PLASMA PHYSICS

SUMMER INSTITUTE
PRINCETON UNIVERSITY
1964

LECTURE NOTES

• PLASMA SOURCES	Nathan Rynn
	Harold P. Eubank
• VACUUM	Francis F. Chen
	Gerhard Lewin
• COIL DESIGN	Edward G. Apgar
• MICROWAVES	Robert G. Mills
	Robert W. Motley
• MISCELLANEOUS	Frank K. Bennett

Princeton University
Plasma Physics Summer Institute
1964

LECTURE NOTES

Plasma Sources
Vacuum

Coil Design
Microwaves

Miscellaneous

Nathan Rynn
Harold P. Eubank
Francis F. Chen
Gerhard Lewin

Edward G. Apgar
Robert G. Mills
Robert W. Motley
Frank K. Bennett

Preface

This volume is one of a series originally prepared for the use of participants in the Summer Institute held at Princeton University June 25-August 3, 1962. An addendum to the section on "Production of Laboratory Plasmas" has been prepared by Francis F. Chen, and the section on "Particle Beams for Plasma Measurements" has been rewritten by Harold P. Eubank. Other sections have not been updated since 1962 although some minor changes have been made. As in the original edition, notation and choice of units have been at the discretion of individual authors; no attempt to obtain uniformity has been made.

May 15, 1964

TABLE OF CONTENTS

THE Q DEVICE

by

Nathan Rynn

Introduction

In the early part of 1959 the writer undertook the problem of making a quiescent plasma in something approaching thermal equilibrium and subject to reasonable control in the laboratory. The objective was to provide an alternative approach to the violently unstable plasmas then existing in the stellarators. It seemed wise, at the time, to avoid the pitfalls of high temperature plasmas and to concentrate on making one at a low temperature. This threw open the entire spectrum of elements as possible plasma species. Further thought seemed to indicate that the lower the ionization potential of the gas, the simpler the problem. This sort of reasoning inevitably leads to the choice of the element with the lowest ionization potential, cesium (3.87 ev), as the plasma species. Many people have worked extensively with cesium plasmas, or ions, for many years. Langmuir and Kingdon[1] did the early work and discovered the principle that a hot metal surface will singly ionize the atoms of a gas that comes in contact with it, provided that the ionization potential of the gas is less than the work function of the metal. Mohler[2] did a great deal of definitive work with cesium discharges. The writer got the idea for the Q-machine after seeing the work of K. Hernquist,[3] of RCA Laboratories, on thermionic energy converters; Langmuir and Taylor[4] studied the effect of surface layers of cesium on tungsten,

to mention some of the bettern known areas of study. Thus, an extensive technology of cesium was available and ready to be put to use in a possible device.

One attractive idea for making a thermal plasma is to make a hohlraum of hot tungsten containing cesium vapor. Dreicer[5] has shown that an interesting plasma can be generated at attainable wall temperature that is in true thermal equilibrium. The difficulty is that it would be necessary to work through walls at temperatures of the order of 2500^0 K or higher, and this would require an involved technology. As an alternative, it was decided to try to make a cesium plasma utilizing contact ionization by tungsten and using a strong magnetic field for confinement. The writer discussed his ideas with several people in this Laboratory but two in particular deserve special mention. E. A. Frieman gave considerable guidance in deciding what sort of device to build from the theoretician's point of view, and W. M. Hooke was very helpful in discussing the experimental details. In particular, Dr. Hooke suggested that the cesium be delivered to the tungsten plates by means of atomic beam ovens.

Theoretical and Other Considerations

Figure 1 is a schematic of the device. Hot tungsten plates, heated by electric bombardment, are placed at each end of a cylindrical vacuum vessel. A beam of cesium vapor is introduced by means of a collimator arrangement, strikes the hot tungsten plate, and is singly ionized. The plates are hot enough to emit electrons; the mixture of electrons and ions form a plasma that streams into the central region where it is confined in the radial direction by the coaxial

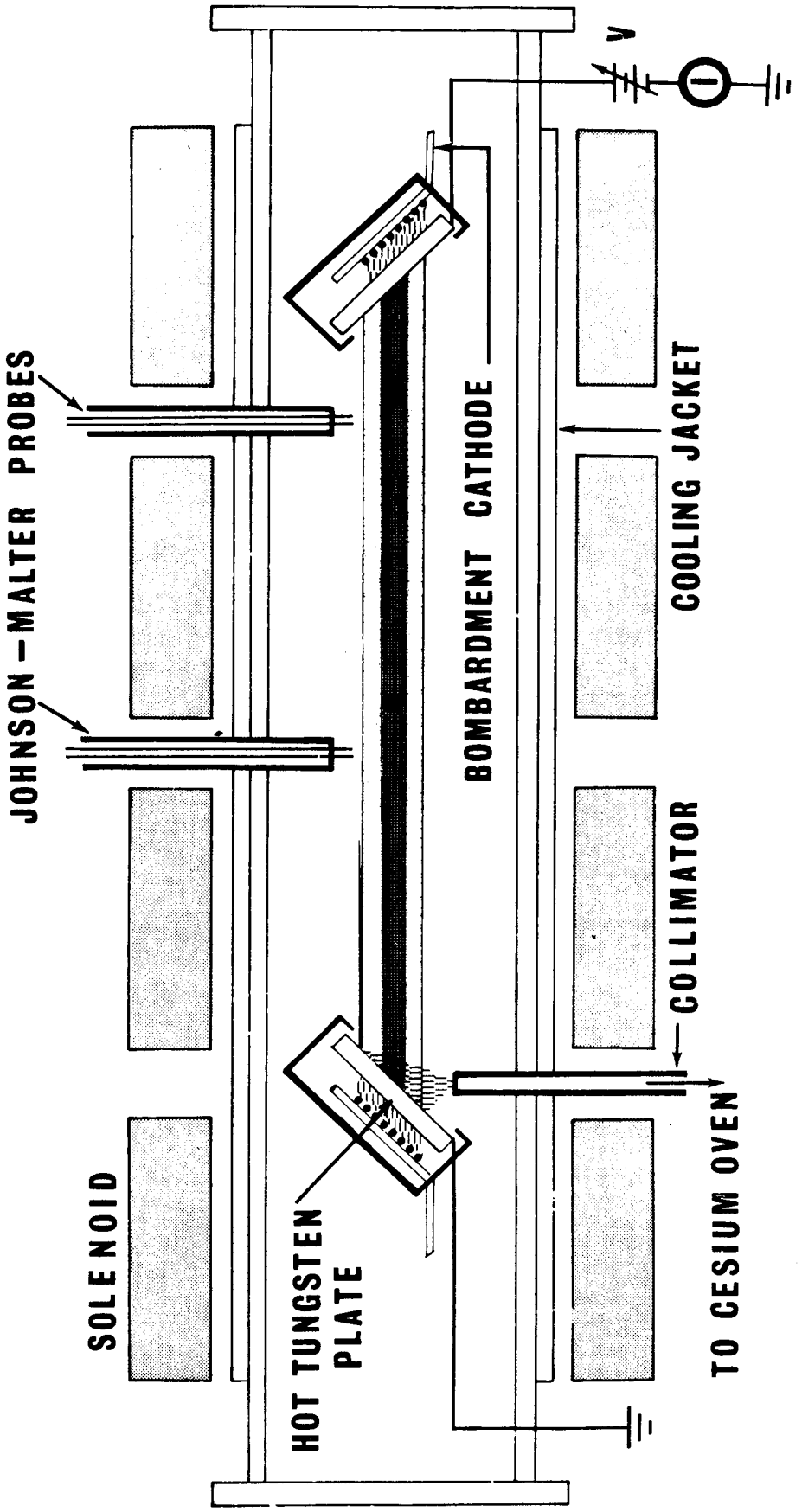

Fig. 1. Schematic of the Q machine.

magnetic field produced by the solenoid. The hot plate at the other end serves as an ion reflector since, in principle, every ion that strikes the plate is adsorbed on the surface and immediately re-evaporated as an ion.* Electrons, of course, are absorbed into the metal lattice and then reemitted according to the Richardson equation. Thus the plasma is confined axially and radially. The vacuum chamber walls are cooled so as to condense out neutral cesium atoms that result from recombination and that are part of the general background. Typically, peak densities of the order of 3×10^{12} cm^{-3}, with fractional ionization of better than 99%, are achieved. Under these conditions the base pressure is of the order of 10^{-6} torr and the neutral cesium vapor pressure is of the order of 10^{-8} torr. It should be noted that although we have been speaking of cesium on tungsten, other combinations can and have been used. Potassium is used quite often and recently we have made a sodium plasma by using a hot rhenium plate.

Since a prime purpose of the machine is to check the theory of a magnetically confined plasma, it is important that the ion gyration radius be small compared to the plasma diameter. If one were to require a minimum of ten gyro radii across a plate diameter of three centimeters, this sets a minimum magnetic field requirement of three kilogauss for cesium, 1.7 kilogauss for potassium and about 1.3 kilogauss for sodium. If we restrict ourselves to air-core, water-cooled solenoids in the present state of the art, this puts a lower

*There is no direct experimental evidence for this assumption. It was first made by Langmuir and his associates and interpretations based upon it seem to work out well.

limit on the size of the device. This is basic and although other workers have made similar devices using cesium confined by fields as low as a few hundred gauss,[6,7,8] it is difficult to see how they can be used to verify the basic theory with which we are concerned. However, this is not to imply that some of these devices are not quite elegant. Some interesting and useful experiments have been performed on them. Pyle[9] was able to generate a cesium column 100 centimeters long with a three kilogauss field, but his plasma was not quiescent.

The theory of the machine has already been published in the Review of Scientific Instruments.[10] The treatment there starts out with the Boltzmann equation and is rather elaborate for the problem at hand. What I propose to do here is to go through a much simpler, but adequate, analysis that emphasises the physical processes involved.

Table I lists some useful relations and numbers. The mean squared distance, $\langle \Delta x \rangle^2$, traveled by an average particle in a random walk is

$$\langle \Delta x \rangle^2 = N a^2 \tag{1}$$

where N is the number of steps and a the length of the step. It can be shown[11] that the maximum distance that a plasma particle will step across a magnetic field due to an electron-ion collision is one electron gyration radius. If we wish to get an estimate of the time, t_D, that it will take for a particle to diffuse across the plasma, we need only set $\langle \Delta x \rangle$ equal to the plasma diameter, 1.4 cm, note that N is the diffusion time divided by the electron-ion collision time, and solve (1) to get $t_D = 1.96$ sec. The electron gyration radius was

TABLE I

(Unless otherwise noted, all values are for cesium at 2000° K (.17 ev), at a density of 10^{12} cm^{-3} and a confining field of 10,000 gauss.)

	Atomic Wt.	Ion. Pot., ev	Work Function, CV	Melting Point, °C
Cesium	132.8	3.87	1.81	28.5
Potassium	39.1	4.32	1.6	62.3
Tungsten	183.9	8.1	4.52	3370
Tantalum	181.5	--	4.19	3027

* * * * *

Thermal velocities: $v_e = 2.78 \times 10^7$ cm/sec; $v_i = 5.59 \times 10^4$ cm/sec

Gyration radii: $a_e = 1.54 \times 10^{-4}$ cm; $a_i = 0.079$ cm

Collision times: ($\ln\Lambda \sim 6$)

Electron-ion (90°) (Spitzer Eq. 5-22): 1.43×10^{-9} sec

Self-collision" (Spitzer Eq. 5-26): $t_{ci} = 1.96 \times 10^{-6}$ sec; $t_{ce} = .4 \times 10^{-8}$ sec

Collision lengths: $\lambda_{ie} = .04$ cm; $\lambda_{ii} = \lambda_{ee} = .11$ cm

Critical frequencies: $f_{ci} = 1.2 \times 10^5$ sec^{-1}; $f_{ce} = 2.8 \times 10^{10}$ sec^{-1}

$f_{pi} = 1.8 \times 10^7$ sec^{-1}; $f_{pe} = .9 \times 10^{10}$ sec^{-1}

Recomb. coefficient (Mohler): $\alpha = 3 \times 10^{-10}$ cm^3/sec

Radiative: $\alpha \sim 10^{-12}$ cm^3/sec;

electron-electron-ion $\alpha \sim 3 \times 10^{-11}$ cm^3/sec

Debye length: 3.1×10^{-4} cm

chosen as the stepping distance because classical diffusion is ambipolar, i.e., both charges diffuse out at the same rate, so that there is no net electrical current. The ambipolar diffusion coefficient is always of the same order as the diffusion coefficient of the slower moving species. Across the field this is the electrons because of the small gyration radius. Along the field the ions are slower-moving and it is the ion diffusion time that corresponds to the ambipolar diffusion. Since this is an almost fully ionized plasma, the significant collisions are coulomb collisions and the mean free path for ions is the same as that for electrons.[14] The collision time is longer by the square root of the mass ratio. The value for $\langle \Delta x \rangle^2$ is the square of the length of the plasma (50 cm), since we want to compare the time of traverse along the plasma with that from axis to edge. Using the mean free path for the stepping distance gives a diffusion time of .31 sec for cesium at a density of 10^{12} cm^{-3}. Note that for a density of 5×10^{11} cm^{-3}, $t_{D\perp}$ becomes 4 seconds while $t_{D\parallel}$ becomes .15 sec. This implies that 10^{12} cm^{-3} is an upper limit for a cesium plasma at 2000° K and 50 cm long if we want the plasma to be "one-dimensional". It should be remembered that these estimates are based on the assumption of zero current.

Recombination is an important loss process in this type of plasma. The recombination coefficient, α, is defined by the relation

$$\frac{dn}{dt} = -\alpha n^2 \qquad (2)$$

where n is the density.

Simple integration of (2) will show that $1/\alpha n$ has the nature of a relaxa-

tion time, which will be referred to as the "survival time," t_s. It is a measure of the length of time an electron-ion pair survives before recomining. It would be interesting to compare t_s and t_D but lack of knowledge of α makes it difficult. For a density of $10^{12}/cm^3$, we can choose $\alpha = 10^{-10}$ $cm^3 sec^{-1}$, Mohler's value, or $\alpha = 10^{-12}$ $cm^3 sec^{-1}$, the radiative value.[12] The first gives $t_s = 1$ sec, the second .01 sec, so that for these densities the average plasma particle recombines "out" before diffusing out. If one assumed $\alpha = 10^{-10}$ $cm^3 sec^{-1}$, then a plasma particle on the axis will diffuse less than a millimeter before recombining when B = 10 kilogauss. Other workers[13] have extended the theory of recombination to show that under certain conditions, α is density dependent. This can be an important effect for the Q machine. However, it complicates the calculations and the basic ideas are not lost if it is assumed that Eq. (2) is valid.

The operating limits of the machine can also be derived by means of a straightforward analytical procedure. Assume end plates of infinite radius, or no variations in the radial and azimuthal directions. Assume the plasma geometry is that shown in Fig. 2 with no applied electric field. The equation of continuity for ions is

$$\frac{\partial n_i}{\partial t} + \frac{\partial (n_i v_i)}{\partial z} + \alpha n_i^2 = 0 \tag{3}$$

where v_i is the ion drift velocity. The equation of continuity of momentum for ions is

$$\frac{\partial}{\partial t}(m_i n_i v_i) + \frac{\partial}{\partial z}(m_i n_i v_i^2) = \frac{\partial p_i}{\partial z} - \alpha n_i n_e m_i v_i \tag{4}$$

where m_i is the ion mass. We have assumed that the ion density, n_i, is equal

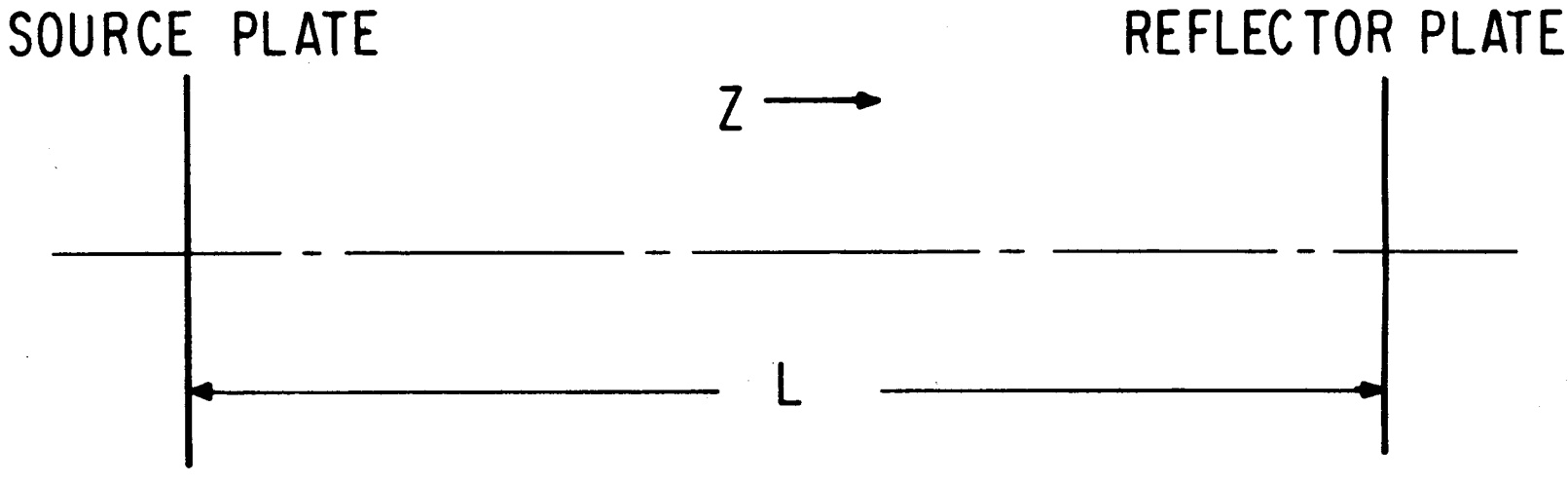

Fig. 2.

to the electron density, n_e, and that the pressure, p, is isotropic so that $p = nkT$. Since the current is zero, $v_i = v_e$ and the net transfer of momentum between electrons and ions is also zero. We have also assumed that T_i is constant. Equation (4) may be rewritten as:

$$m_i n\left[\frac{\partial v_i}{\partial t} + 2v_i\frac{\partial v_i}{dz}\right] + m_i v_i\left[\frac{\partial n}{\partial t} + v_i\frac{\partial n}{\partial z} + \alpha n^2\right] = -kT_i\frac{\partial n}{\partial z} \quad . \tag{5}$$

Substituting (3) into (5) results in

$$m_i n\left[\frac{\partial v_i}{\partial t} + v_i\frac{\partial v_i}{\partial t}\right] = -kT_i\frac{\partial n}{\partial z} \quad . \tag{6}$$

Since this is the equation for fluid flow, it could have been written down immediately except for the fact that this would have obscured the role of the recombination loss. The recombination loss does not show up in (6) because when an electron-ion pair recombines it is completely removed from the plasma. A similar procedure is followed for the electrons, the only difference being the use of v_e for v_i and T_e for T_i. Since the only heat sources are the end plates (we assume perfect insulation along the plasma edge) it seems reasonable to assume that T_e and T_i are equal. Adding the two equations, dropping the time variation for the steady state solution, and remembering that $m_i >> m_e$, gives

$$nv\frac{\partial v}{\partial z} = -\frac{2kT}{m_i}\frac{dn}{dz}$$

or

$$\frac{1}{2}\frac{\partial(v^2)}{\partial z} = -\frac{2kT}{m_i}\frac{\partial(\ln n)}{\partial z} \quad . \tag{7}$$

This integrates out to

$$n = n_o e^{-mv^2/kT} \tag{8}$$

where n_o is the density at $v = 0$. Substituting (8) in (3) gives, for the steady state,

$$(1 - \frac{mv^2}{2kT})\frac{\partial v}{\partial z} = -\alpha n_o e^{-mv^2/4kT} \quad . \tag{9}$$

If we assume that

$$m_i v^2 << 4kT \ , \tag{10}$$

then

$$v \cong -\alpha n_o (L - z) \tag{11}$$

since v is zero at the reflector plate. Suppose we arbitrarily decide that no more than a 1% variation in density over the length of the plasma is permissible. From Eq. (8) we get $n = .99n_o$; for $T = 2000^{\circ}$ K we find that $v = 7.1 \times 10^3$ cm sec^{-1}. Substituting these values into (11) for $z = 0$, and using the conservative value of $\alpha = 10^{-10}$ cm^3 sec^{-1}, gives a maximum length of 71 cm for this plasma at a density of 10^{12} cm^{-3} in order to preserve "one-dimensionality". This agrees with the value obtained above. It is interesting to see what the input neutral flux must be. This flux must be equal to the product of the density and the drift velocity at the source plate or approximately 7×10^{15} cm^{-2} sec^{-1} for $\alpha = 10^{-10}$ cm^3 sec^{-1}. This is very nearly equal to the number of particles lost

by recombination in a cylinder one square centimeter by 50 cm long.

The radial density distribution may be calculated quite simply under the assumption of no axial or azimuthal variation of density. The radial particle flow, $\bar{\Gamma}$, is given by

$$\bar{\Gamma}_{\perp} = -D_{\perp} \nabla_{\perp} n \tag{12}$$

where the classical radial diffusion coefficient, $D_{\perp}$, is given by[15]

$$D_{\perp} = \frac{\eta_{\perp} kT}{B^2} n = \frac{2\eta\, kT}{B^2} n = An \tag{13}$$

where $\eta_{\perp}$ and η are the resistivity across and along the magnetic field, B, respectively. The equation of continuity of particles in the radial direction is

$$\frac{\partial n}{dt} + \nabla_{\perp} \cdot \bar{\Gamma} + \alpha n^2 = q \tag{14}$$

where q is a source term and represents the number of particles created per unit volume per second. This enters in this way because we have assumed no axial variation and this assumes, essentially, that the incoming neutrals strike the source plate and are reflected between the plates many times before diffusing out. Thus, the area source at one end is converted into a cylindrical source. Substituting (12) and (13) into (14) and taking the steady state solution results in

$$\frac{d^2(n^2)}{dr^2} + \frac{1}{r} \frac{d(n^2)}{dr} - \frac{2\alpha}{A} = -\frac{2q}{A} \,. \tag{15}$$

The simplest solution is to have q constant, $n = n_o$ at $r = 0$, and $n = 0$ at $r = 0$, the plasma radius. Then

$$\left(\frac{n}{n_o}\right)^2 = \frac{I_o(r/R) - I_o(r_o/R)}{I_o(r/R) - 1} \tag{16}$$

where

$$\frac{1}{R} \equiv \frac{2\alpha}{A} \tag{17}$$

and

$$q = \frac{\alpha n_o^2 I_o(r_o/R)}{I_o(r_o/R) - 1} \quad . \tag{18}$$

Figure 3 shows some plots of (16) for $r_o = 2.5$ cm. Next visualize a cylindrical source generated by illuminated circular area of radius $r_1 < r_o$ on the source plate. For $r < r_1$, the solution will be much like (16). For $r > r_1$, $q = 0$ and the solution is a sum of modified Bessel functions of the first and second kinds. For a large enough plate the solution is, essentially, $k_o(r/R)$. Figures 4 and 5 show some plots of these solutions taken from Ref. 10.

Constructional Details

One of the most critical components of the Q machine is the atomic beam oven. Considerable work has been done in this field and probably the best thing for one to do to familiarize oneself with the subject is to read Chapter I of Ramsey[16] and the paper by Giordmaine and Wang.[17] Only a very sketchy review of the subject can be given here.*

*See also References 18, 19 and 20.

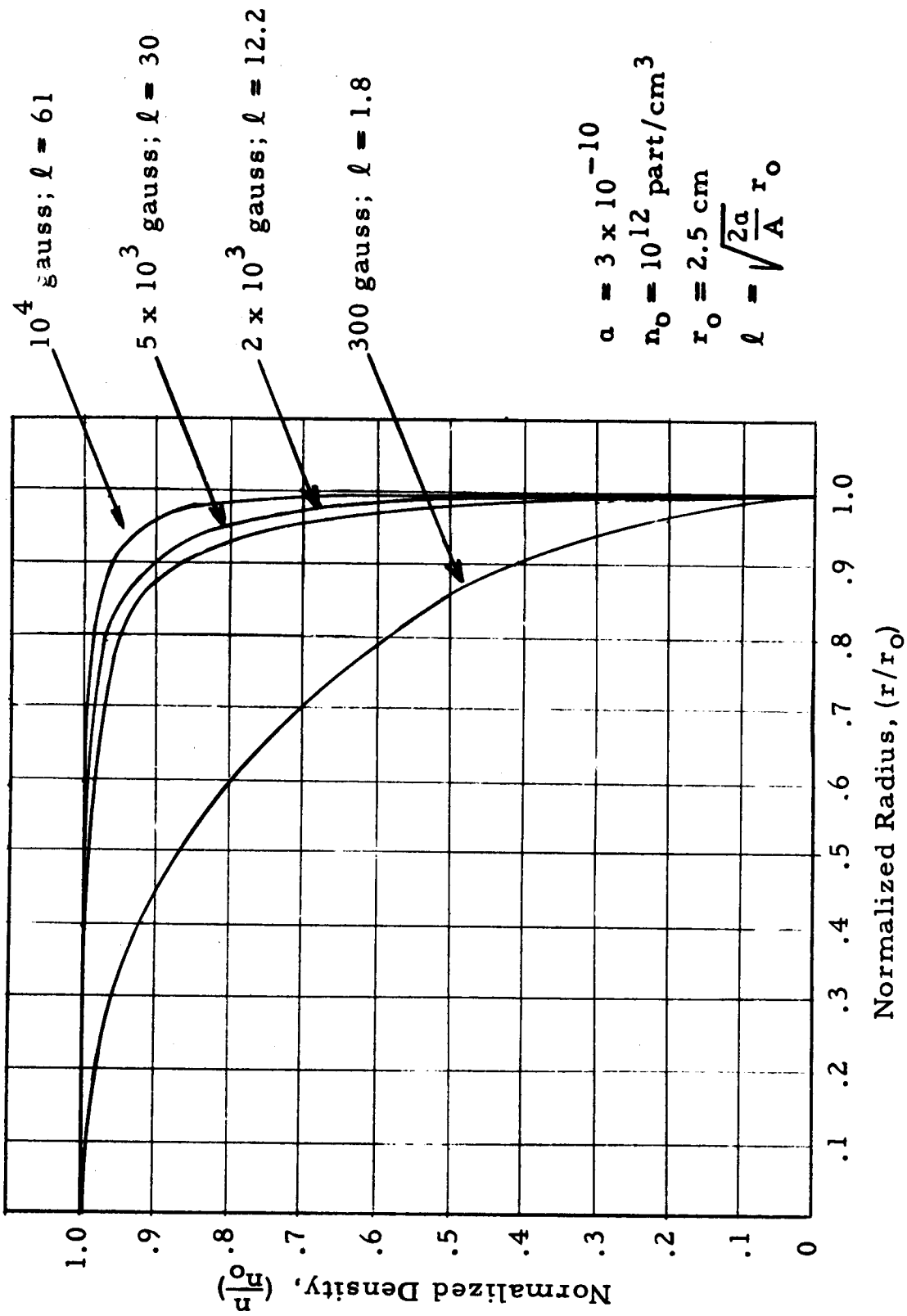

Fig. 3. Relative density as a function of radius with a uniform neutral flux distributed across the source plate.

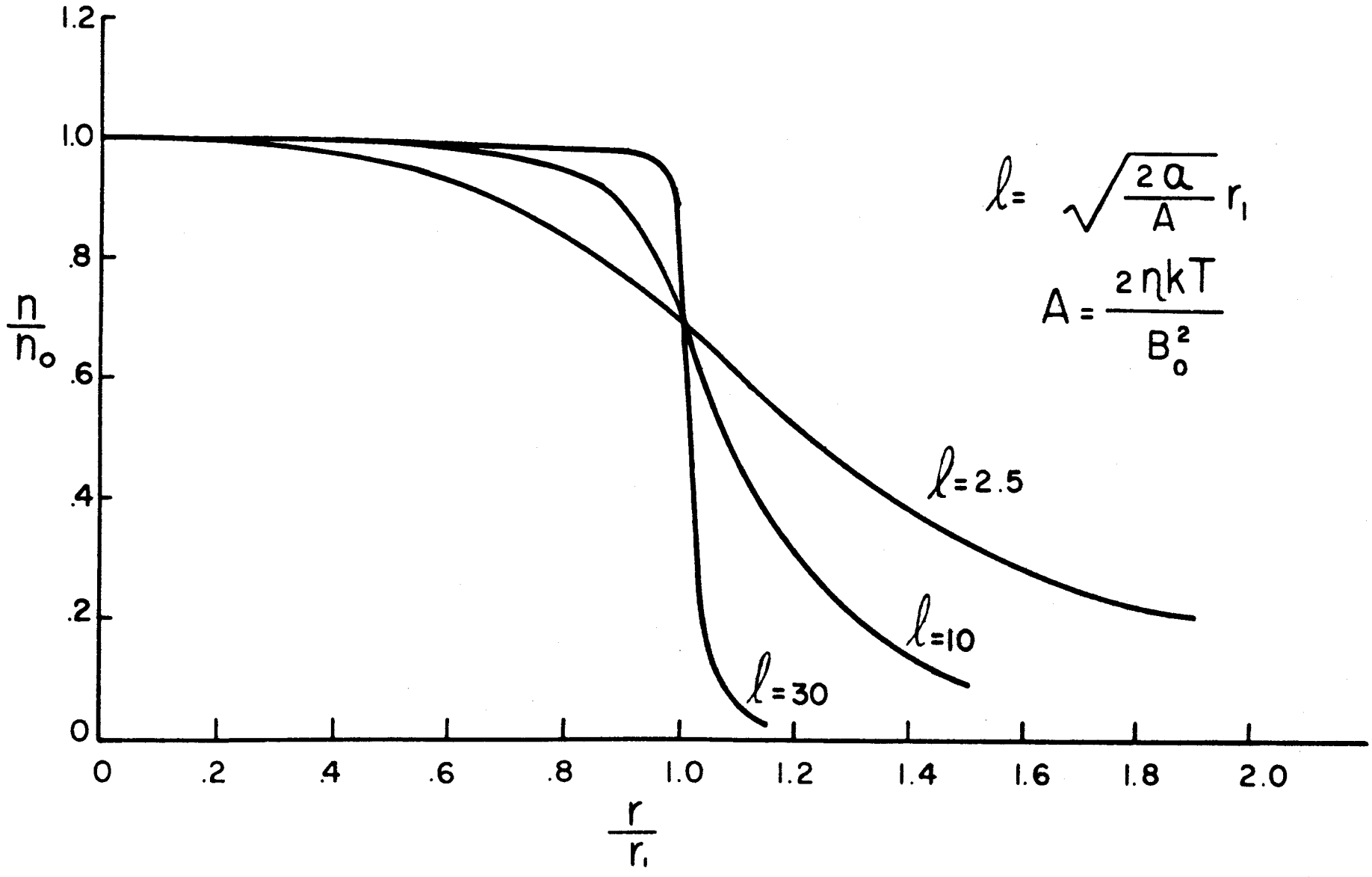

Fig. 4. Relative density versus radius for a partially "illuminated" source plate of infinite radius.

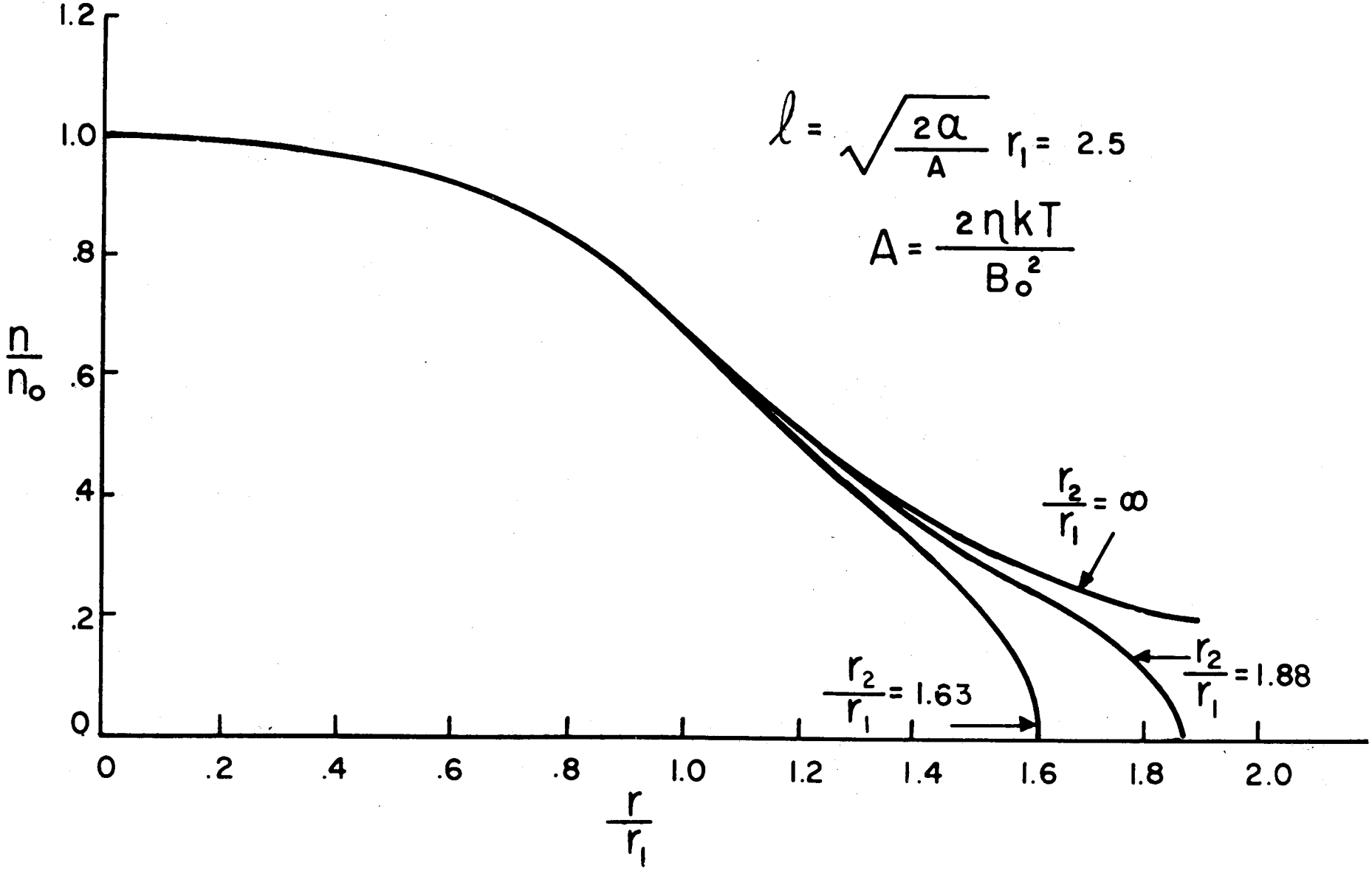

Fig. 5. Relative density versus radius for a partially "illuminated" source plate of finite radius.

Efficient molecular beam collimation is best done by making a bundle of many parallel tubes. One way of doing this is to alternately stack leaves of corrugated metal foil with smooth strips giving the effect of thousands of parallel tubes. It is best to make the radius of the tubes as small as possible, preferably .001 to .002 in. radius. The greater the transparency the better the collimating efficiency.[20] Figure 6 shows three collimators that have been used in the Q machine.

Making good atomic beam ovens is difficult and requires much effort. In order to get the requisite fluxes it is necessary to move the sources as close as possible to the plates. This makes them area sources instead of point sources. The plane of the source must be parallel to the plane of the source plate. Alignment is important. Two ways of accomplishing this have been indicated in the figures. One is to aim an "external" collimator at the center of the plate. In the case of the "hypodermic needle" collimator of Fig. 6, nothing else is needed. The broader collimators must be bent at 45° to be aimed at right angles to the plate or they must be cut at a 45° bias. Figure 7 shows a collimator mounted integrally with a gun.

The alkali metal can be generated in two ways, first, by making a mixture of the alkali chloride and calcium filings. At 400° C or higher a chemical reaction occurs, calcium chloride is formed and the free alkali metal vapor is released. This is the method used in the assembly of Fig. 7. A second method, useful in the external collimators, is to use the pure metal. Cesium must be put into glass ampoules and a means devised to break them inside the vacuum system.

Fig. 6. Some collimators that have been used in the Q machine. The bottom line shows schematics of the collimators; the center line the neutral flux distributions and the top line typical plasma density profiles. The "hypodermic needle" was used with vaporized alkali metal. The other two used a chemical reaction between calcium filings and the alkali chloride.

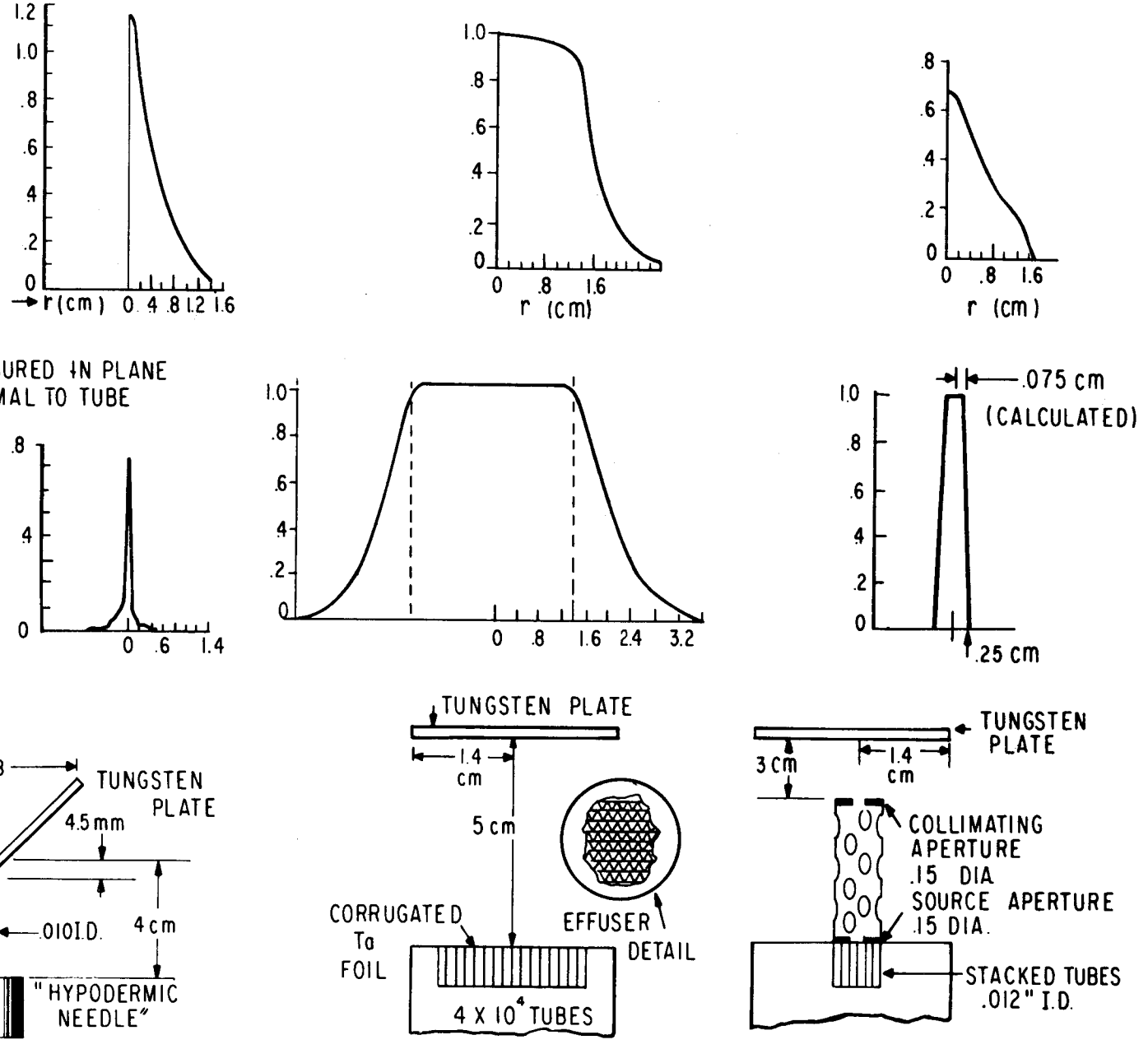

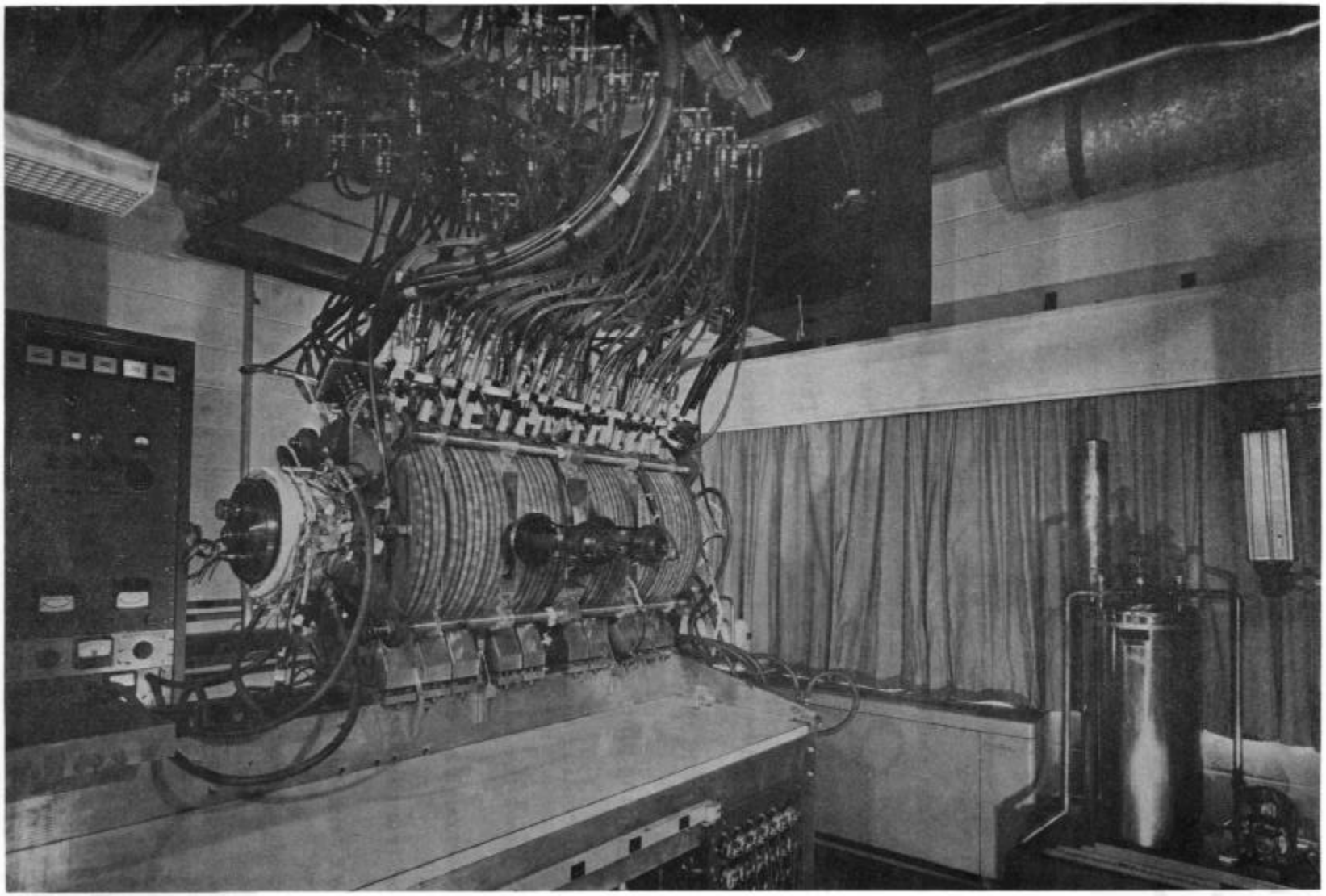

610647

Figure 7. Photograph of a gun and collimator combination. The comminator shown is the one in the right hand column of Fig. 6

Potassium and sodium may be purchased as bars packed in kerosene. These can be removed, cut to size, cleaned, placed in the beam oven, and then placed under a vacuum without disastrous results, provided reasonable precautions are taken.

The guns are shown schematically in Fig. 1 and pictorially in Figs. 7 and 8 The plates are .080 thick tungsten formed into an ellipse that will project into a circle of 1.4 cm radius when held at 45° to the plasma axis. They are held by three tungsten rods .125 in. in diameter. The entire assembly is carefully shielded, both electrically and thermally. The most critical item is the electron bombardment heater. This must be made strong enough to withstand the strong magnetic field with the heating current going through it. This problem was solved by putting nine lengths of .015 dia. tungsten wire in parallel, heating them with dc and coating them with thorium oxide (thoria). Using thoria as the electron emitter allows the filaments to be run at a temperature low enough so that they will have enough strength to withstand the magnetic field. The gun assembly is insulated from the mounting arrangement and mounted on two heavy rods fastened to the end flanges as indicated in Fig. 8. All the leads for the bombardment heaters, oven heaters, necessary thermocouples, etc. go through this flange also. The entire unit is mounted horizontally in the vacuum tube. Typically, the bombardment heaters require about 80 amperes at about 3.5 volts when the plates are radiating away 1.5 kilowatts and drawing about one ampere of bombardment current. Note that it is necessary to put a shield at the heater potential behind the heater to keep electrons from going in the reverse direction.

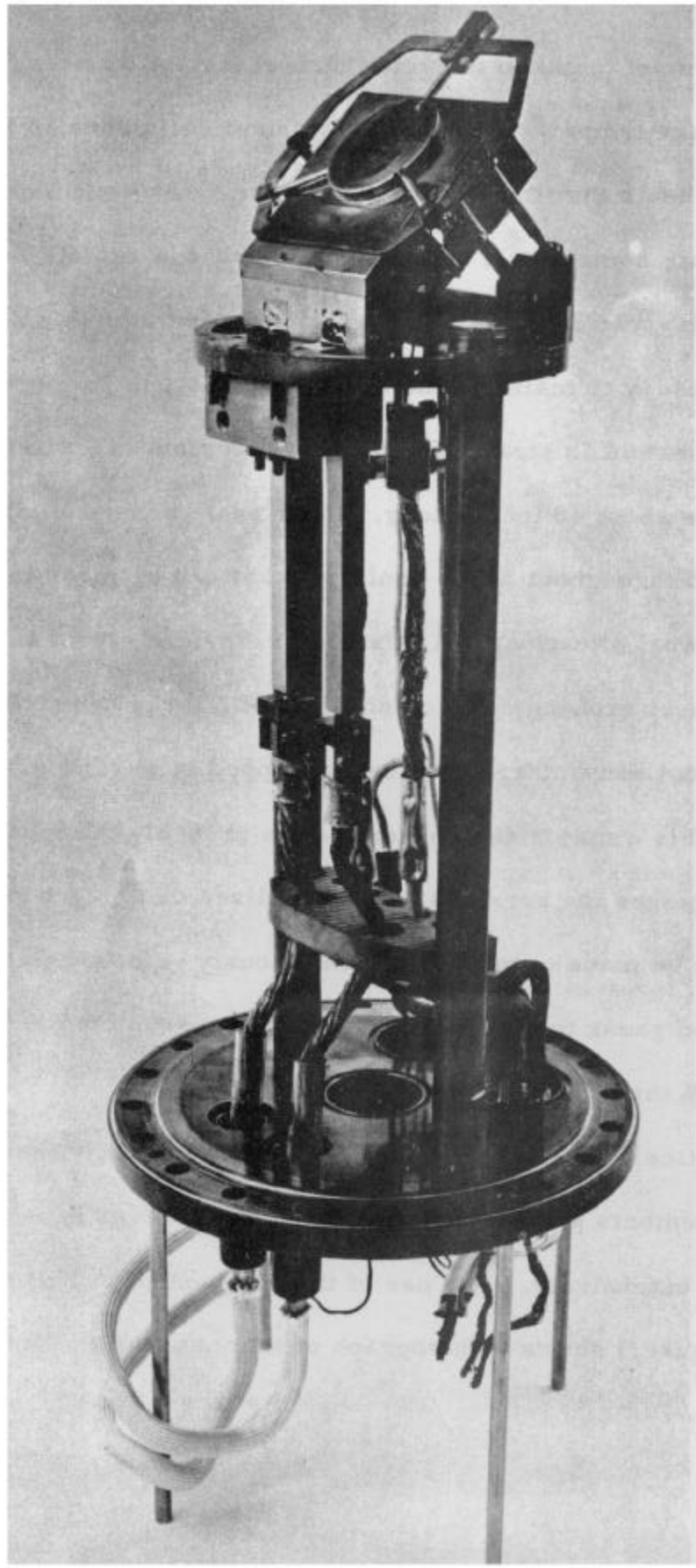

Fig. 8. Photograph of gun mounted on an end flange. The entire unit is bolted on one end of the machine. Gold gaskets ensure a vacuum seal.

Also, precautions must be taken to avoid thermal instability brought about by operating the heaters temperature-limited. When this is done an increase in plate temperature heats the filaments a little more, they emit more electrons, which heats the plate some more, and the whole process rapidly runs away. This can be avoided with some care. The plate temperature is determined by the electron flux necessary to maintain the desired density.

The vacuum vessel is straightforward and consists of a six-inch diameter stainless steel tube about 40 inches long. Hard-seal gaskets of either gold or aluminum are used throughout. The cooling jacket can be made in a variety of ways to suit individual situations. A mixture of ethylene glycol and water is passed through a heat exchanger which consists of a large dewar flask filled with more ethylene glycol and water. Dry ice is dropped in to chill it.

The solenoid is a major design item and is probably the most expensive component and requires the services of a specialized design group. This particular solenoid can be made to produce a continuously variable magnetic field from a few hundred gauss to nine kilogauss. The variation in the field strength is no more than 5% throughout its useful length.

The diagnostics are mostly probes, single and double. These are mounted on bellows arrangements so as to be bakeable. Microwaves have been used occasionally but not extensively. The use of this diagnostic will probably increase in the future. Figure 9 shows a photograph of the installation, and Fig. 10 shows a system diagram.

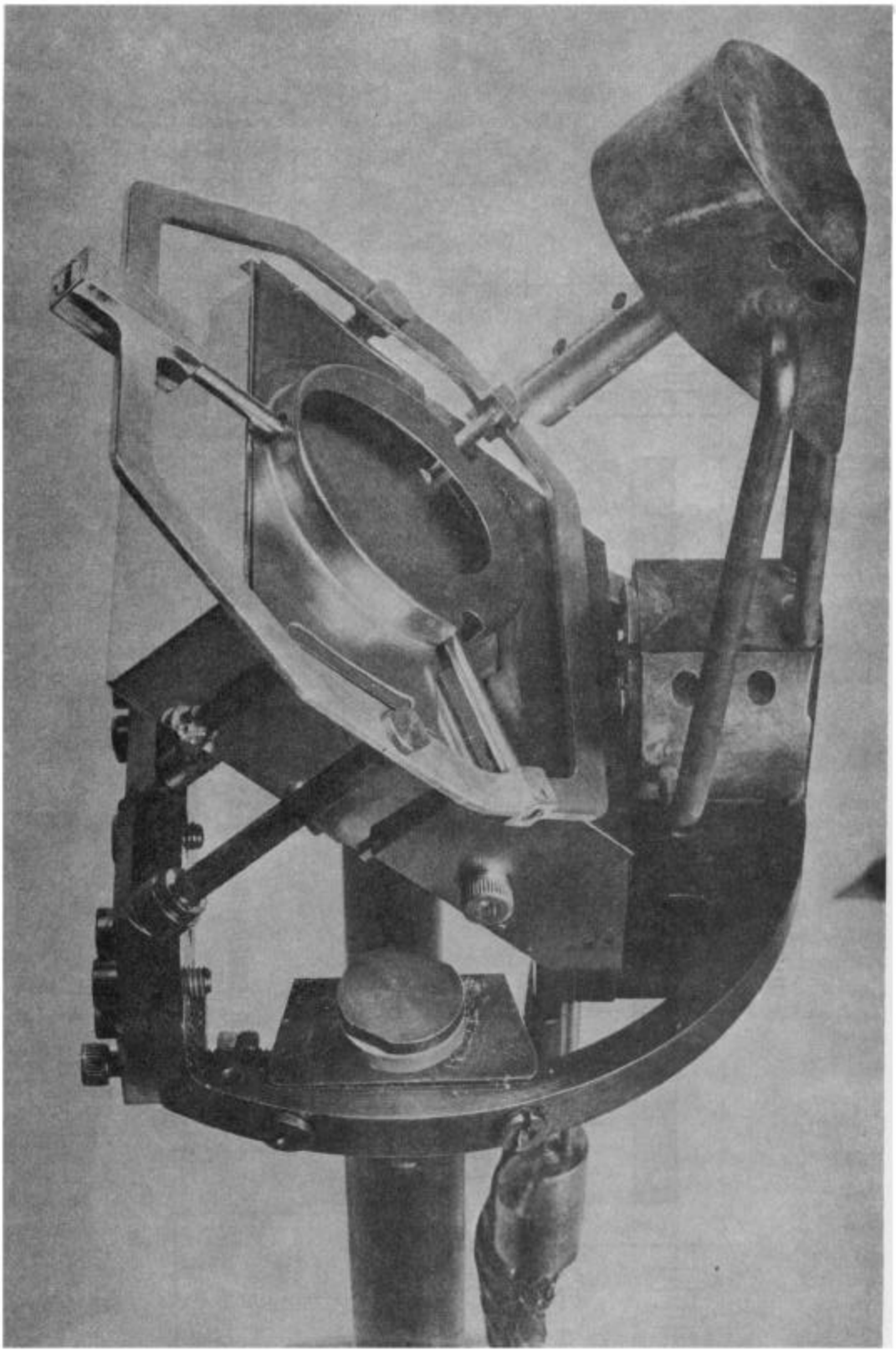

620233

Figure 9. Photograph of the Q Machine

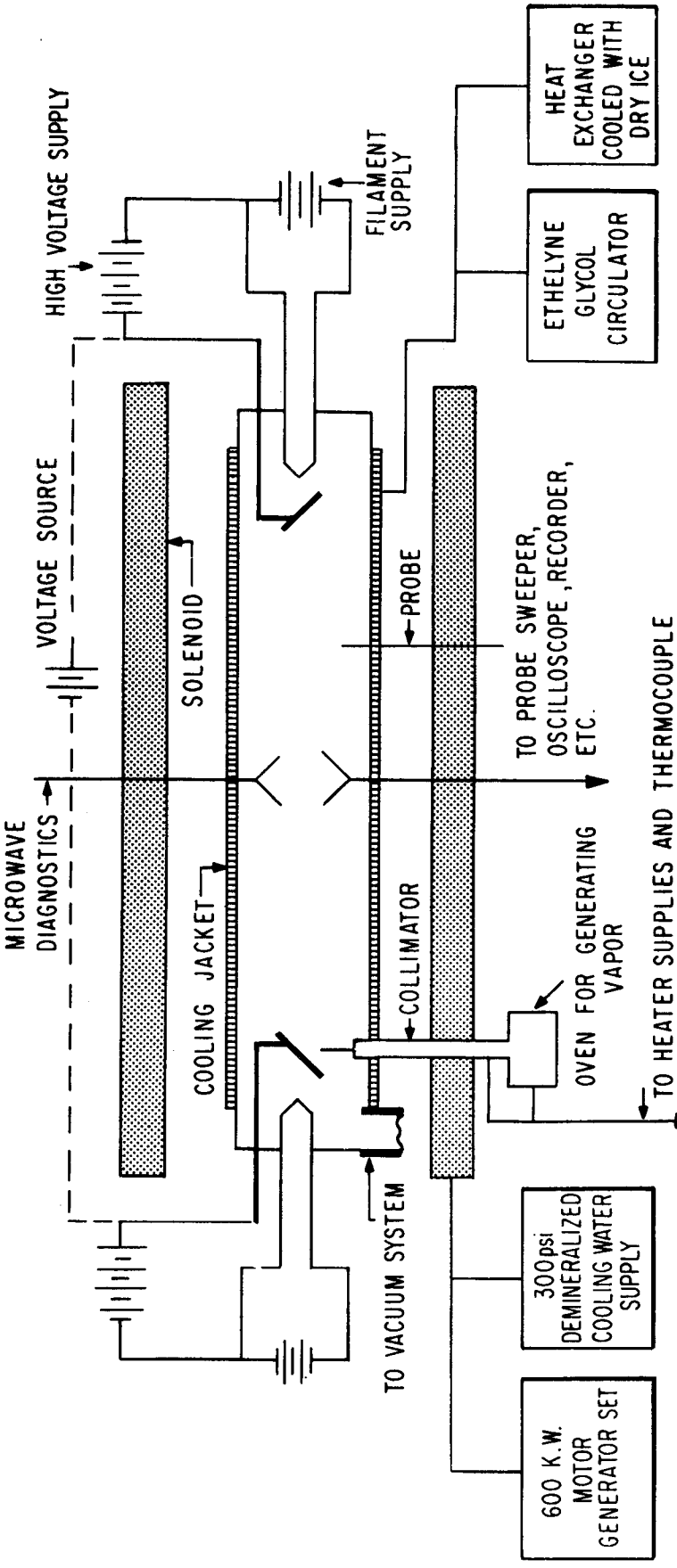

Fig. 10. Block diagram of Q machine installation.

Concluding Remarks

It is not necessary to use atomic beam ovens. The alkali metal can be introduced into a temperature controlled appendix, cooler than the walls, which are kept hot, so that the rate of delivery of metal vapor to the plates is controlled by the temperature of the appendix. This type of operation, designated as the vapor pressure mode, is particularly well suited to small devices. Since the plasma volume and, hence, the recombination loss is small in these devices the background pressure need not be high and reasonably high densities with high fractional ionization can be produced. Knechtli and Wada[6] have made such a device using a weak confining field. Such a device can be made at a substantially lower cost than a large Q machine. Figure 11 shows a schematic.

As was mentioned in the section on theory, the success of the device depends upon the existence of classical diffusion. Consequently, in order to show the Q machine worked and did indeed produce a quiescent plasma, it was necessary to perform an experiment designed to demonstrate classical diffusion. This was done[21] and we can say with reasonable certainty that the Q machine can produce a quiescent plasma of densities of the order of 10^{12} cm^{-3}, with controlled density profiles and high fractional ionization. Further details will be found in Refs. 10 and 21.

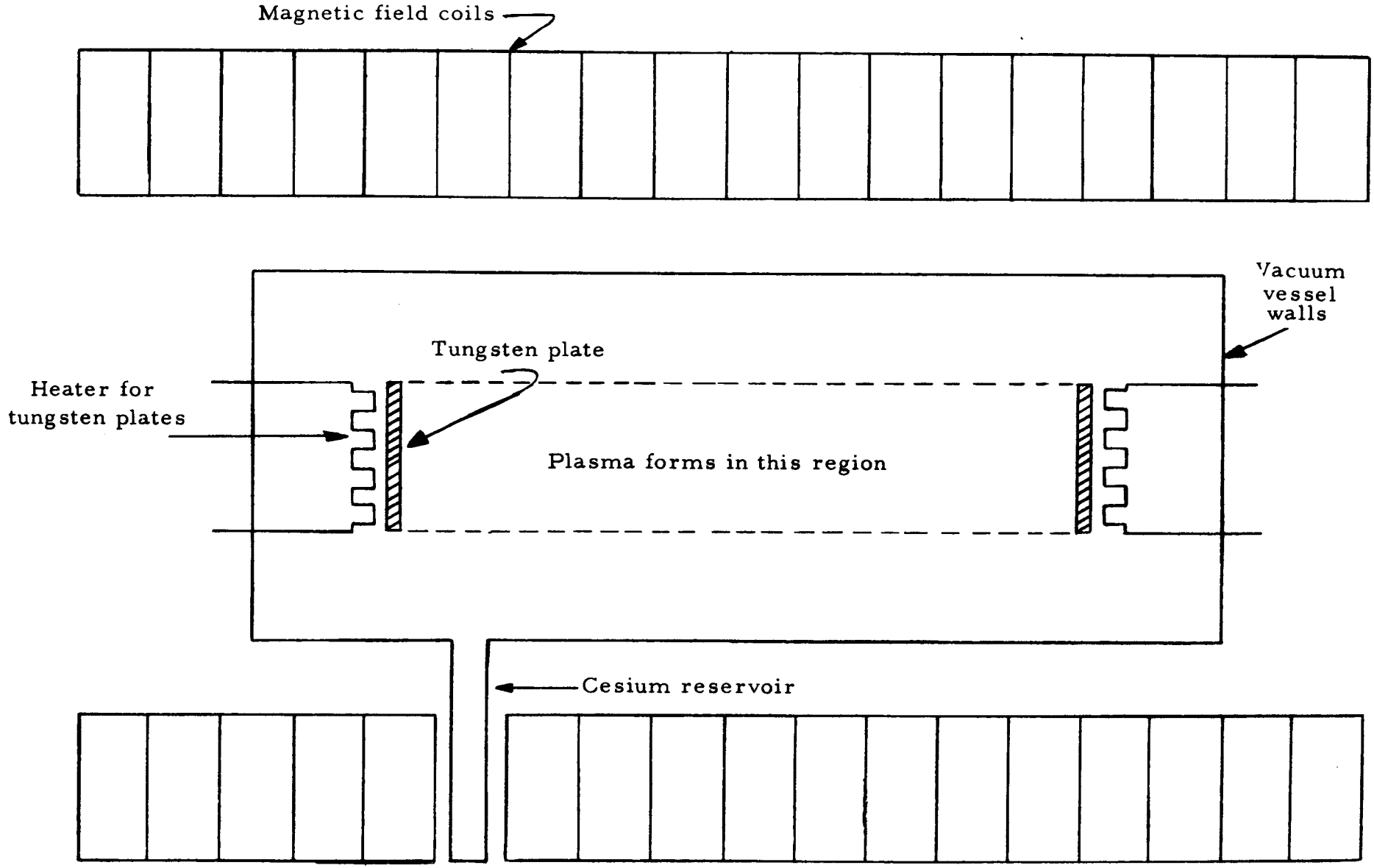

Fig. 11. Schematic of the Q machine in the vapor-pressure mode.

REFERENCES

1. I. Langmuir and K. H. Kingdon, "Thermionic Effects Caused by Vapours of Alkali Metals," Proc. Roy. Soc. A107, 61 (1925).

2. F. L. Mohler, J. Research, Natl. Bur. Standards, 19, 447, 559 (1937).

F. L. Mohler and C. Boeckner, J. Research, Natl. Bur. Standards, 2, 489

3. K. G. Hernqvist, M. Kanefsky and F. H. Norman, RCA Rev. 19, No. 2, 244-258 (June 1958).

4. J. B. Taylor and I. Langmuir, "The Evaporation of Atoms, Ions and Electrons from Cesium Films on Tungsten," Phys. Rev. 44, No. 6, Second Series (1933).

5. H. Dreicer, "Plasma in Equilibrium," Proc of the Conference on Controlled Thermonuclear Reactions (Princeton, October 1955), pp. 507-511; TID-7503.

6. J. Y. Wada and R. C. Knechtli, Proc. I.R.E. 49, No. 12, 1926 (1961).

7. M. A. Allen and G. S. Kino, Phys. Rev. Letters 6, 163-165 (1961).

8. R. B. Hall and G. Bekefi, Bull. Am. Phys. Soc., Ser. II, 5, No. 4, 314 (1960).

9. R. V. Pyle, A. Paulikas, H. Rugge and J. W. Stearns, Bull. Am. Phys. Soc., Ser. II, 5, No. 5, 366 (1960).

10. N. Rynn and N. D'Angelo, Rev. Sci. Inst. 31, No. 12, 1326-1333 (1960).

11. A. Simon, An Introduction to Thermonuclear Research (Pergamon Press, New York, 1959), Chap. IX.

12. F. L. Mohler, loc. cit. (1937).

13. N. D'Angelo, Phys. Rev. 121, 505 (1961).

E. Hinnov and J. G. Hirschberg, Phys. Rev. 125, 795-801 (1962).

14. L. Spitzer, Jr., Physics of Fully Ionized Gases (Interscience, New York, 1956).

15. A. Simon, op. cit.

16. N. F. Ramsey, Molecular Beams (Oxford, Clarenden Press, London, 1956), Chap. I.

17. J. A. Giordmaine and T. C. Wang, Jour. Appl. Phys. 31, 463-471 (1960).

18. L. B. Loeb, The Kinetic Theory of Gases (McGraw-Hill, New York 1934) (also reprinted by Dover, New York).

19. J. C. Helmer, F. G. Jacobus, P. A. Sturrock, Jour. Appl. Phys. 31, 458-463 (1960).

20. G. R. Hanes, Jour. Appl. Phys. 31, 2171-2175 (1960).

21. N. D'Angelo and N. Rynn, Phys. Fluids, 4, 1303-1306 (1961).

PLASMA GUNS

by

Harold P. Eubank

We use the term "plasma gun" to denote those devices employed for the acceleration of self-generated plasmas to velocities such that energetic ions result. "Plasma guns" constitute a special class of plasma sources. The discussion will treat only those guns in which the acceleration results from plasma properties, i.e., collective effects in high density plasmas. Although electrostatic acceleration of ions followed by space charge neutralization results, strictly speaking, in a plasma gun, the acceleration process is a single particle phenomenon and will not be considered here.

We might divide the subject into two groups: I) Guns with electrodes so shaped as to produce directed beams of plasmas, II) Assymmetric electrodeless θ pinches.

At the present time, group I appears to offer better energy transfer from the power supply into kinetic energy of the plasma, values up to $\sim 40\%$ having been reported.[1] In addition, the mean ion energy appears more favorable in group I.

Electrode Guns

The early work of Ehlers et al[2] on pulsed ion sources for accelerators has led to the development of a plasma gun employing hydrogen (or deuterium) loaded electrodes. Such guns have constituted the primary source for plasmas

injected into the magnetic mirror containment device at UCRL Livermore.[3]

Metals such as titanium, zirconium and hafnium have the ability to absorb enormous quantities of hydrogen in ratios better than 1 hydrogen atom per base metal atom. A more modest loading ratio of about 1:5 is usually employed to reduce electrode embrittlement to a tolerable level. Guns employing such hydrogenated electrodes will yield plasmas composed of the various atomic species which appear in the electrodes.[4] As radiation cooling of plasmas by high Z impurity ions is an energy loss mechanism to be minimized to whatever extent possible in fusion devices, such plasma guns would be of little use were it not for the fact that the plasma protons, having similar energy distributions to that of the impurity ions,[4] will have higher mean translational velocity and thus run ahead of the slower moving impurities. With suitable flight paths along guiding magnetic fields and appropriately phased magnetic barriers the impurity level of the final trapped plasma may be reduced to acceptable levels.[3]

The small physical size of these guns and complexity of the plasma flow produced by the multi-electrode system has not permitted an extensive examination of the internal currents and magnetic fields as in the case of the larger, pulsed gas, coaxial systems. For energy inputs of several hundred joules muzzle plasma densities are of the order of 10^{15} cm^{-3} and total ion outputs in the neighborhood of 10^{17} - 10^{18}. The plasma ions ejected from the gun have highly non-isotropic velocity distributions, the energy associated with velocity perpendicular to the gun axis is of order 1/10 that associated with motion parallel to the axis. Typical mean ion energies are about 500-1000 ev;[4] the dependence of the energy distribution on the rate of rise of the gun current is not

known. The electrons in the ejected plasma are probably nearly Maxwellian and have a temperature ~10-20 ev.

In an effort to reduce electrode contaminants, Marshall[1] has injected the desired atomic species into the electrode region with a fast pulsed valve.[6] The electrodes are coaxially arranged and the gas is admitted from the inner electrode into the annular region where the discharge occurs.

Extensive parametric studies of such guns have been carried out by the Los Alamos group, with capacitor voltages from ~20 to ~100 kv and stored energies from ~500 to ~10,000 joules. There appears to be no advantage gained from voltages greater than ~25 kv and the energy required is determined primarily by the type of plasma desired and thus the gas loading. For injected gas loads of ~1 atm. cm^3 ion outputs ~10^{19} are observed with average ion energies in the hundred ev range; whereas, for smaller gas loads and carefully minimized system inductance, recent work[6] indicates mean ion energies in excess of 10 kev with ion energies observed up to 100 kev. Under these conditions densities at the muzzle are ~10^{14} cm^{-3} and efficiencies ~20%.

Most important is the fact that the energy content of the fast neutrals which arise from charge transfer between fast ions moving through the injected gas appears to be < 10% of the total ion energy and furthermore the concentration of impurity ions is no greater than a few per cent of the total.[7]

Detailed measurements on the plasma between the electrodes[8] have shown the existence of a well-defined planar current sheet. In general the behavior is in agreement with theoretical treatments of the acceleration process.[9-12] From

magnetic probe measurements yielding both position and pressure difference across the sheet as functions of time, it is found that the observed velocity is best fitted to theory by the assumption of constant sheet mass contrary to the "snow plow" model. The constant sheet mass is consistent with the observed planar surface over the length of the barrel. As the radial sheet current is primarily due to electrons, these tend to move ahead of the ions due to the Lorentz forces. As a result an axial Hall field is set up which provides the mechanism for acceleration of the ions. Magnetic probe data indicate, in addition, the presence of axial currents through the sheet which are comparable to the total gun current.

The process whereby the large ion energies in the kev region (ion velocities much greater than observed sheet velocities) are produced is not clearly understood. Large voltage spikes ~ 50-100 kev with durations of tenths of microseconds have been observed across the gun terminals as the plasma leaves the muzzle, although no correlation between the size of these spikes and the ion energy is apparent at this time.

Electrodeless Guns

θ pinches with single turn conically shaped coils provide a propulsive force on a plasma and have been extensively employed as plasma guns.[13-20] There exists such a variety of conditions under which such guns have been operated (e.g., cone angle, rate of rise of current, degree of preionization employed, etc.) that it is difficult to compare the experimental evidence from different sources and formulate a picture of the plasma production and propulsion.

In some cases there is evidence of ejected plasma with well-defined structure.[18, 20] Ion energy analysis indicates that the ions have energies extending into the kev region.[16, 17]

Considerable attention has been given to the plasma formation and in the case of little or no pre-ionization it is definitely established that the main plasma burst is created and ejected during the second half cycle. It has been proposed[13-15] that the primary effect of the first half period occurs during the second quarter where the drift velocity is such as to carry electrons into the vacuum wall. Collisional processes then lead to the formation of a nearly fully ionized layer at the wall. During the third quarter cycle this ionized sheet is driven inward by the contracting magnetic field producing ionization and heating of the remaining gas. Presumably Lorentz forces on the electrons of the current sheet then give rise to axial propulsion from j_θ and B_r which eject the electrons from the muzzle. Axial space charge fields in turn accelerate the ions.

REFERENCES

1. John Marshall, Phys. Fluids 3 134 (1960).

2. K. W. Ehlers, J. D. Gow, L. Ruby and J. M. Wilcox, R. S. I. 29, 614 (1958).

3. F. H. Coensgen, W. F. Cummings and A. E. Sherman, Phys. Fluids, 2, 350 (1959).

4. See "An Ion Energy Analyzer for 167ff Plasma Measurements".

5. John Marshall, Proceedings of the Second United Nations International Conference on Peaceful Uses of Atomic Energy, (United Nations, Geneva, 1958), Vol. 31, p. 341.

6. J. E. Osher (private communication).

7. S. Ya Lukyanov, I. M. Podgornyi and S. A. Chuvatin, Zhur, Tekh. Fiziki 31, 1026 (1961). Translated: Soviet Physics - Technical Physics 6, 750 (1962).

8. L. C. Burkhardt and R. H. Lovberg, Phys. Fluids, 5, 341 (1962).

9. Philip J. Hart, Phys. Fluids, 5, 38, (1962).

10. Sidney W. Kash, in Plasma Acceleration, edited by S. W. Kash, Stanford University Press, Stanford, California, 1960.

11. A. Dattner, in Proceedings of the Fourth International Conference on Ionization Phenomena in Gases, Uppsola 1959, North-Holland Publishing Company, Amsterdam 1960, Vol. II, p. 1151.

12. O. K. Mawardi, M. N. Naraghi and R. B. Block, Bull. Amer. Phys. Soc. 7, 159 (1962).

13. T. H. Jensen, H. G. Voorhies, and F. R. Scott, Bull. Amer. Phys. Soc. 7, 141 (1962).

14. H. G. Voorhies, T. H. Jensen and F. R. Scott, Bull Amer. Phys. Soc. 7, 142 (1962).

15. T. H. Jensen and H. G. Voorhies, General Atomic Report #GA 2867.

16. W. Bieger, D. Dorn, D. Knoll and H. Tuczek, Bull Amer. Phys. Soc. 7, 142 (1962).

17. Ralph Waniek, Heinz Fischer and K. Park, Bull. Amer. Phys. Soc. 6, 196 (1961).

18. Ralph Waniek, Heinz Fischer and Sang Lee, Phys. Fluids 4, 928 (1961).

19. C. Leloup, J. P. Poffe, D. Veron and F. Wallbroeck, Bull. Amer. Phys. Soc. 6, 187 (1961).

20. D. R. Wells, Bull. Amer. Phys. Soc. 7, 292 (1962).

PRODUCTION OF LABORATORY PLASMAS

by

Francis F. Chen

To do experimental research in plasma physics, one needs a source of plasma. This source should be accessible and not be located in outer space, and hence we are concerned with the ways of producing a plasma in the laboratory. We shall, however, consider only those plasmas in which controlled experiments in a fairly well known environment can be done, and not those plasmas, of the type often encountered in thermonuclear research, in which the main interest is the production and analysis of the plasma itself. Our point of view, then, is that of an experimentalist seeking the easiest way to construct a laboratory plasma generator of a versatile nature, that is, suitable for a number of experiments which he might have in mind. In order to be a little more definite, these experiments might have to do with, say, waves and resonances in a plasma or instabilities of a plasma.

The extent to which a given machine approaches the ideal one can be measured by criteria such as these:

1. Degree of ionization
2. Plasma density
3. Electron temperature
4. Ion temperature
5. Range of magnetic field

6. Physical size of plasma

7. Duration of plasma

8. Uniformity and reproducibility

9. Quiescence

10. Accessibility

11. Cost and ease of fabrication

12. Range of ion mass

These criteria will be discussed in relation to the requirements of different types of experiments. A number of devices will then be described in relation to these criteria.

A. Criteria

1. Degree of ionization. In a weakly ionized gas the motions of the charged particles is controlled by collisions with the neutral atoms. These collisions include inelastic collisions, which a) distort the electron velocity distribution and b) provide a large source of energy loss via radiative transitions. Thus a weakly ionized plasma is more complicated than a fully ionized gas, in which the only collisions which occur are Coulomb collisions between charged particles. If a magnetic field is used for confinement, it will operate more efficiently if there are fewer neutral atoms for charged particles to collide with. Unless one wishes to study the properties of the neutral atoms, it is in general desirable to have the degree of ionization as high as possible. How high this is

depends on the ratio of the collision frequency f_o against neutrals to the frequency f of the plasma phenomena under study. The plasma frequencies f_{pi} and f_{pe} are proportional to $n^{1/2}$, while f_o is proportional to n_o. If $\delta = n/n_o$ is the degree of ionization, then obviously f_p/f_o is maximized if δ is maximized. If δ must remain constant, then it is best to operate at low densities, since $f_p/f_o \propto n^{1/2}/n_o \propto \delta^{1/2}/n_o^{1/2}$. If magnetic field phenomena (e.g., ion cyclotron waves) are to be investigated, then the relevant cyclotron frequency must be compared with f_o. Since frequencies characteristic of electrons are very high because of their small mass, much higher neutral pressures (up to 1 mm) can be tolerated when studying electron phenomena than when studying ion phenomena (less than 1 μ). Finally, a convenient way to distinguish between a "weakly" ionized gas and a "highly" ionized gas is that in the former the conductivity is primarily limited by collisions with neutrals, whereas in the latter it is primarily limited by collisions between charged particles.

2. Plasma Density. The absolute value of the plasma density is important because it determines the Debye length $h = (kT_e/4\pi ne^2)^{1/2}$. If the density is so low that h is comparable to the dimensions of the discharge, then the gas is not really a plasma at all, since it cannot exhibit the quasi-neutrality characteristic of a plasma. Since the plasma frequencies are proportional to $n^{1/2}$, it is in general desirable to have n as high as possible in order to raise the frequency far above the neutral collision frequency (the neutral density being assumed fixed in this case) and above the rate at which the plasma as a whole is changing, if it is not strictly in steady state. However, above $n \cong 10^{14}$ experimentation

becomes cumbersome because few measurement techniques are available in this range.

3. Electron Temperature. The primary effect of the electron temperature is to determine the conductivity, since in a fully ionized gas $\sigma \sim T_e^{3/2}$. When neutral collisions are unimportant, it is the finite resistivity which causes damping of oscillations, and in those cases where resistive damping is an important effect to overcome (as in the generation of hydromagnetic waves), it is desirable to have a high electron temperature. The effects of finite temperature on dispersion relations for plasma waves can be studied only with high kT_e. On the other hand, a low temperature may be desirable if zero-temperature theories are to be verified.

4. Ion Temperature. There are comparatively few effects in basic plasma physics which depend critically on the ion temperature, and most experiments can be performed with cold ions. This is fortunate, since it is more difficult to achieve high kT_i than high kT_e. This is because the neutral pressure must be very low to prevent ions from losing energy rapidly through charge-exchange collisions with the neutrals, and because electrons can be heated merely by passing a current through the plasma, whereas ions cannot. One important effect of ion temperature is its influence on ion wave instabilities. If $kT_i << kT_e$, the drift velocity between the ion and electron distributions need be only $(kT_e/M)^{1/2}$ before ion wave instabilities develop. However, if $kT_i = kT_e$, the velocity must be much larger: $(kT_e/m)^{1/2}$. Thus a plasma with $kT_i << kT_e$ is much more likely to be unstable and to exhibit oscillations.

5. Range of Magnetic Field. For investigations connected with cyclotron frequencies, hydromagnetic effects, transverse diffusion, etc., it is desirable to be able to vary the magnetic field over a large range. At the low end, one is limited by the difficulty of maintaining high density, percentage ionization, and electron temperature without the aid of a strong magnetic field used for confinement. At the high end, one is limited by sheer economics. Although fields up to about 1 or 2 kG are easily achievable in the laboratory, fields in the 10-100 kG range are feasible only with much time and expense, particularly if a large volume is necessary. An ideal plasma machine would produce a plasma of the same characteristics over a large range of magnetic field. The uniformity of the field would also be important in precise experiments.

6. Physical Size. From the standpoint of the experiment, the size of the plasma is governed by the wavelengths involved and the size of the probes or other diagnostics which have to be used. From the standpoint of producing the plasma, the size is limited at the low end by the diffusion rate to the walls and at the high end by the cost, particularly of the magnetic field.

7. Duration of Plasma. In order to achieve high values of n, kT_e, and B, it is much easier to produce a plasma in pulses than steady-state. The power requirements for the magnetic field, for example, can be greatly reduced if the duty cycle can be much less than unity. However, measurements are much more difficult to make in a pulsed plasma, since time resolution is required, and there is always a problem of pickup of transients. As one example, a frequency analysis can easily be made in a steady plasma by means of conventional slow-

sweeping analyzers; this is, however, slow and tedious with a pulsed source. The ultimate limitation on the length of time the plasma must remain essentially constant is imposed by the relevant frequencies involved -- either the frequency of oscillation or the reciprocal of the exponentiation time of an instability. For electron phenomena, for which the frequencies may be in gigacycles, a microsecond would be a sufficient duration. For Alfven waves, acoustic waves, or other phenomena associated with ions, the frequencies are must lower -- perhaps as low as kilocycles -- and the plasma must remain steady for well over a millisecond.

8. Uniformity and Reproducibility. Since theories of uniform infinite plasmas are much easier to work out, an ideal plasma is everywhere uniform in n, kT_e, and kT_i. The density, however, must fall to zero at the wall of any finite system, so that there must be some macroscopic gradients. This point is covered under (6), the physical size of the plasma. In addition to this, however, there should not be microscopic structure in the plasma which would produce local non-uniformities. Moreover, the plasma should exhibit the same physical characteristics under identical operating conditions day after day, or pulse after pulse in the case of pulsed systems.

9. Quiescence. The existence of oscillations in plasmas has been recognized since the earliest days of the science of gas discharges. These oscillations occur even more readily in a magnetic field. Obviously in a study of plasma waves or instabilities it is desirable to use a plasma which has no oscillations to begin with. Such a quiescent plasma is almost impossible to

create. In only one instance, that of the cesium plasma, has quiescence been demonstrated, and in this case only for $kT_i = kT_e$. A criterion which might be used for quiescence is that the fluctuations in local potential be much less than the voltage equivalent of the electron temperature. This is because if a plasma is electrostatically unstable, one would expect the disturbances to grow until they are limited by non-linear effects which come in when $eV > kT_e$. One should note that apparent quiescence can be achieved if the neutral pressure is so high that oscillations are damped out; this, of course, would also defeat the purpose of most experiments. Finally, experiments with electrons are here again easier to do, because low frequency fluctuations in a plasma, which are the most common, would not necessarily affect phenomena at very high frequencies.

10. Accessibility. Not the least important criterion for a good plasma source is that it should be easily accessible to diagnostic equipment. When a magnetic field is used, therefore, the coils should have gaps between them and be large enough in diameter so that the vacuum chamber is accessible for the insertion of probes, pickup coils, microwave horns, spectroscopic windows, and other necessities of life, in directions both parallel and perpendicular to the axis of the discharge. It would also be extremely convenient if the vacuum chamber can be opened to air without a long delay before the vacuum is regained.

11. Cost and Ease of Fabrication. This requires no comment other than that this consideration may occasionally be of importance.

12. Range of Ion Mass. The gases in which the discharge will operate will determine the variation possible in the value of M.

B. Devices

A single device which would be ideal for all experiments is of course not possible. We can, however, list a number of devices which one might consider for a laboratory plasma source and discuss how each one performs relative to the above criteria. A detailed description of each type of machine would be out of the scope of this lecture, but as an example we shall give later such a treatment of one device, the reflex arc, with which we have had some experience in this Laboratory.

The devices to be discussed are as follows, in more or less historical order:

1. Positive column
2. Mercury arc
3. R.F. and microwave discharges
4. Shock tube
5. Reflex discharges
6. Hollow cathode discharge
7. Cesium plasma
8. "Hot house" discharge
9. Deuterium, lithium, and carbon arcs
10. Mirror machine
11. Stellarator afterglow.

1. Positive Column. Perhaps the earliest known form of plasma is the positive column of a glow discharge between two cold electrodes. The structure

of such a discharge is complicated near the cathode, but sufficiently far away, in the positive column, a fairly uniform, weakly ionized plasma is obtained. This is perhaps still the easiest way to create a plasma. In the positive column a balance is achieved between loss of plasma radially to the walls and ionization produced by electron-neutral collisions. The energy is supplied by a longitudinal current driven by an electric field which is fairly constant along the length of the column. If sufficient voltage is applied between the anode and the cathode, there is essentially no restriction on the maximum length of the column. A typical diameter is 1 cm, and lengths over 3 meters have been obtained.

The degree of ionization is very small, of the order of 10^{-6}. The range of pressures for this type of discharge is from 0.1 mm to hundreds of mm. The maximum current is of order 10 amps/cm^2, and the maximum density of order 10^{10}. Electron temperature is in the range 1-4 ev, depending on the ionization potential of the gas; kT_e decreases with increasing pressure and radius. The ions are generally in thermal equilibrium with the neutral gas at several hundred degrees K. A longitudinal magnetic field decreases the radial diffusion and therefore decreases the electric field necessary to sustain the discharge. If a field larger than a few hundred gauss is used, however, the column becomes unstable and develops a helical distortion. Striations are also known to occur, causing non-uniformities in density. In order to avoid these it is necessary to operate at high pressure and high current. Accessibility is good. A number of different gases can be used. Operation is steady-state. The plasma is pseudo-quiescent because of the high neutral pressure. This also limits the usefulness

to hi low-frequency experiments unless the characteristics of a weakly ionized plasma are themselves of interest.

2. Mercury Arc. The low pressure mercury arc was used by Langmuir in his experiments and is still perhaps the most commonly used plasma generator. This differs from the glow discharge in that an externally heated cathode is used to supply the electrons. Since secondary emission by ion bombardment is unnecessary, the voltage required is reduced from hundreds of volts to tens of volts. Another consequence of a thermionic electron supply is that the pressure range is extended to much lower pressures, of the order of 10^{-4}, 10^{-5}, or even 10^{-6} mm. The normal operating pressure is around 1 μ, as opposed to 1 mm for the glow discharge. There is sufficient scattering of electrons that the discharge usually fills the entire glass chamber regardless of the positions of the cathode and anode and the size and shape of the vessel. Far from the cathode the electron distribution is Maxwellian even at low pressures.

The electron temperature is again of the order 1-4 ev. Ion energies are difficult to measure but kT_i should be somewhat above the gas temperature. Currents of several amperes/cm^2 can be drawn, and the maximum density is of the order $10^{11} - 10^{12}$ cm^{-3}. The percentage ionization thus could be several per cent, much higher than in the positive column. The price one pays is that neutral damping of natural oscillations does not prevent these from occurring, and the arc is in general not quiescent. Magnetic fields and grids have been used to minimize the fluctuations, but they are always present. These are at low frequencies (below 10 mc), so that again very high-frequency experiments

are possible, but low-frequency experiments are complicated by the natural oscillations.

Advantages of the mercury arc are its simplicity, reproducibility, accessibility, range of B (down to zero), range of size and shape, and steady-state operation. Other masses may be used, but the discharge has not been studied as thoroughly as for mercury.

3. R.F. and Microwave Discharges. A plasma can be produced in a vacuum chamber with or without electrodes by means of an externally imposed oscillating electric or magnetic field. This may be an ac electric field between two parallel plates, for instance, or an ac magnetic field produced by windings around an electrodeless toroidal tube. At microwave frequencies a gas can be ionized in a microwave cavity. The mechanism of production depends on the pressure and the imposed frequency. At high pressures and low frequencies the discharge is merely a succession of glow discharges in opposite directions. At very high frequencies electrons are driven back and forth by the field without hitting the wall. Ionization is produced by electrons colliding with neutrals in the course of this oscillation. At r.f. frequencies and low pressures, when both the mean free path and the excursion during an oscillation are large compared with the size of the chamber, ionization is produced mainly at the wall. This is not an interesting case because the plasma then depends on the state of the wall surface. At higher pressures, the discharge starts the same way, but ions which accumulate in the center of the chamber because of their inertia provide a space charge which prevents the electrons from hitting the wall. Thus once

the discharge is started ionization is produced only in the gas.

The density that can be achieved depends on the power input to the plasma. Obviously it is easier to get large power at r.f. frequencies than at microwave frequencies. Percentage ionization is fairly low. For example, a large r.f. generator capable of putting 1000 volts across the plasma at 16 mc can give a density of perhaps 3×10^{10} cm^{-3} at a few microns pressure. Below this pressure collisions with the walls become important. At higher pressures, e.g., 10 mm, correspondingly higher densities can be achieved (e.g., 10^{12}).

The electron temperature is again in the 1-4 ev range, and the ions are essentially cold. The discharge is produced uniformly and without dc current, and so is likely to be quiescent. There is a macroscopic density gradient determined by diffusion to the walls. While the r.f. voltage is on, there are large signals which can interfere with measurements, but the frequency can be chosen out of the range of that of the measurements. The r.f. can also be turned off before the measurements; this has the advantage over other decaying plasmas in that the original plasma was created uniformly. An arbitrary magnetic field and gas can be used. The main disadvantages are the low ionization and the high power required, often necessitating pulsed operation.

4. Shock Tube. A dense plasma can be obtained by using shock waves. An arbitrary gas is compressed behind a diaphragm. Upon rupture of the diaphragm, a shock front travels at a supersonic speed down a tube, producing ionization. This occurs only at relatively high initial pressure (1-10 mm), and the pressure behind the shock is about ten times higher. The ion density is of

order 10^{16}-10^{17} cm^{-3}, giving about 10% ionization. Because of the high densities, the electrons, ions, and neutrals are all in thermal equilibrium at 1 to 1.5 ev. Decay time of the plasma is of order 100 μsec. Shock tubes have been used primarily for excitation of neutrals and spectroscopic studies of their radiation. Plasma and magnetic field phenomena are damped by the very high neutral density. Pulsed operation is necessary, and the duty cycle is extremely small. Magnetically driven shocks can produce better plasmas, but these high-powered devices fall outside the scope of this review.

5. Reflex Discharge. The prototype of this is the Philips Ionization Gauge, which employs a magnetic field to confine electrons radially. The geometry is shown schematically in Fig. 1.

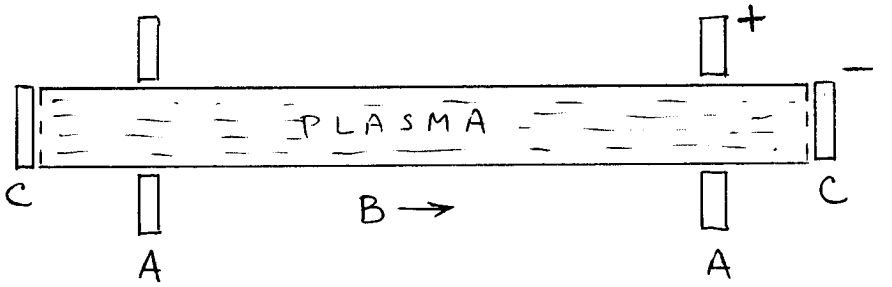

FIG. 1

Electrons emitted by the cathodes are trapped longitudinally by the potential well of the anodes and radially by the electric field. Ions are allowed to flow to the cathodes but travel slowly because of their mass. Higher ionization can be achieved for a given pressure in this geometry than in a straight arc because the electrons can travel many times from cathode to cathode and therefore have

a path length through the gas many times the actual length of the discharge. With this general geometry a number of quite different devices have been invented. Qualitative differences in behavior can occur if one changes the operating pressure, the magnetic field strength, the size of the apparatus, the voltage applied, the anode diameter, and particularly the emission characteristics of the cathode. Two disadvantages common to all these variations are the susceptibility to low frequency oscillations and the need for a minimal magnetic field (about 100 gauss) to confine the electrons.

a) Cold cathodes. Since electrons are emitted by secondary emission from ion bombardment, a large voltage of the order of 1000 v is usually necessary. The discharge is not reproducible over long times because the state of the cathode surface changes. High densities (up to 10^{14} cm^{-3}) can be obtained at moderate currents (0.1 amp/cm^2), but high pressures are required ($\sim$100 μ). The discharge can be made quite large (e.g., 3" dia. x 6' long) with essentially constant plasma conditions throughout; however, the plasma is unstable and has large local fluctuations. At intermediate pressures (10-100 μ), macroscopic instabilities develop. At low pressures ($\sim$1 μ), the density is low ($\sim 10^{10}$ cm^{-3}) but the plasma is more quiescent, although coherent oscillations can be observed between the cathode and anode. Quiescence also occurs even at high pressures if the magnetic field is low enough ($\lesssim$ 200 gauss). Electron temperatures are of the order of 10 ev; ion temperatures are slightly above the gas temperature. Operation can be steady-state. A number of gases can be used. Accessibility is good and construction fairly easy. The main disadvantages are lack of quiescence,

high neutral density, and lack of long-term reproducibility.

b) Hot cathodes. If an emitter is substituted for at least one of the cathodes, an arc is formed; and the voltage is lowered to the order of 70 volts. Operation at lower pressures becomes possible (1-10 μ). Densities are of order 10^{12} to 10^{13} at 1 amp/cm^2, and electron temperatures of order 3-8 volts. Thus the degree of ionization is a few per cent, much higher than with cold cathodes. A large range in size and magnetic field can be covered. Accessibility is good, and the discharge is reproducible and operates in steady-state. Construction is a little more difficult because of the need for externally heated cathodes. The plasma is more quiescent than in the cold cathode case, but still there are low frequency oscillations. At low magnetic fields most of the gradients (in potential, density, temperature) are along the axis; at high fields they are radial. The radius is limited at high fields since the discharge is concentrated mainly near the anodes because of the difficulty of transverse diffusion.

c) The Neidigh arc. A particular modification of the hot cathode reflex discharge has been studied at Oak Ridge. This has the geometry shown in Fig. 2.

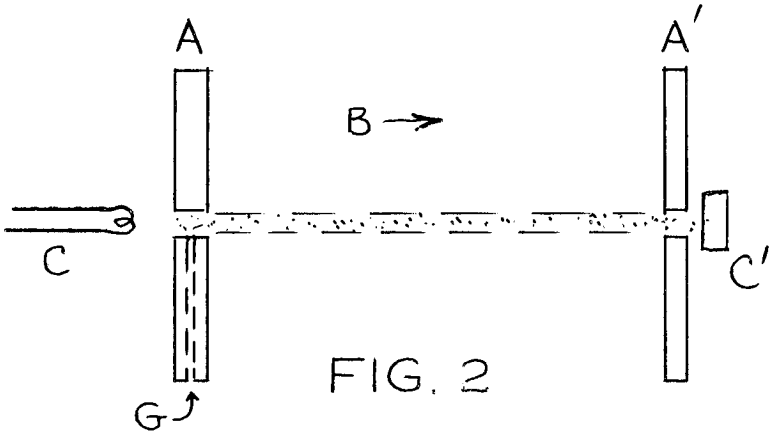

FIG. 2

A small filament forms the cathode, which is biased about -150 volts relative to the large anode plates, and the anti-cathode C' is left floating. At uniform pressures around 1μ, the operation is essentially as described in the previous paragraph, except that the plasma of interest is not that in the main arc but that which has drifted out to the space between the anodes. The electron temperature is apparently about 20 ev. It is conjectured that the ionization is less than 10% here, as compared to over 50% inside the arc. If the gas is introduced through the anode A by a small pipe G, and the pressure in the main chamber is reduced to 10^{-5} mm by fast pumping, a different mode of operation occurs. The arc column becomes diffuse and non-uniform axially, and very energetic ions (several hundred ev) appear in the exterior region. This modification has the advantages of high ion temperature (if the ions are thermalized) and low neutral density, but has the serious disadvantage that the plasma is asymmetric and unstable.

d) The P-4 arc. Another special manifestation of the reflex principle is a large device used at UCRL-Livermore. This has the geometry shown in Fig. 3.

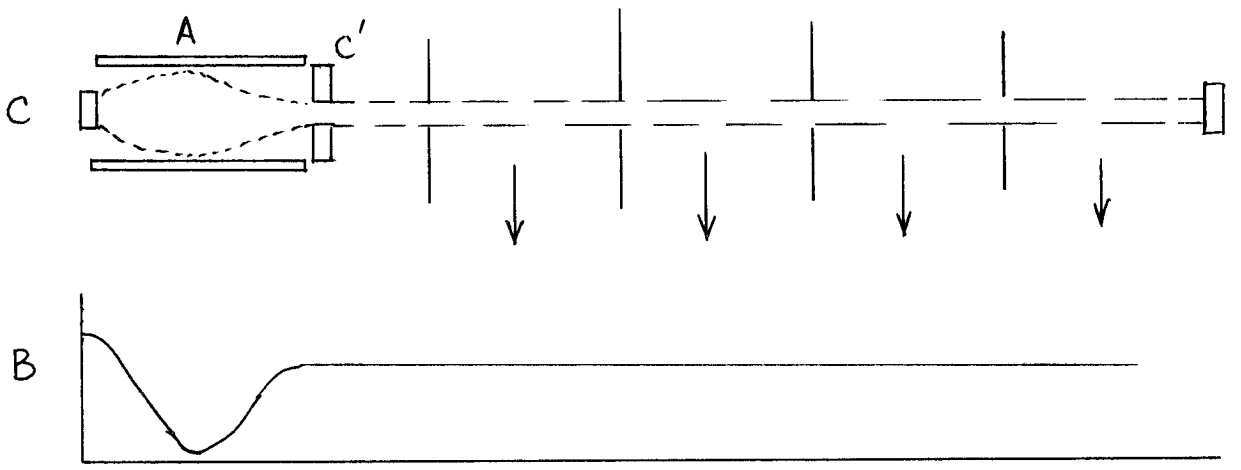

FIG. 3

A solid tungsten cathode, heated by the discharge, is used. The opposite cathode has a large hole, through which the plasma streams out of the discharge region into a long (20') differentially pumped chamber. In this region the neutrals are removed to a pressure of order 10^{-5} mm. Since the plasma density is of order 2×10^{13}, ionization is almost 100%. A magnetic mirror is used in the reflex region to help confine the electrons axially, since the large hole in the cathode diminishes the electrostatic repulsion. In the weak field region the field is actually too weak to confine the plasma radially; the exact mechanism of the discharge is unknown. Its operation depends critically on the adjustment of the field shape in the source region. In the experimental region the field is of order 1000 gauss. Electron temperatures are of order of tens of ev, and ion temperatures of order 8 ev. The diameter is about 1". Thus this device produces a fairly large, highly ionized, dense, hot plasma in steady state. Uniformity and accessibility are good. Disadvantages are its large cost and need for critical adjustment.

e) Rotating plasmas. If the anode inside diameter is made large compared to the cathode diameter and a large pulsed voltage is applied, the plasma drifting outside the reflex discharge is driven into a rapid rotation by the radial electric field crossed with the longitudinal magnetic field. Such devices fall under the category of plasma sources being studied for their own sake and are not generally useful for controlled experimentation.

6. Hollow Cathode Discharge. This source, used largely at M. I. T., combines some of the features of the mercury arc and the Neidigh arc. The geometry

is shown in Fig. 4.

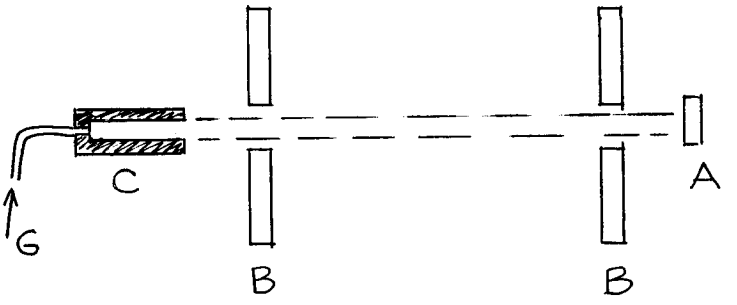

FIG. 4

This is not a reflex arc, so that operation with or without a magnetic field is possible. The cathode is a hollow rod of tantalum or tungsten, heated to emission by the arc itself. Thus large current densities are necessary ($\sim$10-1000 amps/cm^2). The gas feed is through the cathode, and most of the ionization occurs in the high pressure region inside the cathode. By fast pumping the pressure in the main chamber is reduced to the order of 10^{-3}. Since the plasma density is of order 10^{13}-10^{14}, the percentage ionization is 25-75%. The electron temperature is of order 2 ev. So far the diameter has been restricted to 1/2" or less, and it is the plasma outside the main arc that is likely to be quiescent and therefore useful. A number of gases can be used. Operation is restricted to steady-state since the cathode is self-heated. Reproducibility and accessibility are good, and construction is fairly easy. Uniformity in the exterior region is necessarily limited by the radial gradient but may be sufficient for most purposes.

7. Cesium Plasma. This is the only known quiescent plasma. It is achieved without electric fields by thermal ionization of cesium or potassium on hot tungsten plates. Since the work function of tungsten is greater than the ionization potential, neutral atoms become ionized upon contact with the metal. Electrons are injected into the plasma by thermionic emission by the same plates. This device will be described in detail in another lecture.

The densities attainable range up to 10^{12} or 10^{13} cm^{-3}, and ionization is almost 100%. The electron and ion temperatures are approximately equal to the temperature of the tungsten plates, about 0.2 ev. A magnetic field is used for confinement, and in the particular device used here in Princeton the minimum field is 1000 gauss. Operation is necessarily steady-state. Reproducibility is only fair. Uniformity is good. Accessibility and ease of construction are poor. There is no restriction on size. Ion masses are restricted to the elements with the proper ionization potentials, mainly cesium and potassium. Aside from the complexity of the device, the main disadvantage is that the temperatures are low and equal. Thus the resistivity is high even though there are few neutrals. This limits the range of experiments that can be performed. The electrons can be heated to a few volts by passing a current through the plasma, but then it is no longer quiescent. Much work has been done on the instabilities that develop when such a current is imposed.

8. "Hot house" Discharge. This is a pulsed discharge used at Berkeley to produce a high density, large diameter plasma. The geometry is shown in Fig. 5.

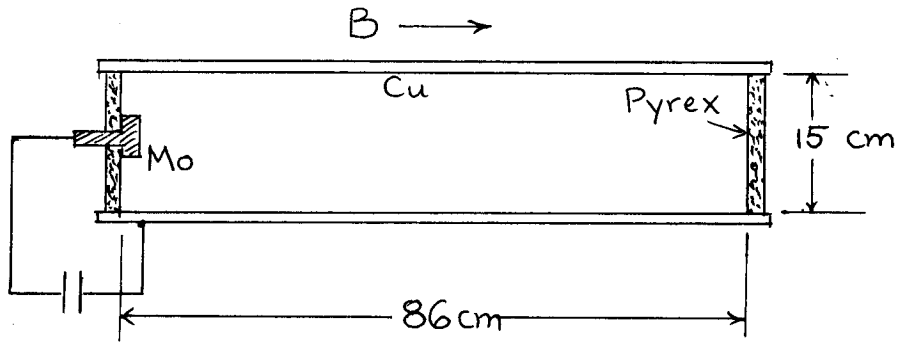

FIG. 5

A 10 kv pulse is applied between the central button and the copper chamber wall. A rotating shock front then proceeds down the tube. The exciting voltage is removed when the front reaches the other end. The plasma left behind is apparently uniform and decays with a time constant of the order of 200 μs, long enough for many experiments. The main feature of this plasma is its high density, 6×10^{15} cm^{-3}, obtained at a pressure of 100 μ of H_2. Ionization is above 90%. Ion temperature is about 1 ev. The range of magnetic fields successfully used is 7-20 kg. The pressure can be reduced to 1 μ, but the composition is less pure. Pulse to pulse reproducibility is fair. Accessibility is good. Other gases may be used. Aside from its limitation to pulsed operation, the main disadvantage is that the density cannot be arbitrarily reduced. In the 10^{15} cm^{-3} range the only density measurement available is by Stark broadening.

9. Deuterium, Lithium, and Carbon Arcs. Intense, high current arcs have been extensively used at Oak Ridge for plasma production. From our point of view, perhaps the most interesting is the deuterium arc. This has the

geometry shown in Fig. 6.

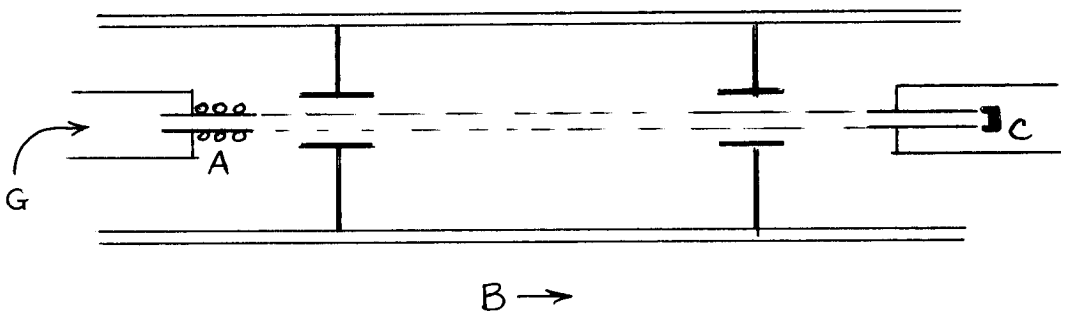

FIG. 6

The cathode is tungsten, heated by the arc itself, and the anode is a water-cooled copper tube 1" in diameter. In contrast to the hollow cathode discharge, the gas is fed into the anode, and most of it is ionized there. Large pumps and baffles remove neutrals from the two ends, reducing the neutral pressure in the central chamber to 5×10^{-5} mm. The arc is hollow, the density being highest near the outside of a 1" dia. cross-section; the density is about 2×10^{14} cm^{-3}. At 150 amps and 90 v, the arc produces an electron temperature of order 40 ev and an ion temperature of 16 ev. There is a relative drift of ions and electrons which may cause instabilities; however, the quiescence has not been thoroughly studied. A magnetic field of about 7 kG is used for confinement. This arc produces a very pure plasma of a light element, with high density and high temperatures. It is, however, quite difficult to construct, and accessibility is only fair. It is limited to dc operation. The main disadvantages are the small region of uniformity and lack of control over the range of densities and temperatures.

An arc using lithium has been built at Oak Ridge, in which the plasma is

allowed to stream behind a hollow cathode. The density in this stream is of order 10^{11}, at $kT_e \sim 10$ to 20 ev. Arcs in carbon vapor from carbon electrodes have also been studied extensively but are not used for pure experiments. These give ion temperatures of order 100 ev at currents of order 200 amps.

10. Mirror Machine. Although primarily used for producing hot ions for thermonuclear reactions, this device has been found to be quite stable and hence may be of interest from the point of view of basic experiments. Hot electrons are injected by deuterium-loaded titanium sources developed at UCRL-Livermore. Impurities from the source can be discriminated against by time of flight. The plasma is of density $\sim 10^{11}$-10^{12} cm^{-3} and electron temperature ~ 10 ev. Once injected into the mirror, the plasma is confined by it and decays with a time-constant of order 10 ms. Such stability occurs only for certain special operating conditions. The plasma can be heated up to 25 kev by magnetic compression, but this makes the machine costlier. Disadvantages are pulsed operation, non-uniform density, and anisotropic velocity distribution.

11. Stellarator. The stellarator is also primarily a device of thermonuclear interest, but it can provide two types of plasma useful for experimentation. The first is the plasma during ohmic heating, which has densities from 2×10^{12} to 2×10^{13} cm^{-3} and temperatures of 5-25 ev. The density decays due to "pumpout", but the characteristic times are quite long: up to 5 ms. Advantages are the extreme purity of the plasma, the large size (10^5 cm^3), and the uniform magnetic field in the straight sections. Disadvantages are primarily the large cost and difficult accessibility. A second type of plasma has been

produced by Stodiek by passing a very small current (amounting to only a few watts of heating) through the plasma during the afterglow. This current maintains a constant temperature of 0.2 to 2 ev, sufficient to prevent fast recombination. The plasma, of density 2×10^{11} to 2×10^{12} cm^{-3}, is about 80% ionized. Although there is no ohmic heating current, the plasma is still unstable and exhibits "pumpout"; however, the confinement time is long -- of order 10 ms.

ADDENDUM

Since these notes were written in early 1962, a number of new methods of plasma production have appeared in the literature.

12. Modified Mercury Arcs. A common form of the mercury arc employs a pool of mercury as the cathode; electron emission then occurs from a hot cathode spot on the surface of the mercury pool. The advantage of this method is that the cathode is virtually indestructible and can supply currents of up to 100 amps. Allen and Magistrelli have been able to use this type of cathode for other gases, such as helium, as well. Their discharge tube is shown in Fig. 7.

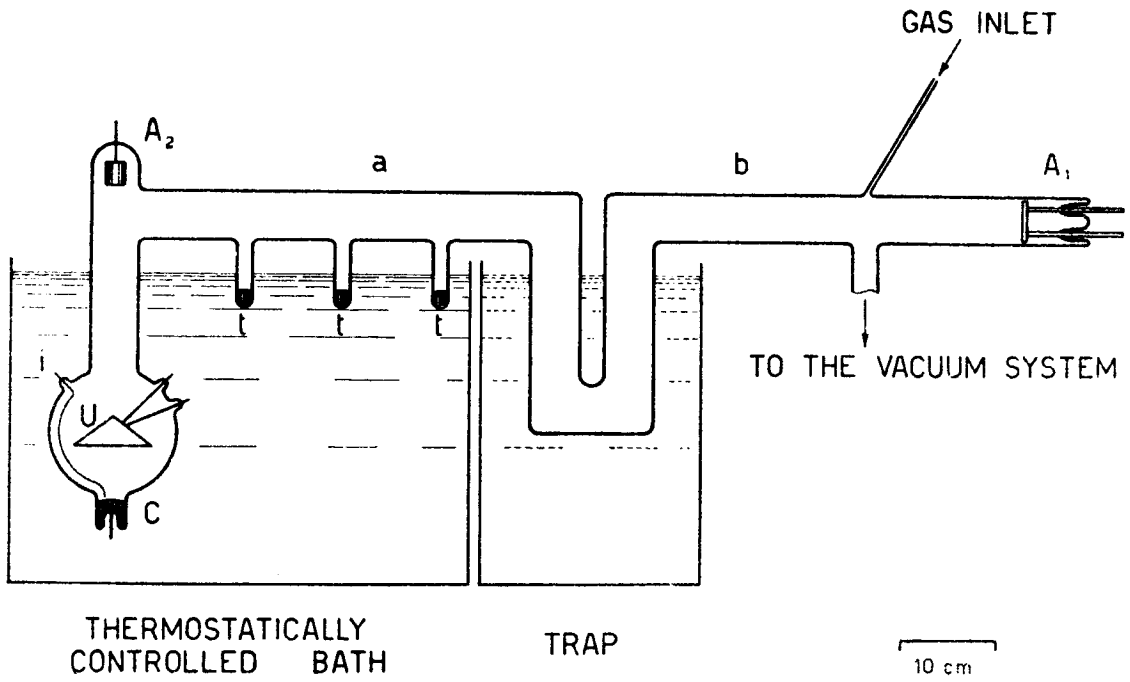

Fig. 7

C is the mercury pool cathode, U an umbrella for diverting the direct stream of electrons, i an igniter, A_1 and A_2 the primary and auxiliary electrodes, and t additional pools of mercury for controlling the pressure. Without the large U-bend, the tube would be a conventional one. In the U-bend, the mercury vapor is condensed out in a dry-ice trap. The electrons diffuse into the right-hand region, where they ionize the input gas. In this manner, a spectroscopically pure helium discharge has been obtained.

A back-diffusion mercury arc has been used by Ikegami, Takayama, et al, to produce a quiescent, low-density plasma. Their apparatus is shown in Fig. 8.

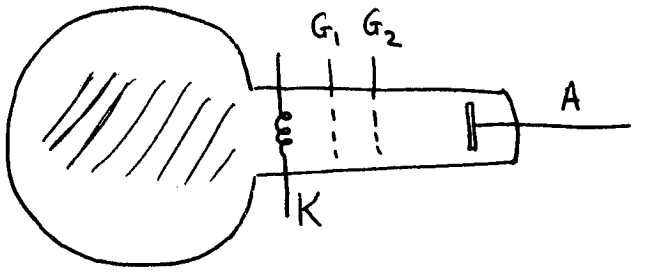

Fig. 8

A plasma of density 10^5-10^6 cm^{-3} and electron temperature $\lesssim 0.2$ ev in 0.2 to 2 microns of Hg reaches the glass bulb by diffusing through the hot-filament cathode K. By means of grids G_1 and G_2 it is possible to bring the noise level down to thermal levels and to vary n without varying kT_e or the plasma potential.

13. Lithium Arc. Results by Fumelli on a reflex discharge in lithium vapor at around 2000 gauss show that an almost fully ionized plasma can be

obtained, with densities of 10^{12}-10^{13} cm^{-3} and kT_e's of 1-10 ev. Since lithium is a solid at room temperature, the entire vacuum chamber acts as a pump to remove the neutrals, which are introduced at the hot cathode. Neutral pressures are in the 10^{-7} torr range. However, the plasma shows the low-frequency oscillations that plague reflex discharges. Recently Li^{+++} has been observed with a mass spectrometer.

14. High-Current Discharge. For the observation of hydromagnetic waves a large diameter, highly conducting, dense plasma is necessary. Jephcott has successfully employed a straight discharge between stainless steel plates, as shown in Fig. 9.

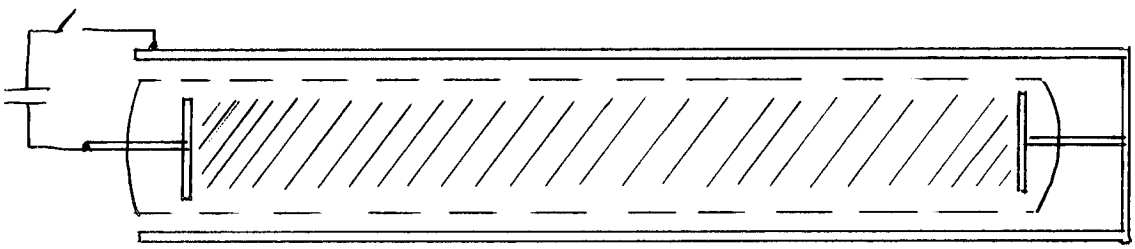

Fig. 9

The quartz vacuum chamber was 10 cm in diameter by 200 cm long, and there was a pulsed confining field of 16 kilogauss. By discharging a condenser bank through 50 μ of argon or neon at a peak current of 12 kA, a plasma of density 10^{15} cm^{-3}, electron temperature 2 ev, and ion temperature 1.7 ev could be produced. The plasma was apparently free from gross non-uniformities and

asymmetries in spite of the presence of a large current. Experiments were performed during the 10-20 μsec when B and I were constant to 0.01%. The magnetic field was high enough that little pinching occurred at this current. The main disadvantage, aside from the short duration of the plasma, is the lack of complete ionization. Although the percentage ionization is around 50%, this is not so high that ion-neutral collisions can be neglected in an Alfvén wave experiment.

15. Cyclotron Resonance. It is possible to create a plasma in a microwave cavity by injecting a high-powered burst of microwaves at the electron cyclotron frequency. The electrons are trapped by magnetic mirrors. Using 5 kw at 11 Gc, Ard et al report densities up to 10^{12} at kT_e up to 80 kev, with a lifetime greater than 100 ms. These parameters are still open to some question. Hooke et al have created plasmas with $n = 10^{13}$ cm^{-3}, kT_i = 300 ev, kT_e = 10 ev by ion cyclotron resonance. Since megawatt powers are necessary, this is not a simple apparatus.

16. Beam-Plasma Discharge. When a high-current electron beam is injected into a gas, it can build up a hot plasma by first ionizing the atoms by collisions, and then interacting with the weak plasma formed to produce a catastrophic increase in ionization rate. The beam-plasma interaction occurs mainly near the electron plasma and cyclotron frequencies, but radiation at ionic frequencies has also been observed. This type of discharge is being studied at M.I.T. and at Oak Ridge. Alexeff et al report a plasma with $n = 4 \times 10^{11}$ and kT_e = 32 kev produced with a 5 kev beam. The plasma is

confined by magnetic mirrors. The detailed nature of the plasma is not yet known.

17. Duoplasmatron. A device called the "duoplasmatron" or "cabinet" has been used in Munich and at General Atomic for the study of diffusion. A plasma is formed by a sort of von Ardenne ion source and is injected along a uniform magnetic field. The density falls off radially with a characteristic distance of about a centimeter. At $p = 10^{-5}$ torr, peak density is 2×10^{10}, and kT_e and kT_i are around 12 and 10 ev, respectively. At $p = 10^{-3}$ torr, n is 5×10^{13}, and kT_e and kT_i are 1 and 0.1 ev, respectively. Radial electric fields exist in the plasma, and different types of oscillations are observed.

The performance of these devices is summarized in Table I. Operating conditions, of course, vary for any one type. The numbers and limits given are representative ones only.

TABLE I

Device	Fractional Ioniz.	n cm^{-3}	kT_e (ev)	kT_i (ev)	B (gauss)	Size	Duration (sec)	Unif. Reprod.	Quiescence	Accessibility	Gases	Cost
Positive column	10^{-6}	$0\text{-}10^{10}$	1-4	.03	0+	unlim.	dc	good	pseudo	good	many	low
Mercury arc	10^{-2}	$0\text{-}10^{12}$	1-4	.03	0+	unlim.	dc	good	fair	good	Hg, noble	low
R.F. + μwave disch.	10^{-3}	$0\text{-}10^{11}$	1-4	.03	0+	usually small	usually pulsed	good	good	fair	any	med.
Shock tube	10^{-1}	$<10^{17}$	1-1.5	1-1.5	0+	any	10^{-4}	fair	pseudo	fair	any	med.
Reflex disch. cold cath.	10^{-2}	$0\text{-}10^{14}$	10	.1(?)	> 100	any	dc	poor	poor	good	many	low
Reflex disch. hot cath.	10^{-1}	$0\text{-}10^{13}$	3-8	.1(?)	>100	< 2" dia.	dc	fair	fair	good	many	med.
Reflex disch. Neidigh	10^{-1}	10^{12}(?)	20(?)	$> 10^2$	$> 10^3$ (?)	small core	dc	poor	poor	fair	many	med.
Reflex disch. P-4	.95	$< 2 \times 10^{13}$	20(?)	< 8	10^3	1" dia.	dc	good	fair	good	mainly He	high
Hollow cath. disch.	.9	$\sim 10^{13}$	2	.1(?)	0+	small core	dc	fair	fair	good	many	med.
Cesium plasma	.99	$0\text{-}10^{12}$	0.2	0.2	$>10^3$	any	dc	fair	good	fair	Cs, K, Ba	high
"Hot house" disch.	.9	6×10^{15}	?	1	$\geq$7000	6" dia.	2×10^{-4}	fair	good(?)	good	many	high
Deuterium arc	.98	2×10^{14}	40	16	$\geq$7000	annular 1" dia.	dc	fair	fair(?)	poor(?)	D_2, Li	high
Hot electron mirror	.9 ?	$< 10^{12}$	10	?	>1000 (?)	any	10^{-2}	fair	good(?)	poor	D_2	high
Stellarator	.99	$< 3 \times 10^{13}$	20	20	$> 10^4$	large	10^{-3}	good	fair	v.poor	any	v.high

TABLE I (cont.)

Device	Fractional Ioniz.	n cm^{-3}	kT_e (ev)	kT_i (ev)	B (gauss)	Size	Duration (sec)	Unif. Reprod.	Quiescence	Acces-sibility	Gases	Cost
Stellarator afterglow	.8	10^{12}	1	1	$>10^4$	4" dia.	10^{-2}	good	fair	v. poor	any	v.high
Backstream-ing arc	10^{-7}	10^6	.2	.1?	0	small	dc	good	good	good	Hg	low
Lithium arc	.99	6×10^{12}	1-10?	?	2000	large	dc	fair	poor	good	Li	high
Hi-current discharge	.5	10^{15}	2	1.7	16K	large	10^{-4}	fair?	good?	fair	A,Ne	high
El. cyclotron resonance	.9?	10^{12}	80K	?	4K	med.	10^{-1}	?	?	poor	any	high
Ion cyclotron resonance	.99	$>10^{13}$	10	300	20K	med.	10^{-4}	good	good	poor	H_2	high
Beam-plasma	.9?	10^{12}	>20K	?	>1K	small-med.	dc	poor	poor?	good	any	med.
Duoplasma-tron	<.5	10^{13}	1	.1	.7-4K	small core	dc	?	poor?	good	any?	med.

BIBLIOGRAPHY

1. Glow discharge

Gordon Francis, Handbuch der Physik, Vol. 22, p. 53 ff (Springer-Verlag, Berlin, 1956).

2. Mercury arc

Irving Langmuir, Collected Works (ed. by C. G. Suits), Vol. 4 (Pergamon Press, Oxford, 1961).

3. R.F. and microwave discharges

Gordon Francis, Ionization Phenomena in Gases, Chap. 4 (Butterworths Scientific Publications, London, 1960).

4. Shock tubes

R. A. Alpher and D. R. White, Phys. Fluids 2, 153 (1959).

O. Laporte and T. D. Wilkerson, J. Opt. Soc. Am. 50, 1293 (1960).

5. Reflex discharges

a) J. Backus, J. Appl. Phys. 30, 1866 (1959), and 31, 400 (1960).

R. L. Jepsen, J. Appl. Phys. 32, 2619 (1961); Proc. I.R.E. 49, 1920 (1961).

b) F. F. Chen, R. Bingham, and W. L. Harries, Phys. Rev. Letters 8, 234 (1962), and Princeton Plasma Physics Laboratory Rpt. MATT-63.

Consoli, Geller, and LeGardeur, Proc. Munich Conf. on Ionization Phenomena in Gases, 1961.

Salz, Meyerand, Lary, and Walch, Phys. Rev. Letters 6, 523 (1961).

c) R. V. Neidigh and C. H. Weaver, Proc. 2nd U. N. Conf. on Peaceful Uses of Atomic Energy, Geneva 1958, Vol. 31, 315; also Oak Ridge Natl. Lab. Rpt. No. ORNL-1890 (1955).

d) Gardner, Barr, Gall, Hall, Kelly, and Oleson, Univ. of Calif. Rad. Lab. Rpt. No. UCRL-5904 (1960).

6. Hollow cathode discharge

Lidsky, Rothieder, Rose, Yoshikawa, Michelson, and Mackin, J. Appl. Phys. 33, 2490 (1962).

7. Cesium plasma

N. Rynn, Rev. Sci. Instr., 35, 40 (1964).

M. A. Allen and G. S. Kino, Phys. Rev. Letters 4, 163 (1961).

Wada and Knechtli, Proc. IRE, 49, 1926 (1961).

8. "Hot House" discharge

Wilcox, Baker, Boley, Cooper, de Silva, and Spillman, J. Nuclear Energy, Pt. C, 5, 337 (1962).

9. Deuterium and carbon arcs

Gibbons and Mackin, Proc. 5th Intl. Conf. on Ioniz. Phenomena in Gases, Munich (1961).

10. Mirror machine

Post, Ellis, Ford, and Rosenbluth, Phys. Rev. Letters 4, 166 (1960).

Perkins and Post, Phys. Fluids 6, 1537 (1963).

11. Stellarator

PPL Annual Report, MATT-Q-21 (1964).

12. Modified mercury arcs

J. E. Allen and F. Magistrelli, Nature 194, 1167 (1962).

Ikegami and Takayama, Inst. of Plasma Physics (Nagoya), Report IPPJ-10 (1963).

Uramoto, Fujita, Ikegami, and Takayama, IPPJ-19 (1963).

13. Lithium arc

M. Fumelli, Euratom-CEA (Fontenay-aux-Roses, France), Report EUR-CEA-FC-155 (1962).

14. High-current discharge

Jephcott and Stocker, J. Fluid Mech. 13, 587 (1962).

15. Cyclotron resonance

Ard, Becker, Dandl, Eason, England, and Kerr, Phys. Rev. Letters 10, 87 (1963)

Hooke, Tenney, Brennan, Hill, and Stix, Phys. Fluids 4, 1576 (1961).

16. Beam-plasma discharge

Alexeff, Neidigh, Peed, Shipley, and Harris, Phys. Rev. Letters 10, 273 (1963).

Getty and Smullin, J. Appl. Phys. 34, 3421 (1963).

17. Duoplasmatron

Boeschoten and Schwirzke, Nucl. Fusion 2, 54 (1962).

PLASMA PHYSICS VACUUM TECHNIQUES

by

Gerhard Lewin and Edward G. Apgar

Introduction

The next three lectures deal with the vacuum techniques which are used in plasma physics. The purpose of the vacuum technique is to provide the proper environment for plasmas. This need arises mainly in the following cases:

(1) Classical gas discharges and alkali-metal vapor converters;

(2) Investigation of rocket propulsion in the laboratory;

(3) Thermonuclear research.

In general, the first employs techniques which have been known for many years. They are used in the development and manufacture of gas discharge and other electronic tubes. The second constitutes a special case of the outer space simulation chambers. Large amounts of gas or vapor have to be removed at a moderately high vacuum. The third case requires different arrangements depending on the particular experimental approach. In view of the diversity of the requirements, we are going to present a general treatment of vacuum technique with emphasis on more recent developments and plasma applications.

To convey a feeling for vacuum conditions, Table I gives some gas-kinetic data for nitrogen. Column 1 is the pressure in torr for typical vacua. (The torr is now commonly used and is equal to mm Hg.) Column 3 is the cor-

responding mean free path. Column 5 shows that, in ultra-high vacuum only, the time required to form a monolayer is large compared to the average time spent in conducting an experiment. Therefore, ultra-high vacuum is required whenever clean surfaces are needed. But, generally, even in ultra-high vacuum a surface is covered with gas unless this gas is removed by a cleaning process. As the gas is pumped out of the volume of the container, the gas adsorbed on the wall becomes of increasing importance. If a monolayer were suddenly released from the wall of a tube of one cm diameter, the pressure would rise 10^{-1} torr.

Table I

Gas-Kinetic Data for Nitrogen

	1 Pressure (torr)	2 Molecules (cm^3)	3 Mean Free Path (cm)	4 Molecules incident on cm^2/sec	5 Time to Form Monolayer (sec)
Atmospheric Pressure	760	2.6×10^{19}	7×10^{-6}	2.3×10^{23}	4×10^{-9}
Vacuum Pressure	1	3.6×10^{16}	5×10^{-3}	3×10^{20}	3×10^{-6}
High Vacuum Pressure	10^{-6}	3.6×10^{10}	5000	3×10^{14}	3
Ultra-High Vacuum Pressure	10^{-10}	3.6×10^{6}	5×10^{7}	3×10^{10}	2.88×10^{4}

Kinetic Theory of Gases (Gerhard Lewin)

We shall discuss only those aspects of the kinetic theory of gases which are of importance in vacuum work and will present pertinent equations without derivations. The equation of state for an ideal gas is

$$PV = NkT \tag{1}$$

where

P = pressure

V = volume

T = absolute temperature (^{o}K)

N = total number of molecules

k = Boltzmann constant = 1.37×10^{-16} erg/^{o}K or 10^{-19} torr $cm^3/^{o}K$.

At the low densities with which we are concerned, the real gases behave like the ideal gas.

The number of molecules incident on the unit area per second is

$$\nu = \frac{1}{4} n v_a \tag{2}$$

where

n is the number of molecules in unit volume,

v_a is the average velocity of a molecule.

$$v_a = \left(\frac{8kT}{\pi m}\right)^{1/2} = 14551 \left(\frac{T}{M}\right)^{1/2} \quad \text{cm sec}^{-1} \tag{3}$$

where

m = mass of a molecule

M = molecular weight.

The mean free path of a molecule is

$$\lambda = \frac{1}{\pi n r^2} = \frac{kT}{\pi P r^2 \sqrt{2}} \tag{4}$$

where r is the gas-kinetic radius of a molecule.

$$\lambda_{(\text{nitrogen})} = \frac{5 \times 10^{-3}}{P_{\text{torr}}} \quad \text{cm} \quad .$$

At high pressures, heat is conducted away by convection. As the pressure is decreased, macroscopic motion of the gas ceases and molecular conduction takes over. The thermal conductivity is

$$K \cong \eta c_v \tag{5}$$

where η is the viscosity and c_v is the heat capacity per unit mass at constant volume.

$$\eta \cong 0.1 \frac{m v_a}{r^2} \quad . \tag{6}$$

It is interesting to note that the viscosity and heat conductivity are independent of pressure. This result was one of the early triumphs of the kinetic theory of gases.

When the number of collisions with the wall is large compared to the number of collisions between molecules, we have the condition of molecular flow. In the ideal case, the molecules will not be specularly reflected. They will remain at the wall a short time. Upon leaving, all directions have equal probability and their energy corresponds to the temperature of the wall. It can usually be assumed with good approximation that the reflection of common surfaces is diffuse; but the heat transfer is not always perfect, hence the accommodation coefficient α has been introduced which gives the efficiency of heat transfer in a single wall collision. If T_i is temperature of the incident molecule,

T_w ($T_w > T_i$) is wall temperature and T is temperature of the leaving molecule,

$$\alpha = \frac{T - T_i}{T_w - T_i} \quad . \tag{7}$$

It varies for metals usually between 10% and 100% depending on the gas and the surface condition.

If a chamber with a high wall temperature is connected with a chamber of a lower temperature, a pressure difference will exist due to the temperature difference. If the diameter of the connecting tube is large compared to the mean free path, we have the condition of viscous flow; the pressure must be the same on both sides, and in view of (1), the densities will be inversely proportional to the temperatures. But in the molecular flow region, wall collisions predominate. Since in equilibrium equal numbers of molecules pass in either direction, the density is inversely proportional to the velocity or

$$\frac{P_2}{P_1} = \left(\frac{T_2}{T_1}\right)^{1/2} \quad . \tag{8}$$

This is called thermal transpiration. It has to be taken into consideration if equipment consists of parts at different temperatures; for instance, if a pressure gauge with walls at room temperature is connected to a high temperature furnace.

Evaporation of substances is another important phenomenon. If the evaporating molecules are not reflected back to the surface, the rate of evaporation is

$$g = .058\, P_{torr} \left(\frac{M}{T\ K}\right)^{1/2} g\ cm^{-2} sec^{-1} \quad . \tag{9}$$

If we have a certain number of molecules or quantity of gas Q flowing each second through a pipe of conductance C with pressures P_1 and P_2 at the ends of the pipe,

$$Q = C(P_1 - P_2) \quad . \tag{10}$$

The analogy to an electrical current is obvious. As in the latter case, the rules for parallel and series connection of conductances apply, namely,

$$C = C_1 + C_2 \text{ for parallel connection} \tag{11}$$

$$\frac{1}{C} = \frac{1}{C_1} + \frac{1}{C_2} \text{ for series connection.} \tag{12}$$

We have to discriminate between molecular and viscous flow. The conductance of a pipe of diameter d and length L in the viscous region is

$$C_v \alpha \frac{d^4}{\eta \lambda} \bar{P} \tag{13}$$

for nitrogen at 293° K

$$C_{v_{(\text{nitrogen})}} = 187 \frac{d^4 \text{ cm}}{L \text{ cm}} \bar{P}_{\text{torr}} \text{ liters/sec} \quad . \tag{14}$$

Most of the time we deal with molecular flow, i.e., wall collisions only and diffuse reflection. Then the conductance of a long pipe is

$$C = \frac{\pi}{3} \left(\frac{kT}{2\pi m}\right)^{1/2} \frac{D^3}{L} \quad . \tag{15}$$

This becomes for nitrogen at 293° K

$$C_{(\text{nitrogen})} = 12.2 \frac{D^3 \text{ cm}}{L \text{ cm}} \text{ liters/sec} \quad . \tag{16}$$

If the pipe is short, (16) gives too high a conductance since the conductance of the entrance aperture is neglected. For L/D = 4, C is 30% less than the value computed from (16).

Recently L. L. Levenson, N. Milleron, and D. H. Davis[8] determined molecular flow conductances for tubes and pipes of various shapes and constrictions theoretically by a Monte Carlo calculation and confirmed the results experimentally.

The conductance of an aperture of area A is for molecular flow

$$C = \left(\frac{kT}{2\pi m}\right)^{1/2} A \quad . \tag{18}$$

For nitrogen at 293° K,

$$C_{(\text{nitrogen})} = 11.7\, A_{cm^2} \quad \text{liters/sec} \quad . \tag{19}$$

The Pumping Process (Gerhard Lewin)

It is customary to measure the pump action in terms of a pumping speed, S, expressed in liters/sec. S is the volume of gas removed from the container each second at the pressure existing at the time. A reason for this definition is that the pumping speed of many pumps is approximately constant over a large range of pressures. The total mass of gas removed each second is called the throughput of the pump and is expressed in torr liters/sec; it decreases as the pressure drops.

Figure 1 is a schematic representation of the evacuation of a vacuum container of volume V. The schematic shows three main sources of gas: Q_W gas desorbed from the wall, Q_L gas leaking into the container, and Q_P gas streaming back from the pump. The basic equation describing the pump action is

$$-V\frac{dp}{dt} = SP - Q_W - Q_L - Q_P \quad . \tag{20}$$

The amount of gas removed from the container is equal to the amount of gas entering the pump less the influx of gas which comes from the three sources. Eventually, an equilibrium will be established and the pressure will not drop any further. After the initial pumpdown, the gas sources Q determine what gas is present in the container rather than the gas initially filling the volume V.

When the ultimate pressure P_u is reached dP/dt is zero and

$$P_u S = Q_W + Q_L + Q_P \tag{21}$$

$$S = \frac{\Sigma Q}{P_u} \quad . \tag{22}$$

We can define an effective pumping speed S_e which takes the various gas sources into account. From (22) follows

$$S_e P = SP - \Sigma Q = S(P - P_u)$$

$$S_e = S(1 - \frac{P_u}{P}) \quad . \tag{23}$$

If Q_L is rendered negligible by proper technology and Q_W by a bakeout, the backstreaming from the pump determines P_u. S_e is a function of pressure; it becomes zero at the ultimate pressure.

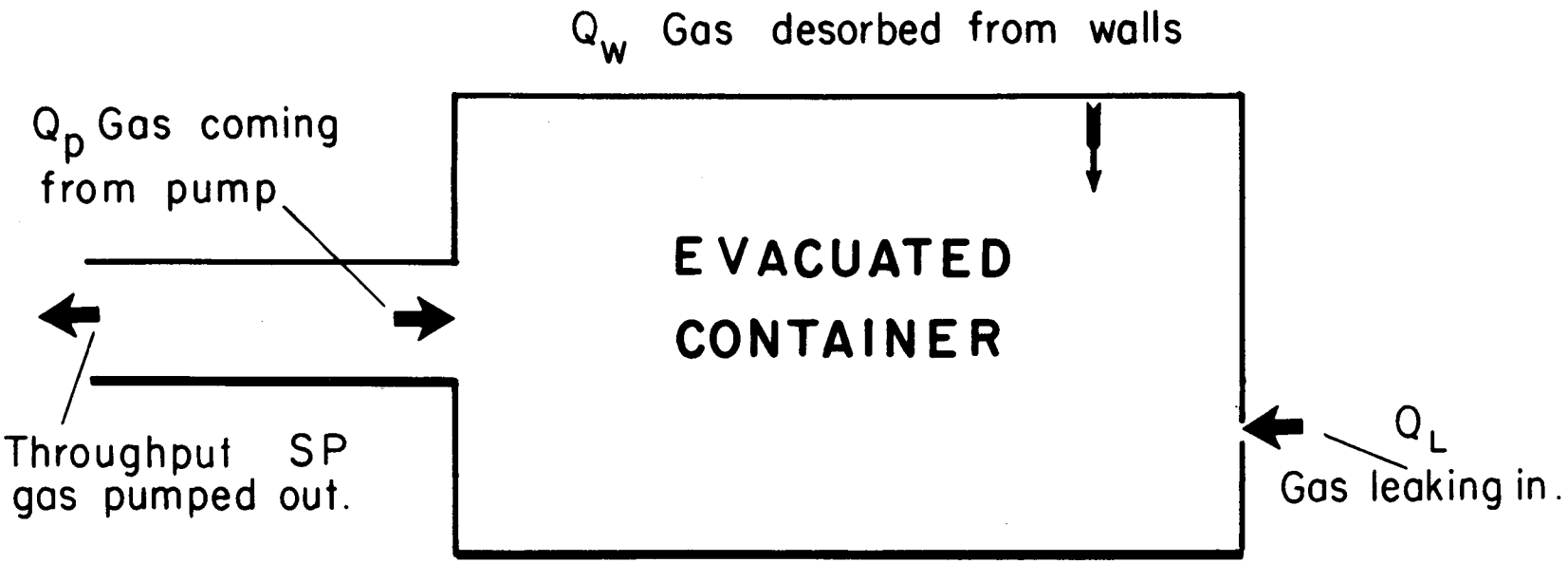

EVACUATION EQUILIBRIUM

Q_L and Q_P are usually constant and Q_W changes only slowly with time. If we consider those time intervals where the various Q's are either negligible (as during initial pumpdown) or nearly constant, we can integrate (20) and obtain in view of (22)

$$P - P_u = (P_o - P_u)\, e^{(-S/V)t} \quad .$$

P_o, the pressure at $t = 0$, is large compared to P_u; therefore

$$P = P_o\, e^{(-S/V)t} + P_u \quad . \tag{24}$$

If the pump of speed S is connected to the vacuum system through a pipe of conductance C, the pumping speed of the combination is, in view of (12),

$$S_c = \frac{S\,C}{S + C} \quad . \tag{25}$$

Hence, $C \geqq S$ to take advantage of the inherent speed of the pump.

If we have a surface of area A which adsorbs all gas hitting it or a "black hole" of area A which exhibits no backstreaming, it follows from (19) that such area has a pumping speed for nitrogen of $11.7\, A_{cm^2}$ liters/sec.

Surface Effects (Edward G. Apgar)

Surface effects are particularly important in the vacuum considerations of plasma physics experiments because they determine the equilibrium base pressure, its constituents and also, in the presence of a gas discharge, the influx of material into the plasma. Thus, in addition to adsorption and desorption effects which affect the degree of vacuum and contamination of the working gas one must also expect sputtering, ion pumping, re-emission and enhanced desorption due to the efflux of particles and radiation from the plasma.

Adsorption. Adsorption is the term applied to the existence of a higher concentration of a component at the surface of a liquid or solid than is present in the bulk. It should be distinguished from absorption which refers to a more uniform penetration. The term "sorption" is used more generally for both cases since they are frequently difficult to separate. The term "occlusion" is now restricted to the case of sorption of gases by metals. The gas or vapor is called "adsorbate" and the surface "adsorbent."

When a molecule of gas strikes a surface, it can rebound or else stick and be released at some later time. If the average sticking time becomes comparable to the mean flight time, then adsorption effects can influence the pressure. The sticking time, τ, depends on the desorption energy for the gas surface combination and the surface temperature. It can be represented approximately by[9]

$$\tau = \tau_o \exp(E_d/RT) \tag{26}$$

where τ_o is usually approximately 10^{-13} sec and the energy E_d can vary between approximately 1 k cal to 100 k cal (1.0 ev = 23.06 k cal/mole). Even if a molecule stays on the surface, it can engage in surface diffusion, dissociation, and chemical reactions. These also are functions of temperature and an energy characteristic of the particular gas surface combination. Fig. 2 shows the dependence of τ on E_d and T.

The study of adsorption dates back nearly 200 years to the discovery of the power of charcoal and other porous substances with large surface to mass ratios to take up large volumes of certain gases following heat treatments. In

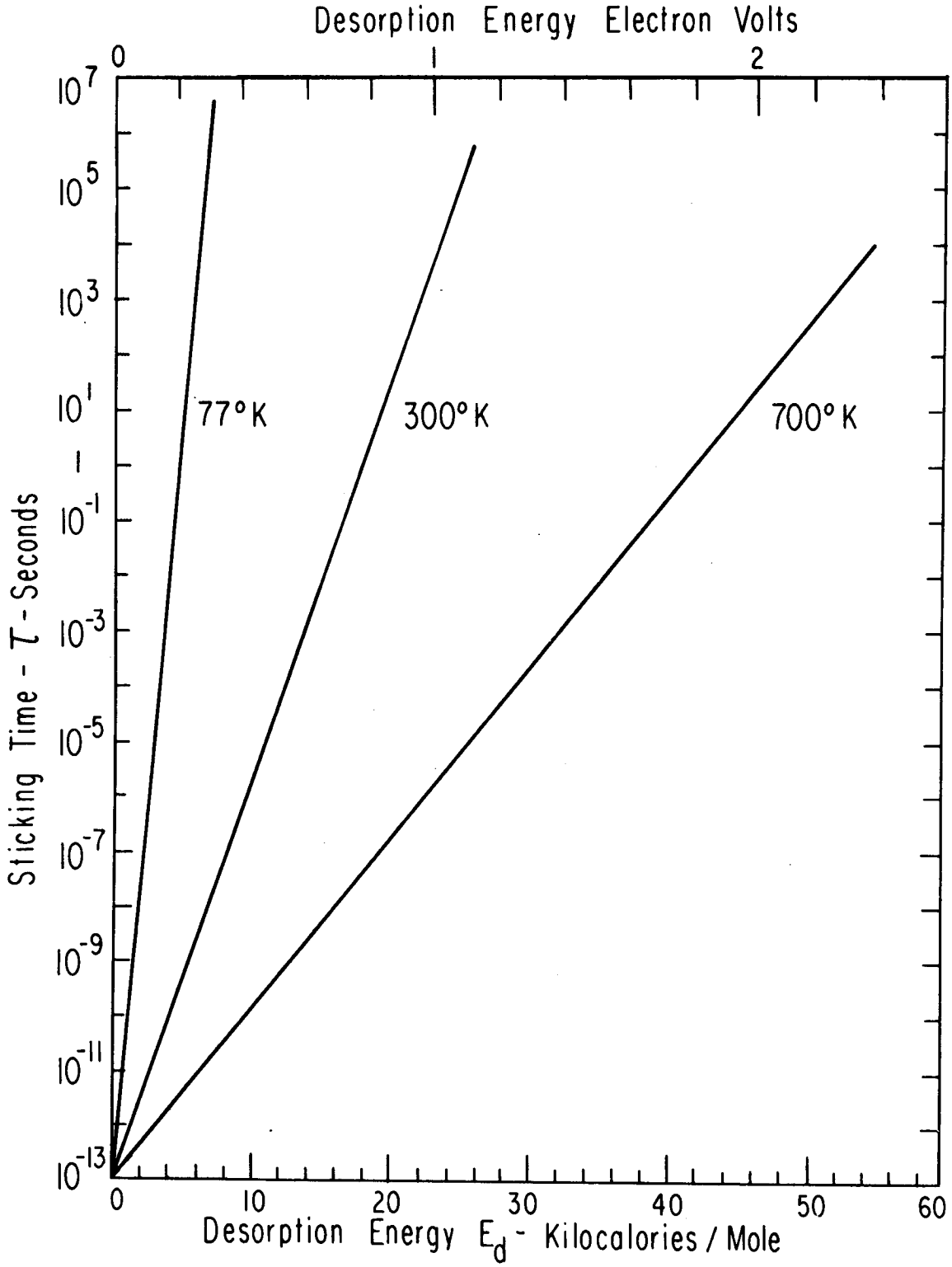

FIGURE 2. DEPENDENCE OF STICKING TIME ON DESORPTION ENERGY AND TEMPERATURE

general increasing the pressure or decreasing the temperature will increase the amount adsorbed. This is connected with the evolution of a heat of adsorption which can be detected in a calorimeter during the actual process of adsorption. Figure 3 shows the microscopic interpretation of the energies involved in adsorption.[10] This figure shows the energy given off during adsorption of a single particle (a) for the case of "weak binding", or "physical" adsorption, namely, E_p and (b) for the case of strong binding or chemical adsorption, namely, E_c. In the latter case, an activation energy E_a must be supplied. This means the energy of desorption in Eq. (26) is:

$$E_d = E_c + E_a \quad . \tag{27}$$

Much data on adsorption is in terms of "isotherms," i.e., plots of amount adsorbed vs. pressure at constant temperature and the shapes of these curves led to the earliest theories of the nature of the adsorption process. Figure 4 shows typical curves for physical adsorption. Case (a) occurs when only part of a surface, up to a monolayer, is covered by an adsorbate. In (b) no limit exists; any number of layers form as the pressure increases to the saturated vapor pressure P_s, and in (c) after the initial monolayer forms a further increase in pressure adds more layers.

Up to the time of Langmuir's work, adsorption was thought of as a progressive condensation of the adsorbate into a film on the absorbent. The variation of adsorption with pressure was often found to follow the empirical equation (known as the Freundlich isotherm)

$$\frac{x}{m} = k p^{1/n} \tag{28}$$

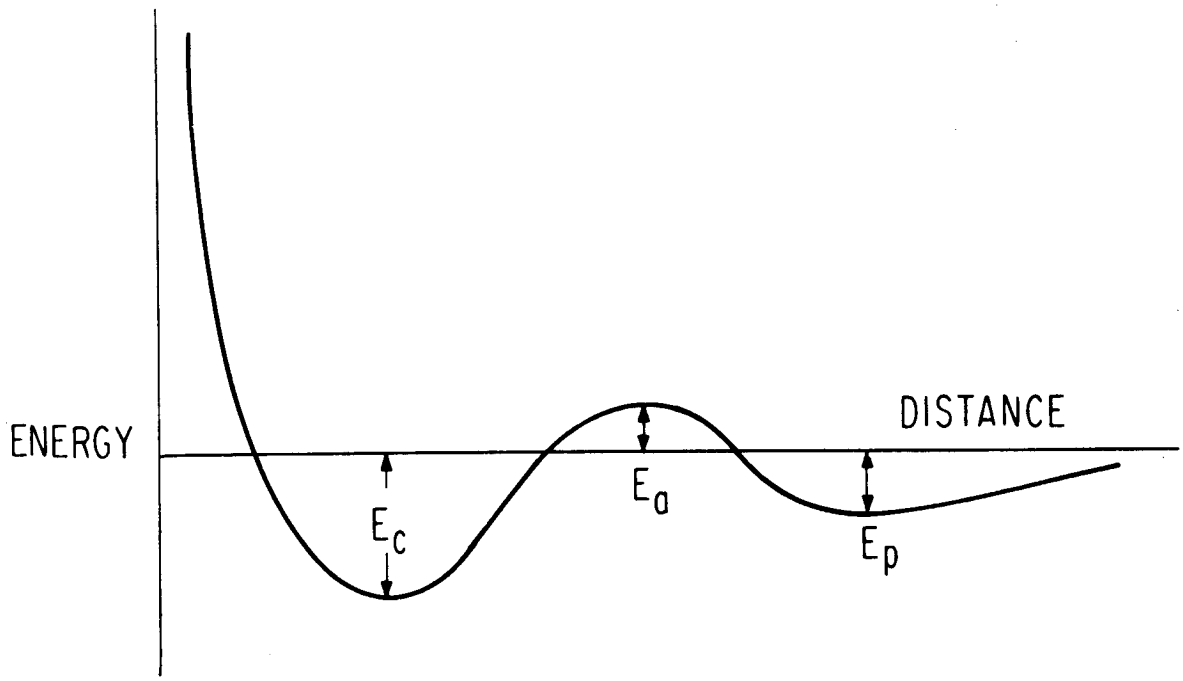

FIGURE 3. VARIATION OF POTENTIAL ENERGY OF ADSORPTION WITH DISTANCE E_c - CHEMISORPTION ENERGY, E_a - ACTIVATION ENERGY, E_p PHYSICAL ADSORPTION ENERGY.

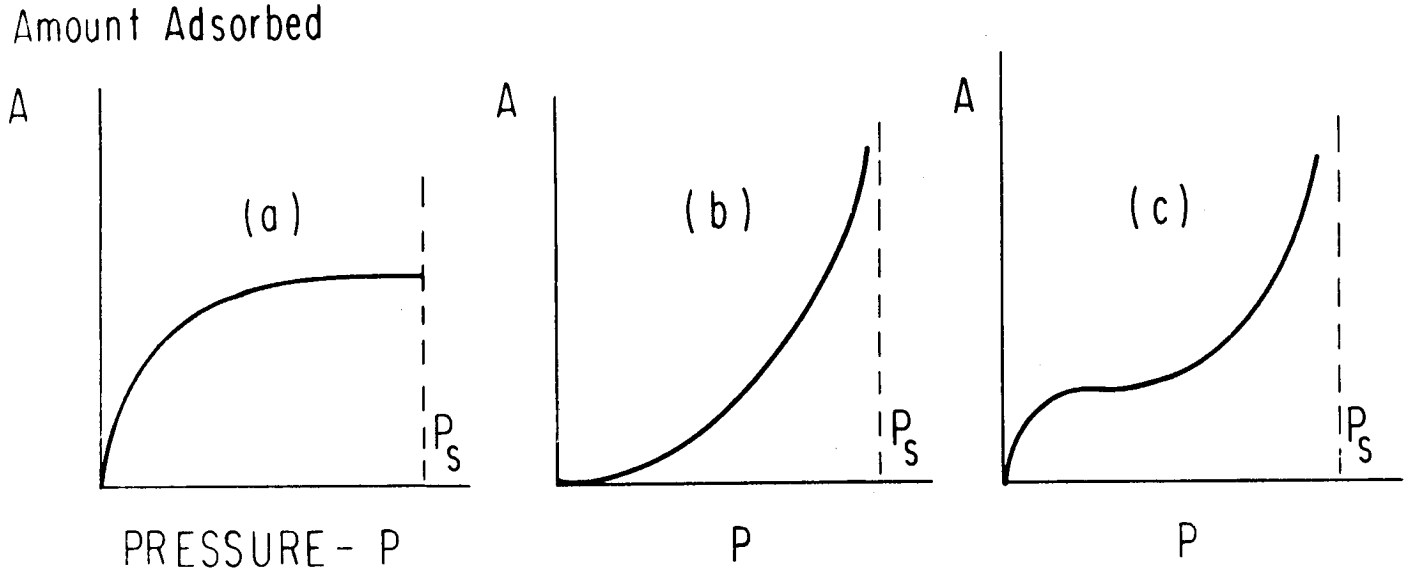

FIGURE 4. TYPICAL ISOTHERMS FOR PHYSICAL ADSORPTION

where x is the mass of gas adsorbed by m grams of absorbent at pressure p, and k and n are constants for a fixed temperature and system. Equation (28) is primarily useful for plotting adsorption data of type (a) in Fig. 4. Theoretically it corresponds to adsorption where a distribution of heats of adsorption exist.

Langmuir introduced the idea that the energy of adsorption is as great as the energy of ordinary chemical reactions and (since chemical forces decrease very rapidly with distance) that adsorbed layers of gas would in general be only one molecule in thickness. He also postulated that a certain average heat of adsorption existed for the whole adsorbent surface so that the probability of desorption is proportional to surface coverage. Thus at equilibrium when the rates of adsorption and desorption are equal

$$(1 - \theta)\alpha\mu = \nu\theta \tag{29}$$

where θ is the fraction of available surface covered at any instant, α is the probability that a single molecule striking the surface will remain bound, μ is the rate at which molecules strike 1 cm^2/sec, and ν is a constant at a given temperature. However, μ is proportional to pressure and θ is proportional to the amount of gas x adsorbed by a mass m of adsorbent, so

$$\frac{x}{m} = \frac{k_1 k_2 p}{1 + k_1 p} \tag{30}$$

where k_1 and k_2 are again constants.

This Langmuir isotherm fits much experimental data such as case (a) in Fig. 4. It breaks down when more than one adsorption energy is present for

when multi-molecular adsorption occurs as shown in cases (b) and (c) of Fig. 4. In this case the derivation can be generalized as was done by Brunauer, Emmett and Teller.[11] This isotherm called the BET equation is useful in determining surface areas since it allows one to determine the amount of gas necessary to form the first monolayer. From the size of the molecule being adsorbed one then calculates the surface area. This is the most widely used method of surface area determination.

A monomolecular layer of gas can be defined in terms either of the number of adsorbed particles per cm^2 when they are considered to be in a close packed hexagonal array or as the number of particles per cm^2 when there is one adsorbed particle for each surface atom or for each adsorbing site. The first definition depends on knowing a molecular diameter. This is computed from the density of the condensed phase of the gas in a close packed face centered cubic lattice. Table II gives some values for the surface density N_s of monolayers of different gases,[2] based on the close-packed definition.

Table II

Gas	H_2	He	A	N_2	O_2	CO	CO_2	CH_4	NH_3	H_2O
10^{-15} N_s	1.52	2.42	0.85	0.81	0.87	0.81	0.53	0.52	0.46	0.53

One sees that an approximate value for a monolayer of any gas is 10^{15} molecules per cm^2. However, there are two possible errors in an uncritical use of this number. First the density will be limited by the density of adsorbing sites.

Thus an adsorbed molecule may share bonds with more than one surface atom and the monlayer value would be smaller than the number given in Table II. The second and larger error is due to lack of accurate knowledge of the true surface area. Accurate measurements are usually made with the BET method applied to powdered samples. Microscopic examination of surfaces can give a rough estimate. Ratios of true to apparent area range from 1 to 1000 for common materials and are very sensitive to methods of surface preparation. For an aged tungsten filament the ratio of 1.4 has been used. Rolled metal foils have ratios in the range of 2 to 10, while for mechanically polished metal the values range from 10 to nearly 100. Chemical etching can give ratios greater than 1000. Thus the adsorption of a monolayer can remove between 10^{14} to 10^{18} molecules per cm^2 of surface from the gas phase.

An extensive literature on adsorption exists due partly to the important industrial applications of adsorption effects, i.e., catalysis. Much of this data was measured at relatively high pressure and with complex absorbents such as charcoal, powdered metals and metal oxides. In most cases the preliminary heat treatment rarely exceeded 1000° K which is insufficient to remove surface impurities such as oxygen from many substances. In fact, to prepare a tungsten surface free of adsorbed oxygen, prolonged heating at 2200° K is necessary. In addition, unless the base pressure around the sample is in the ultra-high vacuum region it can quickly re-contaminate the sample surface before the admission of the test gas. Also in the cases of gases with only moderate adsorption energies, ultra-pure quality is necessary to prevent a small trace of a

more active gas such as O_2, N_2, CO, H_2O from adsorbing rapidly and changing the character of the surface. These considerations are based on the fact that a gas-surface combination with a sticking probability of near unity can form a monolayer in a few seconds at a pressure of 10^{-6} torr, as pointed out in Table I. As a result, it is now evident that much adsorption data was taken in the past on surfaces which were not well understood although by careful experimental technique reproducible data was achieved which was characteristic of the specific surface treatment and relevant to the intended applications. Modern techniques show that even in the absence of impurities small changes in annealing technique with polycrystalline samples, which result in different crystal sizes and orientations, can produce large effects on adsorption energy and sticking probability. Techniques developed to study adsorption on known reproducible surfaces include (1) experiments on thin filaments of refractory metals such as tungsten which can be flashed to temperatures which will remove all adsorbed layers. Changes in thermionic emission are used as indications of cleanliness or re-adsorption. (2) Evaporation of a metal, in ultra-high vacuum, to prepare a fresh surface, (3) sputtering away surface contamination by ion bombardment of an inert gas, (4) field ion microscope technique which displays adsorption effects of individual atoms, (5) electron diffraction to study asorption on clean surfaces (this can only detect appreciable fractions of a monolayer). By these methods a body of knowledge is being accumulated which is applicable to conditions in ultra-high vacuum systems and plasma physics devices. The adsorption energies and sticking probabilities have been measured for many combinations of the common gases and pure metals.

Unfortunately, the experimental techniques are difficult and considerable differences sometimes exist between the results of different workers. In addition, the surfaces in typical vacuum systems and plasma devices may have been altered by cleaning and baking techniques so as to differ from the ideal surfaces used in adsorption experiments.

Physical adsorption, sometimes called van der Waals adsorption, is due to weak forces of the same nature as those involved in condensation and departures from the ideal gas lows. Physical adsorption is non-specific and, while the energy E_p may vary, occurs for virtually all combinations of adsorbent and adsorbate. Somewhat arbitrarily the figure of 8 k cal/mole is used as the dividing line between the two types of adsorption. The condensation coefficient C is the probability that a single molecule striking a surface will become physically adsorbed. This is different from the accommodation coefficient, defined in Eq. (7), which is a measure of the degree of thermodynamic equilibrium established between a surface and incident molecule.

Chemisorption usually involves greater adsorption energies than 8 k cal/mole, and also often requires an activation energy, as shown in Fig. 3. However, for many gas-surface combinations E_a is small enough that we may neglect it and consider the energies of adsorption and desorption equal. Frequently, a surface will physically adsorb and chemisorb the same gas simultaneously. In some cases, such as H_2O on metals, the physical adsorption of a molecule occurs first, after which it undergoes chemisorption.

Recently an abnormally low sticking probability at very small coverages has been observed[12] and a possible explanation offered in terms of nucleation centers.[13] Chemisorption is involved when electron exchange effects occur and when dissociation takes place such as with O_2, N_2 and H_2 on tungsten. Following this, surface chemistry reactions can occur, such as formation of H_2O, CO or CH_4. Figure 5 shows data of Becker[14] on the sticking probabilities s on tungsten. The important indication is that (a) all the s values are initially between 0.1 and 1.0, and (b) each curve exhibits a flat region up to a certain value of coverage. For N_2 it extends to about 0.8×10^{14}, for CH_4, C_2H_4, H_2, and O_2 it is about 1.7×10^{14} and for CO it is 3.5×10^{14}. Apparently the N_2 monolayer forms first, followed by four other gases at about twice the coverage and the CO monolayer at four times the coverage. It is known that O_2 and H_2 dissociate on W while CO remains molecular, bound by its carbon atom. After the first monolayer we see that s decreases rapidly with increasing coverage. With second and third monolayers s approaches the range of 0.01 and 0.001. This means adsorption continues at greatly reduced rates. Thus for the case of N_2 and CO, the formation of a second monolayer would take nearly 1000 times as long as the first. Thus if the pressure were maintained at 10^{-6} torr adsorption effects would continue for more than 15 minutes. Clausing[15] has recently measured s for gases adsorbed on vapor-deposited titanium films. Table III shows how sensitive s is to method of surface treatment. The film deposited in the

presence of He shows higher sticking probabilities for some unknown reason (possibly related to a larger surface area). Even more striking is the improvement noted in going from 10° C to -195° C. Notice that near room temperature s for H_2 and N_2 is about 0.2 while s for CO is near unity. CO is seen to be "active".

Table III

Initial Sticking Probability on Titanium Films

Gas	High Vacuum				2×10^{-3} torr He	
	Continuous Evaporation		Batch Evaporation		Batch Evaporation	
	10° C	-195° C	10°C	-195° C	10° C	-195° C
H_2	0.07	0.14	0.05	0.24	0.19	0.85
D_2					0.14	0.78
N_2	> 0.20	> 0.50	0.08	0.85	0.17	0.93
CO	0.86		0.38	0.95	0.66	
CO_2	>0.50		> 0.4	0.98	0.92	
He	< 0.0005					
A	< 0.0005					
CH_4	< 0.0005					

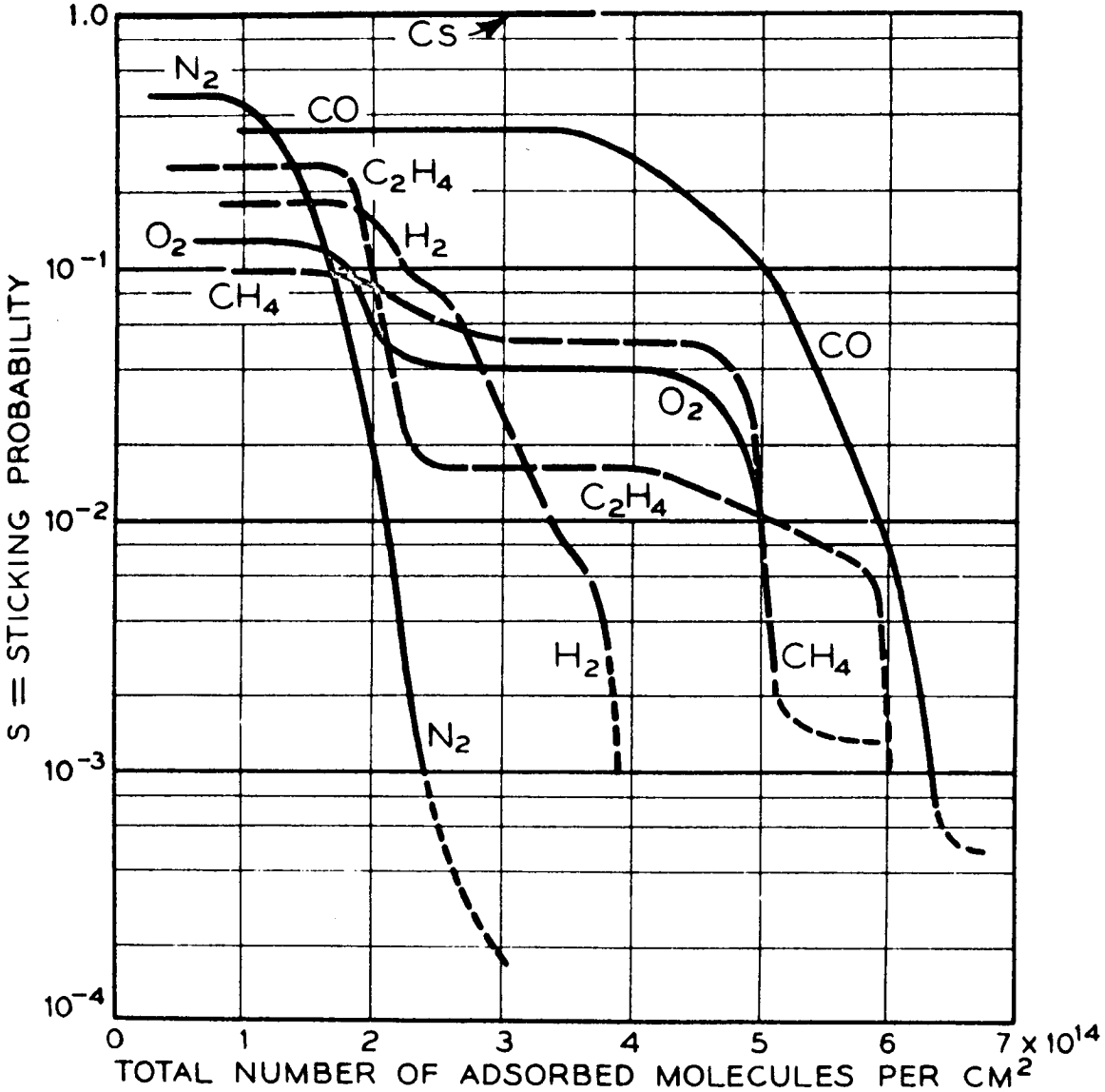

FIGURE 5. STICKING PROBABILITIES OF VARIOUS GASES ON TUNGSTEN

Values of initial sticking probabilities such as these are useful in calculating the initial pumping speed of a given area of absorbent but other information such as the true area and desorption energy are needed to obtain the capacity or total amount that can be pumped. Thus the total number of molecules being held in equilibrium is, for less than a monolayer,

$$N = \frac{1}{4} n \bar{v} s \tau \tag{31}$$

where τ, as shown in Eq. (26), depends on E_d, the desorption energy. Some values for the initial heats of adsorption are given in Table IV for various gas-surface combinations.

Table IV

Initial Heat of Adsorption on Polycrystalline Samples in k cal/Mole[3,17]

	W	Ta	Ti	Ni	Fe	Cu	Av	Ag	Charcoal
H_2O									9.5
H_2	45	45	--	31	32	9	< 3	< 3	50
N_2	95	140	140		40				
CO	80			32	32	9.3	8.7		
O_2	194	212	236	107	136				72
C_2H_4	102	138		58	68	18	21		

The value of E_d for a particular gas determines whether or not it can limit the base pressure in a system. Obviously, in the extreme limit of very small E_d the sticking time will be so short the gas will rapidly pump out. In the other limit of a large E_d the sticking time will be so long that the rate of flow of gas into the

volume will be small. In both cases after the initial pumpdown, the outgas rate will be small. However, in the region of intermediate E_d values the outgassing can continue for inconveniently long times and it is then that baking will accelerate the removal of adsorbed gas. J. P. Hobson[16] has assumed a certain model and calculated that E_d values in the range of 15 to 25 k cal/mole are those that benefit greatly from baking at 300° C. In Table IV not many values of initial heats are in this range but as coverage increases we can expect the values of E_d for the common gases CO, N_2, O_2, H_2 to decrease to the point where their effects will limit the base pressure of system.

Adsorption effects on the surface surrounding a vacuum not only limit the pressure in the volume but can be the controlling feature in the approach to equilibrium between two volumes connected by a limiting conductance. Important applications where this effect is encountered are 1) pumping out a volume through a tube of small conductance and large surface area, 2) outgassing through microscopic cracks and pores, 3) determining pressure with an ion gauge connected to a system by a small diameter tubulation. Hayashi[18] treats in detail the effect of diffusion in the presence of adsorption in vacuum devices. Blears[19] demonstrates the errors possible in pressure readings by tubulation gauges in the presence of oil vapor. Apgar[71] has demonstrated similar errors with permanent gases also.

Effects of Wall Bombardment. In addition to adsorption and desorption processes between the gas phase and the discharge tube walls in the absence of a discharge, some mention should be made of the effects of wall bombardment by plasma products. A brief summary of effects produced by low energy 50 to

100 ev particles follows.

a) Ion pumping. Hydrogen ions can penetrate up to several lattice distances and be temporarily trapped. In the absence of specific information on H_2, data for other gases shows that in general the range of ions in solids for energies < 30 kev is < 10^3 lattice spacings and is approximately proportional to energy. Ions of 1 kev can penetrate approximately ten lattice spaces into Al. When the lattice becomes saturated diffusion to the surface will just neutralize the entrapment, i.e., reemission. (For 400 ev to 5000 ev argon ions incident on metal, saturation is reached at about $10^{14}/cm^2$ to $10^{15}/cm^2$.) H_2 ions at 50 ev would saturate at much smaller values. Impurity ions in a discharge would penetrate several lattice spaces and be strongly bound. With reasonably low impurity levels saturation would require a long time.[20] Cooling of the walls to L. N. temperatures greatly increases the sorption capacity and reduces reemission.

b) Sputtering. The sputtering yield of low energy H_2 ions[21] is of the order of 0.01 while for heavier ions it is roughly 1. Thus, sputtering by H_2 along is low, but a small impurity content exerts a disproportionate effect. Sputtering yield values show a systematic correlation with the atomic number of the metal involved. Be, Al, Cu, Ag and Au have high values, while Hf, Ta, W and Zr show low values. Sputtering also can release ion pumped gas and other gaseous impurities.

c) Enhanced desorption. Exposure of a wall to plasma products not only increases the desorption of gas but affects the amount and state of the gas adsorbed. Thus, bombardment of an oxide surface containing some carbon impurity atoms by H^+ ions can result in the formation of adsorbed H_2O, CO and

CH_4 which can subsequently be desorbed by plasma product efflux. In addition a wall with a history of H^+ bombardment can yield H_2 gas back into the volume. In general residual surface gases and these "reaction products" can certainly be desorbed by the effects of ion bombardment and surface thermal transients while it is less certain that photon[22,23] and electron effects[24] are of importance.

Pressure Measurements (Edward G. Apgar)

The apparatus of plasma physics requires pressure measurements for a variety of purposes. For example, one must measure fore pressures of diffusion pumps, the relatively high pressure of the working gas in a discharge device, the low base pressure in a clean device in the absence of injected gas, and the partial pressures of impurities. Also measurements are sometimes required under unusual conditions. Thus the presence of a magnetic field complicates the operation of a gauge near a plasma. In addition, if a high speed large conductance gauge geometry is mounted facing a plasma both magnetic field and plasma pickup effects must be dealt with.

High Pressures. In the range from several torr to 10^{-3} torr thermal conductivity gauges are useful because they are compact, rugged and continuous-reading. They consist of heated wire filaments mounted in envelopes. At pressures where the mean free path becomes comparable with the gauge dimensions the energy loss by conduction between the filament at T_2 and its surroundings at T_1 is proportional to the accommodation coefficient, pressure and the temperature difference $T_2 - T_1$. This energy loss may be converted into a tem-

perature decrease detected by a thermocouple or an increase in power required to maintain a filament at constant temperature and resistance. The main source of error is the fact that the accommodation coefficient depends on the gas composition and surface condition. These can change unpredictably. At low pressures radiation losses become appreciable and are another source of error. Advantages are that the low temperature of operation prevents filament reactions with the gas being measured and a sudden burst of high pressure is not injurious.

The pressure region from several torr down to 10^{-5} torr can be measured by a special variety of hot filament ionization gauge, the WL7676.[25] (The geometry of this gauge will be discussed later.) The advantage over the thermal conductivity gauge is the decreased low pressure limit and the greater accuracy when the gas composition is known. The sensitivity of this gauge for some different gases is given in Table V.

Table V

Sensitivity Factors for High Pressure Gauge WL-7676

Gas	Sensitivity
He	.06[26]
N_2	.40[26]
CO	.42[26]
H_2	.21[26]
D_2	.24[27]
H_2O	.56[28]

where sensitivity s is defined in the usual way:

$$I = sI_e p \quad , \tag{32}$$

I being the ion current, I_e the ionizing current, and p the pressure.

The McLeod gauge is not ordinarily used directly on plasma apparatus because of its size, fragility, and the fact that considerable caution is necessary to obtain accurate readings. However it is important because it is an absolute device, independent of gas composition (permanent gas, excluding vapors), which is very useful for calibrating and checking all other gauges from the range of many torr down to 10^{-6} torr. In this gauge an initial volume V of gas at pressure P is compressed by a Hg column into a capillary where the final pressure is given by the difference between two Hg columns. The pressure P is indicated on a scale calibrated by the application of Boyles Law. This eliminates the direct measurement of condensable vapors (which depart from an ideal gas), in particular H_2O. The presence of such a vapor in a system will cause a difference between the indications of an ion gauge and McLeod gauge. Another potential source of error is due to the cold traps between the McLeod gauge and the system necessary to contain the Hg vapor. Certain gases will condense, producing a much lower pressure in the gauge than in the system. Thus the trap temperature must be selected with the gas composition in mind, and time allowed for adsorption effects to reach equilibrium.

Low Pressures. The extreme low pressure region down to 10^{-10} torr requires the well known hot filament ionization gauge structure[29] hereafter referred to as the BA gauge. An ionization gauge measures pressure in terms

of the ion current collected from a region of ionizing collisions between neutral gas molecules and energetic electrons. The calibration depends on the gas composition and electrode geometry. In the high pressure gauge the filament, accelerating grid, and collector are all parallel and closely spaced so that the ion collection and electron paths are unaffected up to a pressure of several torr. In the BA gauge the filament is outside a cylindrical grid structure which contains the ion collector electrode along its axis. The electrons are accelerated by the approximately 150 V potential drop between the filament and grid and pass through the grid structure. A very small fraction make ionizing collisions with neutrals. The ions are then drawn to the collector because of the high potential of the grid relative to the collector.

In both gauges the low pressure limit is determined by the current of photo-electrons released from the ion collector by soft X-rays produced at the grid by ionizing electrons. The large area of the collector in the high pressure gauge causes a correspondingly high X-ray current (equivalent to 10^{-5} torr) while the very small area of the BA gauge collector produces an X-ray limit corresponding to approximately 6×10^{-11} torr. In Table VI below are listed some sensitivity factors for the Westinghouse WL-5966 BA gauge.[31]

Table VI

Sensitivity Factors for the WL-5966 Gauge

Gas	He	Ne	A	N_2	H_2	CO	CH_4	N_2O
s	2.4	3.7	16.4	11.5	5.0	13.0	18.0	14.2

In using these factors when the system composition is known, it is convenient to routinely read the pressure as an equivalent N_2 pressure and then multiply by the appropriate factor, i.e., 4.8 for He, 2.3 for H_2, when true pressures are required. In the absence of a partial pressure analyzer and at very low pressures where the gas composition is easily influenced by factors beyond control the conversion of gauge ion current to true pressure is difficult and one must be content with an equivalent N_2 pressure.

In addition to errors due to the low pressure X-ray limit and lack of knowledge of gas composition, various other effects are important including gauge pumping, outgassing, impurity reactions, oscillations[32] and high pressure non-linearity.

The last effect is most easily handled. At very low pressures a value of I_e = 10 ma is necessary for sufficient sensitivity, but above 10^{-4} torr departure from linearity sets in for several reasons.[33] Setting I_e to 0.1 ma or less, the region up to 10^{-3} torr is made accessible.

The effects of gauge pumping and outgassing are most important when the gauge is mounted with a low impedance (1 ℓ/sec or less) tubulation to the system or else even with a large conductance tubulation connected to a small volume

system. A thorough initial outgassing period of 3/4 hour or until the electrodes glow yellow is necessary with the usual ion gauge before it can detect pressures in the ultra-high vacuum range. Subsequent outgassing periods of five minutes will usually suffice in a clean system. In addition to simple outgassing from the electrodes, chemical reactions can produce gas products which lead to erroneous results. Thus carbon and oxygen impurities in the gauge materials react with H_2O to produce CO and CH_4 and with H_2 to produce H_2O. Another gauge reaction which causes an increase in pressure is the cracking of oil vapor products from the pump system. It has been shown[34] that a large conductance gauge can steadily crack oil molecules and release the products into the system. With a small conductance gauge adsorption effects in the tubulation reduce the oil vapor influx to the point where the cracked products can be "pumped" by the gauge. Then the small tubulation gauge will read a lower pressure than a large tubulation gauge on the same system. This observation was first explained by Blears.[19] On the other side of the "gauge effect" coin are the various pumping mechanisms. A small but important effect at very low pressures is the ion pumping effect. This effect is quite general and includes both inert and active gases.[35,36]. Positive ions are driven into the surface of the gauge electrodes or enevelope and thus removed from the gas phase. Initial pumping speeds of about .01 liter per second occur. Gradually saturation and re-emission bring about a slow decline. Chemisorption of the active gases N_2, O_2, CO, H_2O and H_2 on electrodes or the envelope freshly cleaned by outgassing can produce very high initial pumping speeds of many liters/sec. This too saturates with time and can be ignored

one day or so after outgassing. Another effect is filament pumping of certain gases. Thus H_2, O_2 and CH_4 all undergo specific reactions at the surface of a hot filament which tend to remove them from the gas phase. Speeds of the order of tenths of a liter/sec are common.

Errors in pressure reading by a gauge due to outgassing or pumping can be reduced by using a "nude" or large conductance mounting. However in this case if the system pumping speed is low or the experiment involves accurate measurement of low partial pressures the gauge effects can still be troublesome. The extent of this source of error is discussed in detail by E. Apgar.[71]

Brief mention should be made of two special ion gauges which do not rely on a hot filament electron source, the Alphatron* and the Penning type.

The former uses a polonium source to supply alpha particles which ionize the gas. The ion current is then detected in the usual way. Advantages are the absence of a hot filament, the large pressure range, 1000 torr to 10^{-4} and non-delicate construction. Accidental exposure to atmospheric pressure has no effect. As disadvantages it is moderately bulky and heavy, cannot be baked or cleaned out effectively, and requires precautions in use due to the radioactive source.

The Penning type gauge, also called "P. I. G.", produces ions by means of a cold cathode discharge in crossed electric and magnetic fields. The principle advantages are its simplicity and ruggedness of construction and lack of hot filament. It is not easily damaged by brief exposure to high pressures. Its disadvantages include the need for a dangerously high anode voltage (6 kv), a

*Marketed by National Research Corp.

permanent magnet, its appreciable ion pumping effect, and delayed starting at low pressures. In its simple form the pressure range is from 10^{-2} torr to 10^{-6} torr. However, a special model is available, NRC Model 552, which is claimed to operate between 10^{-4} torr and 10^{-14} torr.

Another gauge for the extremely low pressure range has been developed by J. M. Lafferty[37] in which the electron trajectories have been lengthened by an axial magnetic field, as in a magnetron, giving greater ionizing efficiency. With electrostatic focussing of the ions onto an electron multiplier detector pressures as low as 4×10^{-14} torr are measurable. The technique is claimed to be capable of detecting even lower pressures. Pressures in this range would still be of questionable interest in plasma physics because of the difficulty of relating them to the surface conditions of the discharge vessel.

In plasma devices gauges often have to be operated in the presence of magnetic fields and plasma products. In general magnetic fields much above 50 gauss will reduce the gauge sensitivity or completely cut it off because of disturbances in the electron and ion paths. However special orientations are possible in which the ion and electron motion is parallel to the field and useful sensitivities are possible.[38] Plasma products such as ions, electrons, photons and electromagnetic pickup are difficult to keep out of a gauge structure which is supposed to respond only to neutrals. Shielding by biased grids alone seems ineffective. However a solid metal baffle between the plasma and gauge structure has been used successfully on fast ion gauges at this Laboratory. These gauges were developed to measure changes in neutral pressure at the boundary of a plasma

permanent magnet, its appreciable ion pumping effect, and delayed starting at low pressures. In its simple form the pressure range is from 10^{-2} torr to 10^{-6} torr. However, a special model is available, NRC Model 552, which is claimed to operate between 10^{-4} torr and 10^{-14} torr.

Another gauge for the extremely low pressure range has been developed by J. M. Lafferty[37] in which the electron trajectories have been lengthened by an axial magnetic field, as in a magnetron, giving greater ionizing efficiency. With electrostatic focussing of the ions onto an electron multiplier detector pressures as low as 4×10^{-14} torr are measurable. The technique is claimed to be capable of detecting even lower pressures. Pressures in this range would still be of questionable interest in plasma physics because of the difficulty of relating them to the surface conditions of the discharge vessel.

In plasma devices gauges often have to be operated in the presence of magnetic fields and plasma products. In general magnetic fields much above 50 gauss will reduce the gauge sensitivity or completely cut it off because of disturbances in the electron and ion paths. However special orientations are possible in which the ion and electron motion is parallel to the field and useful sensitivities are possible.[38] Plasma products such as ions, electrons, photons and electromagnetic pickup are difficult to keep out of a gauge structure which is supposed to respond only to neutrals. Shielding by biased grids alone seems ineffective. However a solid metal baffle between the plasma and gauge structure has been used successfully on fast ion gauges at this Laboratory. These gauges were developed to measure changes in neutral pressure at the boundary of a plasma

in times of the order of milliseconds or less. The Penning type[39] is simply two disk-like cathodes with a ring shaped anode at high potential. If the gauge is located close to the plasma column then the application of a confining magnetic field will permit a discharge in which the current to the cathode is a measure of the neutral density. The gauge tested had a time constant of 1 millisecond.

The hot filament high speed gauge[40] was designed with a flat, large aperture, structure to have a time constant of 90 μsec for H_2. In this gauge the electrons and ions move to the grid and collector along paths parallel to the magnetic field. A high frequency power supply for the filament reduces stress due to the magnetic field.

Partial Pressure Measurements. For many purposes a knowledge of total pressure is insufficient and in fact unless we know the gas composition in order to apply the correct gauge sensitivity factor, even total pressure measurements can be greatly in error. In the very low pressure region the apparatus and technique for total pressure measurements becomes increasingly complex so in the long run the adoption of a partial pressure measuring device is usually worth the extra expense and effort. Elaborate experiments on surface effects are sometimes carried out using ion gauges only leading to ambiguous results which would easily be resolved by a knowledge of gas composition. In plasma physics research there are several possible applications for a mass spectrometer (which identifies gas composition on the basis of the molecular mass to charge ratio).

One can monitor the residual gas composition after pumpdown. This will

provide immediate evidence as to the source of the vacuum limitation, i.e., leaks, normal outgassing of H_2O and CO or a hydrocarbon indicating oil contamination of the surfaces. A mass spectrometer set to detect a probe gas such as He can serve as a substitute for a leak detector and give high sensitivity if the system pump speed is throttled down. Also a mass spectrometer is useful for routine analysis of the purity of the working gas. With a clean system, impurities of several parts in 10,000 can make a noticeable effect on plasma purity by virtue of wall adsorption effects. Monitoring the impurity background between discharges gives indirect evidence as to the exchange of impurity between the plasma and walls and shows the rate of clean-up as a result of discharges. Although mass spectrometry is a well known and widely used technique, its application to ultra-high vacuum devices and plasma physics has, until recent years, been limited because of the requirements of bakeability, small size, and high sensitivity. The bakeable feature has followed the development of reliable seals and metal gaskets (such as gold and copper), rugged lead-throughs for the base connections and ion collector and low leakage, precise supports for the electrode system. Platinum plating has been found to help prevent formation of insulating metal oxide layers. The small size is necessary to minimize surface effects in the mass spectrometer itself. High sensitivity, necessary for detection of pressures in the 10^{-10} torr or lower range has come from the availability of reliable, high gain, low drift dc amplifiers as well as electron multiplier devices able to withstand moderate baking. In the last year in the United States alone, at least three such instruments have been made commercially available.

A well known type of mass spectrometer of the magnetic deflection type is one in which ions created by energetic electrons are accelerated by a potential V through a magnetic field H where they are sorted out in circular paths of different radii R according to their charge to mass ratio, e/m.[41] If M is the molar mass in grams of the singly-charged ion, then

$$HR = 144(MV)^{1/2} \quad . \tag{33}$$

In the crossed field type category there are several sub-types labeled variously as 60° sector, 90°, 180° and trochoidal. In general the larger instruments have better sensitivity and resolution. However, for UHV purposes a small size is important. Only the peaks for $M < 44$ need be well resolved and multiplier type ion detectors can augment sensitivity. A commercial 180° type with magnetic deflection only, known as the "diatron 20" is useful because of its extreme compactness and simplicity. It can be purchased bakeable or else converted by the user. In this device R = 1, H = 3200 gauss, and with a vibrating reed electrometer capable of measuring currents in the 10^{-16} amp range the lower limit of partial pressure is near 10^{-11} torr. If we define the sensitivity K in the usual way by

$$I = K I_e p \tag{34}$$

then some measured values for K are given in the table below, based on an ion gauge calibration.

Table VII

Sensitivity Factors for Diatron 20

Gas	H_2	H_e	H_2O	CH_4	CO	N_2	CO_2	A	Hg^+
K	.055	.026	.060	.108	.017	.064	.096	.057	.044

The time constant of the diatron 20 is approximately 1 sec, at best, due to vacuum conductance and electronic limitations. Thus pressure changes in the course of a short discharge cannot be resolved. If mounted very close to a confined plasma, electrical pickup and fringe magnetic fields will eliminate the signal near the time of the discharge but after recovery the transient changes in impurity pressures can be studied. Thus, an initial rise in CO pressure after each discharge is interpreted as outgassing from impurity laden walls and indicates a net removal of impurities in progress. An initial drop in CO pressure with a slow recovery indicates clean walls adsorbing CO from the gas phase. Mounting a mass spectrometer on the pump line, away from the discharge, avoids interruptions in signal and provides a smoothed out measure of the flow of impurities.

Another popular mass spectrometer is the Omegatron[42] in which ions are created at the center of an electrode structure by energetic electrons and then accelerated by an rf field into spiral orbits in a steady magnetic field. Again discrimination occurs according to the e/m ratio. It requires a well aligned electrode geometry, a well regulated rf generator voltage, absence of stray fields due to insulating layers, and the ion output cannot be directed into a multiplier. However it is small and simple in structure and has been available commercially in bakeable form for several years, with the drawback of not being demountable for adjustment or repair. Its principal use has been as a vacuum analyzer for research purposes and has not been used on plasma devices.

Two other mass spectrometer types which operate without magnetic deflection are the time of flight and quadrupole resonance devices. These send the ion beams in a nearly straight line, have large conductance, high sensitivity, fast response time, and are suited to multiplier detection. They are just about developed to the point where, with sufficient expense and effort, bakeable versions might be expected to be successfully applied to plasma devices. Then the study of impurity reactions with a time resolution of approximately 10 μsec would be feasible.

A special mass spectrometer for plasma physics use was developed by L. Smith which uses the discharge as an ion source and the steady confining magnetic field as the analyzing field for the ions. The ions are drawn to a collector across an accelerating gap whose potential drop can be varied to select the different e/m ratios.[43] The sensitivity is such that a few per cent of impurity can be detected. It gives both a qualitative analysis of the gases present and the different states of ionization of the same species. Thus in a He discharge H^+, O^+, O^{++}, O^{+++}, C^+, and CO^+ ions were detected, while in a neon discharge ionization up to Ne^{4+} was detected in the A2 stellarator.

A major application of mass spectroscopy is in leak detection where the electrode system and voltages are pre-set to detect the specific ion of the probe gas. A standard commercial He leak detector can respond to a flow of 10^{-9} torr liters/sec or a leak of approximately 10^{-12} liters/sec. Devices with a

background of D_2 gas, such as fusion reactors, will have a D_2^+ ion, of M = 4, which will obscure the He^+ signal. In such cases a different detector and probe gas must be used or else an existing mass spectrometer on the device can be used with A or Ne probe gas.

Vacuum Equipment - General Considerations (Gerhard Lewin)

The main use of the vacuum equipment with which we are concerned is in experimental research investigation. It is often quite complex and may contain novel components. It has been our experience that it is of utmost importance to stress the reliability aspect, otherwise operating time will be severely limited by breakdowns. To check reliability by testing is costly and time-consuming, although this can often not be avoided. It is preferable to use proven designs rather than to adopt prematurely attractive innovations. An example is the gold seal design of the "C" stellarator. It is the corner type gold seal.[44] Since its introduction many new metal-to-metal joints have been suggested. But the "C" machine has about 75 detachable metal-to-metal joints. Obviously, we hesitate to change over to a new type of joint unless it has been proven by large-scale usage for several years. Reliable information can often be gained from the experience of the electronic tube industry, but caution is indicated if we want to use joints which contain dissimilar components which have to be baked. Eletronic tubes are baked once or twice during manufacture, while plasma vacuum equipment may be baked many times. Hence, fatigue cracks could develop. In

one instance, we received several ceramic-to-metal seals from a tube company. We heat cycled two seals between room temperature and 420° C. One failed after 12 cycles and the other one after 15. Stress analysis is helpful to establish scaling laws after one size has been successfully tested. An example is the design of glass and ceramic seals.[45] In case of numerous installations at one laboratory, standardization of components is helpful to facilitate maintenance and to reduce the number of items which have to be stocked.

Fore Pumps. Pumping is usually done in several stages, since pumps operate only in a limited pressure range. Fore pumps reduce the pressure from atmospheric pressure and high vacuum pumps evacuate to the final pressure. If extreme requirements for freedom from oil do not exist, oil-sealed fore pumps with rotary piston are in common use. With two stages in series, the practical limit is the 10^{-3} torr range. Most of these pumps can be operated with a so-called gas ballast which prevents the deterioration of the pump oil by the absorption of pumped condensing vapors, in particular water vapor. Sometimes these fore pumps are connected to root pumps which operate at pressures of about 10^{1} to 10^{-4} torr.

If oil-free systems are desired, water aspirators can be used with refrigerated water. They will pump down to about 20 torrs. Steam ejector pumps have high pumping speeds. By using several stages in series, the low pressure limit can be extended to 10^{-3} torr.[46] Steam backstreaming under no load condition and the necessity to provide live steam can be objectionable. Another approach is the use of sorption fore pumps which are now commercially

available. They consist of a vacuum tight vessel which contains an adsorbent. When cooled to liquid nitrogen temperatures, the sorption will reduce the pressure to the 10^{-2} torr range. When warmed up again to room temperature, the gas desorbs.

Diffusion Pumps. The main high vacuum pump used to be the diffusion pump. Diffusion pumps contain either oil or mercury as pump fluid. Usually several stages are connected in series in one pump. The pump ceases to operate at the limiting fore pressure, when the vapor jet breaks down due to too many collisions with the pumped gas. The maximum fore pressure for oil diffusion pumps is in the lower 10^{-1} torr range. The last stage on the fore pressure side sometimes has an ejector nozzle to increase the fore vacuum tolerance. The ejector stage may be built into a separate pumping unit since it also requires higher vapor pressures. Such a pump is called a booster pump. Oil booster pumps have high pumping speeds in the 10^{-3} to 10^{-1} torr range. The fore pressure limit is in the 10^{0} torr range. Mercury pumps are often designed for higher fore pressures in the torr range. A four-stage mercury diffusion pump of 80 liters/sec speed is commercially available, which has a limiting fore pressure of 35 torr. Hence, it can be used with a water aspirator as fore pump.

The low pressure limit of diffusion pumps without traps is given by the vapor pressure of the pump fluid. Mercury has a pressure of 10^{-3} torr at room temperature. Diffusion of the mercury into the vacuum system is prevented by a liquid nitrogen trap. To avoid permanent transfer of the mercury from the pump to the trap, a freon baffle is put on top of the pump. This baffle operates

at a temperature of -30 to -35° C, slightly above the freezing point of the mercury. At this temperature, the mercury vapor pressure is about 10^{-6} torr. Most of the mercury condenses at the baffle and drops down into the pump.

The vapor pressure of pump oils at room temperature is in the 10^{-8} to 10^{-7} torr range. Without suitable trapping an appreciable amount of oil may stream back into the vacuum system. The backstreaming is reduced by good pump design, especially by providing special caps over the top jet.[47] The oil is cracked during the boiling process. Self-fractionating pumps remove volatile components from the oil through the fore vacuum. If the fore pressure is reduced by the use of another diffusion pump as a fore pump, ultra-high vacuum can be attained with refrigerated (-30° C) traps only.[48, 49] Also liquid nitrogen traps can be used. They have preferably cold walls to prevent the creepage of oil into the vacuum system. Adsorption traps using molecular sieves or aluminum oxide have also been employed successfully at room temperature to arrest the oil vapor.[50] They eventually saturate. New oils have been recently reported. Pressures of 5×10^{-10} torr and less than 4×10^{-11} torr, respectively, have been reached without any traps or refrigerated traps only.[49, 51] When evaluating results reported in the literature, it must be kept in mind that metal pumps are more likely to crack oils than glass pumps and that the walls between the gauge and the pump act as adsorption traps.

Most published data refer to air or nitrogen. If lighter gases than nitrogen are pumped, the ultimate pressure may be increased by back diffusion of these gases from the fore vacuum. This back diffusion can be kept at a

tolerable level by the use of a sufficient number of stages and lower fore pressures. Some data on back diffusion of helium and hydrogen were reported by Dayton.[52]

High Vacuum Sorption and Ion Pumps. The sorption of gases by surfaces is not only utilized in fore pumps and traps as mentioned above, but also in high vacuum pumps. Obviously, saturation effects will reduce the effectiveness with time. The sorption is usually performed by metal layers, especially titanium. In many cases these layers are evaporated directly on the wall of the vacuum vessel. This results in very high initial pumping speeds. Noble gases are not adsorbed at room temperature. They (and other gases) can be pumped into metal layers if the gas is ionized and the ions are buried in the metal. The pumping action of the ionization gauges is well known. Ion pumping exhibits saturation effects also. It is often combined with sorption pumping. Ion-sorption pumps are commercially available. Often the PIG discharge is used and the cathodes are made of titanium. The sputtered titanium is the adsorbing metal film. In one design one pair of cathodes is used for sputtering while another pair at a more positive potential acts as collectors.[53] Ion-sputter pumps have a memory effect with regard to the nature and amount of gas previously pumped. The typical behavior of a commercial two-element pump of 150 liters/sec speed is described by Normand and Knox.[54] These pumps have a fore pressure limit of about 10^{-2} torr. Since the power increases with pressure, a runaway condition can exist at higher pressures if the pump is gassy. The pumping speed falls off rapidly below 10^{-8} torr. Ion-sputter pumps

have the advantage of basic simplicity and absence of contaminating vapors. Their through-puts are rather small. They are not suited for installations with high gas loads. It would be highly desirable that the memory effect be taken into consideration in the rating sheets which can be easily misinterpreted otherwise. Titanium films in commercial pumps are also deposited by evaporation. Such pumps have been described in the literature.[55, 56] The theory and design of ion-sorption pumps is given in the review article of Holland.[57]

Sorption of evaporated metal has been studied extensively in conjunction with the need for improvement of the vacuum in high energy ion injection machines, such as OGRA. The coating is deposted on or near the wall of the discharge container. Clausing's results given in Table III (p. 81) show the improvement gained by cooling the substratum. Simonov and co-workers[58] found that the so-called Azotites (liquid nitrogen cooled titanium surfaces) are required to obtain satisfactory pumping action for hydrogen atoms and ions in OGRA. At the low temperature hydrogen is adsorbed without dissociation and no methane or water vapor production occurs. The critical temperature varies with the metal and is approximately -170° C.

Hunt and co-workers[59] found that hydrogen is rapidly adsorbed at solidified gas films of A, N_2, O_2, H_2O, N_2O and CO_2 at 11° K. The initial sticking probability is between 0.1 and 1 for coverages up to about 1 monolayer. Lazarev and Fedorova[60] pumped hydrogen by adsorption on activated charcoal cooled to liquid hydrogen temperature. Preliminary tests indicated that the same method could be used for helium when the carbon is cooled to liquid helium temperature.

Cryogenic Condensation Pumps. Adsorption of gases at cooled surfaces may be considered a special case of cryogenic pumping although, in a narrower sense cryogenic pumping is the removal of gas by condensation on a cold surface. Again high speed can be obtained by cooling the container wall directly. The pumping speed is given by Eq. (18) if the vapor pressure of the condensate can be neglected and the sticking coefficient is one. The advantage compared to adsorption pumping which has similar speed initially is that no saturation occurs. Therefore, this type of pumping is used in plasma propulsion test chambers where large quantities of gas have to be removed. When designing a cryogenic system, care must be taken to avoid spots of intermediate temperatures inside the vacuum system. Here vapor may condense initially and be given off later on, causing intermediate vapor pressures to persist inside the system for a long time. Cryogenic pumping is usually done with either liquid helium (boiling point -269° C) or liquid hydrogen (boiling point -253° C). P. A. Redhead[61] obtained pressures in the 10^{-13} torr range by dipping a finger-like extension of a small laboratory vacuum system into liquid helium. At -269° C hydrogen has a vapor pressure of 10^{-6} torr; apart from helium, it is the only substance that still has an appreciable vapor pressure at that temperature. At -253° C only hydrogen, helium, and neon still have appreciable vapor pressures; the vapor pressure of carbon monoxide at that temperature is less than 10^{-10} torr. D. J. Santeler[62] recommends this type of pumping for large chambers for simulating conditions in space. He suggests the use of panels cooled with liquid hydrogen, these being shielded against the radiation from the chamber by other panels cooled with

liquid nitrogen. Russian workers[63] have investigated two liquid hydrogen pumps having pumping speeds of 4000 and 13,000 liters/sec, respectively. Richly and co-workers[64] evaluated the use of a liquid nitrogen cooled condenser for sodium vapor, used on a test stand for plasma propulsion systems. Since hydrogen has such a high vapor pressure, Grobman[65] used the following scheme. He added oxygen and combined it with the hydrogen at a palladium catalyst with the formation of water vapor. The water was then condensed at liquid nitrogen cooled surfaces.

Molecular Pump. A pump which has gained some renewed popularity lately is the molecular pump. A pump of 140 liters/sec speed for air is commercially available. An ultimate pressure of less than 10^{-9} torr can be reached without traps after a mild bake, the only one possible. The ratio of fore pressure to high vacuum pressure increases rapidly for heavier gases. This explains the absence of oil vapor on the high vacuum side. The pumping speed decreases slightly as the molecular weight increases. This pump can be used as a combination pumping and gas injection system for hydrogen and helium in the 10^{-4} to 10^{-3} torr range by admitting the gas on the fore vacuum side.[66]

Hardware and Processing. Hardware for high vacuum systems has been commercially available for many years. Recently ultra high vacuum components and systems are also offered. Systems made of metal, ceramic and glass only with metal gaskets are used in ultra-high vacuum applications for bakeout at 450° C. After some pumping these systems have low gassing rates even without bakeout. Typical gassing rates of metals are 10^{-8} to 10^{-10} torr liters/cm^2/sec

after some pumping only and 10^{-15} to 10^{-16} torr liters/cm^2/sec after a 12-hour bake. Dayton[67] gives a comprehensive list of published outgassing rates of many different materials. Steinherz[68] studied the gassing of large cylindrical vacuum chambers of 3 1/2-5 ft diameter and 8-10 ft length. He calculated that the outgassing of the organic (neoprene?) gaskets constitutes a major gas source. Bakeouts for several hours at 260° C resulted in a pressure in the 10^{-9} torr range. Without bakeout the minimum pressure is about 10^{-8} torr. Teflon may be used as a gasket instead of neoprene. It is less gassy, but requires higher pressures and helium permeates through it. Recently Viton-A is becoming popular. It has low gassing rates similar to teflon if it is vacuum degassed before use (10^{-8} torr liter/cm^2/sec).[69] Metal gaskets are made mainly of gold, aluminum, and copper. We had some failures of copper due to oxidation during prolonged bakes and prefer the corner gold seal as stated above. If the mating flanges are larger than 8" or have different heat capacity, uniform and constant pressure should be assured by springs (Belleville washers).

Metal joining techniques are well known from the electronic tube processing. In particular, inert gas shielded arc welding is a very dependable method well suited for the assembly of experimental equipment. For metal-to-ceramic seals, we prefer the titanium hydride washer type seal on account of its excellent reliability (Ref. 44, Grove, p. 12)

All metal parts should be degreased and all components baked in vacuum before leak testing. Organic contaminants can also be removed by an air bake. At 450° C carbon will be removed from a surface in air at the rate of

7×10^{-4} grams/cm^2/hr. Feder and Koontz[70] discussed the detection and removal of organic contaminants. High temperature vacuum treatment removes adsorbed and absorbed gases. Only adsorption will recur when the parts are exposed to the atmosphere after cooling. Usually final cleaning of the assembled equipment is done by either bakeout or passing of a discharge. The latter procedure is often the simpler one if large equipment is involved. Several textbooks are available on the materials technology for vacuum engineering.[4, 5, 6] Reference 6 is the most comprehensive one.

GENERAL TEXTS

1. M. V. Ardenne, Tabellen der Elektronenphysik Ionenphysik und Übermikroskopie, Vol. 11, D. Kinetic Theory of Gases and High Vacuum Technique, p. 617-817 (Deutscher Verlag der Wissenschaften, 1956).

2. S. Dushman, J. M. Lafferty, eds., Scientific Foundations of Vacuum Technique, 2nd ed. (John Wiley and Son, 1962).

3. P. A. Redhead, J. P. Hobson, and E. V. Kornelson, Ultra High Vacuum, Advances in Electronics (in press).

4. W. H. Kohl, Materials and Techniques for Electron Tubes (Reinhold Publishing Company, 1960).

5. Max Knoll, Materials and Processes of Electron Devices (Springer, 1959).

6. W. Espe, Werkstoffkunde der Hochvakuumtechnik, Vol. I, 1959; Metals and Carbon, Vol. II, 1960; Glass, Silica, Ceramics, Mica, Asbestos, Vol. III; Sundry Materials Used in Vacuum Work (Deutscher Verlag der Wissenschaften).

REFERENCES

7. Guthrie and Wakerling, Vacuum Equipment and Techniques (McGraw-Hill, 1949) p. 43.

8. L. L. Levenson, N. Milleron, D. H. Davis, Molecular Flow Conductance, UCRL Rpt. No. 6253, presented at Intl. Congress on Vacuum Techniques and Applications, Paris, 1961.

9. J. H. deBoer, The Dynamical Character of Adsorption (Oxford, 1953) p. 30.

10. R. Gomer, The Science of Engineering Materials (John Wiley, 1957) p. 222.

11. S. Brunauer, P. H. Emmett and E. Teller, Jour. Am. Chem. Soc. 60, 309 (1938).

12. D. Lee, H. Tomaschke, and D. Alpert, "Adsorption of Molecular Gases on Surfaces and Effect on Pressure Measurement," Proc. 2nd Intl. Vac. Congress, Washington, 1961 (in press).

13. T. N. Rhodin, "Nucleation of Metal Oxide," Conference on Clean Surfaces, New York, N. Y., April 1962.

14. J. A. Becker, Solid State Physics 7, 379 (1958).

15. R. E. Clausing, "A Large Scale Getter Pumping Experiment Using Vapor Deposited Titanium Films," Proc. 2nd Intl. Vac. Congress, Washington, 1961 (in press).

16. J. P. Hobson, "Desorption of Adsorbed Gas and Re-emission of Gas Previously Pumped by Ionic Pumping," Proc. 2nd Intl. Vac. Congress, Washington, 1961 (in press).

17. B. M. W. Trapnell, Chemisorption (Butterworth, London, 1955).

18. C. Hayashi, 1957 Vac. Symp. Trans., p. 13.

19. J. Blears, Proc. Roy. Soc. A188, 62 (1946).

20. R. B. Burtt, J. S. Colligon, J. H. Leck, Br. Jour. Appl. Phys. 12, 396 (1961).

21. G. K. Wehner, General Mills Electronics Group Tech. Progress Rpt. No. 2240 (1961).

22. W. J. Lange and H. Riemersma, Westinghouse Scientific Paper No. 808-D801-P-3.

23. H. J. Karr, E. A. Knapp, and J. E. Osher, Phys. Fluids 4, 424 (1961).

24. G. E. Moore, J. Appl. Phys. 32, 1241 (1961).

25. G. J. Schulz and A. V. Phelps, Rev. Sci. Instr. 28, 1051-1054 (Dec. 1957)

26. Melling, AIEE, CP60-401.

27. Sheffield, PPL, unpublished, 10/3/60.

28. Futch, RSI 32, 1263 (1961).

29. R. T. Bayard and D. Alpert, Rev. Sci. Instr. 21, 571 (1950).

30. P. A. Redhead, Rev. Sci. Instr. 31, 343 (1960).

31. D. Mullaney, private communication.

32. P. A. Redhead, 1960 Vac. Symp. Trans., p. 108.

33. G. J. Schulz and A. V. Phelps, Rev. Sci. Instr. 28, 1051 (1957).

34. R. A. Haefer and J. Hengevoss, 1960 Vac. Symp. Trans., p. 67.

35. L. J. Varnerin and J. H. Carmichael, J. Appl. Phys. 28, 913 (1957).

36. N. W. Robinson and F. Berz, Proc. 1st Intl. Vac. Conf., Namur (1958) p. 378.

37. J. M. Lafferty, "Further Developments in the Hot Cathode Magnetron Ionization Gauge," Proc. 2nd Intl. Vac. Congress, Washington, 1961 (in press).

38. G. Martin, "Observations on the Operation of Hot Filament Gauges in Homogeneous Magnetic Field," Proc. 2nd Intl. Vac. Congress, Washington, 1961 (in press).

39. E. G. Apgar, PPL Tech. Memo. No. 120.

40. G. Lewin, G. Martin, Rev. Sci. Instr. 33, 447 (1962).

41. A. O. C. Nier, Rev. Sci. Instr. 11, 212 (1940).

42. H. Sommer, H. A. Thomas, and J. A. Hipple, Phys. Rev. 82, 697 (1951).

43. M. S. Jones and L. G. Smith, MATT-29, p. 8.

44. D. J. Grove, 1957 Vac. Symp. Trans., p. 9.
J. T. Mark and K. Dreyer, 1959 Vac. Symp. Trans., p. 176.

45. G. Lewin and R. Mark, 1957 Vac. Symp. Trans., p. 44.

46. V. V. Fondrk, 1957 Vac. Symp. Trans., p. 88.

47. B. D. Power and D. J. Crawley, Vacuum 4, 415, (1954).

48. R. A. Haefer and J. Hengevoss, Vakuum Technik, 9, 225 (1960).

49. B. D. Power and F. C. Robson, "Experiences with Demountable Ultra High Vacuum Systems," Proc. 2nd Intl. Vac. Congress, Washington, 1961 (in press).

50. M. A. Biondi, Rev. Sci. Instr. 30, 831 (1959).

51. K. Hickman, Nature 187, 405 (1960).

52. B. B. Dayton, Rev. Sci. Instr. 19, 793 (1948).

53. A. R. Hamilton, "Some Experimental Data on Parameter Variations with the Triode Getter-Ion Pump," Proc. 2nd Intl. Vac. Congress, Washington, 1961 (in press).

54. C. E. Normand and F. A. Knox, "Test of the Vac-Ion Pump, VA-1415," ORNL Rpt. 60-1-26, Jan. 7, 1960.

55. H. Huber and M. Warnecke, Advances in Vacuum Science and Technology, Vol. 1: "The Titanium Pump to Sustain Vacuum Electron Tubes," 1960.

56. R. G. Herb, Advances in Vacuum Science and Technology, Vol. 1: "Evapor-Ion Pump Development at the University of Wisconsin," 1960.

57. L. Holland, J. Sci. Instr. 36, 105 (1959).

58. V. A. Simonov, G. F. Kleimenov, A. G. Mileshkin, V. A. Kochnev, Salzburg Conf. on Plasma Physics and Controlled Thermonuclear Fusion Res., Sept. 4-9, 1961, Conf. Paper CN-10/255.

59. A. L. Hunt, C. E. Taylor, J. E. Omohundro, UCRL-6626, Dec. 4, 1961.

60. B. G. Lazarev and M. F. Fedorova, Soviet Physics - Technical Physics 6, No. 7, Jan. 1962, p. 624.

61. P. A. Redhead, 1958 Vac. Symp. Trans., p. 148.

62. D. J. Santeler, 1959 Vac. Symp. Trans., p. 129.

63. B. G. Lazarev, E. S. Borovik, M. F. Evedorova, N. M. Tsin, Ukrain. J. Phys. 2, 175 (1957).

64. E. A. Richley, R. J. Cybulski, T. A. Keller, "Experimental Evaluation of High Vacuum Condensers in Large Vacuum Facilities," Proc. 2nd Intl. Vac. Congress, Washington, 1961 (in press).

65. J. Grobman, "A Technique for Cryopumping Hydrogen," NASA TN-D-863.

66. E. G. Apgar, G. Lewin, D. Mullaney, Rev. Sci. Instr., 33, 985 (1962)

67. B. B. Dayton, 1959 Vac. Symp. Trans., p. 101.

68. H. A. Steinherz, Trans. Vac. Metallurgy Conf. 1960, p. 315.

69. A. Schram, "Desorption in Vacuum," Intl. Congress on Vacuum Techniques and Applications, Paris, 1961.

70. D. O. Feder and D. E. Koontz, Symposium on Cleaning of Electronic Device Components and Materials, ASTM Special Tech. Publication No. 246.

71. E. G. Apgar, "Difference Between Nude and Enclosed Ion Gauges on an Oil-Free System," Proc. of the 2nd European Symposium, "Vacuum", Frankfurt, 1963.

Some recent books on high vacuum technique include:

R. W. Robertson, T. A. Van der Slice, High Vacuum and Its Application, Prentice Hall, 1963.

A. E. Barrington, High Vacuum Engineering, Prentice Hall, 1963.

H. A. Steinberg, Handbook of High Vacuum Technology, Reinholt, 1963.

A. Guthrie, Vacuum Technology, John Wiley and Sons, 1963.

MAGNETIC FIELD AND COIL DESIGN

by

Robert G. Mills

Maxwell's Equations

All macroscopic electromagnetic fields are described by Maxwell's equations which can be written as:

$$\begin{aligned} \nabla \cdot \bar{D} &= 4\pi c^2 \sigma \\ \nabla \cdot \bar{B} &= 0 \\ \nabla \times \bar{E} &= -\frac{\partial \bar{B}}{\partial t} \\ \nabla \times \bar{H} &= \frac{1}{c^2}\frac{\partial \bar{D}}{\partial t} + 4\pi \bar{j} \end{aligned} \tag{1}$$

where the symbols have the usual meanings. The field vectors are related to each other by the relations

$$\begin{aligned} \bar{D} &= \bar{E} + \bar{P} \\ \bar{B} &= \bar{H} + \bar{M} \end{aligned} \tag{2}$$

when $\bar{P}$ and $\bar{M}$ are the polarization and magnetization vectors present in materials. Thus Maxwell's equations can be written in the following form:

$$\begin{aligned} \nabla \cdot \bar{E} &= 4\pi c^2 \sigma - \nabla \cdot \bar{P} \\ \nabla \cdot \bar{B} &= 0 \\ \nabla \times \bar{E} &= -\frac{\partial \bar{B}}{\partial t} \\ \nabla \times \bar{B} &= \frac{1}{c^2}\frac{\partial \bar{E}}{\partial t} + 4\pi \bar{j} + \frac{1}{c^2}\frac{\partial \bar{P}}{\partial t} + \nabla \times \bar{M} \quad . \end{aligned} \tag{3}$$

At this point rigor is generally abandoned because in materials $\overline{P}$ and $\overline{M}$ may be non-linear tensor functions of $\overline{E}$ and $\overline{B}$, awkward to handle analytically. For the most part we shall be able to ignore the properties of materials, setting $\overline{P}$ and $\overline{M}$ equal to zero. Furthermore, we shall not need the first equation. Consequently our fields will be described by the following equations:

$$\nabla \cdot \overline{B} = 0$$

$$\nabla \times \overline{E} = - \frac{\partial \overline{B}}{\partial t} \qquad (4)$$

$$\nabla \times \overline{B} = \frac{1}{c^2} \frac{\partial \overline{E}}{\partial t} + 4\pi \overline{j} \quad .$$

These are differential equations which summarize a variety of experimental observations. The physical significance is often clearer from integral forms of these equations, which are in a sense better representations of the physics of the situation. For example, the first of these three (by the divergence theorem) states that through a closed surface of any size or shape as much magnetic flux enters as leaves. In particular, it does not mean (as stated in some sources) that magnetic field lines are necessarily either closed or coming from and going to infinity. Applying Stokes' theorem to the second relation gives an equivalent statement that the number of volts per turn induced about any closed contour is measured by the rate of change of magnetic flux through that contour. Similarly the last equation means that the line integral of $\overline{B} \cdot \overline{d\ell}$ around any closed contour is measured by the total current through the contour.

D. C. Magnets

Elementary Considerations

For static magnetic systems, we may write

$$\nabla \times \overline{B} = 4\pi \overline{j} \quad \text{or equivalently}$$

$$\oint \overline{B} \cdot \overline{d\ell} = 4\pi I \quad . \tag{4a}$$

In systems of high symmetry this can be applied directly. For example, the field surrounding an infinite wire is given directly by

$$B\,2\pi r = 4\pi I \quad \text{or}$$

$$B = \frac{2I}{r} \quad \text{(emu)} \quad . \tag{5}$$

The field within an infinite solenoid can be derived by considering a short section of a thin toroidal coil and applying symmetry, thus

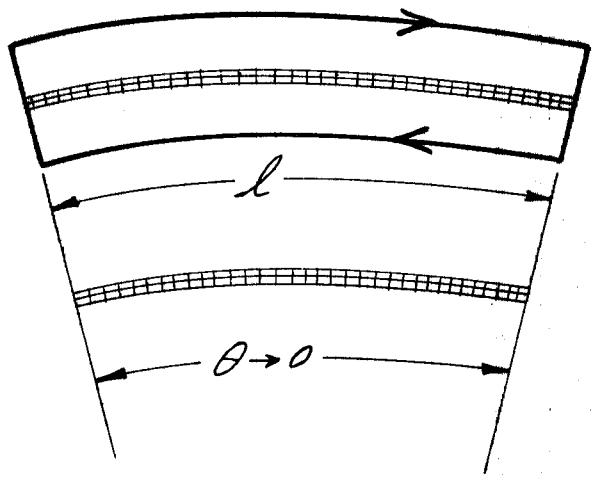

if there are n turns, each carrying current I, we get

$$B\ell = 4\pi n I \quad \text{or}$$

$$B = \frac{4\pi n I}{\ell} \quad \text{(emu)} \quad . \tag{6}$$

B is in gauss when I is in emu and ℓ in cm. For I in amperes,

$$B = 0.4\pi(n/\ell)I \quad .$$

An important "rule of thumb", accurate to about one per cent, to be carried in your memory is

$$B = \frac{1}{2}(nI/\ell)$$

where B is in gauss and nI/ℓ in ampere-turns per inch. Thus a 100 kilogauss field requires 200,000 ampere-turns per inch.

Analysis

In an academic course it is customary to introduce the vector potential and the Biot-Savart law and from them derive the fields of certain current configurations as examples and exercises. From the practical point of view, this most general approach should be reserved for the more difficult problems and known results for relatively simple configurations applied to analyze a field. We shall adopt this latter approach and illustrate the application of progressively more advanced techniques to more difficult problems.

1. Simple Configurations

The field of a straight wire and that of an infinite solenoid are given above in (5) and (6). A third simple configuration is a circular loop. The analysis, although more complex than the simple symmetrical cases given above, is essentially straightforward. It may be found in Smythe,[1] Sec. 7.04. The result is:

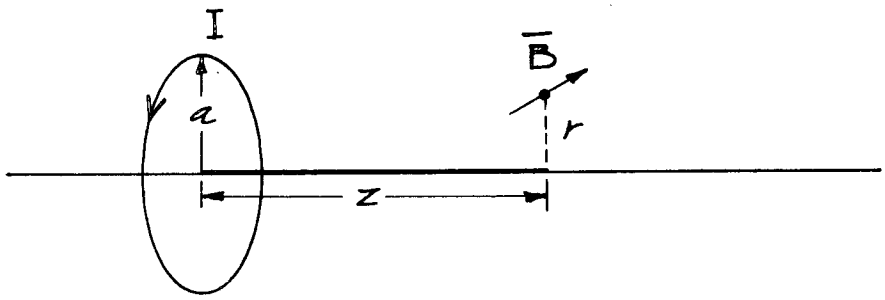

$$B_r(r,z) = \frac{2zI}{r[(a+r)^2+z^2]^{1/2}}\left[-K+\frac{a^2+r^2+z^2}{(a-r)^2+z^2}E\right]$$

$$B_z(r,z) = \frac{2I}{[(a+r)^2+z^2]^{1/2}}\left[K+\frac{a^2-r^2-z^2}{(a-r)^2+z^2}E\right] \qquad (7)$$

where K and E are complete elliptic integrals of the first and second kind, and $k^2 = 4ar[(a+r)^2+z^2]^{-1}$ (the eccentricity of the ellipse which is needed to find K and E from tables). Only on the axis does this reduce to a simple analytic expression, where $B_r = 0$ and

$$B_z(z) = \frac{2\pi a^2 I}{(a^2+z^2)^{3/2}} \quad . \qquad (8)$$

The field produced by a circular loop can also be expressed by expanding it in a series of associated Legendre functions. The derivation is given in Smythe,[1] Sec. 7.06 and will not be repeated here.

A great deal of the analysis of practical systems consists fundamentally of these results for single loops. The design techniques include various methods of combining these results in a convenient manner.

2. Straight Systems

Axial Symmetry

Desk calculators; tables. One should avoid using a method of greater complexity than is necessary for the task at hand. For relatively long solenoids, relation (6) above may be adequate, but it should be kept in mind that in the end plane of a semi-infinite solenoid, the field will (by symmetry) be one-half that of an infinite solenoid. Thus, if the solenoid is not long, (6) will give a field significantly higher than will be achieved at a given current.

Many practical coils consist essentially of an array of circular turns all carrying the same current, the array having a rectangular cross-section. If one is interested primarily in the field on axis, hand calculation is not out of the question. From (8) above, one can integrate directly to find B(z).

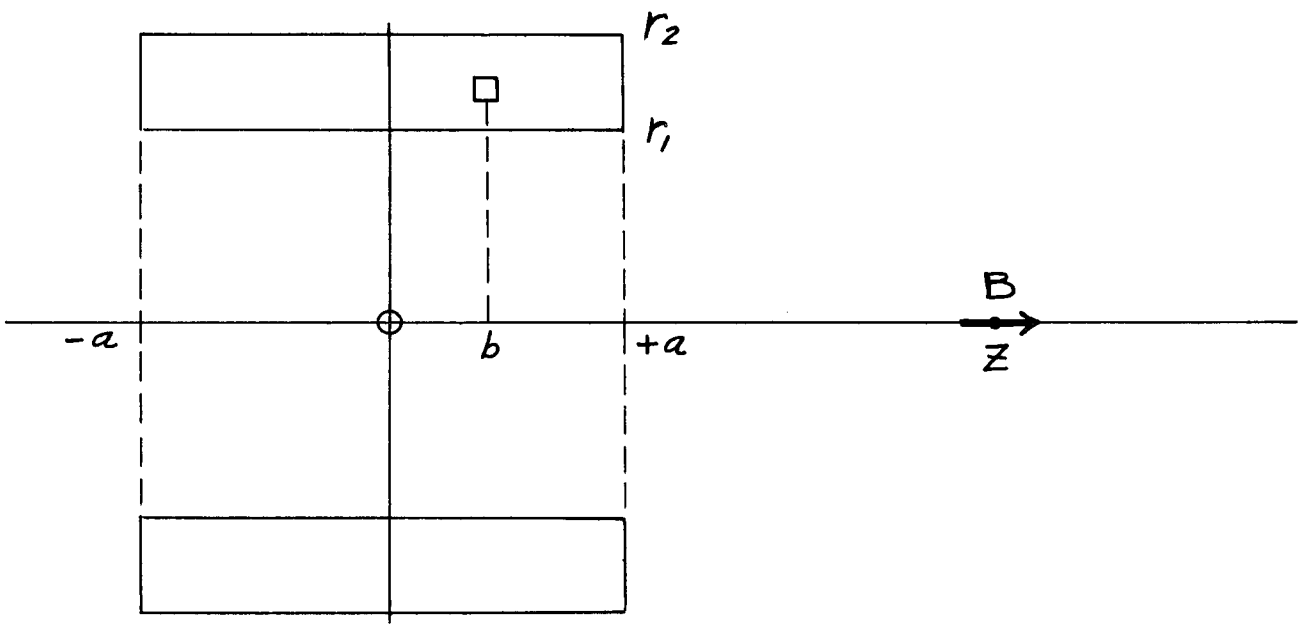

$$dB_z = \frac{2\pi r^2 j\, dr\, dz}{[r^2 + (z-b)^2]^{3/2}} \tag{8a}$$

$$B(z) = 2\pi j \int_{r_1}^{r_2} \int_{-a}^{+a} \frac{r^2\, dr\, db}{[r^2 + (z-b)^2]^{3/2}}$$

which gives

$$B(z) = 2\pi j \left[(z+a) \ln \left(\frac{r_2 + [r_2^2 + (z+a)^2]^{1/2}}{r_1 + [r_1^2 + (z+a)^2]^{1/2}} \right) - (z-a) \ln \left(\frac{r_2 + [r_2^2 + (z-a)^2]^{1/2}}{r_1 + [r_1^2 + (z-a)^2]^{1/2}} \right) \right]. \tag{9}$$

Here j is the effective uniform current density in abamperes/cm^2 in the rectangular cross-section of the coil as shown in the sketch. Clearly any set of standard coils arranged into an axially symmetric system could be analyzed by desk computer by using this result. The process would be tedious, but might be justified if only one analysis of a given situation were required. On the other hand, only values on the axis are given, and this may not be sufficient information for many purposes. Hand calculations involving relation (7) for off-axis fields are even more laborious.

Fortunately, tables are available to simplify this difficult task. One valuable collection of data[2] is based on the principle that if one has values of

B_z and B_r at all points in space generated by a thin semi-infinite solenoid of unit radius and unit linear current density, one can determine the field of any linear, axially-symmetric system. The actual system is represented by a finite (as few as possible) number, n, of semi-infinite solenoids, and the field at any point computed by addition of the n appropriate values for each component as taken from the tables.

The very useful Legendre polynomial method has been developed by Garrett.[3] This method applies to systems made of circular coils, and the solutions converge in any sphere within, but not including, any of the conductors. (This method also gives the less-often wanted field outside of a sphere containing the entire coil system.)

Since this method gives the field throughout a volume, it is superior to the elliptic integral method which gives the field at a point. If one must prepare an analytic solution for such a system, Garrett's method should be considered first. Numerous useful references are available to assist in field calculations and are listed in the bibliography.[4, 5, 6, 7, 8]

There are numerous approximation methods which may be of use for hand calculation; one, for example,[4] giving a simple formula for the variation in field strength along the axis of an infinite solenoid made up of current loops of radius R separated from each other by a space λ.

$$B = \frac{4\pi I}{\ell}\left[1 + 2\pi\left(\frac{R}{\lambda}\right)^{1/2} e^{(-2\pi R/\lambda)} \cos\frac{2\pi}{\lambda} z\right], \quad R >> \lambda .$$

An extension of this gives the field off-axis (but only in the neighborhood of the axis) and also gives expressions for practical coils. Another very helpful reference is due to Montgomery.[5]

The above methods are satisfactory for isolated problems, but rapidly become far too time-consuming if any appreciable volume of work is to be done. The following more powerful methods should then be utilized.

Conducting Analog. Resistance networks, conducting paper, rubber membranes and electrolytic tanks have been used to solve Laplace's equation for years. However, the most useful form for the solution of magnetic field problems of axial symmetry was developed by K. E. Wakefield in 1954. This device has been described in Project Matterhorn reports,[9,10] and a more complete description of its application is in preparation.[11] In this device the network represents the r, z plane, and current is introduced into the network at points to represent the current in a circular loop of the problem being solved. All the input currents are collected at the axis. The equipotential lines in the analog represent magnetic field lines of the problem.

The analogy is apparent from the following considerations. The analog represents a conducting sheet in which the conductivity varies inversely as one coordinate (called r) and is independent of the other (called z). The potential, v, in such a situation is governed by the following relation:

$$\frac{\partial^2 v}{\partial r^2} - \frac{1}{r}\frac{\partial v}{\partial r} + \frac{\partial^2 v}{\partial z^2} = k_1 r j \quad .$$

Compare this with the following relation for magnetic flux ϕ in an axially symmetric situation

$$\frac{\partial^2\phi}{\partial r^2} - \frac{1}{r}\frac{\partial\phi}{\partial r} + \frac{\partial^2\phi}{\partial z^2} = k_2 r j \quad .$$

Thus by scaling the proportionality constants, k_1 and k_2, constant potential lines represent lines of constant enclosed flux.

In the hands of a skilled operator, this device becomes a rapid and accurate tool for synthesis, a much more difficult problem than analysis, a point to be developed below.

Analysis of unusual configurations such as a stellarator's divertor can be done rapidly on such a unit. An afternoon's work can provide the data to give the magnetic fields everywhere in the system, the mutual inductance between the separate coils in the system, and the Lorentz force density at every point.

Although physically finite, the analog board is able to represent semi-infinite and infinite systems, either by the use of one or two reflecting boundaries or one or two remote boundaries. This is done in a reasonable size by changing the effective mesh size in the end portions. The central region is uniform and linear, but, of course, has a finite mesh size and a limit on its accuracy which is about one per cent.

Digital Computers. Access to a modern digital computer removes much of the objection to the slow analytic methods described above, although it is easy to find magnetic problems that tax their capacity and take many hours to complete. Examples of codes worked out here at Princeton by U. Christensen

for the IBM 650 are the following:

FIASCO (No. 366) calculates the field on the axis of a coaxial coil system. The system can consist of finite coils with rectangular cross-sections and of semi-infinite coils going to either plus or minus infinity. Use is made of (9) above.

FITS (No. 274) is similar to FIASCO with the coils represented by current sheets or circular filaments. Use is made of (8).

Helical Symmetry

All the above has been analysis of systems of axial symmetry. Occasionally the magnetic designer is interested in systems of helical symmetry. These are systems in which the field is a function of two variables, r and u, with u defined by

$$u = \ell\theta - kz \quad .$$

An analog has been constructed for solving this class of problems and has been described by Wakefield.[12] Although of great interest for stabilizing winding design and for helical inflectors, these geometries are of limited general application and will not be pursued further here.

3. Toroidal Systems

The ideal hollow toroidal coil is as elementary a problem as the straight wire or the infinite solenoid. The field is zero outside the coil, and within the coil varies as 1/r where r is the radius from the point in question to the axis of

torus. In fact our solution for the infinite solenoid in a previous section was this solution in the limit as $r \to \infty$. Unfortunately practical closed configurations are sufficiently different from the ideal case that this result is of little use. In some cases this result can be made the zeroth order of an expansion, but this perturbation method is generally restricted to applications in theory rather than for specification of coil structure to provide a desired field. In practice the coils will have access gaps, and frequently the assembly will have straight legs connecting the torus into a racetrack. If the sole purpose of the assembly is to create a given amount of flux within the container, detailed knowledge of the flux path is unnecessary, but if (as in a stellarator) the designer intends that the greatest possible volume of flux exist in which no flux line intersects a material wall, the problem becomes more complex. Keeping in mind the 1/r field variation within a torus, consider the joining of two ideal semi-infinite solenoids to an ideal semi-torus to form one end of a racetrack.

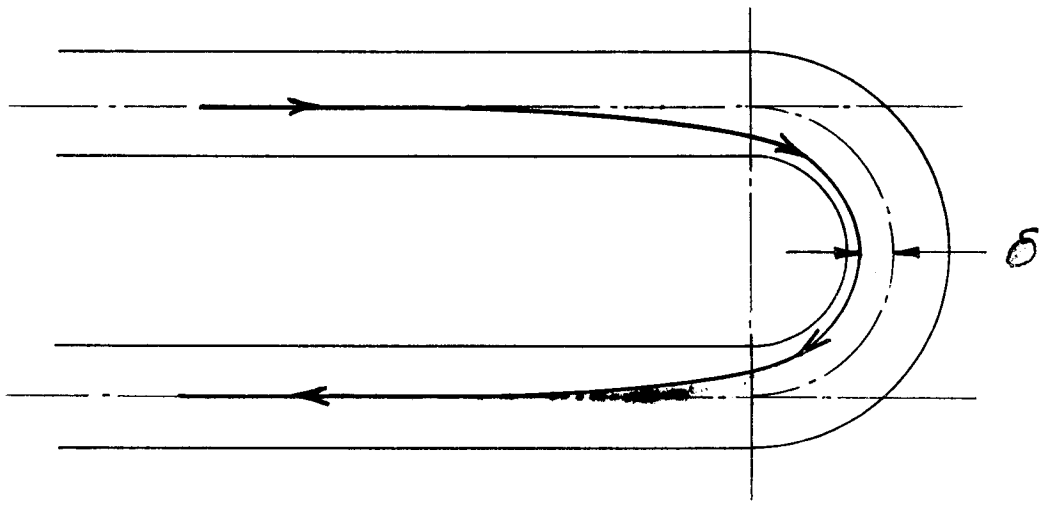

The magnetic field line which lies on the axis of a straight section remote from the bend will be displaced by δ within the tube centerline of the turn. It "takes a short cut" around the bend. If uncorrected, this would produce a serious loss of aperture in a plasma container. Thus in practice, toroidal systems retain little if any symmetry. The design of this type of system has been described by Christensen.[13] The method consists of tilting individual coils in the neighborhood of the end of the straight section about an axis perpendicular to the plane of the track to steer the line outwards. One must know the characteristics of the field of a single coil, which is discussed below, in order to apply the method.

4. General Systems

The Biot-Savart Law. It is customary in field analysis to introduce the solenoidal vector, $\overline{A}$, called the magnetic vector potential, such that

$$\overline{B} = \overline{\nabla} \times \overline{A} \quad . \tag{10}$$

Since

$$\overline{\nabla} \times \overline{B} = 4\pi \overline{j} \quad ,$$

and $\overline{\nabla} \cdot \overline{A} = 0$, we may take the curl of (10) to get $\nabla^2 A = 4\pi \overline{j}$. This is Poisson's equation with the solution

$$\overline{A} = \int\int\int \frac{\overline{j}\, dv}{r} \quad . \tag{11}$$

In the case of a system made up of a thin wire carrying a current I, $\overline{j}\, dv = j\, dA\, \overline{ds} = I\, \overline{ds}$ and (11) may be written

$$\overline{A} = \oint \frac{I\, \overline{ds}}{r} \quad . \tag{12}$$

This relation is frequently of use in analysis. The vector field $\overline{A}$ is determined first from these relations, and then $\overline{B}$ is found with (10). However (10) may be applied directly

$$\overline{B} = \overline{\nabla} \times \overline{A} = \int\int\int \overline{\nabla} \times \left(\frac{\overline{j}}{r}\right) dv \,, \quad \text{or}$$

$$\overline{B} = \int\int\int \frac{\overline{j} \times \overline{r}}{r^3} \, dv \quad . \tag{13}$$

This (the Biot-Savart law) is sometimes written as

$$dB = \frac{I \sin\theta}{r^2} \, ds \,,$$

but note that this is not a vector equation, since $\overline{dB}$ and $\overline{ds}$ are at right angles. A better form is

$$\overline{dB} = \frac{I \overline{ds} \times \overline{r}}{r^3} \quad . \tag{14}$$

Biot and Savart established this in 1820, but only for straight currents. It is sometimes called Ampere's law. Ampere investigated the forces between two closed current-carrying loops.

Attention should be called to the fact that (14) has quite a different meaning from that of (8a). The latter is a correct statement as it stands, whereas (14) represents part of an entire system which must be integrated to give meaningful results. Incorrect results may be developed if (14) is applied unthinkingly for only part of a circuit. A simple example is the following: consider two current elements, A and B, of separate circuits located as shown in the following sketch.

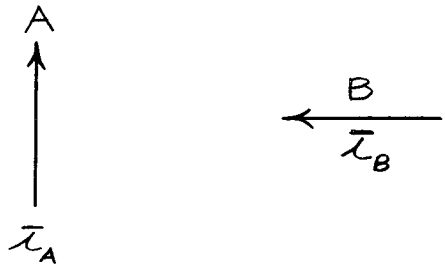

Apply (14) and consider the Lorentz force, $\bar{j} \times \bar{B}$. One concludes that current element A exerts a force on current element B, but current element B has no effect on element A, a result which would have bothered Newton. Of course, if the two entire loops are treated, the two forces are equal and opposite.

When integration of (13) and (14) over an entire conductor system is carried out, one can solve for an arbitrary arrangement. Although this would be difficult analytically, it is well suited for digital computer techniques.

Digital Computer Analysis. Relation (14) is used in FORTRAN program CIHELIF 263, written by U. Christensen. This program calculates the field produced by current filaments which may be portions of circles, helices, or straight lines. The integrations are done by Simpson's rule.

It should not be inferred, however, that lack of symmetry requires that the Biot-Savart law be applied. For example, COLF 298, written by Christensen and Rabinowitz, will calculate the field produced by any number of regular coils in any position in space. For points off-axis the coils are approximated by a number of circular current filaments in accordance with Lyle's Theorem[14] and the field evaluated with the help of Hasting's approximations for elliptic integrals. Lyle's Theorem is most useful in the region near the axis and midplane of a coil. At remote points one should check to make sure that excessive errors are not being introduced by the use of this theorem. If they are, other representations of the current distribution should be used.

5. Analysis and Synthesis

All of the above has been directed to the problem of determining the magnetic field generated by a given set of currents. Unfortunately, most magnetic design problems are the inverse of this, viz., to find a current distribution that generates a desired field. This problem of synthesis is considerably more difficult, and direct solutions are rare.

If one is interested in generating a vacuum field that is everywhere parallel to an arbitrary bounding surface and fulfills a given set of other requirements, this can be synthesized directly for any required field distribution (provided, of course, that $\nabla^2 \bar{B} = 0$ within the vacuum). This can be seen by applying (4a) to a region of the boundary.

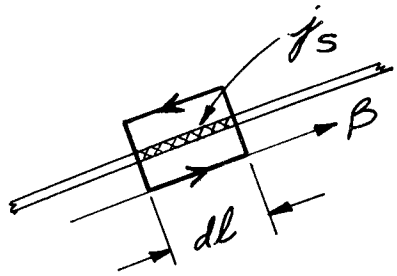

A surface current, j_s, must be provided such that

$$4\pi \int j_s \, d\ell = \oint \bar{B} \cdot d\ell = B(x, y, z)\, d\ell$$

where $d\ell$ is taken parallel to B. This is equivalent to stating

$$\bar{j}_s = \frac{\bar{B} \times \bar{n}}{4\pi}$$

where $\bar{n}$ is a unit normal to the surface. With this surface distribution of cur-

rent, the required field is produced within the container, and there is zero field outside. To the author's knowledge this has not yet been made use of in practice, although it has been suggested for a pulsed apparatus in which the current distribution is automatically provided.[15]

The problem of direct specification of practical coils with spaces between them in terms of the required fields within has not yet been solved as far as the author is aware. There is room here for important contributions to the art.

In practice, synthesis amounts to repeated analyses, improving the proposed system by trial and error. This is the reason why the analog board is such a powerful tool, particularly in the early stages of a design problem. An experienced operator will be able to guess at an almost suitable conductor arrangement in the first place, and will be able to correct it locally and rapidly in the second.

6. Forces

The Lorentz force density, $\overline{f} = \overline{j} \times \overline{B}$ is the most convenient way to evaluate the total force on an element of conductor, thus the body force $\overline{F}$ is given by

$$\overline{F} = \int\int\int [\overline{j} \times \overline{B}]\, dv \quad .$$

If $\overline{j}$ and $\overline{B}$ are explicitly known, $\overline{F}(x, y, z)$ is determinable.

Another method of force determination makes use of the stress-energy tensor, where one uses a surface integral,

$$F_i = \int_S T_{ij}\, dS_j$$

$$T_{ij} = B_i B_j - \frac{1}{2}\delta_{ij} B_k B_k$$

where a repeated index represents summation over all three components. This is occasionally useful when the current distribution is not explicitly known, or when the field bears a particularly simple relation to a boundary surface. If the field is everywhere parallel to a surface, it can be treated as exerting a pressure, $B^2/8\pi$, against that surface; if everywhere perpendicular, the field transmits a tension of $B^2/8\pi$ across the surface. In general, the field vector, $\bar{B}$, bisects the angle between the vector $\bar{n}$ normal to the surface and the vector $\bar{F}$. But warning: do not take these ideas too literally. The total force on a volume of material is the sum of all these surface terms over the entire surface; individual surface pressures or tensions are meaningless. The stress-energy tensor gives no information as to the location of the forces.

In practice, the stress-energy tensor is often used to assist one's intuitive idea of how big the forces are, but it is the Lorentz force that is used almost exclusively to evaluate them.

Properties of Materials

In all branches of engineering the soaring aspirations of designers come up against the hard facts of the properties of materials, and competent design rests on a foundation of a good understanding of these limitations. This is particularly true in coil design. Time and space limitations allow only an introduction to this subject in these lectures.

Conductors. For materials of interest for coil construction, Ohm's law is given by $\rho\bar{j} = \bar{E}$, and this implies that to maintain a current density, $\bar{j}$, one

must transform electrical energy into heat at a rate $j^2\rho$. With the exception of superconductors, a topic treated separately below, ρ is sufficiently high that the supply of this electrical power, and its removal as heat, is an engineering problem for all solenoids, becoming rapidly more difficult above a few thousand gauss. Copper is the only practical material. Aluminum's resistance is up 60% over copper, too severe a penalty, and silver is far too expensive. OFHC (oxygen-free-high conductivity) copper should be annealed dead soft and a resistivity of two microhm-cm should be assumed in design calculations. The copper cross-section should be designed with generous corner radii to avoid cutting through the insulation which will be wrapped on the conductor.

The resistivity is so high, even for the best available material, that much effort has been expended in designing coils of optimum performance. This work applies generally only to short coils, and those interested in this class of coil should refer to the work of Fabry,[16] Bitter,[17] and Gauster.[6] For long solenoids, the resistance of the magnet can be lowered only by increasing the outside radius, and this improvement is slow (inversely proportional to the logarithm of the ratio r_o/r_i). Bitter magnets of small bore have been built where this ratio reached 10, but systems of larger size would become too bulky and the ratios generally lie in the region of two or three. If a bend is required in the magnet, large o. d./i. d. ratios cannot be used.

At temperatures of 10°-20° K, the normal resistance of many pure materials drops to very low values. Unfortunately the magnetoresistive effect prevents one from taking advantage of this property in some materials

(e.g., copper), but both sodium and aluminum have seemed attractive, and low temperature developmental magnets have been built of these materials at the Lawrence Radiation Laboratory at Livermore and at the Boulder Laboratories of the National Bureau of Standards. The power savings in these materials is sufficient to pay for the refrigerator losses, although the capital investment in the refrigerator tends to be high. Interest in cryogenic normal magnets has decreased with the awakening development of superconductors, but they nevertheless may be of future use.

Insulators. Coils are frequently potted by vacuum impregnation with an epoxy resin, with glass fiber reinforcement. This gives a very strong, satisfactory mounting. However, it is a mistake to depend on this potting for dielectric strength, and one should always assume that there will be low pressure gas bubble voids in the epoxy. Individual conductors should be wrapped, and pancakes should be separated by solid disks of material without penetrating slots. There is always a temptation to skimp on insulation in order to increase the space factor. This is a mistake. Pay no attention to dielectric strength figures of so many hundreds of volts per mil. Never use less than 10 or 20 mils of insulation and preferably maintain 30 or 40.

Supports. Tables and external framework can well be constructed of aluminum provided one can take the increased deflection resulting from a low Young's modulus, but structural members for the magnet itself should be of stronger materials. It will almost always be necessary to use non-magnetic materials; therefore ferrous steels must be austenitic. The 400 series of stain-

less steels is martensitic and not suitable. Furthermore many of the 300 series (18-8), normally austenitic, will develop appreciable permeability under work-hardening or welding due to ferritic transformations. Table I summarizes the properties of a few useful alloys.

Cooling. Heat transfer is a discouragingly slow process. Unless one is contemplating a very large magnet (beyond the size of anything built yet), the cooling problem will be the ultimate physical limitation. For general purposes, hollow copper, carrying deionized water, will be most practical. We recommend holding the inlet pressure to 300 psi and the outlet temperature to 180°F for general laboratory purposes for reasons of personnel safety. In this regime the flow is given by the empirical relation

$$P = \frac{(L/D)V^2}{5000}$$

where P is the pressure in psi and V, in ft/sec, the equivalent velocity determined by the mass flow rate and the diameter, D, of the channel. The cooling rate follows immediately from an allowed temperature rise of 80-100°F of the water passing through the coil. The magnet should be protected by provision to turn it off should the flow fail.

Table II gives comparative operating characteristics of a number of machines which represent reliable, conservative design.

The Auxiliary Use of Iron. Iron can be used advantageously to shape the field if the vacuum B is not large compared to the saturation level. One example of this is in the Q-3 machine where iron rings are used to reduce the field varia-

Table I. Properties of Structural Materials

Name	Yield Stress[2]	Push-Pull Fatigue Stress	Ultimate Stress	Machinability	Cost	Availability	Remarks
305	35,000[1]	28,000[6]	82,000[1]	Good	0.67	Usually by spec.order	Spinning grade makes this more machinable than 304 and 310
A-286	37,000[8] 152,500[8]	40,000[6, 9]	97,000[1] 167,000[8]	Fair with slow speeds and lubric.[7]	1.90	Usually by spec.order	Finish machining usually must be done after final hardening process
HNM	56,000[1] 147,000[4]	75,000[4, 6]	116,000[1] 184,000[4]	Fair with slow speeds and lubric.[7]	0.90	Usually by spec.order	Finish machining usually must be done after final hardening process
K-Monel	90,000[1] 130,000[3]	40,000[1, 5] 45,000[1, 5]	130,000[1] 170,000[3]	Fair with slow speeds and lubric.[7]	1.25	Usually by spec.order	Finish machining usually must be done after final hardening process
304	30,000[1]	27,000[6]	85,000[1]	Good	0.66	Readily	After some cold work or machining, tendency to become slightly magnetic
310	40,000[1]	32,000[6]	95,000[1]	Good	1.08	Readily	Expensive
Tension-wound glass fiber reinf. epoxy			30,000 -60,000[10]	Excellent	2.00 -2.50	Readily	This material varies greatly in strength and price. However it is almost universally easy to machine.

[1] Annealed condition
[2] 0.2% offset.
[3] Cold rolled - full hard age hardened.
[4] Full hard - 2150° 1/2 hour, oil quench.
[5] 10^8 cycles.
[6] 10^7 cycles.
[7] The harder these materials, the more difficult to machine.
[8] This range is extremely wide, and upper and lower limits are included.
[9] Yield 85,000 psi (0.2% offset).
[10] Varies greatly - yield and ultimate are the same. No fatigue data could be found.

Table II. D.C. Coil Performance

Machine	Field	Current	Conductor	Cross-Section	Current Density	kw/ft	Gal/min.[2]	Cooling Velocity ft/sec	ΔP, psi	ΔT, °F
L-2 Open	4,000	400 A	130 ft long 33 T/coil 2 pancakes/coil coil 3/4" thick	.250 x .250 9/64" dia. hole	A/in.^{2} 17,800	40	0.5	10	220 psi/ coil	60
L-2 Closed	8,000	400 A	"	"	"	80	0.5	10	220 psi/ coil	60
E-R*	9,000	2,250	26 ft long 13 T/coil 2 pancakes/coil Nom. 1" thick	1.00" x .33 x .160 (shaved) dia. hole .370" x .330" x .160" dia. hole	20,000[1]	66	1.0	15	105	50
Q-3	29,900	4,400	180 ft long 24 T/coil 2 pancakes/coil 1.36" thick	.770" x .595" x .360" dia. hole	14,900	570	4.9	15.8	300	130
C	12,000	10,150	41 T/coil[3] 334 ft/coil	.51" x 2.81 x[3] (.30 x .80" dia. hole)	8,200[3]	400	5.9[3]	10[3]	60[3]	23
95 kΓ Solenoid (not constructed)	95,000	10,000	90 ft/coil 43 T/coil 2 pancakes/coil 2.2" thick	1.00" x .661" x ($\frac{1}{2}$ x $\frac{1}{4}$ dia. hole)	18,500	1100	7.80	20	300	205
G-1	30,000 max.	1,600	104 ft 2 strands in parallel	.365" x .365" x .220" dia. hole	17,000	250	1.8	16.1	300	105

*The U-bend coils are shaved and cross-section of the coil varies from 1.00" x .330" to .370" x .330". The straight section coils are all .370" x .330".

[1] For straight section coils (worst condition).

[2] All coils in parallel for water cooling.

[3] Varies -- B-41 coil given.

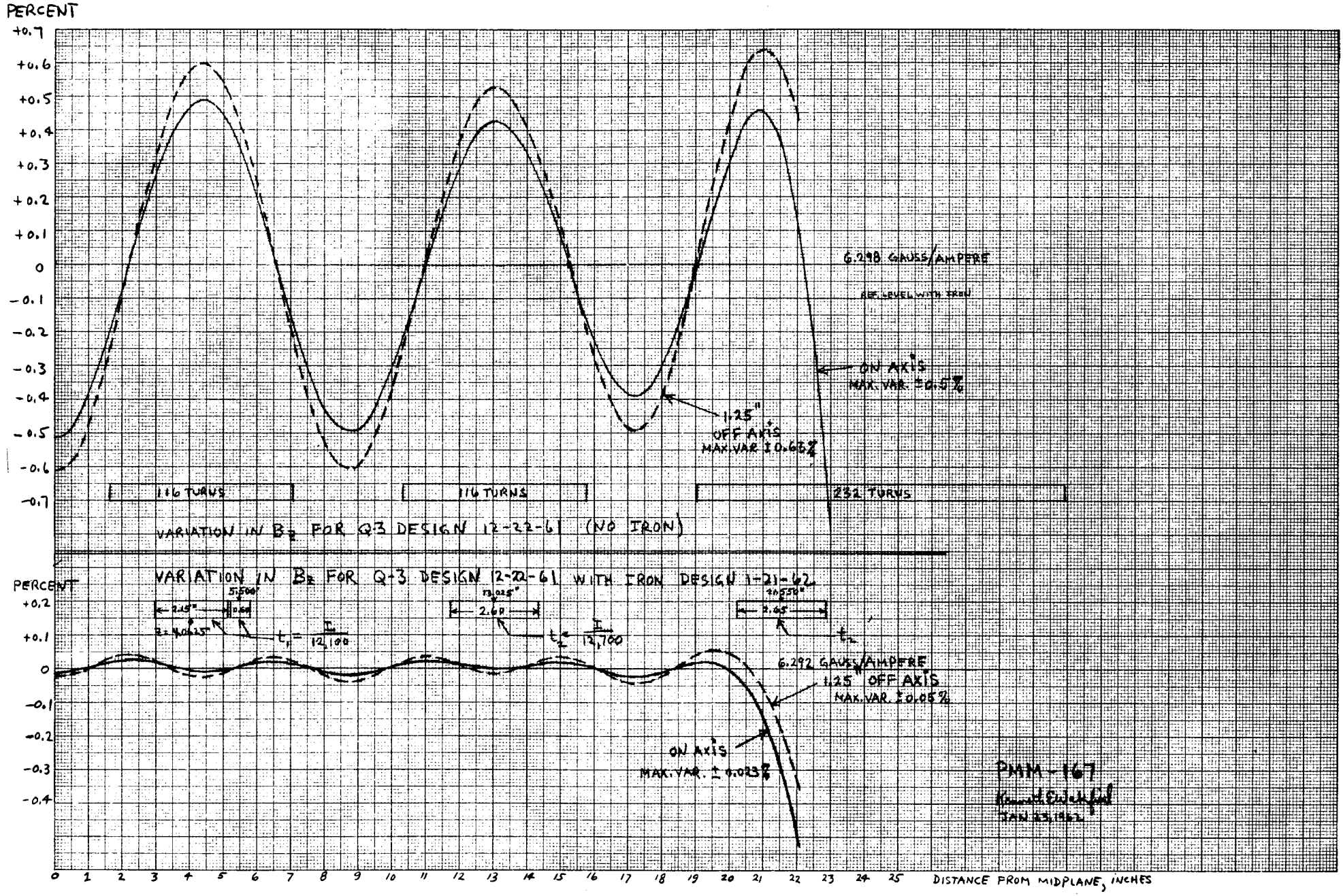

PMM-167
JAN 23, 1962

tion by a factor of twenty from ± 0.5% to ± 0.025%. The iron is, of course, saturated, and different operating levels require different amounts of iron for optimum performance. Figure 1 illustrates the effect.

Pulsed Magnets

The Skin Effect and the Proximity Effect. To treat time-varying fields, we must go back to Eqs. (4), but we shall still drop the displacement current term which is negligible except for very rapidly changing fields. Also substituting $\bar{j} = \bar{E}/\rho$, we get

$$\bar{\nabla} \times \bar{B} = \frac{4\pi}{\rho} \bar{E} \quad .$$

Taking the curl of both sides and making use of the first two equations of (4) we get

$$\nabla^2 \bar{B} - \frac{4\pi}{\rho} \frac{\partial \bar{B}}{\partial t} = 0$$

which is the diffusion equation. Thus a magnetic field diffuses into a metal, or alternatively, a metal (by eddy current induction) tends to shield its interior from an applied magnetic field. For a sinusoidal, externally applied field, $B_o e^{j\omega t}$, the simplest one-dimensional case has the solution within the metal

$$B_o \exp[-(4\pi\omega/\rho)^{1/2} x] \quad .$$

Thus the field (and therefore the current) is confined to a "skin" adjacent to the surface. For copper the skin depth, δ, is given approximately by

$$\delta = 6.6\nu^{-1/2} \text{ cm}$$

e.g., at 60 cps, δ is 0.85 cm. If the dimensions of a conductor are as large or larger than the skin depth, the current will flow in only a part of the conductor and its effective resistance will be higher than the dc value. This is well known in rf circuitry where one is accustomed to considering all the current flowing in the thin outside skin of an isolated conductor. This diffusion property has very surprising effects if we consider the rapid pulsing of a multi-layer coil. The exact solution has been worked out by Tenney and Wells.[18] As illustrated in their paper, an n-layer coil carrying a series current, I, actually has a current of nI flowing on the inside surface of the inner conductor and a current -(n - 1)I flowing on the outside surface of the inner conductor. Since losses go as j^2, it is immediately apparent that any coil which is wound of a conductor thick compared to a skin depth must be a single-layer coil or the resistive losses will be excessive. We therefore divide pulsed coils into slow and fast categories depending on whether the skin depth is large or small compared to the conductor thickness.

Slow Pulses. A pulsed coil will usually require a higher voltage supply than a dc system in order to fulfill the requirements of

$$\overline{\nabla} \times \overline{E} = - \frac{\partial \overline{B}}{\partial t} \quad .$$

In slow pulses, this may be a fairly modest requirement of the order of ten volts per turn, but a machine can easily have a thousand turns or more. A convenient way of supplying the energy is from a charged capacitor bank. The basic circuit is as shown below.

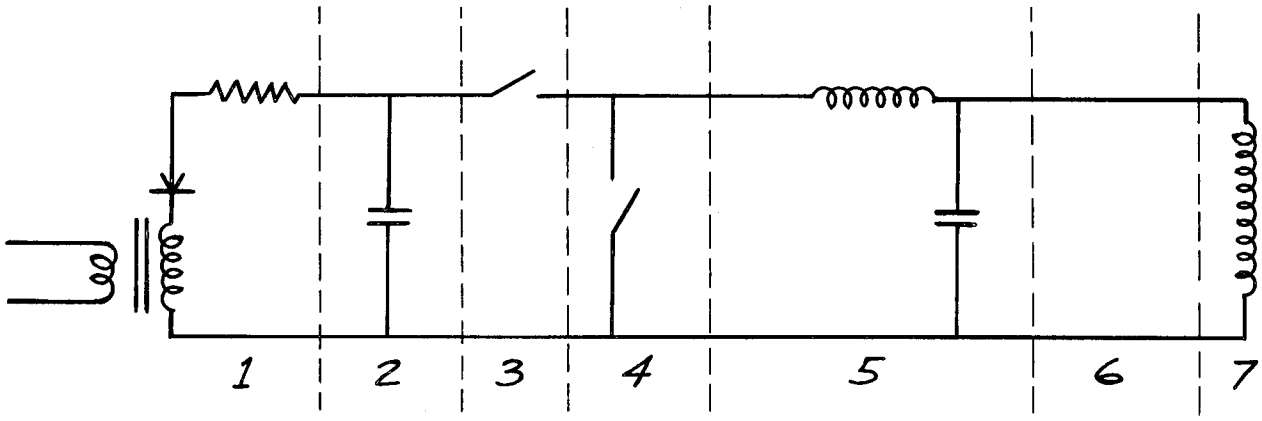

The elements from left to right are: 1) the charger, 2) the storage bank, 3) the firing switch (usually an ignitron), 4) the crowbar switch, 5) the low pass filter to prevent voltage rise on the load faster than the transmission time of the voltage wave along the load, 6) the transmission line between the storage facility and the load, 7) the solenoid.

For slow pulses such a system is adequately described by a series LCR circuit, and it rings. The crowbar closes at V = 0, and the load current decays with its characteristic time constant. The efficiency, η, of transfer of stored energy to peak magnetic field energy is given by

$$\eta = e^{\frac{-\arctan 2Q}{Q}}$$

which can be of the order of 90% in practical designs. The problem of energy conservation is somewhat different for these systems of constant energy from that of dc systems of constant power. A dc coil's power requirement for a given internal field decreases monotonically with increase in outer diameter. In con-

trast, at a given stored energy, the internal field of a pulsed coil will grow rapidly with outer radius in the regime of very thin coils (because R is decreasing, increasing Q and the transfer efficiency), but it will go through a maximum at relatively low o.d./i.d. ratios and then begin to decline because the given energy is now being distributed throughout a larger volume. Nevertheless it is usually wise to design above the maximum point because the fall-off in peak field is not precipitous, and the decreasing R above the maximum transfer point increases the crowbarred time constant so that the crowbarred field is available for a longer useful period. These points are illustrated in Fig. 2.

Fast Pulses. As mentioned above, a fast pulse coil must be single-layered if not a single turn. This tends to make its inductance considerably less than the multi-layered slow pulse coils. This shifts the energy transfer problem from a simple one of Q to the voltage dividing action resulting from the inductance in the storage bank and the transmission line becoming significant compared to that of the load. For this reason transmission lines have to be many parallel lines or large sheets of copper closely spaced.

An interesting form of single turn coil is the flux concentrator, a slotted solid conductor used to shape a pulsed field. Since $\int \bar{B} \cdot \bar{d\ell} = 4\pi I$, for any path, the name is a misnomer, the device being more accurately described as a flux eliminator since the device removes flux from its interior by eddy currents. For a short coil, however, it can be used to intensify a field by distributing B unevenly along the path of integration in accordance with the designer's plan.

Figure 2.

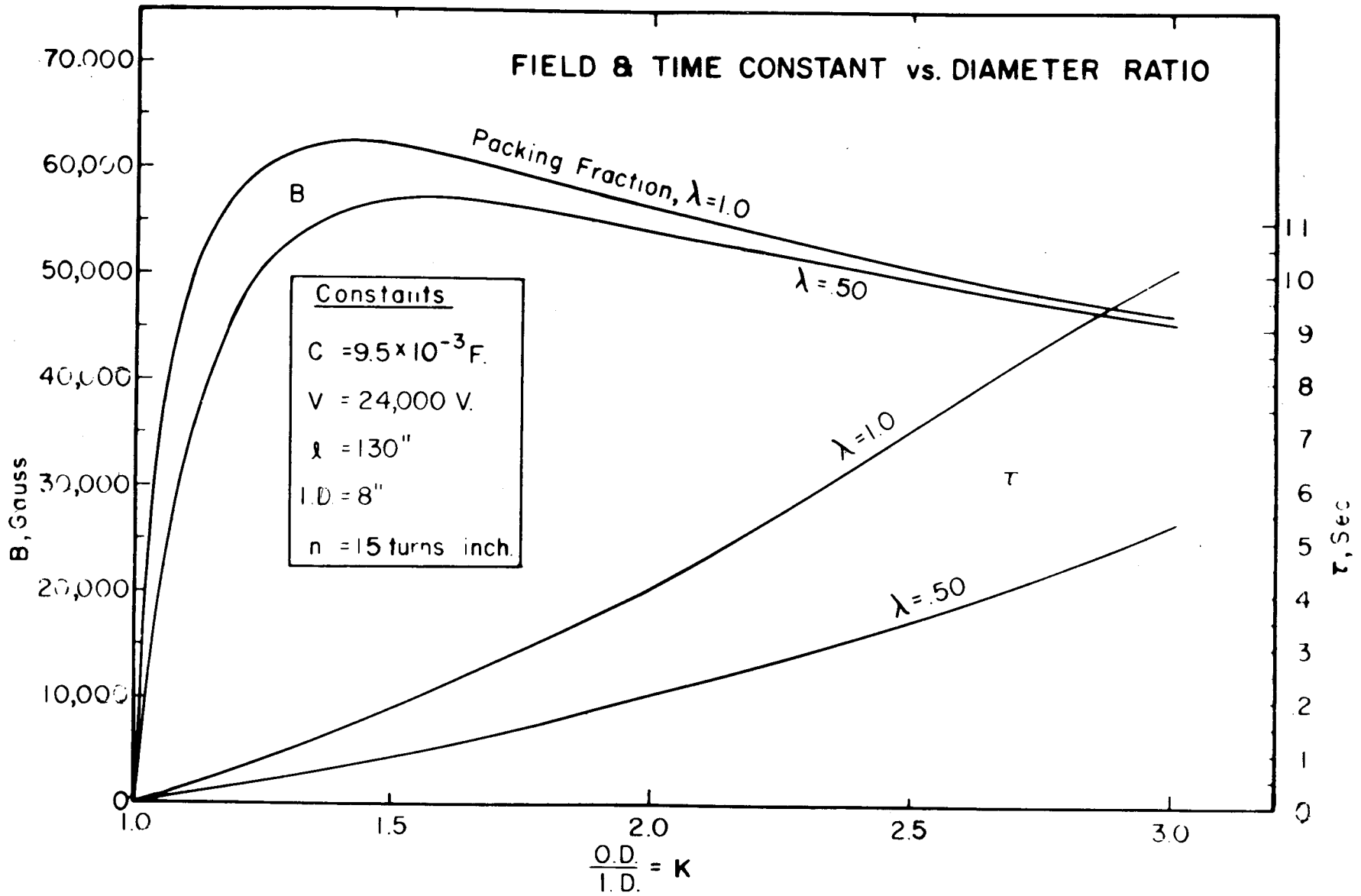
FIELD & TIME CONSTANT vs. DIAMETER RATIO
Packing Fraction, λ=1.0
B
λ=.50
λ=1.0
τ
λ=.50
Constants
C =9.5×10⁻³F.
V = 24,000 V.
ℓ =130"
I.D = 8"
n =15 turns inch.
B, Gauss
τ, Sec
70,000
60,000
50,000
40,000
30,000
20,000
10,000
0
11
10
9
8
7
6
5
4
3
2
1
0
1.0
1.5
2.0
2.5
3.0
O.D. / I.D. = K

True flux concentration has been accomplished by Fowler[19] at Los Alamos, who establishes a high flux inside a conducting cylinder and then collapses the cylinder by implosion via conventional explosives. Multi-megagauss fields have been produced for microseconds.

The question of how high in pulsed fields one can go without destroying the apparatus has been discussed by Furth, Levine, and Waniek.[20] Since the skin depth increases with higher resistivity, good conductivity is of less importance than achieving a high melting point and large specific heat of the conductor. Three to four hundred kilogauss are reasonable, and 750 may be possible with tungsten.

Current Development

Design of the Force Distribution. Forces have always been a serious problem for the designer of coils for high fields. A fifty kilogauss field is roughly equivalent to a pressure of 100 atmospheres. With very few exceptions coils have been designed of circular loops, orienting $\bar{j}$ and $\bar{B}$ at right angles. The design is carried out to produce a given, desired field, usually at a minimum expenditure of power. The resulting forces are accepted, and a suitable mechanical structure designed to withstand them. As the technology develops to higher field strengths, the forces grow ($\sim B^2$), and this problem becomes critical. Interest is now growing in designing coils that will generate forces only in mechanically convenient locations.

The ultimate in such a program would be a force-free coil, i.e., one in which j and B are everywhere parallel. Is such a system possible? The problem

arose in astrophysics,[21, 22, 23] and became of interest in technology.[20, 24] Mathematical solutions for truly force-free fields, i.e., a field in which

$$\bar{\nabla} \times \bar{B} = 4\pi \bar{j}$$

and

$$\bar{j} = \alpha \bar{B}$$

or

$$\bar{\nabla} \times \bar{B} = 4\pi \alpha \bar{B} \tag{15}$$

do exist, but the current systems extend to infinity. Such a system on a finite scale is not possible. According to the virial theorem, a system of energy U must be held together by forces F_i according to

$$\Sigma \bar{F}_i \cdot \bar{r}_i = U \quad .$$

The form of this theorem for a coil system is

$$\int\int\int (\bar{j} \times \bar{B}) \cdot \bar{r} \, dV = \frac{1}{8\pi} \int\int\int B^2 \, dV \quad ,$$

and can be derived directly.[24]

Within this limitation there is room for a great deal of ingenious design, and some experimental coils have been produced.[25, 27] A clear application for a stellarator, for example, would be coils which, when mounted in a racetrack configuration, would have zero net force on each unit coil. Note that this is quite a different situation from "force-freeness". Such systems always require more power than conventional coils.

Superconductivity. Materials of zero electrical resistance would remove two of the big engineering problems in field design -- the supply of electrical

energy to the coil and its removal as heat. It would have no direct effect on the force problem, but since no power penalty would be attached to the types of windings described in the previous section, they would become relatively more attractive than they are when one is designing with conventional conductors. Such materials exist and have been known since their discovery in 1911. Many metallic elements and alloys are superconductors, but numerous problems have delayed their application. The normal to superconducting transition is a phase change which takes place at cryogenic temperatures well below that of liquid hydrogen (20° K). This means that in practice the coil must be cooled by liquid helium (4.2° K), an expensive commodity. Secondly, a sufficiently high magnetic field will quench the superconducting state. A curve of quenching magnetic field versus temperature has a parabolic shape for a pure, ideal (sometimes called "soft") superconductor as sketched here:

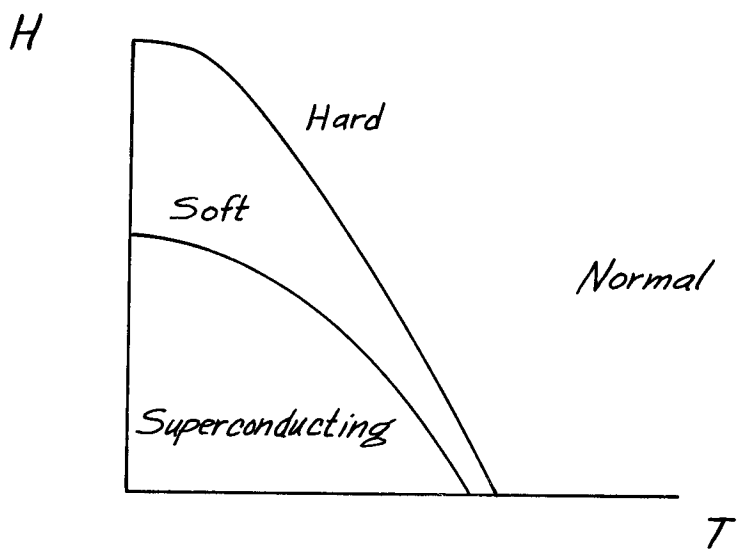

A "hard" superconductor is severely work-hardened and many are brittle intermetallic compounds. These tend to have higher transition temperatures, and steeper phase boundary plots.

Most superconductors have low quenching fields, but development of this fascinating region in technology has been spurred by the appearance of alloys of extraordinarily high capabilities. They are all hard superconductors and present mechanical difficulties not yet thoroughly understood. Nb_3Sn may have application in fields as high as 160 to 180 kilogauss, but is extremely brittle. Alloys of niobium (called columbium in industry) and zirconium may be useful to 70 kilogauss and are quite easy to handle. Available in ten and twenty mil diameter wire, it is still very expensive (50 cents per foot), but is being sold in considerable quantity for experimental coils. At least two companies now market small superconducting solenoids as a commercial product.

Design of a superconducting solenoid begins with a curve giving the constant temperature, critical current versus field characteristics for the wire to be used. Such a curve will be similar to the following sketch which is for 0.020" Nb-Zr alloy (25% zirconium). Unfortunately accurate curves are not available for any particular commercial sample of wire. The characteristics depend on both the mechanical and heat treatment that the sample has received.

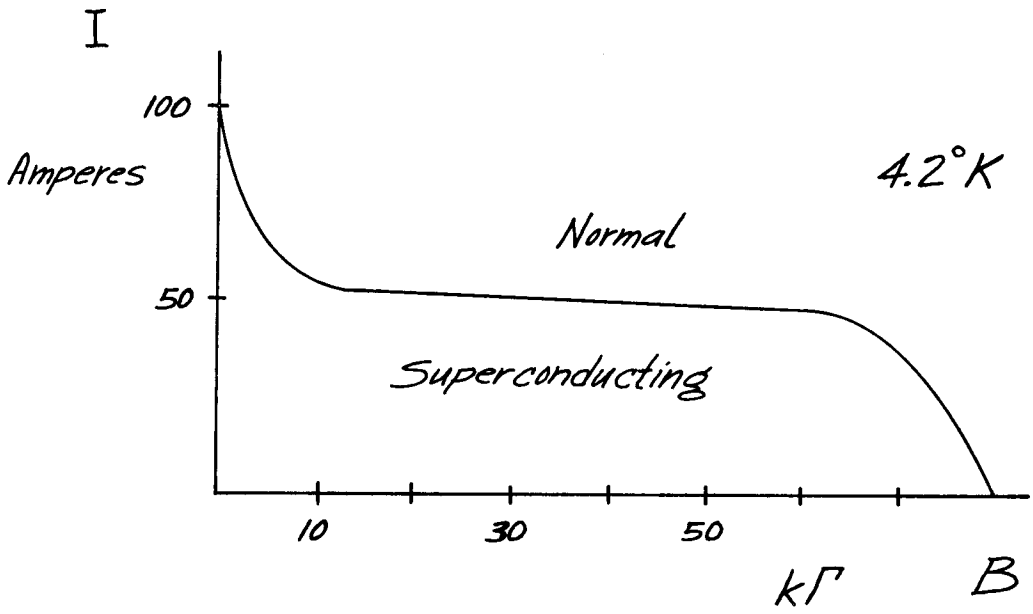

Presumably production control will eventually result in a product of reasonably consistent characteristics. Another phenomenon that has been observed possibly is not related to the production method. It is called "training." After a solenoid has been wound, it is found that cycling through the critical current can push its value upwards. Although this is encouraging, other effects are not. It has been found that a motion of one turn of a coil, or other mechanical disturbance, may trigger off a spontaneous quenching of the state. Numerous laboratories are involved in studying these problems and when the material price has dropped an order of magnitude, practical magnetic devices using superconductors will become important.

REFERENCES

1. W. R. Smythe, Static and Dynamic Electricity (McGraw-Hill Book Co., Inc., New York, 1939).

2. N. B. Alexander, A. C. Downing, ORNL-2828, Oak Ridge National Laboratory (1959).

3. M. W. Garrett, J. Appl. Phys. 22, 1091 (1951).

4. G. R. North, ORNL-2975, Oak Ridge National Laboratory (1960).

5. D. Bruce Montgomery, J. Terrell, AFOSR-1525 (M.I.T.) (1961).

6. W. F. Gauster, Communications and Electronics, AIEE 52, 822 (1961).

7. F. Gaume: Jour. de Recherche du Centre Nationale de la Recherche Scientifique (Bellevue), 43 and 45 (1958), translated to English in Lincoln Laboratory's Rpt. No. M81-12 (1959) and M81-12 Suppl. 1 (1960).

8. M. W. Garrett, Tables of the Internal Magnetic Source Functions U_n for Thick Solenoids and Disk Coils (Edwards Brothers, Ann Arbor, 1953).

9. K. E. Wakefield, PM-S-23 (Princeton Univ.) (1958).

10. U. Christensen, TM-71 (Princeton Univ.) (1959).

11. K. E. Wakefield (to be published).

12. K. E. Wakefield in ORNL-2745, Oak Ridge National Laboratory (1959).

13. U. Christensen in High Magnetic Fields, M.I.T. Press (1962).

14. T. R. Lyle, Phil. Mag. 3, 310 (1902).

15. J. B. Taylor and K. V. Roberts, Phys. Rev. Letters 8, 52 (1962).

16. C. Fabry, L'Eclairage Electrique XVII, 43, 133 (1898).

17. F. Bitter, Rev. Sci. Inst. 7, 479 (1936); 8, 318 (1937); 9, 373 (1939).

18. F. Tenney and D. R. Wells, TM-54 (NYO-7995) (Princeton Univ.) (1958).

19. C. M. Fowler in High Magnetic Fields, M.I.T. Press (1962).

20. H. P. Furth, M. A. Levine, and R. W. Waniek, Rev. Sci. Inst. 28, 949 (1957).

21. S. Chandrasekhar and E. Fermi, Astrophys. J. 118 (1953).

22. S. Lundquist, Arkiv Fysik 2, 361 (1950).

23. R. Lust and A. Schluter, Z. Naturforsch. 12a, 850 (1957).

24. D. R. Wells, R. G. Mills, A. Bahr, R. L. Peskin, TM-111 (Princeton Univ.) (1960).

25. D. R. Wells and R. G. Mills in High Magnetic Fields, M. I. T. Press (1962).

26. K. E. Wakefield in High Magnetic Fields, M. I. T. Press (1962).

27. H. P. Furth, Sci. 132, 387 (1960).

MICROWAVES

by

Robert W. Motley

The lectures on microwaves will be confined to three topics: (1) the propagation of high frequency waves in a highly ionized plasma, (2) a discussion of microwave techniques for measuring time varying electron densities, and (3) a short discussion of thermal noise emitted from plasmas and its measurement by means of a radiometer.

Propagation of Microwaves in Plasma

We consider first the propagation of high frequency waves in a plasma. The term "high frequency" implies that we can neglect the motion of ions. For the description of the waves we will need the Maxwell equations and the Boltzmann or momentum equation, which one obtains by taking the second velocity moment of the Boltzmann equation and averaging over the velocity coordinates. These fluid equations characterize the plasma by an average density n and velocity v. The equations are

$$\frac{\partial \bar{v}}{\partial t} + (v \cdot \nabla)\bar{v} = \frac{e}{m}(E + \frac{\bar{v}}{c} \times \bar{B}) - \frac{\nabla p}{mn} = 0$$

$$\nabla \cdot E = 4\pi e(n - n_o)$$

$$\nabla \times \bar{E} = -\frac{1}{c}\frac{\partial \bar{B}}{\partial t}$$

$$\nabla \times \bar{B} = \frac{1}{c}\frac{\partial E}{\partial t} + \frac{4\pi n e}{c}\bar{v} \quad .$$

Taking the pressure to be $p = nkT$, $\nabla p = \gamma kT \nabla n$, and linearizing,

$$\bar{E} = \bar{E}_1$$

$$\bar{B} = \bar{B}_o + \bar{B}_1$$

$$\bar{v} = \bar{v}_1$$

$$n = n_o + n_1 \quad .$$

Then

$$\frac{\partial \bar{v}_1}{\partial t} - \frac{e}{m}(\bar{E}_1 + \frac{1}{c}\bar{v}_1 \times \bar{B}_o) + \gamma \frac{V^2}{n_o} \nabla n_1 = 0 \tag{1}$$

$$\nabla \cdot \bar{E}_1 = 4\pi e n_1 \tag{2}$$

$$\nabla \times \bar{E}_1 = -\frac{1}{c} \frac{\partial \bar{B}_1}{\partial t} \tag{3}$$

$$\nabla \times \bar{B}_1 = \frac{1}{c} \frac{\partial \bar{E}_1}{\partial t} + \frac{4\pi n_o e}{c} \bar{v}_1 \tag{4}$$

$$V^2 = \frac{kT}{m} \quad .$$

We have four equations and four unknowns, n_1, v_1, E_1, B_1. Dropping the 1 subscript and taking the time derivative of Eq. (4),

$$\nabla \times \frac{\partial \bar{B}_1}{\partial t} = \frac{1}{c} \frac{\partial^2 \bar{E}}{\partial t^2} + \frac{4\pi n_o e}{c} \frac{\partial \bar{v}}{\partial t} \quad .$$

From Eq. (2),

$$\nabla n = \frac{1}{4\pi e} \nabla(\nabla \cdot \bar{E}) \quad .$$

Defining the square of the plasma frequency,

$$\omega_p^2 = \frac{4\pi n_o e^2}{m} \quad ,$$

we have from Eq. (1)

$$\frac{\partial^2 \bar{E}}{\partial t^2} + \omega_p^2 \bar{E} - \gamma V^2 \nabla(\nabla \cdot \bar{E}) - c \nabla \times \frac{\partial B}{\partial t}$$

$$+ \frac{m}{e}\left\{\frac{1}{c} \frac{\partial \bar{E}}{\partial t} \times \bar{B}_o - \nabla \times \bar{B} \times \bar{B}_o\right\} = 0$$

and

$$\nabla \times \nabla \times \bar{E} = -\frac{1}{c} \nabla \times \frac{\partial \bar{B}}{\partial t} \quad .$$

For simplicity we drop the terms in B_o. This procedure is justified only when $\bar{E} \parallel \bar{B}_o$.

$$\frac{\partial^2 \bar{E}}{\partial t^2} + \omega_p^2 \bar{E} - \gamma V^2 \nabla(\nabla \cdot \bar{E}) + c^2 \nabla \times \nabla \times \bar{E} = 0 \quad .$$

This is the wave equation. Assume a solution of the form $\bar{E} = \bar{E}_o e^{-i\omega t + i\bar{k} \cdot \bar{r}}$. Then

$$\nabla \cdot \bar{E} = i\bar{k} \cdot \bar{E}$$

$$\nabla \times \bar{E} = i\bar{k} \times \bar{E} \quad .$$

We consider two cases:

Case 1. $\bar{k} \times \bar{E} = 0$. Electrostatic waves.

$$\omega^2 = \omega_p^2 + \gamma V^2 k^2 \quad .$$

In the zero temperature approximation these waves are purely standing, i.e., $d\omega/dk = 0$. The frequency spectrum is quite narrow:

$$\omega^2 = \omega_p^2\left(1 + \frac{\gamma V^2 k^2}{\omega_p^2}\right) = \omega_p^2(1 + \gamma D^2 K^2)$$

$$(\gamma D^2 K^2)_{max} \approx 1 \ .$$

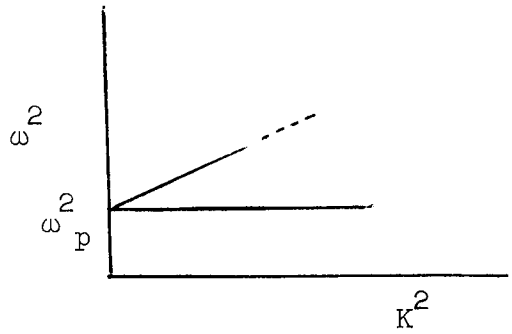

Therefore the frequency spectrum extends from ω_p to about $1.4\omega_p$, where strong Landau damping sets in. One cannot obtain the damping from a fluid analysis such as this. Velocity distribution must be taken into account from the Boltzmann equation.

These electrostatic waves have not been useful in exploring plasmas because they have proved difficult to excite. A type of wave motion in plasma-filled waveguides studied by Trivelpiece and Gould is closely related to these waves. In their work, most of the energy of the wave was present in the region between plasma and waveguide. Therefore the propagation is more sensitive to the exact dimensions of the system than to the intrinsic plasma properties.

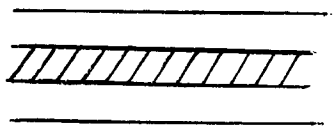

Case 2. $\bar{k} \cdot \bar{E} = 0$. Electromagnetic waves.

For electromagnetic waves $\bar{k} \perp \bar{E}$.

$$\omega^2 = \omega_p^2 + k^2 c^2 \ .$$

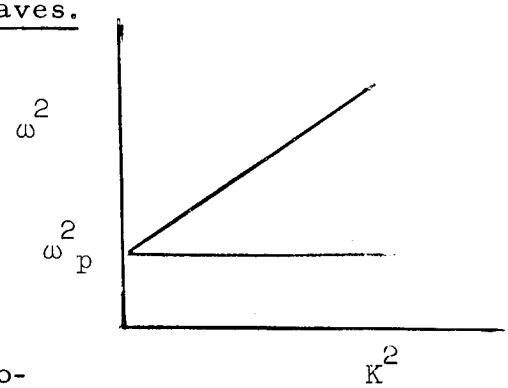

The spectrum of electromagnetic waves extends from the plasma frequency up. Unlike the electrostatic waves there is no high frequency cut-off. It is the above equation which forms the basis for the most generally useful microwave measurement in

plasmas: the determination of ω_p^2 and therefore the electron density.

Practical Systems

In order to obtain a useful sensitivity in the microwave measurement one must use a microwave frequency slightly in excess of the plasma frequency. The following table gives the plasma frequencies ($f_p = \omega_p/2\pi$) corresponding to typical plasma densities

n	f_p		λ_o	Plasmas
10^{10}	0.9×10^9	commercial	33 cm	gas discharges
10^{12}	9.0×10^9	commercial	3.3 cm	cesium plasmas
10^{14}	90×10^9	developmental	.33 cm	stellarators, mirrors
10^{16}	900×10^9	infra-red	.033 cm	pinches

Microwave Cavities. In addition to the frequency criterion for the measurement of electron density, there is also a length scaling criterion. If $\lambda >> D$, where D is a characteristic length of the plasma, the beam technique is not suitable and the microwave cavity technique must be used. For this purpose the TE_{020} mode in a cylindrical cavity is often used. One merely measures the shift in the resonant frequency of the cavity when the plasma sample is introduced. For low densities

$$\frac{\Delta f}{f} \sim \frac{\omega_p^2}{\omega^2} = \frac{n}{n_c} .$$

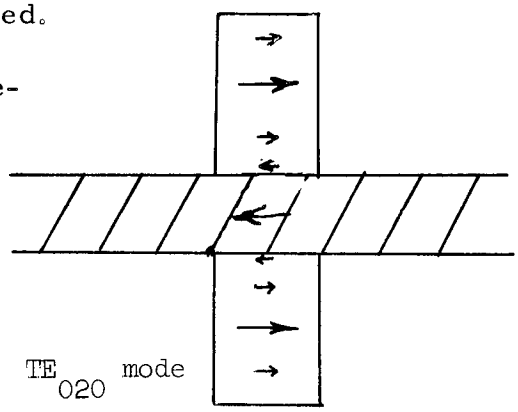

This, the usual technique in gas discharges, is not particularly convenient for

infrequent pulsed discharges. For more details on the microwave cavity technique one should consult the papers of Sanborn Brown.

Microwave Beams. If $\lambda << D$, then it is best to employ a microwave beam. The microwave signal is sent across the plasma and the phase at the opposite side is compared with a reference phase. At this Laboratory we use horn antennas, since they provide a reasonably confined beam in a small area. Our standard frequency is 70 Gc or 4.3 mm; $n_c = 6 \times 10^{13}$. A typical diameter for a B type stellarator is 43 mm; then $L/\lambda_o = 10$. Signals at 35 Gc, which are often used, are marginal in the B devices. We also have an operating 140 Gc or 2 mm system.

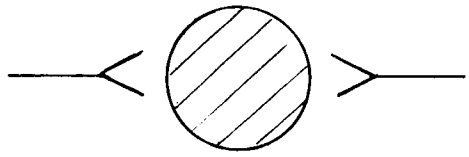

For the purpose of interpreting measured phase shifts the dispersion relation is most convenient in the form of an index of refraction μ,

$$\mu = \frac{ck}{\omega} = \left(1 - \frac{\omega_p^2}{\omega^2}\right)^{1/2} .$$

The phase shift (in fractions of a wavelength) of a signal traversing a length of plasma L is

$$\Delta\phi = \frac{1}{\lambda_o}\int_o^L (\mu - 1)dx = \frac{1}{\lambda_o}\int_o^L \left[\left(1 - \frac{\omega_p^2}{\omega^2}\right)^{1/2} - 1\right] dx \quad .$$

If ω_p^2 is independent of x, and since

$$\frac{\omega_p^2}{\omega^2} = \frac{n}{n_c} \qquad (n_c = \text{critical density})$$

$$\Delta\phi = \frac{L}{\lambda_o}\left[\left(1 - \frac{n}{n_c}\right)^{1/2} - 1\right] \approx \frac{1}{2}\frac{L}{\lambda_o}\frac{n}{n_c} \qquad (\text{if } n << n_c) \quad .$$

If the electron density is small compared with the critical density, the phase shift is a linear function of the electron density.

Microwave Bridges.

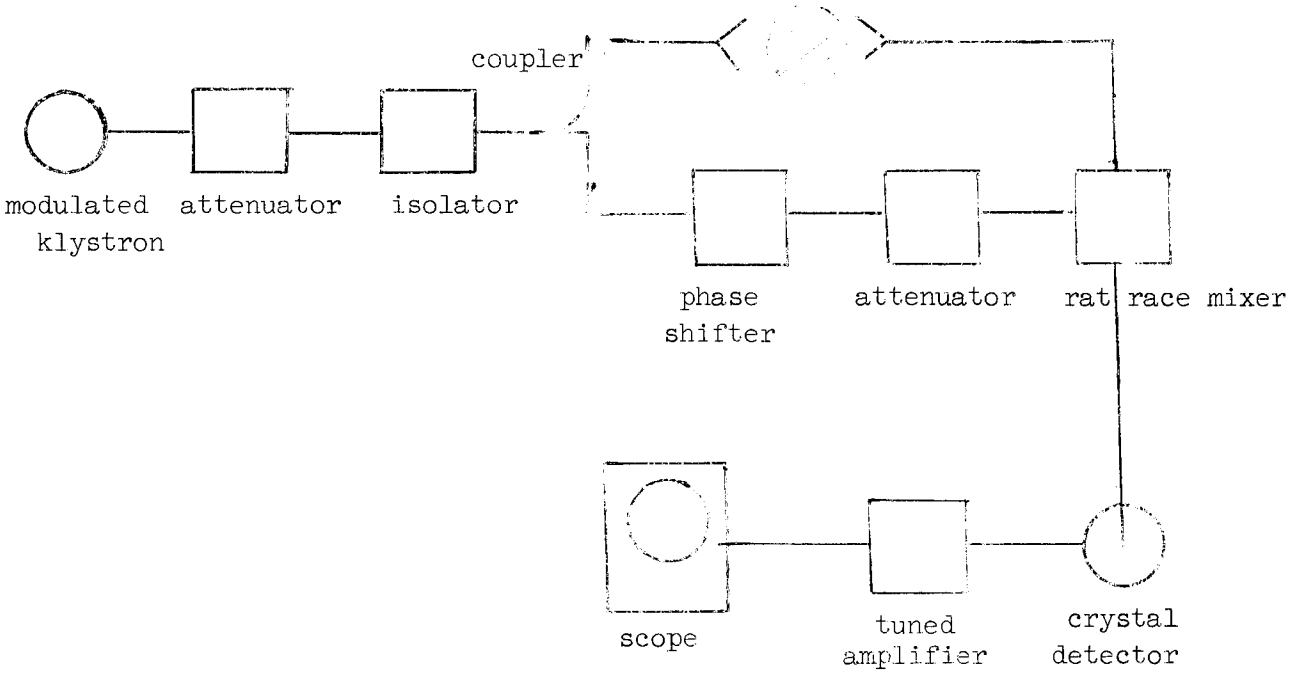

The above sketch shows a typical simple microwave bridge for measuring a transient phase shift. A modulated klystron sends a microwave signal to a bridge, where the power is split by a coupler. Part of the signal is sent through the plasma and part through a reference path. The signals are reunited in a rat race mixer, where they are detected by a silicon crystal. Phase shifts introduced by the plasma cause changes in the output level of the mixer. If there

is a square wave detector,

$$A^2 = (\bar{A}_1 + \bar{A}_2)^2 = A_1^2 + A_2^2 + 2A_1 A_2 \cos(\Delta\phi)$$

where $\Delta\phi$ is the plasma phase shift.

One of our systems square wave modulates the klystron at 455 kc. The detection amplifier is tuned to 455 kc and has a transient bandwidth of 50 kc. With this system one can easily measure phase shifts as small as 10^o and with effort can improve this. The sinusoidal variation of the output signal with phase shift is often a big disadvantage when the plasma density is not increasing or decreasing monatomically, and often leads to confusion in the analysis. For this reason we usually use a more sophisticated bridge for routine measurement of plasma density.

Magnetic Fields. For special purposes it is possible to take advantage of the additional resonances which a magnetic field provides. To derive the dispersion relation in the presence of a field, it is necessary to include the B_o terms in the wave equation. One finds that for certain conditions the refractive index is greater than one, and that "pass and step" bands arise in the frequency spectrum. A particularly interesting mode of propagation is that of a right-handed circularly polarized plane wave along the magnetic field. The dispersion relation is

$$\mu^2 = 1 - \frac{\omega_p^2}{\omega^2} \quad \frac{1}{1 - \frac{\omega_b}{\omega}} \quad .$$

If $\omega_b/\omega > 1$, then there is no sharp cut-off density for this mode, which is

commonly called the "whistler mode" and is of importance in understanding low frequency propagation in the ionosphere.

Density Profile Measurements. If two probing microwave frequencies are used simultaneously, it is possible to infer a first moment of the distribution of electrons across the plasma column. The simplest method is to select one frequency which is just cut off at the center of the plasma. This immediately gives the density at the center n_m

$$n_m = n_{c_1} = \frac{m}{4\pi e^2}\,\omega_1^2 \quad .$$

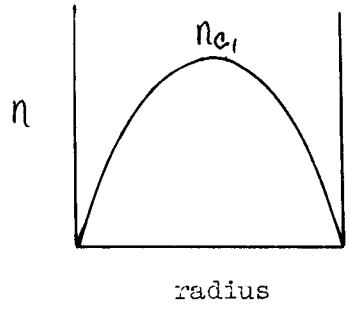

With another higher frequency wave one measures the phase shift and therefore the average electron density over the path length. In the linear approximation

$$n_{av} = \frac{m}{2\pi e^2}\,\Delta\phi_2\,\omega_2^2$$

$$\frac{n_{av}}{n_m} = 2\left(\frac{\omega_1}{\omega_2}\right)^2 \Delta\phi_2 \quad .$$

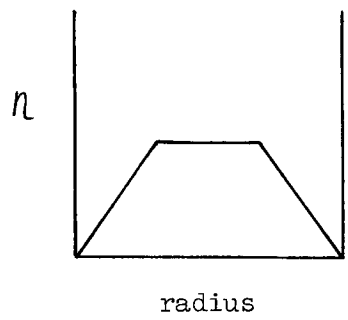

The quantity n_{av} defines the area under the density-radius curve, the peak of which is determined by the cutoff frequency. This technique is limited to a duration of time during which ω_1 is just cut off. There are other more complicated methods which can be used in special circumstances.

Noise

Microwave noise from plasma can furnish much information on the plasma temperature, the velocity distribution of the electrons, and the presence of instabilities. The sources of the noise include bremsstrahlung, cyclotron radiation, Cerenkov radiation, and radiation from the interaction of electron beams with slow waves propagating along the plasma column. We will not consider the coherent radiation from the plasma but will restrict ourselves to some general remarks on thermal radiation.

Thermal radiation from a plasma has its origin in the bremsstrahlung emitted by the electrons in scattering by the ions. At any given microwave frequency picked at random the intensity of the thermal radiation from a warm plasma ($\sim$10 ev) will be extremely weak and difficult to detect. According to Kirchoff's law the emissivity from a hot body is proportional to the absorptivity. Therefore at frequencies near the natural resonances in the plasma, the thermal radiation can approach the blackbody level.

Suppose we inquire into the noise power received by an antenna which is placed in the vicinity of a blackbody. The body extends to infinity in the directions perpendicular to the line from the antenna normal to the body, but is finite in the other direction. The energy density in a frequency interval $d\nu$ is given by the Planck law:

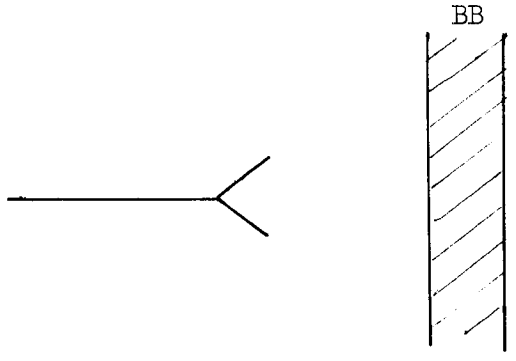

$$U\,d\nu = \frac{8\pi h\nu^3}{c^3} \frac{1}{e^{h\nu/kT} - 1} d\nu \quad .$$

In the Rayleigh Jeans approximation $h\nu/kT << 1$,

$$U\,d\nu = \frac{8\pi kT}{c\lambda^2} d\nu \quad .$$

The energy flux striking the antenna is then

$$J = c\,U\,d\nu = \frac{8\pi kT}{\lambda^2} d\nu \quad .$$

The power delivered to the antenna is then the product of the energy flux and the effective antenna area equals $\lambda^2/4\pi$. Since only one state of polarization is detected,

$$J = kT\,d\nu \quad .$$

The noise power delivered to the antenna is the same as that delivered by a resistor at temperature T. A (blackbody) plasma at a temperature of 2300° K will emit 3×10^{-15} watts over a bandwidth of 1 megacycle. A power level of this magnitude is difficult to detect with an ordinary superheterodyne microwave receiver, which has a noise figure of about 10 (10 Gc). With the aid of a Dicke radiometer, however, the detection of the radiation becomes easy.

The Dicke radiometer is designed to eliminate the effect of fluctuations in the gain of a radiometer system. (See sketch on following page.) The waveguide connecting the antenna to the first detector contains a slotted section with a rotating absorbing wheel. The wheel is driven at 30 cycles/sec and effectively

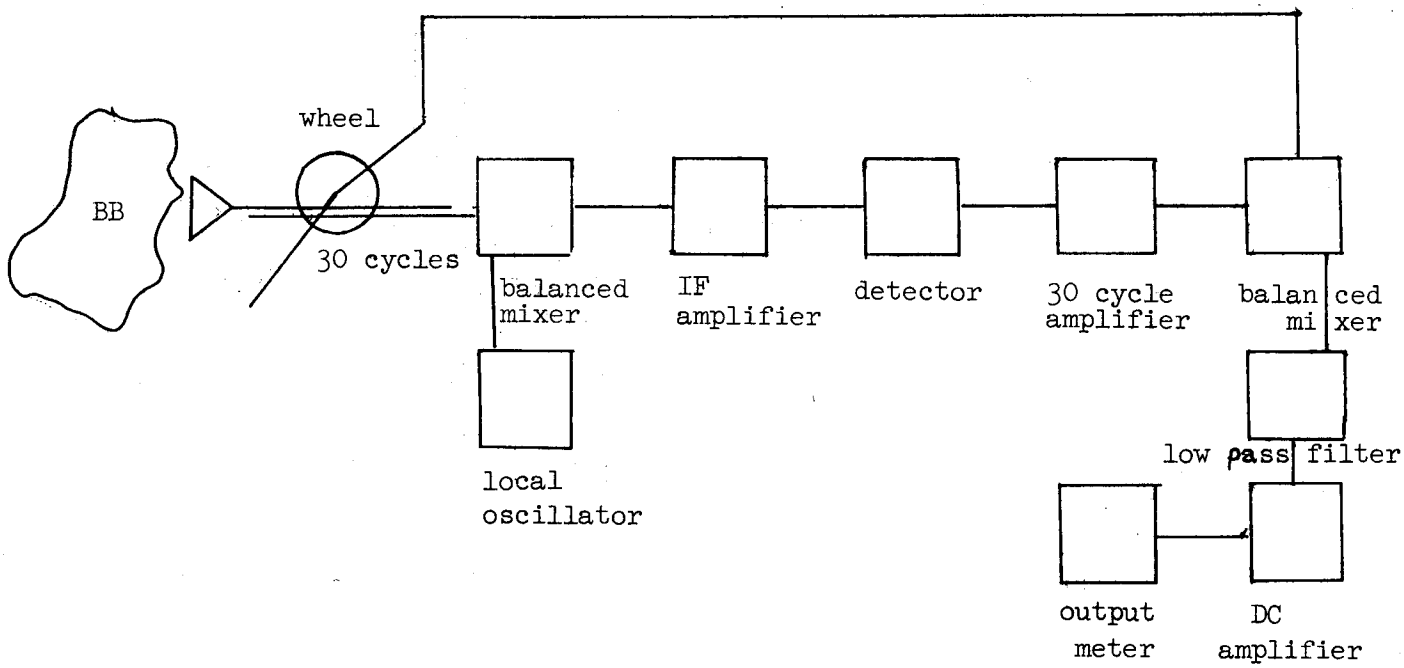

disconnects the antenna at this frequency. The output from the 30 cycle amplifier is proportional to the difference in signals received when the waveguide is connected and disconnected to the antenna. In the short time interval of 1/30 sec the amplifier gain will not change greatly. In order to minimize the fluctuations in the output meter it is advisable to have a large IF bandwidth and a long integrating time in the output circuit. The radiometer can detect 10^{-16} watt if the bandwidth is 16 mc.

REFERENCES FOR FURTHER STUDY

Microwave Techniques in Plasmas

M. A. Heald, "The Application of Microwave Techniques to Stellarator Research," Project Matterhorn MATT-17, Aug. 26, 1959.

Microwave Cavity Techniques

S. C. Brown, "The Interaction of Microwaves with Gas Discharge Plasmas," IRE Transactions on Microwave Theory and Techniques MTT-7, 69, 1959.

Thermal Radiation from Plasmas

Beckefi, Hirshfield, and Brown, "Incoherent Microwave Radiation from Plasmas," Phys. Rev. 116, 1051 (1959).

Radiometers

R. H. Dicke, "The Measurement of Thermal Radiation at Microwave Frequencies," Rev. Sci. Inst. 17, 268 (1946).

very simple relationship between the ion density and measured beam transmission.

A monoenergetic beam of atoms traversing a group of stationary scattering centers of density proceeds according to

$$I = I_o \exp[-n\sigma(v_B)x] \quad , \tag{1}$$

where σ is the scattering cross section, v_B is the beam velocity, and I_o and I the beam intensity upon entering and after penetrating the scatterers to a depth x. For a plasma the idealized scattering centers are replaced by j types of scatterers -- electrons, atoms, and perhaps several kinds of ions -- each of which may undergo k types of velocity-dependent interactions with the beam. If each j class of particles has a velocity distribution such that

$$n_j = f(v_j)dv_j \tag{2}$$

the beam intensity is now given by

$$I = I_o \exp\left[-\frac{1}{v_B}\sum_{j,k}\int \sigma_{kj}(v_r)v_r\, f(v_j)dv_j\, x\right] \quad , \tag{3}$$

where v_r is the relative velocity of the beam-target particles.

As examples of some of the many interactions which will occur we list the following:

1. Resonant charge transfer with plasma ions
2. Non-resonant charge transfer with impurity ions
3. Electron loss to the neutral background gas
4. Ionization of the beam by plasma electrons
5. Elastic scattering by plasma ions and electrons.

If we select for the beam species the primary ionic constituent of the plasma, e.g., a hydrogen beam for a hydrogenic plasma, then process 1 can be made the dominant mechanism leading to beam attenuation. Although the total cross section for process 5 is of the same order as the resonant charge transfer cross section, the differential scattering cross section for beams of kev energy is so strongly forward[1] that for detector acceptance angles $> 0.25^{o}$ in the laboratory system, scattering may be neglected.

Process 2 may under some conditions constitute a necessary correction. As an example, the charge transfer cross section between atomic hydrogen and 0^{+} ions is $\sim 10^{-15}$ cm^{2} at low energies[2] due to the near matching of ionization potentials. For the experiment to be considered the sum of impurity ions is a small percentage of the total ionic density so that process 2 leads to a negligible correction.

Cross sections for electron loss by the fast atoms to the neutral background gas are generally $\leq 10^{-16}$ cm^{2}/atom for beam energies $\leq$5 kev,[3] although they increase to $1\text{-}5 \times 10^{-16}$ cm^{2}/atom at energies of 20-50 kev. If the background gas is hydrogen, the electron loss cross section is 4.2×10^{-17} cm^{2}/atom for 5 kev beam energy. While this effect may produce an observable attenuation of the beam under static background conditions such as employed in stellarators, i.e., a background pressure of 10^{-4}-10^{-3} torr, the linear absorption coefficient would be much less than that due to process 1.

For all of the above mentioned processes the relative velocity of interaction between beam particles and plasma particles is, to sufficient accuracy, just the beam velocity. For ionization by plasma electrons this is, of course, no longer

the case and averages of the quantity $\sigma_i v_r$ must be calculated over the velocity distribution. For this case the beam velocity is much less than electron velocities of interest so that $v_r \simeq v_e$.

The ionization cross section for simple ionization curves such as those of hydrogen and helium may be represented with good accuracy by

$$\sigma_i = e\,\sigma_m \frac{\ell n\, u}{u} \quad , \tag{4}$$

where $u = kT_e/eV_i$, the ratio of thermal to ionization energy, σ_m is the peak value of the cross section, and e (the base of Naperian logarithms) appears as a normalizing constant. For a Maxwellian distribution of electron energies, $\overline{\sigma_i v_e}$ may be computed from tabulated values of the error integral -- $E_i(-\alpha)$. Specifically,

$$\overline{\sigma_i v_e} = 1.54\,\sigma_m v_o \alpha[-E_i(-\alpha)] \quad , \tag{5}$$

where $\alpha = [eV_i/kT_e]^{1/2}$ and $v_o = [2eV_i/m]^{1/2}$.

Such calculations show that $\overline{\sigma_i v_e} \leq 10^{-8}$ cm^3/sec for all kT_e for beams of hydrogen or helium. By comparison the rate coefficient for resonant charge transfer for a 5 kev atomic hydrogen beam is 13×10^{-8} cm^3/sec or more than 10-fold greater. Equation 3 reduces, therefore, to

$$I = I_o \exp[-n_+ \sigma_c x] \quad , \tag{6}$$

whereby n_+ is readily calculated from the measured ratio of I/I_o.

We have confirmed the thoughts outlined above with some measurements made on the B-1 stellarator.*

*In collaboration with Peter Noll and Fred Tappert.

The apparatus, illustrated schematically in Fig. 1, consists of an rf-excited ion source producing some tens of microamperes of a mixture of H^+, H_2^+ and H_3^+ ions. The ions are extracted, focussed and passed through a neutralizing cell where, to maintain plasma purity, we use hydrogen at approximately 1 m torr. An appreciable fraction of the emergent beam is therefore fast neutrals of the above species. This mixed beam then passes into the plasma vessel where the remaining ions are removed by the perpendicular magnetic field. After passage through the plasma in which some fraction of the beam undergoes charge transfer the now-remaining neutrals traverse a stripping cell of helium gas in which a small fraction of these neutrals are converted back to ions. Helium is employed here rather than hydrogen because of its superior efficiency as a stripping agent. The ions so formed are then momentum-analyzed to select the atomic portion of the beam. (The molecular components are also attenuated by the plasma interaction but this attenuation is not so directly correlated to the plasma density.) Finally, at the secondary electron detector the input current is 10^{-9} to 10^{-10} amperes. A detector amplification of about 10^6 is used.

The atomic beam has been employed in two ways. As a dc beam, the pulsed discharge produces an attenuation and varies the output signal. This mode of operation is well suited for small percentage attenuations and when maximum time response is desired. Alternatively, we have modulated the beam at the focus electrode by application of a 100-kc sine wave. The plasma attenuation then produces an amplitude modulation of the 100-kc carrier. This mode of operation offers several advantages. First, the dc level of the beam is not needed to deter-

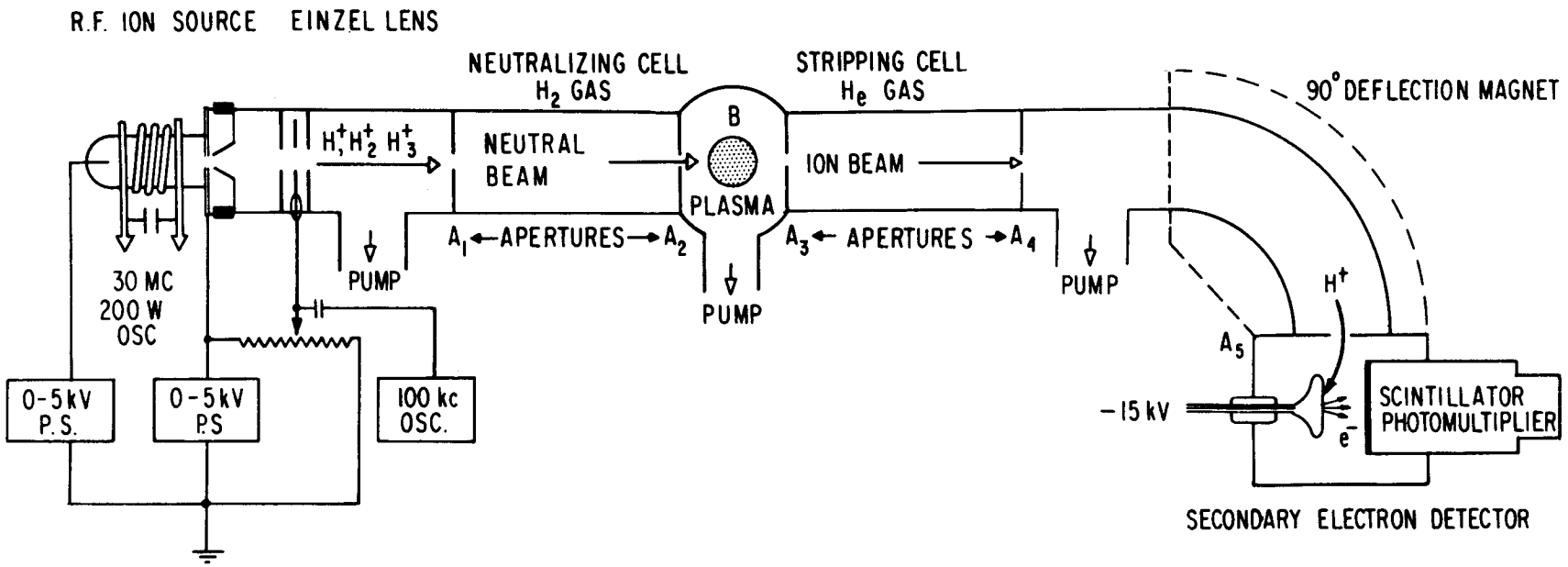

Fig. 1 Schematic representation of atomic beam employed for the measurement of plasma ion density.

mine the attenuation and secondly, reasonably narrow band amplification can be employed to reduce the relative level of noise originating from the pulsed discharge.

Using the B-1 stellarator, with a relatively pure hydrogen plasma, a comparison was made between the atomic beam system and a 4-mm microwave interferometer over the density range 1 to 5×10^{13} cm^{-3}. Such comparison signals are illustrated by Fig. 2. The noise which appears most prominently in the dc beam display arises from the ion source itself and not from density fluctuations within the plasma.

Some density measurements were made with the atomic beam in the 10^{14} cm^{-3} range, above the microwave cut-off at 6×10^{13} cm^{-3}. Two such traces in the 10^{14} range are shown in Fig. 3. At 2×10^{14} cm^{-3} density the beam attenuation is 60%. We would expect that this technique could be used in the measurement of densities to $\sim 10^{15}$ cm^{-3} for which the attenuation is ~99%.

Figure 4 shows the total comparison points between the electron density n_e from the microwave system and the ion density n_+ from the beam system. In computing the proton density from the beam attenuation we have used the charge transfer cross section of Fite, Brackmann and Snow.[4] A best mean-squares fit to the points gives a line of slope 0.9 and an intercept of 0.3×10^{13} cm^{-3}. Although this agreement seems rather good there are disturbingly large deviations from the mean as evidenced by Fig. 4. The fluctuations arising from the ion source, while corresponding to density uncertainties of up to 10^{13} cm^{-3}, are of order 100 kc in frequency and should introduce an uncertainty considerably

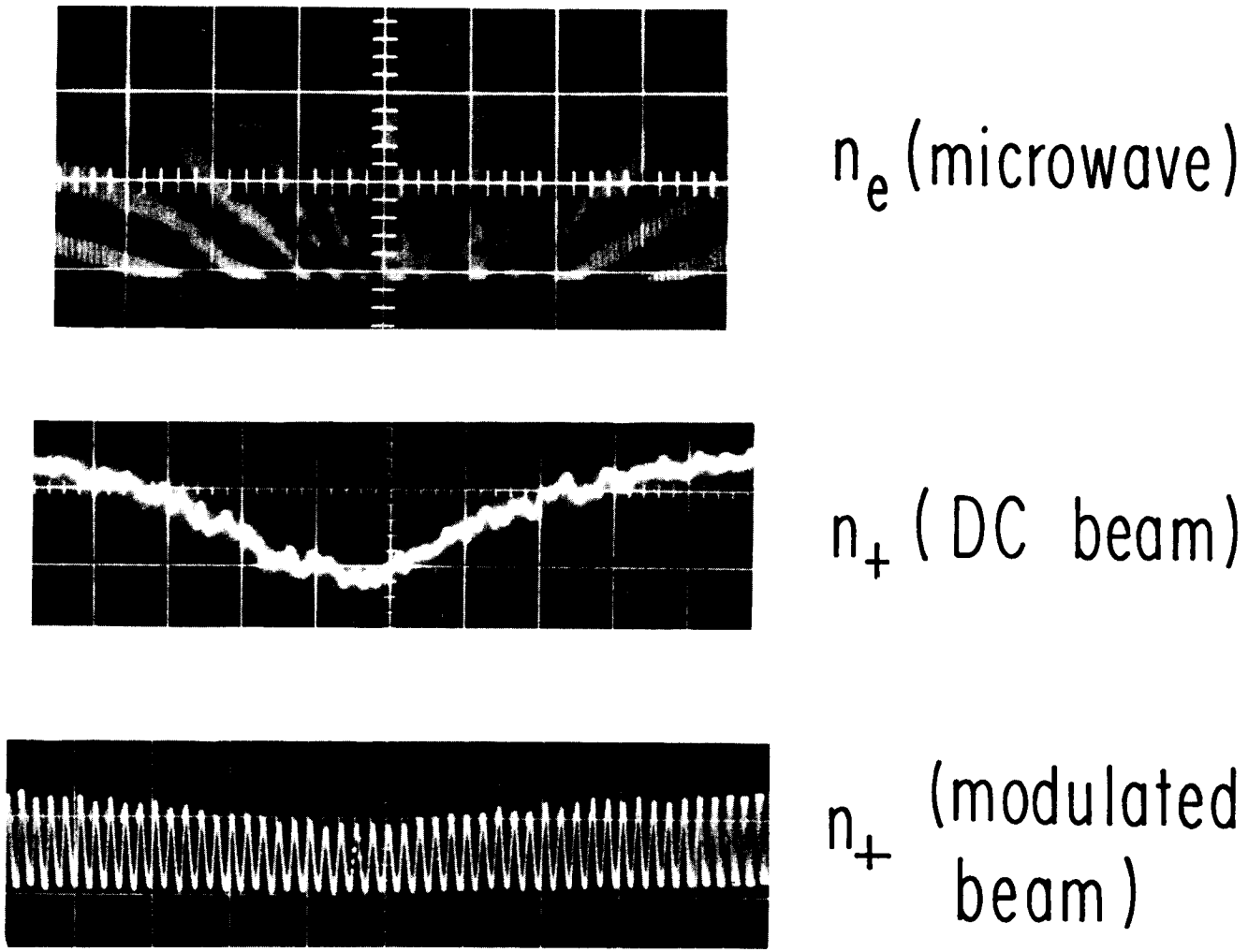

Fig 2. From top to bottom: density traces as recorded by 4mm microwave interferometer, dc atomic beam and atomic beam modulated at 100 kc. Time 50 μs/cm to the right. Machine filling pressure 2 m torr. and beam energy 2.5 keV. The peak density is 4.5×10^{13} cm^{-3}.

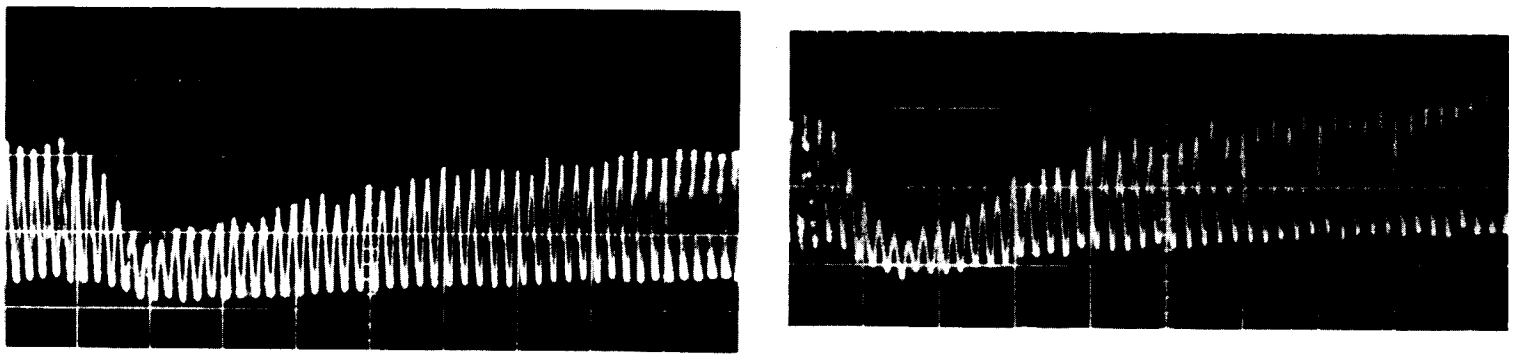

Fig. 3 Modulated beam density traces at indicated machine pressures. Time -50 μs/cm to the right and beam energy 2.5 keV.

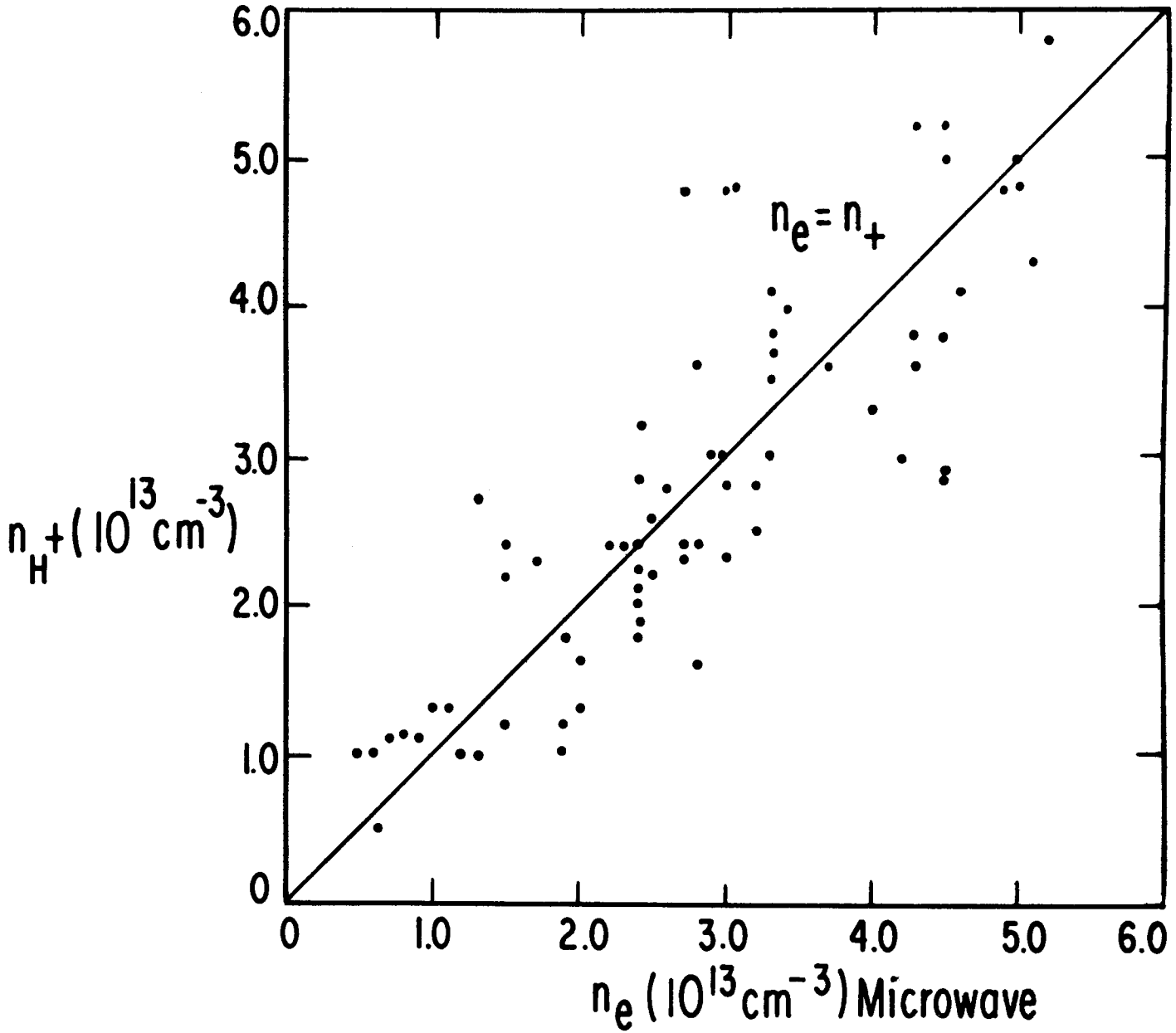

Fig. 4 Comparison points between microwave (n_e) and atomic beam (n_{H^+}) systems. Straight line shown is that for $n_e = n_+$. Best mean squares fit to data points gives a line of slope 0.9 and intercept of $n_{H^+} = 0.3 \times 10^{13} cm^{-3}$.

less than 10^{13} cm^{-3}, since densities were always assessed from smoothed envelopes. The possibility exists that distortions from cylindrical symmetry introduce such discrepancies since the systems measure at 90^{o} to one another. Insofar as we can tell there is no systematic difference between the two systems which can be attributed to electron temperature. We have, in addition, employed a discharge in neon gas to show the absence of large attenuations when resonant charge transfer does not occur.

We believe, therefore, based on the observations reported above, that the neutral-beam transmission system offers considerable merit in the measurement of plasma density.

II. Electron Temperature

From the discussion in Sec. 1 concerning beam attenuation by electron ionization it is clear that, in principle, such measurements can give rise to estimates of electron temperature. The temperature range for such measurements is fairly restrictive, however. To produce a measurable attenuation kT_e must be an appreciable fraction of the ionization energy of the beam particles, i.e., $kT_e \geq 1/4\ eV_i$. On the other hand, the rate coefficient $\overline{\sigma_i v_e}$ becomes increasingly flat vs T_e for $kT_e > eV_i$. For $kT_e = 2eV_i$ the slope of $\overline{\sigma_i v_e}$ is so small that extreme accuracy would be required in the measurement of I/I_o to obtain any degree of accuracy in T_e.

In practice, it is highly desirable to employ a beam species for which electron ionization constitutes the dominant attenuation process. In other words, for a hydrogenic plasma an atomic beam of hydrogen is a poor choice to measure

electron temperature since the beam attenuation is governed primarily by charge transfer which is quite insensitive to plasma temperature. A helium beam has some merit, however, and might be briefly considered as an example. To obtain an estimate of the importance of charge transfer for a 4 kev helium beam with plasma protons we use, from Allison,[3] the charge transfer cross section for protons at 1 kev (same relative velocity) traversing He gas. The result is 5×10^{-18} cm^2/atom from which the rate coefficient $\overline{\sigma_e v} = 2 \times 10^{-10}$ cm^3/sec. This lies well below the peak value of $\overline{\sigma_i v_e}$ for electrons which is $\sim 10^{-8}$ cm^3/sec. To produce a beam of attenuation of 10%, however, requires that the product of electron density and plasma thickness be in excess of 5×10^{14}/cm^2, so that fairly high densities are necessary.

Recent determinations of the absolute cross sections for electron ionization of some alkali atoms[5] indicate two interesting features concerning the use of such beams as probes for electron temperature. Potassium, for instance, has a cross section two orders of magnitude larger than does helium so that much lower plasma densities suffice to yield measurable attenuation. Furthermore, due to auto-ionization from an excited state some 18 ev above the ground level, the temperature dependence of the rate coefficient $\overline{\sigma_i v_e}$ remains quite strong out to $\sim$ 30 ev. The structure of the cross section is shown in Fig. 5 and the resulting rate coefficient numerically calculated from an assumed Maxwellian distribution of electron energies and the experimental cross section is shown in Fig. 6.

The magnitude of the ionization cross section for potassium indicates clearly that ionization by electrons is the only process which need be considered

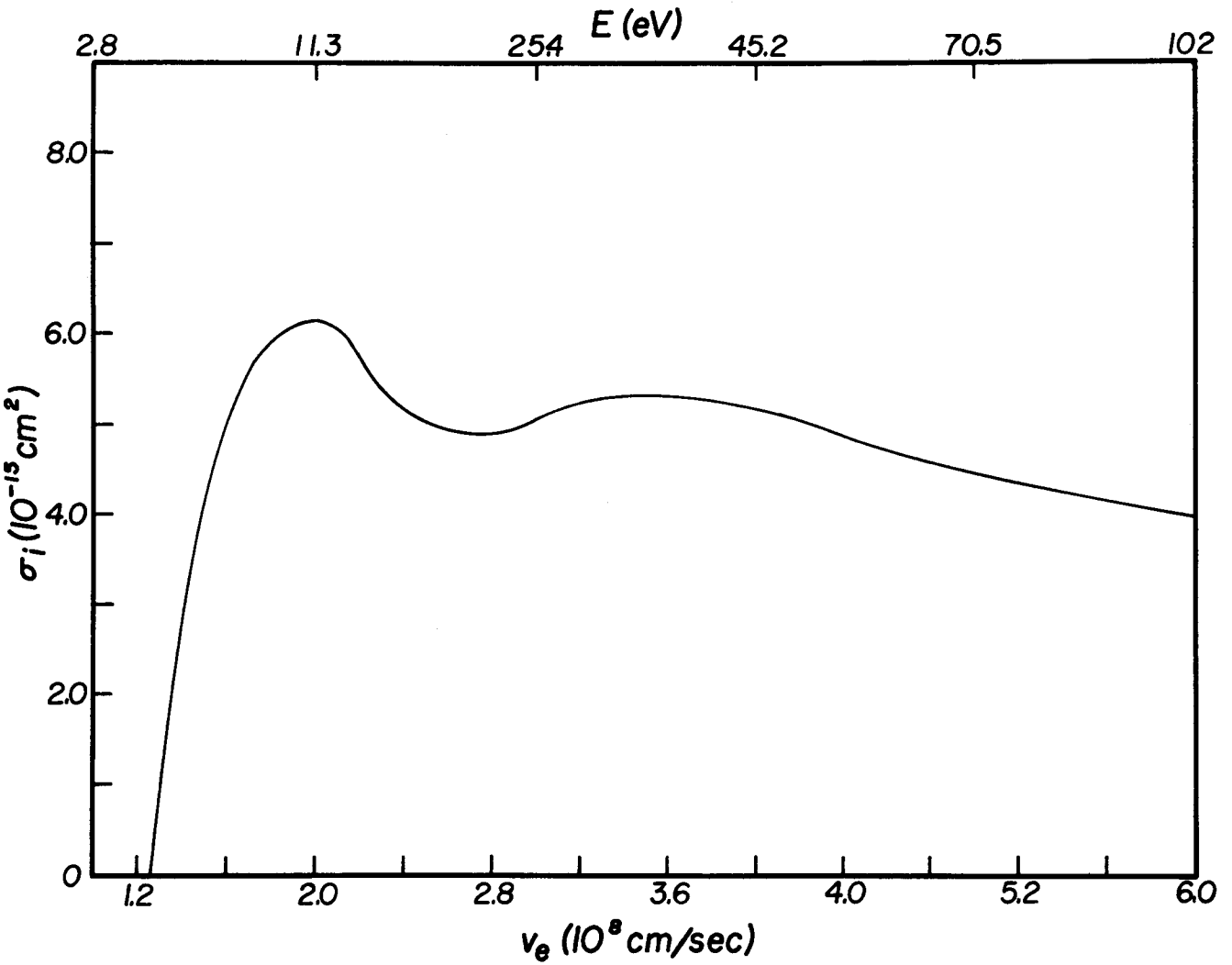

Fig. 5 Electron ionization cross section for potassium (from F. S. Baker and G. O. Brink[5].

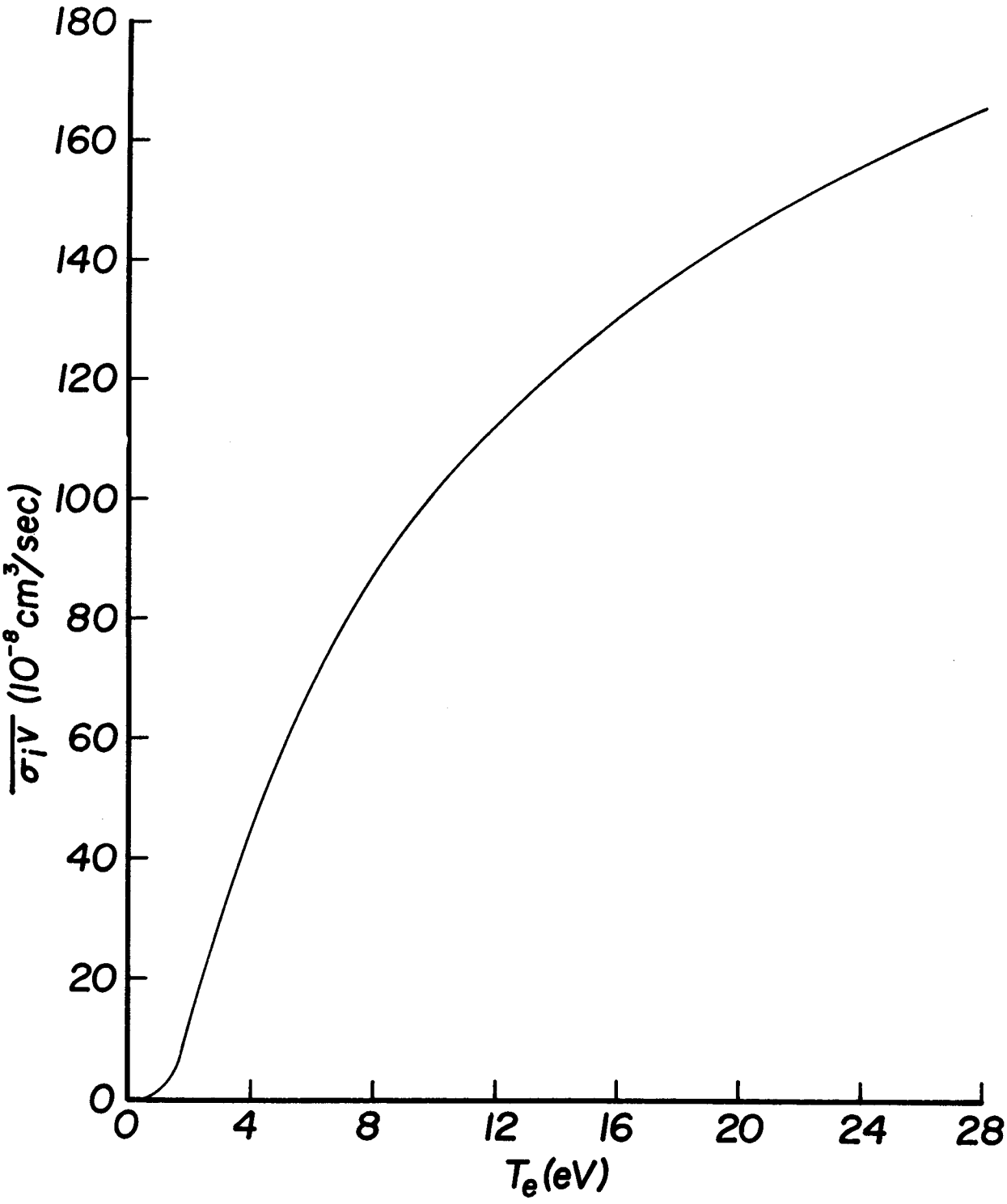

Fig. 6 Rate coefficient for electron ionization of potassium as a function of electron temperature.

in producing attenuation of an energetic potassium beam. Equation (3) reduces, therefore, to

$$I = I_o \exp\left[-n_e \frac{\overline{\sigma_i v_e}}{v_k} x \right] \quad , \tag{7}$$

where v_k is the potassium beam velocity. For a plasma thickness of 4.45 cm (the experimental value) and a potassium beam energy of 3 kev, one obtains the beam transmission I/I_o as a function of electron density and temperature, as shown in Fig. 7.

Experiments were performed on the B-1 stellarator to compare the electron temperature determined from beam attenuation with those obtained from conductivity. The arrangement of apparatus is shown in Fig. 8. Ions are formed by surface ionization on tungsten at 1500° K to yield approximately 1 mA/cm^2. The tungsten is a 0.25 inch diameter porous plug* and is back-fed by an oven at a few hundred degrees centigrade. The entire assembly is resistively heated to the desired temperatures. Ions are extracted and focussed so as to pass through a cross jet of potassium vapor to produce the neutral beam by resonant charge transfer. This gave a working beam at the detector of order 10^{-9} amperes equivalent. Modulation of the beam at 100 kc/sec is again employed in order that band pass filters may be used at the detector output. Otherwise the beam signal is masked by the detector sensitivity to the vacuum ultraviolet radiation from the plasma.

*Obtained from Semicon Associates, Box 832, Lexington, Kentucky.

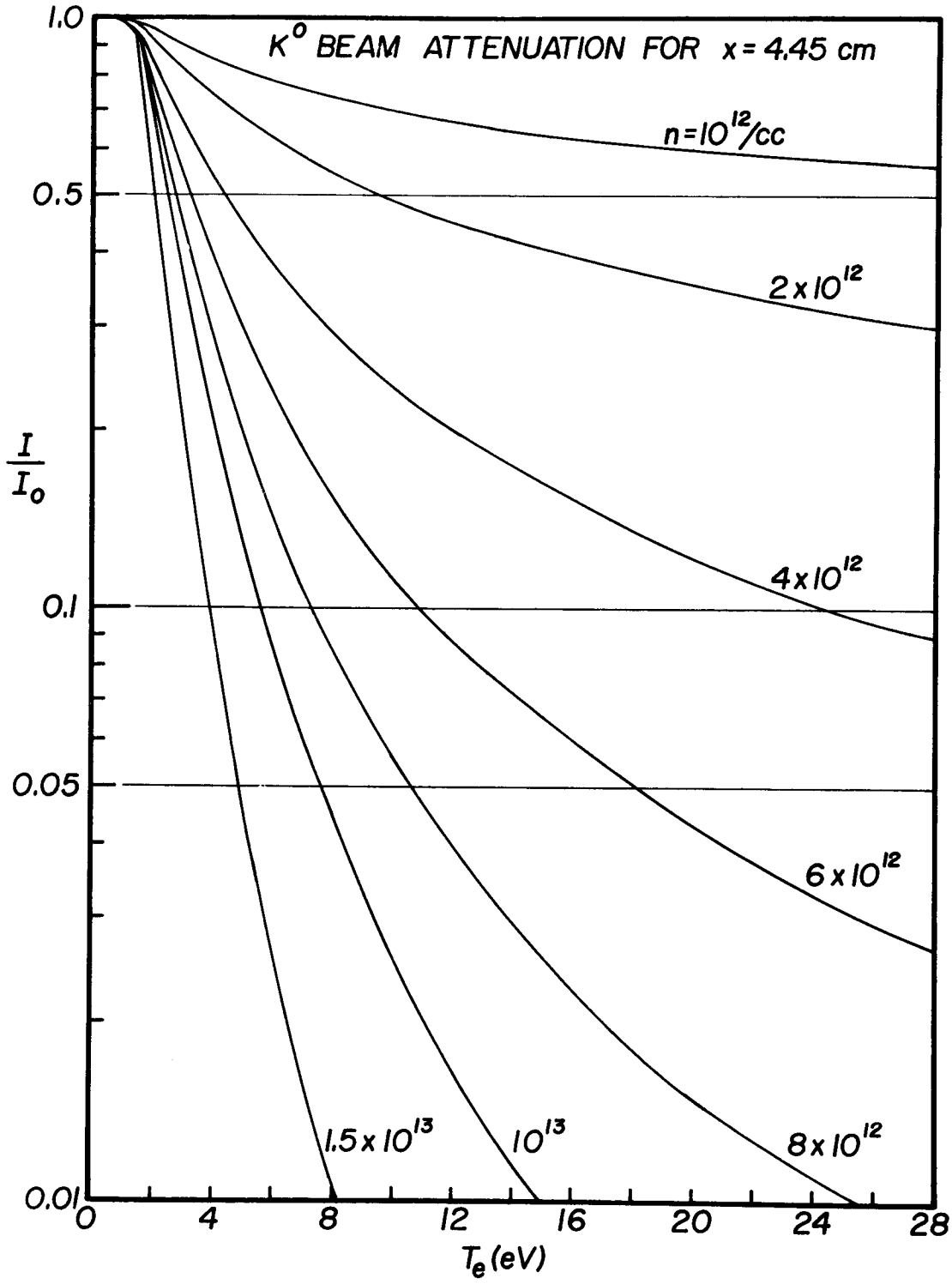

Fig. 7 Potassium beam transmission as a function of electron temperature and density for a plasma thickness of 4.45 cm.

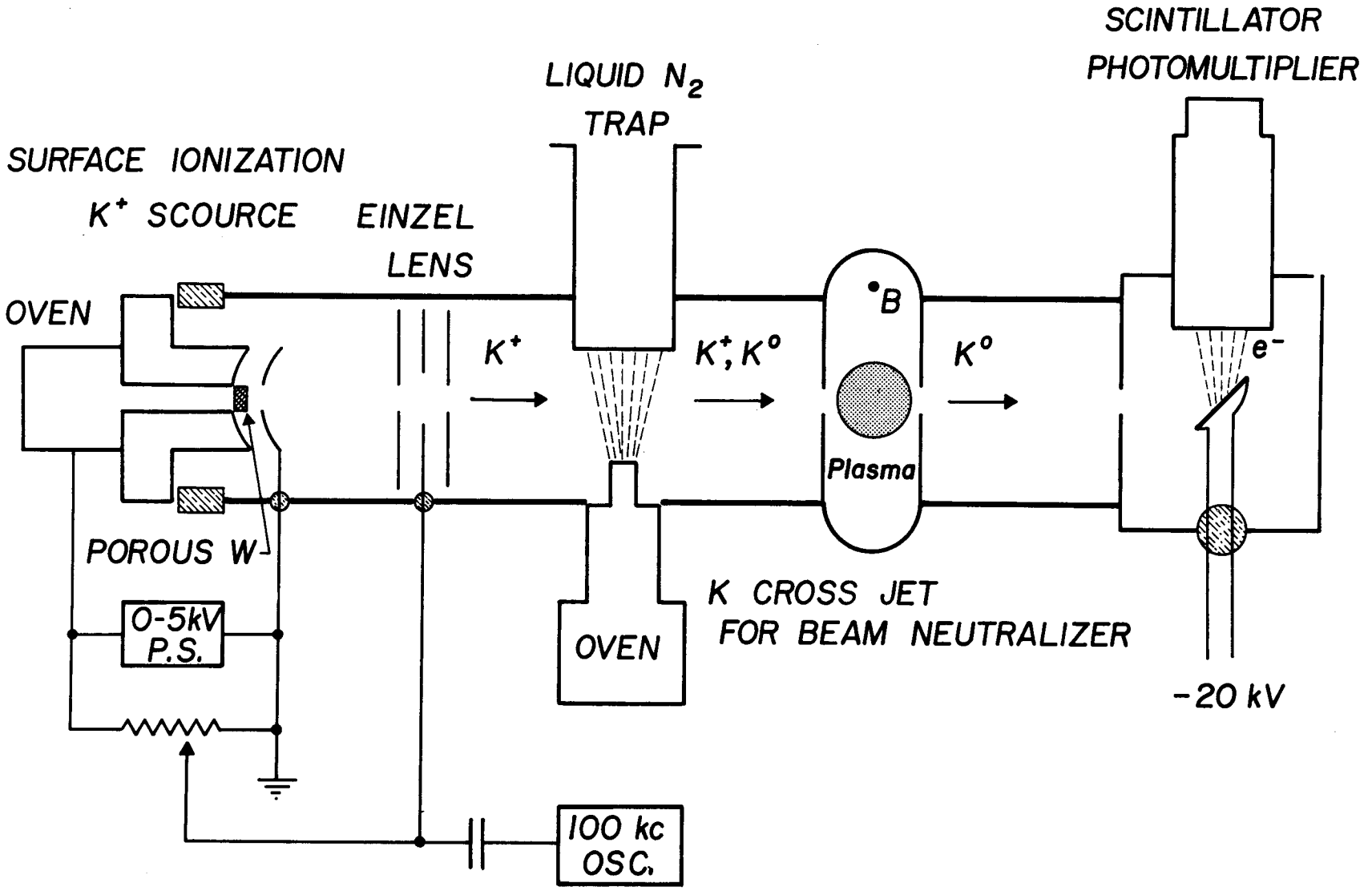

Fig. 8 Schematic drawing of experimental arrangement for measurement of electron temperatures with potassium beam.

The response of the beam system to the electron temperature is illustrated by Fig. 9. The discharge is driven by a 5 kc/sec sine wave for about 1 m sec and the electron density as recorded by a 4 mm microwave interferometer is reasonably flat (incomplete ionization) at $\sim 7 \times 10^{12}/cm^3$. One observes that the temperature, as evidenced by beam transmission, is modulated at twice the driving frequency of the discharge in accordance with the conductivity. The asymmetry indicated by the variation in adjacent minima of beam intensity is too long a story to discuss here. Suffice it to say that the conductivity temperature usually fell within the values one obtains from adjacent minima in beam transmission.

In Fig. 10 we show the comparison data between beam and conductivity measurements. Agreement is usually within ±20%. Measurements beyond 10 ev could not be made with the beam system due to perturbing effects of the ultraviolet radiation from the plasma.

REFERENCES

1. M. R. C. McDowell, Proc. Roy. Soc. (London) A72, 1087 (1958).
2. R. F. Stebbings, W. L. Fete and D. G. Hummer, J. Chem. Phys. 33, 1226 (1960).
3. Samuel K. Allison, Rev. Mod. Phys. 30, 1137 (1958).
4. W. L. Fite, R. T. Brackmann and W. R. Snow, Phys. Rev. 112, 1161 (1958); Phys. Rev. 119, 663 (1960).
5. F. S. Baker and G. O. Brink, Lawrence Radiation Laboratory Rpt. UCRL-7087 (1962).

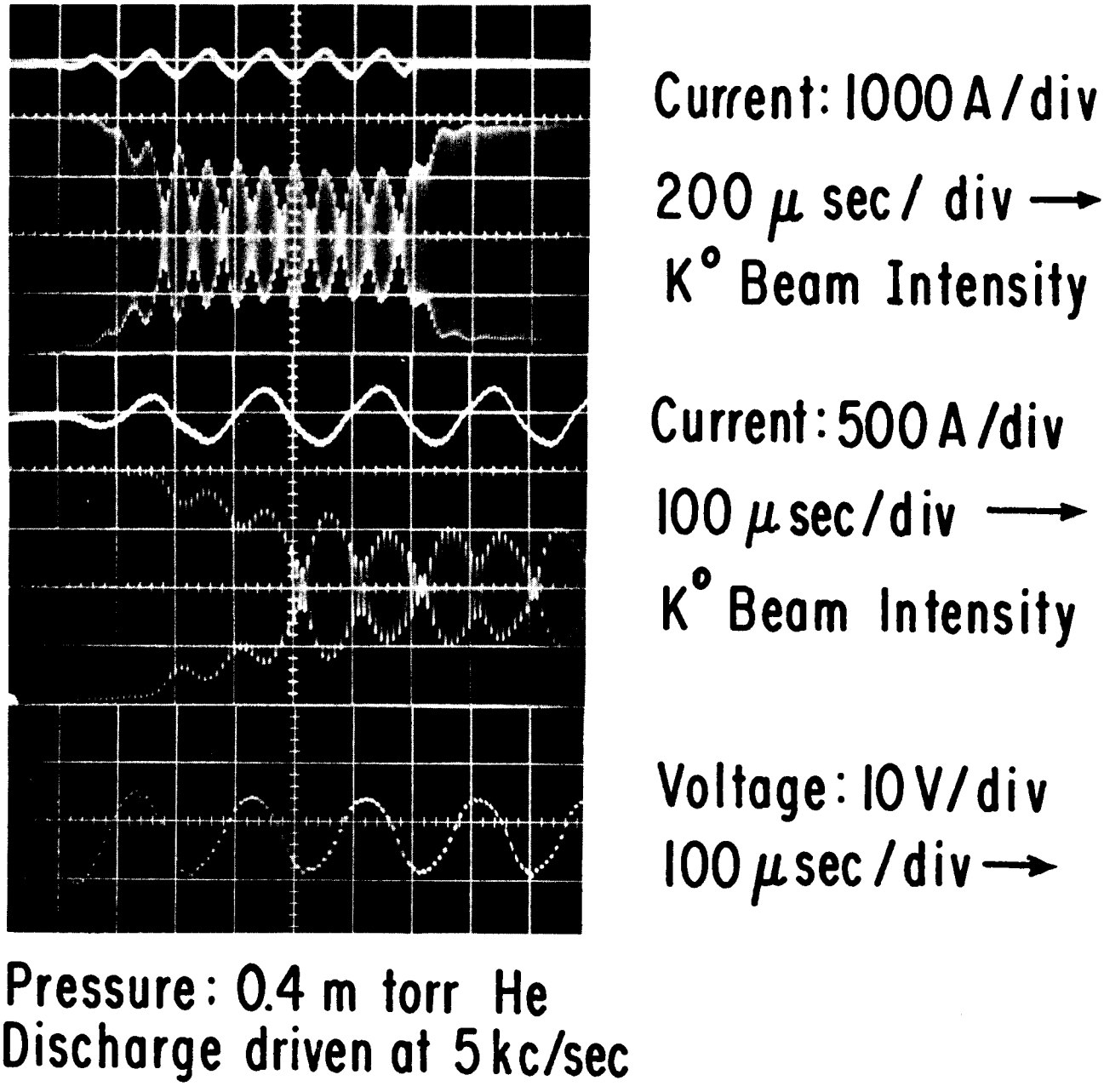

Fig. 9 Discharge driven at 5 kc/sec showing from top to bottom plasma current and beam transmission at 200 μs/div, plasma current, beam and loop voltage at 100μs/div. Temperature modulation is asymmetric but at twice the driving frequency.

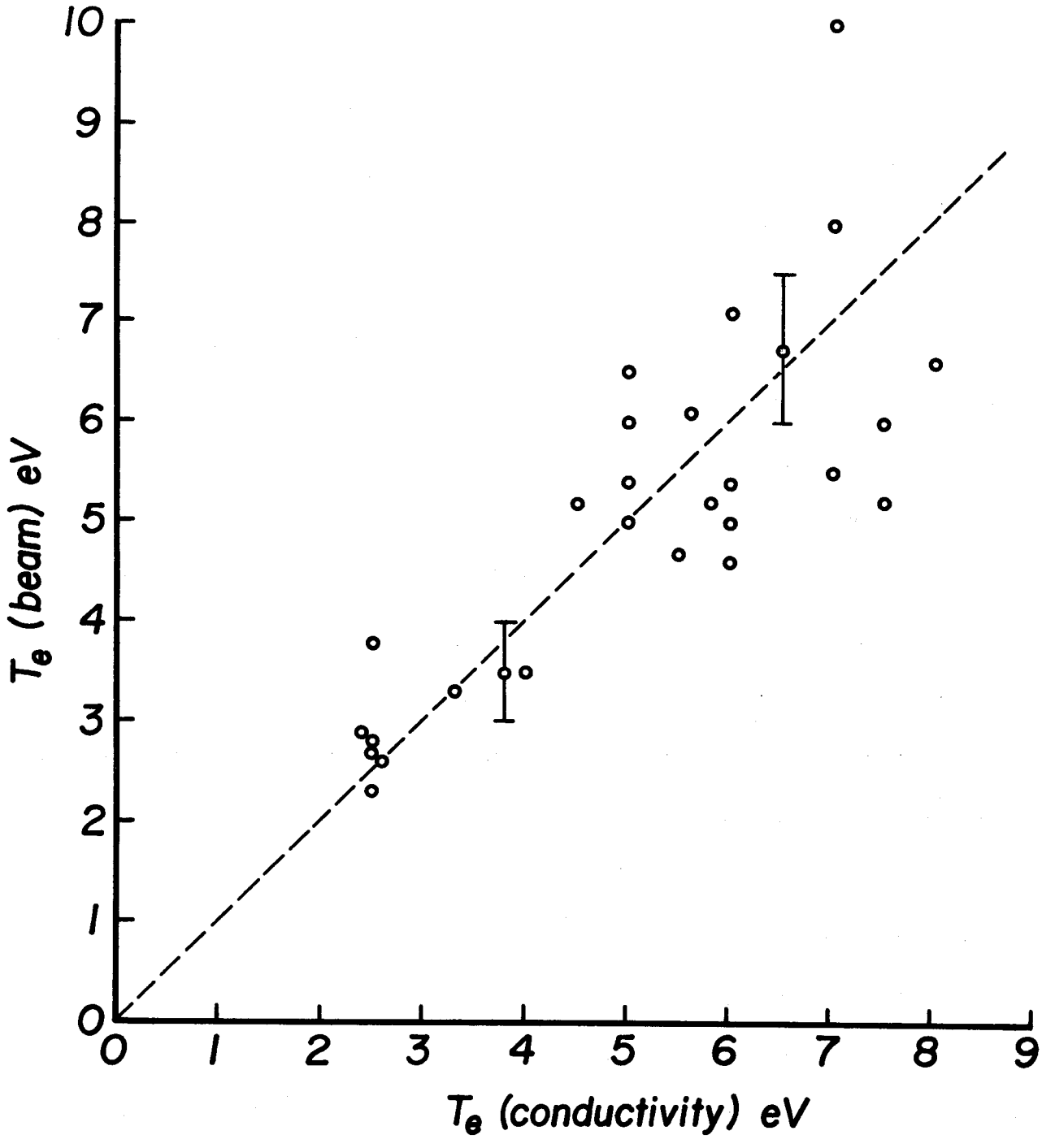

Fig. 10 Comparison points between conductivity temperatures and temperatures recorded with potassium beam. Error bars represent the observed asymmetry in beam measurements with the direction of heating current.

AN ION ENERGY ANALYZER FOR PLASMA MEASUREMENTS

by

Harold P. Eubank and Thomas D. Wilkerson*

The study of plasmas generally requires some knowledge of the plasma composition and the state of motion of the particles. One wants to know the abundance of ions and neutrals and their kinetic energy distributions as functions of position, direction and time. The most direct way to get this information is to separate the species and measure the flux of each as a function of particle energy. We report here the operation of a particle analyzer which appears to be suitable for this purpose. This work was originally undertaken to measure the flux of energetic neutrals out of stellarator discharges. We hope to assess the importance of charge-exchange as an energy-loss mechanism and, under certain assumptions, to infer the energy distribution of ions within the discharge. To date, the analyzer has successfully been used for a composition and energy analysis of the ion output from a pulsed plasma guns of the Livermore type .[1] We believe that the analyzer has sufficiently good sensitivity, time response and energy resolution to be useful for a broad class of plasma experiments. In particular, such instruments should allow new measurements on low density plasmas, where other methods often fail because of low signal-to-noise ratios or departures from thermal equilibrium.

* Now at the Institute of Fluid Dynamics and Applied Mathematics, University of Maryland.

In the following section we will describe in detail the basic elements of the system, namely, the electrostatic analyzer[2] and the detector.[3] A schematic diagram is shown in Fig. 1. Ions pass through the entrance slit (upper left) and into the space between oppositely-charged deflector plates. For a given plate potential ϕ those ions with energy $\sim \epsilon$ are refocused at the exit slit and pass into the detection chamber. These ions are strongly accelerated into an aluminum knob (held several kilovolts below ground) where they give rise to emission of secondary electrons. The secondaries are accelerated into the scintillator (covered with an evaporated aluminum ground-shield) whose resulting light emission is viewed by a photomultiplier. Assuming the necessary calibrations, one can clearly measure the current of ions at any energy and, by varying ϕ, determine the complete ion energy distribution.

This procedure gives ambiguous results when a mixture of charges is analyzed. With a given ϕ, one would actually record all singly-charged ions of energy ϵ, as well as all doubly-charged ions of energy 2ϵ, and so on. An independent determination of particle velocity suffices to separate the components according to their mass-to-charge ratio, m/Z. In a later section of this paper we will show how time-of-flight data provide the m/Z separation for a pulsed plasma source. We also discuss a velocity selector to be used in front of the analyzer for steady or slowly varying plasmas. For some plasmas, such simple methods are not entirely satisfactory because of the m/Z similarity of some constituents and the limits on energy and velocity resolution imposed by the apparatus. Our present system, for example, cannot distinguish between

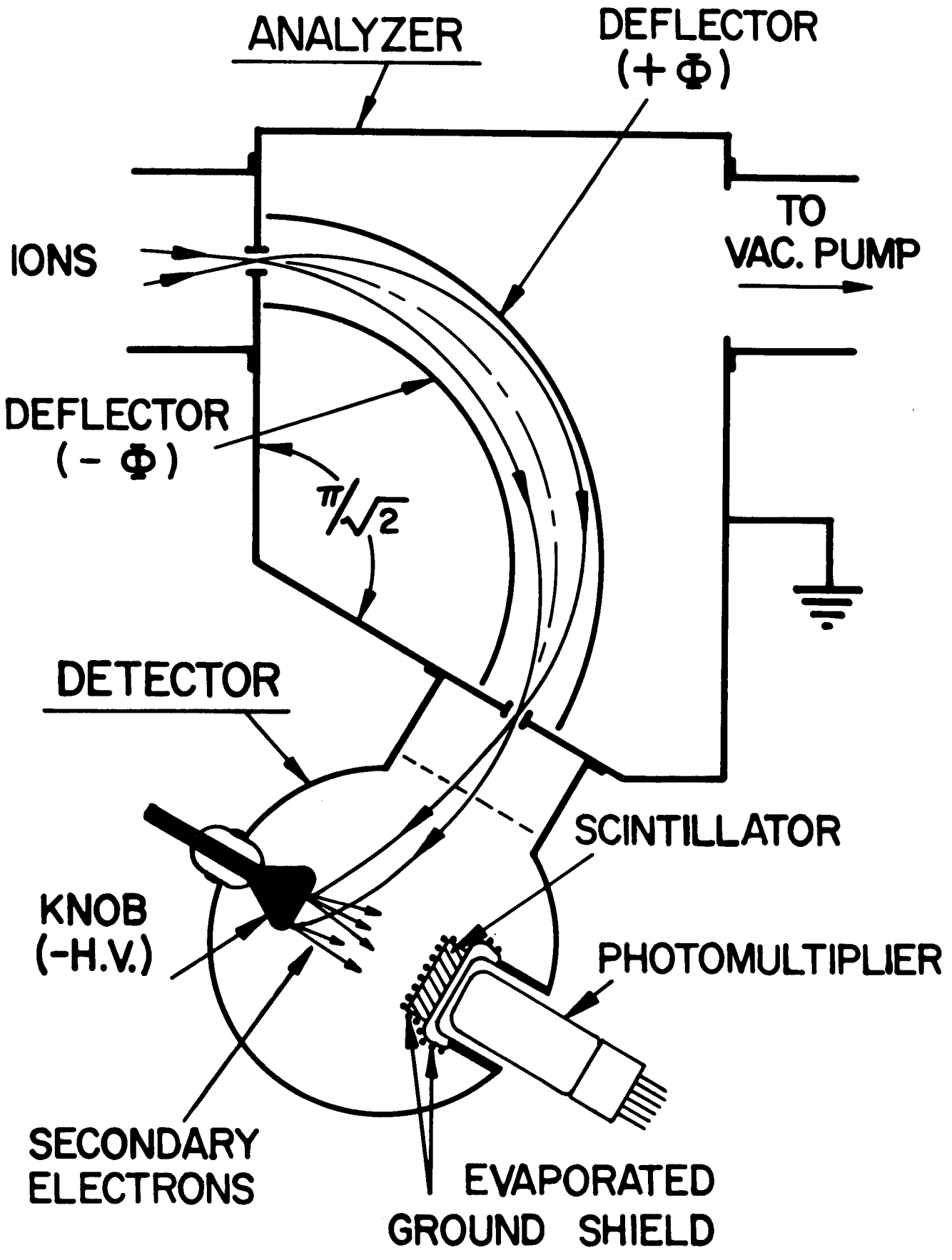

Figure 1. Schematic of electrostatic energy analyzer and detector.

α particles and H_2^+ ($m/Z \approx 2$) or between He II, C IV and OV ($m/Z \approx 4$); however, the measurement of proton current is always unambiguous. When very little is known in advance about composition, one must resort to the higher-resolution methods typical in mass spectroscopy. We may refer to Nier[4] for recent developments in this field, particularly for mass analysis of the upper atmosphere in rocket experiments.

For the study of neutral particles, the analyzer must be preceded by an ionization section in which the ionizing process does not greatly alter the particle energy. Moreover, the ionization efficiency must be known with good precision and should be high enough to satisfy detection requirements. We are now evaluating two methods of ionization: (1) electron collisions in an electron beam perpendicular to the entrance axis of the analyzer, and (2) charge-changing collisions in a gas stripping cell. The second method has successfully been applied by Afrosimov et al in their study[5] of neutral particles emitted by the Alpha plasma with energies above 300 electron volts.

A few more general remarks are in order before we pass on to the details of the apparatus and the experiments. The measurements we have undertaken could, in principle, be accomplished in a variety of ways; however, the adopted methods offer advantages which are worth considering:

1. The analyzer is analogous to a monochromator in that it yields a differential energy spectrum rather than the "integral" spectrum one obtains with repeller-grid systems.

2. Electrostatic analysis requires much less power and weight than magnetic analysis and allows rapid scanning of particle energy distributions.

3. Daly's ion detector[3] combines high sensitivity, short time-constant, simplicity of construction, and operational convenience. Single ions are reliably observed, due to their post-analysis acceleration and the resulting yield of secondary electrons. In quasi-steady operation, the current gain of the system can be made as high as 10^7 to 10^8. The time-constant depends on the response times of the scintillator and the photomultiplier circuit, and can be as low as tens of milli microseconds. Unlike "bare photomultipliers" with beryllium-copper dynodes, this detector can be exposed to the air arbitrarily often with no decrease in sensitivity.

Apparatus

Hughes and Rojansky[2] were the first to demonstrate the particle-focusing properties of cylindrically symmetric, electrostatic potential fields. Later applications appear in the mass spectrograph of Bainbridge and Jordan[6] and the β-decay spectrometer of Backus.[7] With reference to Fig. 1, a positive particle of charge Z and energy ϵ will follow the centerline of the analyzer if

$$\frac{\phi}{\epsilon/Z} = \frac{\Delta r}{r_o} \tag{1}$$

where ϕ is the potential above and below ground of the outer and inner deflector plates, respectively. Δr is the plate separation, and r_o is the radius of the

centerline. Particle "rays" which initially make small angles $\pm\ \alpha$ with the centerline will re-intersect after undergoing the indicated deflection of $\pi/\sqrt{2}$ ($127^{\circ}\ 17'$). The intersection point is displaced inward from the centerline by a small amount $r_o(\alpha^2/3)$ (α in radians). The energy resolution one achieves with an exit slit-width Δs is given by

$$\frac{\Delta\epsilon}{\epsilon} = \frac{\Delta s}{r_o} \quad . \tag{2}$$

Thus the bandwidth of the system increases linearly with particle energy, and one must unfold this dependence in order to derive an energy distribution, $f(\epsilon)$, from the variation of ion current with deflector voltage. That is,

$$f(\epsilon) \propto \frac{j(\phi)}{\epsilon} \propto \frac{j(\phi)}{\phi} \tag{3}$$

where $j(\phi)$ represents the current measured by the detector as a function of analyzing voltage.

Figure 2 is a photograph of the analyzer and detector with their lids removed. The analyzer box was milled out of a single piece of 4-inch thick 2024 aluminum plate. The entrance and exit slits (0.050 in. wide, 0.400 in. high) are cut out of brass inserts which plug into recesses in the sides of the box. The inner deflector is a sheet of copper, and the outer one is a tungsten mesh (95% transparent) which is tantalum-welded onto a curved frame. Both deflectors are supported by rails which stand on ceramic insulators. Electrical connection to the deflectors is provided by vacuum feed-throughs in the bottom of the box; these are adapted to coaxial cable fittings on the outside. The

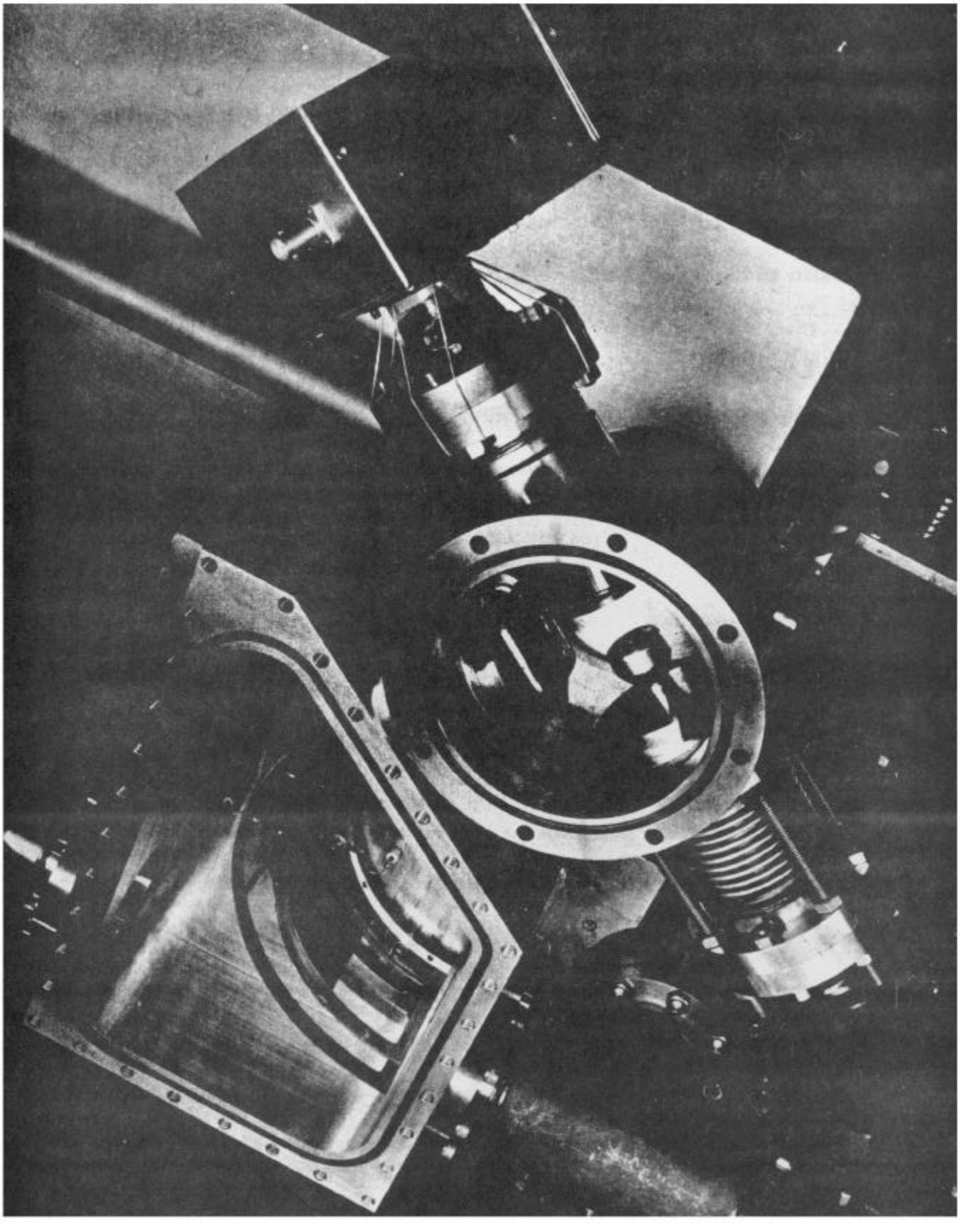

Figure 2. Photograph of analyzer and detector with lids removed.

deflectors are 2-1/2 inches high, 3/4 inches apart, and their median radius is 4 inches. Thus $\phi = 3\epsilon/16Z$ by Eq. (1); i.e., protons of 1 kev energy pass through the analyzer when the deflector potentials are $\pm$ 187.5 volts. The energy resolution given by Eq. (2) is roughly 1% and is no worse than 2% taking account of the width of the entrance slit.

Originally, the inner deflector was also a tungsten mesh until the electron experiments showed that over-deflected particles could course inside the inner mesh and back out into the analyzing space, to appear as a spurious second beam of apparently higher energy than expected. Experiments are now under way to see if solid plates can be used for both deflectors without spoiling the analysis.

The rest of this section is concerned with the response of the detector, or more exactly, what photomultiplier current results from a time-dependent ion current through the analyzer exit slit. In what follows, we assume that all ions strike the aluminum knob similarly, regardless of initial kinetic energy, and that all secondary electrons strike the scintillator in, say, the central part of the disk. Speaking optically, we might say we have no vignetting in the system, i.e., no preferential loss of rays that would distort the observed ion energy spectra. Daly[3] has discussed this problem to some extent. We find that these requirements are readily met by providing an initial optimizing adjustment for the knob position. For this purpose we use a flexible bellows mounting as shown in Fig. 2. The potential lead for the knob (10 to 20 kilovolts negative) is fed through a large Kovar seal on the end of the bellows.

If all particles are collected with equal efficiency, the only remaining

problem is to relate the photomultiplier current to the ion current. We can differentiate two regimes according to whether the mean time between ion arrivals is substantially less or greater than the response time of the system. For the purposes of this paper, we are concerned with the first case and further, with ion currents which do not change drastically during an instrumental response time. In this regime there is a constant (large) ratio, the gain, between photomultiplier and ion currents; the determination of this ratio constitutes the absolute calibration of the detector under these conditions.

The net gain of the detector is governed by three factors, namely, (1) the secondary electron multiplication, γ, at the aluminum knob, (2) the number of photoelectrons in the multiplier per secondary electron incident on the scintillator, and (3) the current gain of the photomultiplier.

Factor (1) is the major source of uncertainty for multiply-charged ions. For protons, previous reports[5] give $\gamma = 4$ for the range 10-15 kev, and we find the same value for 10-25 kev. For other singly-charged atomic ions, γ is not greatly different from 4 for a similar energy range. However, larger values[3,8] of γ occur with multiply-charged ions and molecular ions. Since we are interested primarily in protons and deuterons, we have not yet measured γ for the multiply-charged species emitted by our plasma gun (e.g., C IV and Ti IV). Hence our assessment of their abundance relative to hydrogen could be off by a factor of two or three.

The number of photoelectrons liberated at the multiplier cathode per electron incident on the scintillator is determined (aside from collecting effi-

ciencies) by the secondary electron energy and the ratio w/η; w is the energy loss rate (i.e., per emitted photon) required of electrons passing through the scintillator, and η is the yield (photoelectrons per photon) of the Cs-Sb photocathode in the multiplier tube. One calculates $w/\eta = 2.2$ kev per photoelectron, since the plastic scintillator has 90% the pulse height of stilbene.[9] For 20 kev secondaries, the ideal "particle gain" of the scintillator-photomultiplier system is therefore about 9. Together with $\gamma = 4$ for protons on the aluminum knob, one therefore expects a net proton-to-photoelectron gain of 36. Our observed particle gain is about 20. The 45% defect in sensitivity probably arises from the aluminum coating on the scintillator. (If one chooses a thin coating to minimize electron energy loss, one must sacrifice some reflectivity of the coating for radiation directed away from the photomultiplier). Since the gain of such photomultipliers themselves can be made of order 2.5×10^6, the current gain of the entire detection system can be as high as 5×10^7. Hence, an ion current of 10^6 protons per second into the detector can give a photomultiplier output current of 8 micro-amperes, and one could detect a proton per second by measuring 10^{-12} ampere currents with a one-second time constant.

Ion Analysis of Pulsed Arc Plasma Source

The assessment of ion energies and impurity concentrations is of prime importance in the fusion application of confined plasmas. The usefulness of optical methods is often limited because of low plasma density, the almost complete ionization of the principal species (hydrogen or deuterium), and the unknown

excitation conditions and transition probabilities of impurities. Since we had encountered these problems during an experiment[10] on plasma injection into strong magnetic fields, the analyzer was first used to examine the output from the plasma gun employed in the injection studies. From shielded probe data we knew that the ion velocity distributions extended well above 10^7 cm/sec, and optical measurements had at least identified H, C, O and Ti in the plasma. We knew nothing as to the impurity abundance relative to hydrogen, and wanted particularly to maximize the proton fraction of those ions having velocities greater than 10^7 cm/sec.

To resolve the plasma species with the analyzer, we used the time-of-flight method previously mentioned. The flight path between the gun and the analyzer was made long enough (3.4 meters) to allow an adequate velocity determination in spite of the discharge duration in the gun (2 μsec); e.g., the accuracy was 10% at 1.7×10^7 cm/sec ($\sim$150 ev for protons). For each firing of the gun, the deflector voltage in the analyzer was set beforehand and the detector signal recorded as a function of time. Thus the narrow band in mv^2/Z passed by the analyzer was spread out in time, i.e., inversely as the velocity, and an m/Z spectrum thereby displayed. Such data are shown in Figs. 3 and 4, with time and m/Z increasing to the right. The figures are composites of several scope pictures, the sensitivity for each being given underneath in millivolts/cm. In each figure, ϕ denotes the analyzer deflector potential and, from Eq. (1), gives the ion energy $\epsilon = 16\phi Z/3$. Figures 3 and 4 differ in the voltage V_c to which the plasma gun capacitor was charged, and one sees a substantial increase in im-

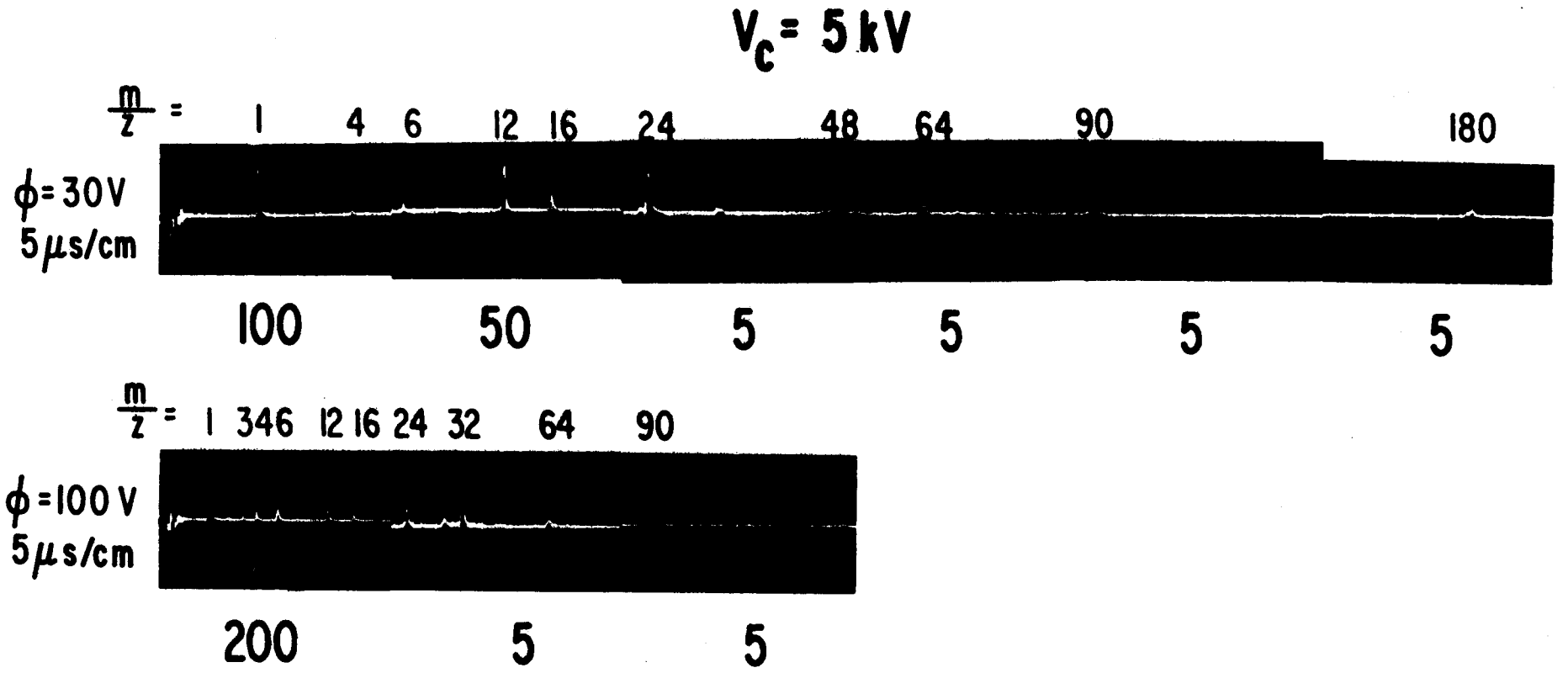

Figure 3. Composite of scope pictures showing m/z display achieved from time-of-flight velocity separation. Scope sensitivity in millivolts/cm given below each picture. ϕ denotes analyzer deflector potential and is related to ion energy by $\epsilon = \frac{16\,\phi}{3z}$, V_c = capacitor voltage.

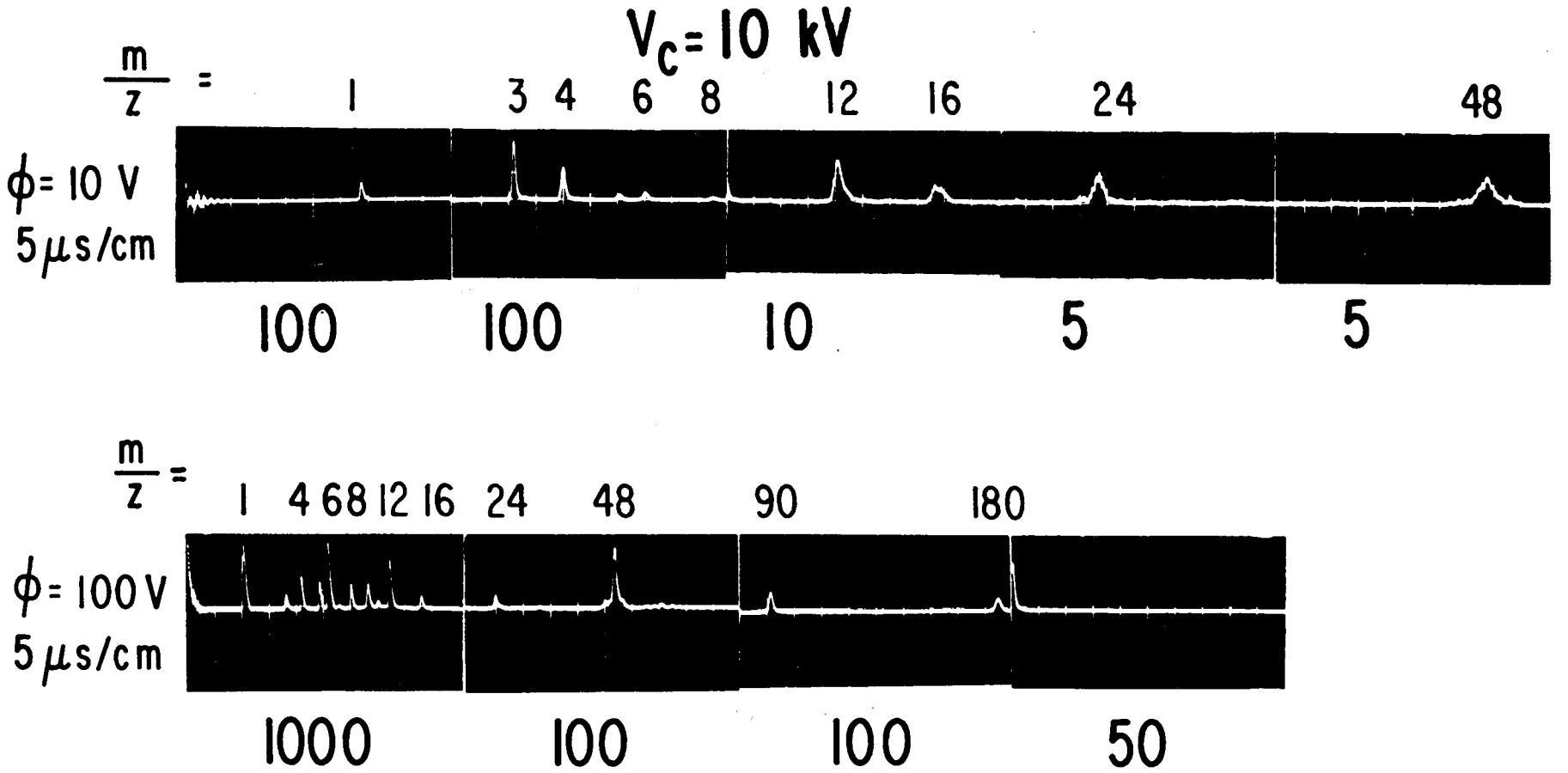

Figure 4. Display similar to that of Figure 3, except at 10 kv capacitor voltage.

purities ($m/Z \geq 3$) when V_c is raised from 5 kv (Fig. 3) to 10 kv (Fig. 4).

The voltage ϕ must be varied to find energy distributions for the various species, and one can simultaneously check all the m/Z data for self-consistency. This procedure is represented graphically in Fig. 5, where ϕ covers the range between 5 and 350 volts. The data points are taken from such peak locations as are shown in Figs. 3 and 4. The solid lines show theoretical values of ϕ (t, m/Z) for the dominant species expected in the plasma. A few ions can be identified with some certainty, particularly the protons at $m/Z = 1$. The likely contender for $m/Z = 3$ is CV; carbon is a commonly encountered impurity with plasma guns of this type. Copper and tantalum are used in the gun assembly, and the ions Cu II, Ta II and Ta III appear at $m/Z = 64$, 180 and 90, respectively. The primary electrode material is titanium and we indeed see Ti II and Ti III at $m/Z = 48$ and 24. The resolution is not good enough for distinctions between higher ionized states of titanium and states of carbon and oxygen, e.g., Ti V vs C II or Ti IV vs O I at $m/Z = 12$ or 16, respectively.

The proton energy distribution data are contained in the amplitudes of the peaks whose locations have been shown in Fig. 5. To find a proper relative distribution, however, one must divide out the linear increase of analyzer bandwidth with energy (Eq. 3). This involves an arbitrary choice of that energy ϵ^* at which the raw data is simply divided by unity. If the same such choice is made in deriving several distributions, they may all be intercompared although the absolute scale for all may still be arbitrary. Such a comparison is shown in Fig. 6 which gives the relative proton energy distribution ($\epsilon^* = 533$ ev) for

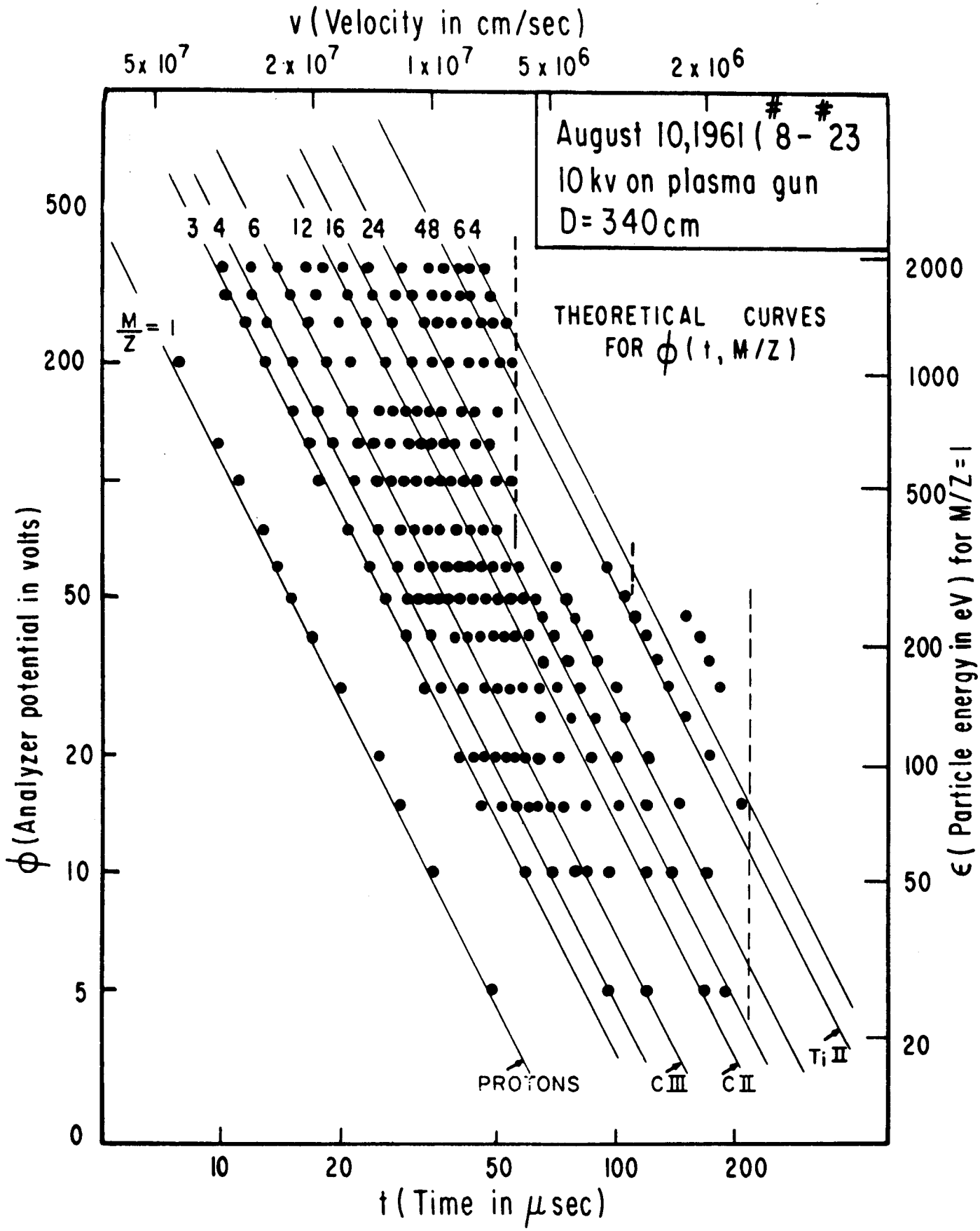

Figure 5. Graphical summary of m/z species indicated from data such as shown in Figure 3 and Figure 4. Solid lines are calculated values of $\Phi(t, m/z)$ for the dominant species expected in the plasma.

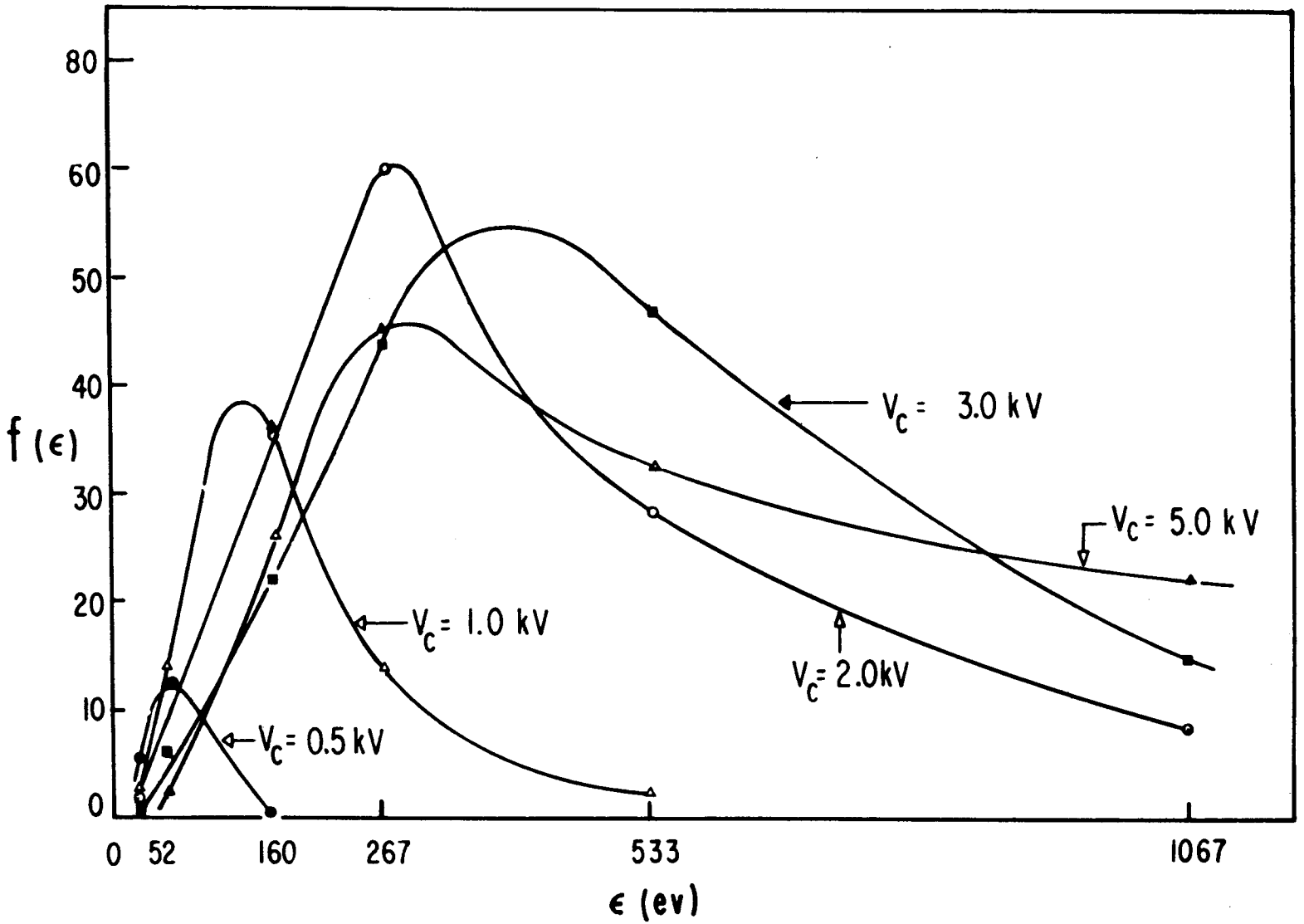

Figure 6. Proton energy distribution (normalized to 533 ev, see text) as a function of source capacitor voltage.

various voltages on the plasma gun capacitor. Absolute energy distributions are discussed at the end of this section. We see that voltages > 2 kv do not yield any striking gains in either the flux or mean energy of the protons.

In fact, Figs. 7 and 8 show that higher voltages are disadvantageous, the extra stored energy going primarily into high impurity yields. Not all the information is yet available, however, for a rigorous comparison of distributions between protons and other species. First, even if all these ions were identified, there would still be uncertainties of order 2 or 3 in the secondary electron coefficient and, hence, in the instrumental sensitivity for these species relative to protons. Secondly, as long as the absolute charges Z remain unknown, the scales of energy and distribution over energy are determined only up to multiplicative constants. Much work remains to be done on this phase of the analysis. Nonetheless, the present procedures are quite useful for isolating the proton component for subsequent study and allowing some empirical evaluation of plasma gun performance.

Absolute scales for the energy distributions have not been given, even for protons, since the 3.4 meter separation between the gun and the analyzer slit (stopped down to ~1 mm x 1 mm) were chosen quite arbitrarily. Further, the hydrogenation level in the titanium washers of the gun was not known since the initial loading had been made several months previous. Another variable arises from the angular dependence of plasma emission from the gun. The absolute sensitivity for protons was checked in other experiments with an RF ion source, using independent measurements of proton current together with

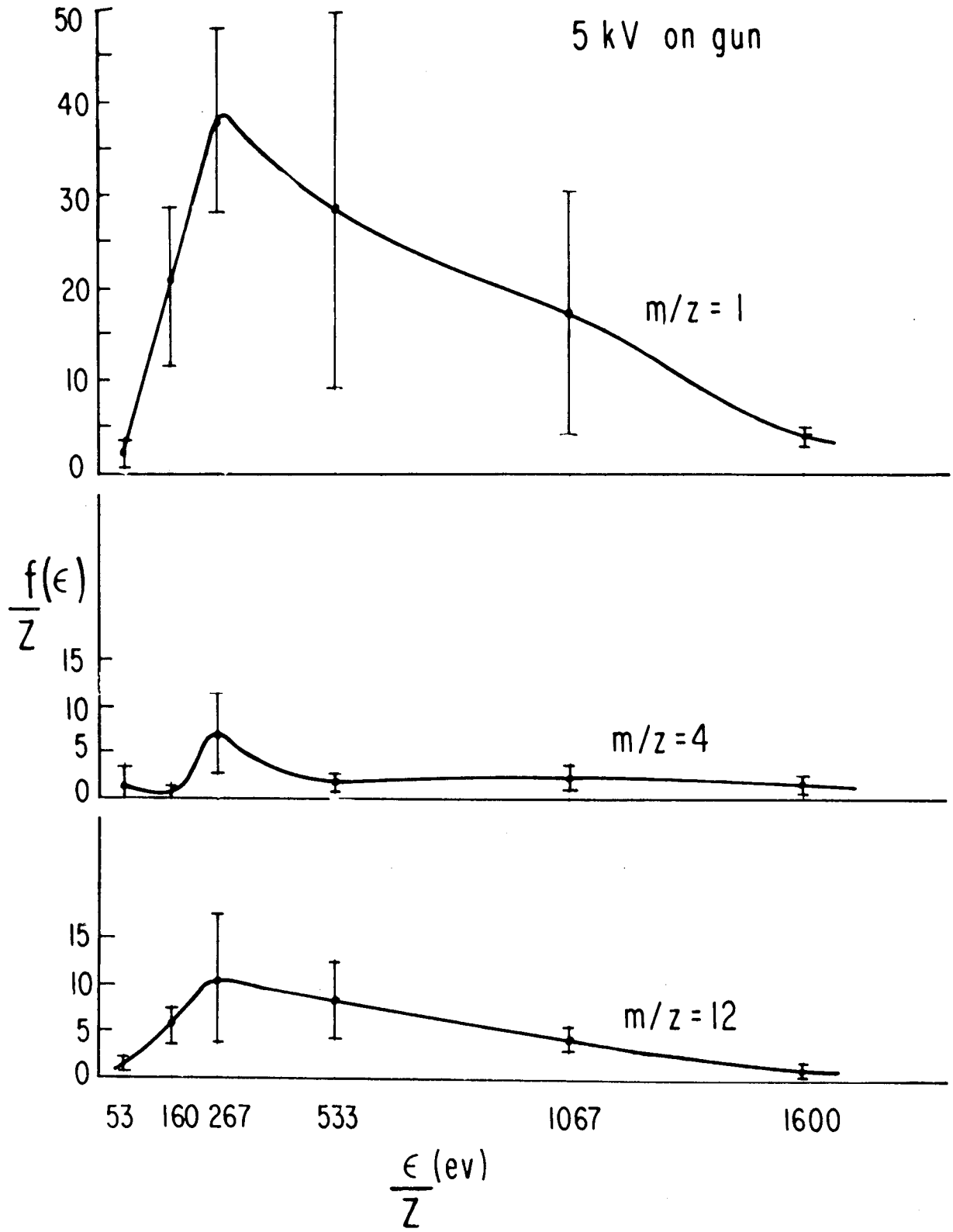

Figure 7. Energy distributions for m/z = 1,4 and 12 at 5 kv capacitor voltage. Each point and error bar represent the average and mean deviation over about 10 gun firings.

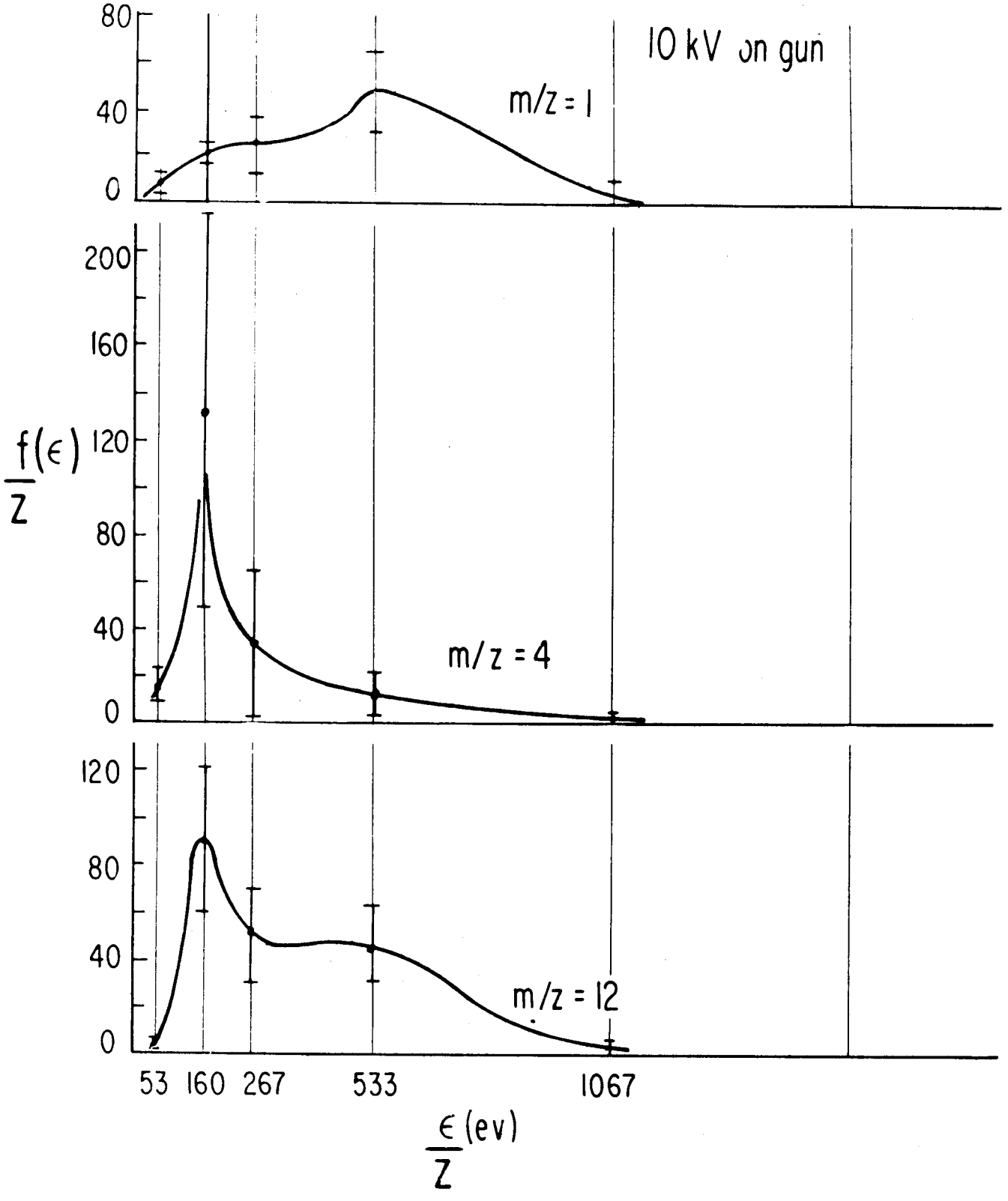

Figure 8. Energy distribution for m/z = 1,4 and 12 at 10 kv capacitor voltage, showing marked enhancement of impurities over 5 kv distributions.

the relative distributions taken by the analyzer.

Further Developments

In this section we discuss additional techniques being developed to extend the usefulness of the analyzer, namely, velocity selection and measurements of neutral particles.

Often particle velocities cannot be determined by a simple time-of-flight method, since the plasma under study may last long enough to make the time-origin of the particles quite uncertain. To solve this problem by increasing the flight path, one would need very large apparatus for the plasmas which will hopefully be studied in the future. (A kilometer would be required for 10% ion velocity measurements on a 5 kilovolt plasma confined for 100 microseconds.) We have, therefore, considered using various velocity selectors for m/Z discrimination, particularly the well known $\underline{E} \times \underline{B}$ type in which $\underline{v}$, $\underline{E}$ and $\underline{B}$ are mutually perpendicular. Since we are primarily interested in the range of atomic masses below 40, the required resolution is not exceptional, and fairly large apertures may be used for beam definition.

A very simple device of this sort employing permanent magnets giving $B \approx 600$ gauss has been tested in conjunction with the energy analyzer. The measured resolution in velocity, as determined by the use of an RF ion source, is approximately 7% for mass 28 ions at 1000 ev. A typical mass spectrum illustrating the performance of the selector is shown in Fig. 9. Better resolution, if required, could readily be obtained by a reduction of apertures.

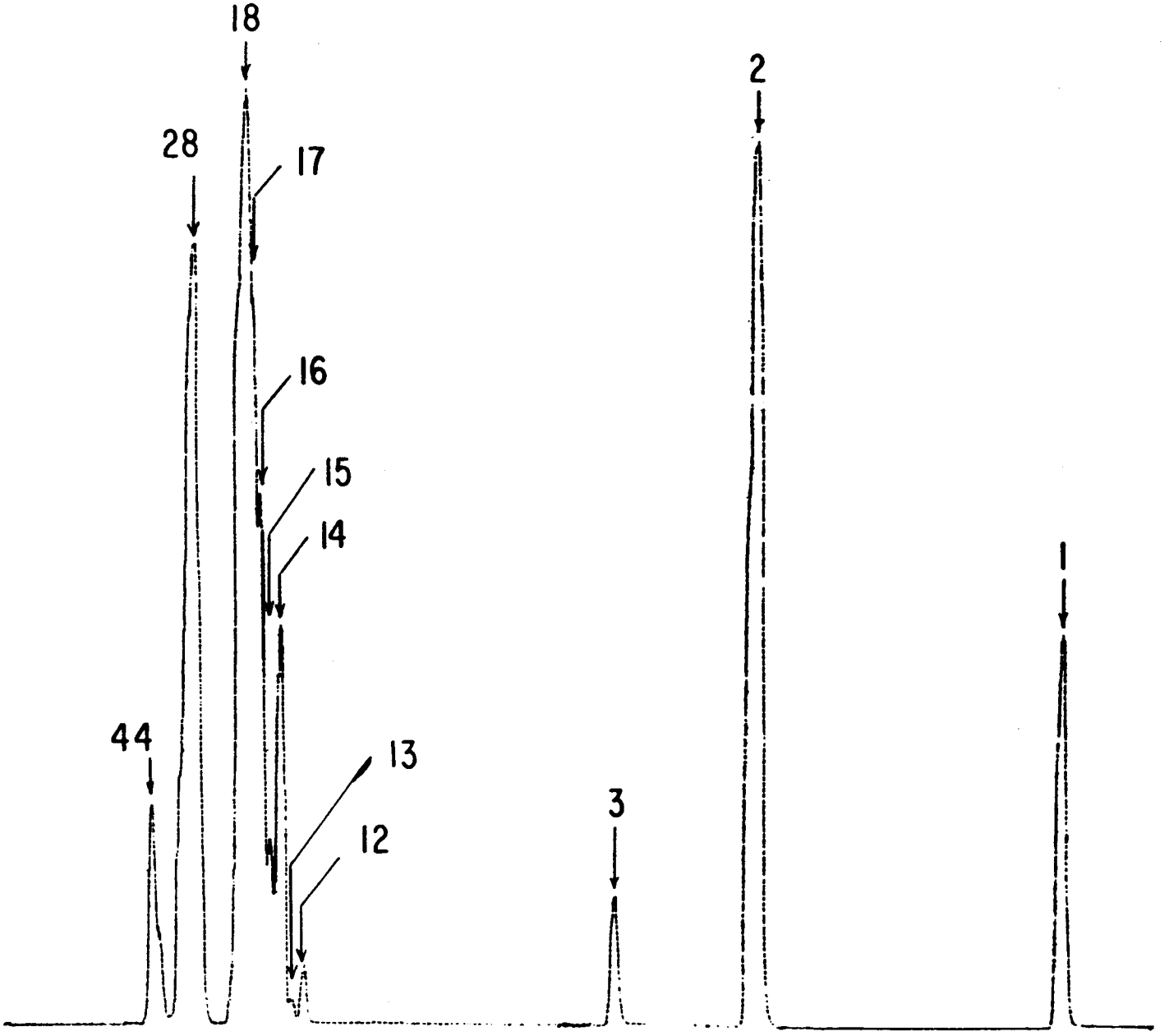

Figure 9. Display of m/z peaks obtained with small E x B velocity selector. The ion beam is dc and is obtained from an rf discharge in H_2 gas. Calibration was based on m/z values 1, 2 and 3 which are H^+ H_2^+ H_3^+ .

Neutral particle analysis and detection is of considerable interest in studies of confined plasmas, particularly when the energies of plasma ions are in the kev range and, therefore, their cross-sections for non-resonant charge exchange are very large. (Energetic neutrals are produced from positive ions by electron capture.) For such cases, the ability of neutrals to cross the magnetic field makes the neutral flux interesting as a probe of the ion energy distribution within the plasma, while creating a potentially serious drain on the plasma heat content. From either point of view, one can clearly make good use of flux and energy distribution measurements on neutral particles. This, of course, requires an ionization of the neutrals prior to analysis.

Various methods of ionization are possible in principle. The most attractive appears to be stripping in a gas cell, and our initial efforts in this direction will be discussed below. However, for neutral particle energies of order 100 ev or less, the electron loss cross sections are so low that scattering of the neutral beam is no longer a negligible perturbation. To work in the 1-100 ev range, it appears that one must ionize by photon or electron impact. In either case, one wants as high a flux of the ionizing agent as possible, so as to maximize the detection efficiency.

For electrons this immediately raises the question of space charge, i.e., the requisite beam density is high enough to make a potential well so deep as to alter the energy distribution of ions formed in the beam. One may be able to neutralize the electron space charge by the build-up of cold ions from the background gas. This would require great care, however, and the likelihood of avoiding perturbations to ions of a few ev energy seems rather remote.

Photoionization is appealing in principle, but faces practical difficulties

for the present. To be "competitive" with ionization by electrons, the required photon flux, i.e., the radiative power in the vacuum ultraviolet, seems prohibitive for steady-state operation. An alternative is to use short bursts ($\sim \mu$sec) of intense arc radiation to sample the neutral flux from more slowly varying plasmas. One such radiation source is the plasma gun described earlier. Since the cross-illuminating arc must be vacuum-coupled to the ionization region, and such arcs inevitably give rise to an energetic plasma, extensive baffling by mechanical and/or electromagnetic means is required to keep the plasma out of the neutral beam during the time of data collection.

In view of these difficulties, we have concentrated on the gas-stripping method which one can apply to neutral particles with energy > 100 ev. The Russians, for example, have achieved detectable ionization of 300 ev hydrogen atoms with nitrogen as a stripping agent.[5] We have succeeded in detecting helium-stripped hydrogen atoms over the energy range 160-1300 ev by the following procedure.

The source of energetic hydrogen neutrals was the plasma gun we have discussed earlier. The presence of hydrogen atoms with velocities above 10^7 cm/sec had previously been shown by monochromator observations of the Balmer lines. To effect the atom-to-ion conversion, we preceded the analyzer with a helium cell; the cell was appropriately slitted and differentially pumped so that helium pressures of 5×10^{-5} to 5×10^{-4} torr could be maintained with the pressure elsewhere of order 10^{-6} torr. The cell, in turn, was preceded by a pair of deflection plates for sweeping out the plasma ions. With 300 volts be-

tween these plates, and the extra cell evacuated, the "ordinary" (i.e., ion) signal disappeared entirely from the detector. By then admitting helium to the cell, we recorded strong proton signals arising from atoms stripped in the helium. We found that energy distributions could be taken of the converted protons, just as with the "ordinary" protons discussed previously.

For this low energy range, we do not yet know how to reconvert the measurements into absolute energy distributions for the neutrals H I. The electron-loss cross-section, σ_{01}, in helium has been measured only down to 5 kev by Fogel et al.[11] One of the authors (Eubank) is now extending the cross-section measurements down to ~ 300 ev for hydrogen atoms in hydrogen and helium. Preliminary helium results show a strong energy dependence with values of order 10^{-18} to 10^{-17} cm^2. The source of neutrals is a mass-analyzed beam of protons passing through a hydrogen cell. Absolute energy distributions of the resulting neutrals are derived from (1) the proton current, (2) the proton distribution as measured by the analyzer, and (3) the known values of the pickup cross-section, σ_{10}, for protons in hydrogen.[12] The calculated flux of neutrals into the stripping cell and the analysis of emerging protons then suffice to determine the electron-loss cross-section, σ_{01}, as a function of energy for whatever stripping gas is employed. (Hydrogen stripping may be required for the stellarator application to prevent possible contamination of the gas in the main discharge.) As well as being of fundamental interest, these data on stripping cross-sections will allow the absolute calibration of the analyzer as a neutral particle detector.

REFERENCES

1. F. H. Coensgen, W. F. Cummins, and A. E. Sherman, Phys. Fluids 2, 350 (1959).

2. A. L. Hughes and V. Rojansky, Phys. Rev. 34, 284, 291 (1929).

3. N. R. Daly, Rev. Sci. Inst. 31, 264, 720 (1960). This work relates to sensitive mass spectroscopy. A similar detector (in conjunction with a crude energy analysis) is described four months later in Ref. 5. It is not clear what priority, if any, can be established for this important development.

4. A. O. Nier, Rev. Sci. Inst. 31, 1127 (1960).

5. V. V. Afrosimov, I. P. Gladkovskii, Yu S. Gordeev, I. F. Kalinkevich, and N. V. Fedorenko, Zhur. Tekh. Fiziki 30, 1456, 1469 (1960). Translated: Soviet Physics - Tech. Physics 5, 1378, 1389 (1961). This work is particularly interesting for the ingenious method of flux calibration.

6. Bainbridge and Jordan, Phys. Rev. 50, 282 (1936).

7. J. Backus, Phys. Rev. 68, 59 (1945).

8. H. S. W. Massey and E. H. S. Burhop, Electronic and Ion Impact Phenomena (Oxford University Press, London, 1956), App. III.

9. J. Sharpe, Nuclear Radiation Detectors (John Wiley and Sons, Inc., New York, 1955), Table II, p. 40.

10. H. Eubank and T. D. Wilkerson, Phys. Fluids 4, 1407 (1961).

11. M. Fogel, V. A. Ankudinov, D. V. Pilipenko, and N. V. Topolia, Zhur. Eksptl. i Teort. Fiz. 34, 579 (1958). Translated: Soviet Phys. - JEPT 7, 400 (1958).

12. J. B. Hasted, Proc. Roy. Soc. A205, 421 (1951); A212, 235 (1952).

MEASUREMENT OF PULSED CURRENTS AND MAGNETIC FIELDS

by

Frank K. Bennett

One of the most common ways of measuring a pulsed magnetic field or a current producing such a field is by the use of a "pick-up" coil and associated "integrator". Some of the problems worth considering in the design of such coils and integrators are:

1. High and low-frequency limitations imposed by the integrator
2. High-frequency limitations imposed by resonances of the coil
3. Means of calibration of the system
4. Methods of making a current-measuring system insensitive to the spatial distribution of the current
5. Methods for measuring the peak value of the field or current to a higher degree of precision than that obtained in the time-resolved data
6. Corrections for the effects of a large extraneous field in the presence of a smaller field to be measured.

This discussion will not pretend to be all-inclusive, but will emphasize techniques which have been useful in the Plasma Physics Laboratory at Princeton. The actual problems dealt with are in no sense special except insofar as particular time scales are of interest and insofar as due regard must be taken of the presence of other large fields which preclude the use of magnetic materials with

their attendant non-linearities.

Typical System with RC Integration

A typical problem involves measuring the current flowing in the closed loop of plasma in a stellarator. A suitable pick-up coil will give a signal proportional to the time derivative of the magnetic field produced by this current, and hence proportional to the time derivative of the current. Integration of this signal with respect to time will finally yield an output signal proportional to the current. A simplified experimental arrangement is shown diagrammatically in Fig. 1, in which a toroidally wound pick-up coil and a simple "RC" integrator are employed.

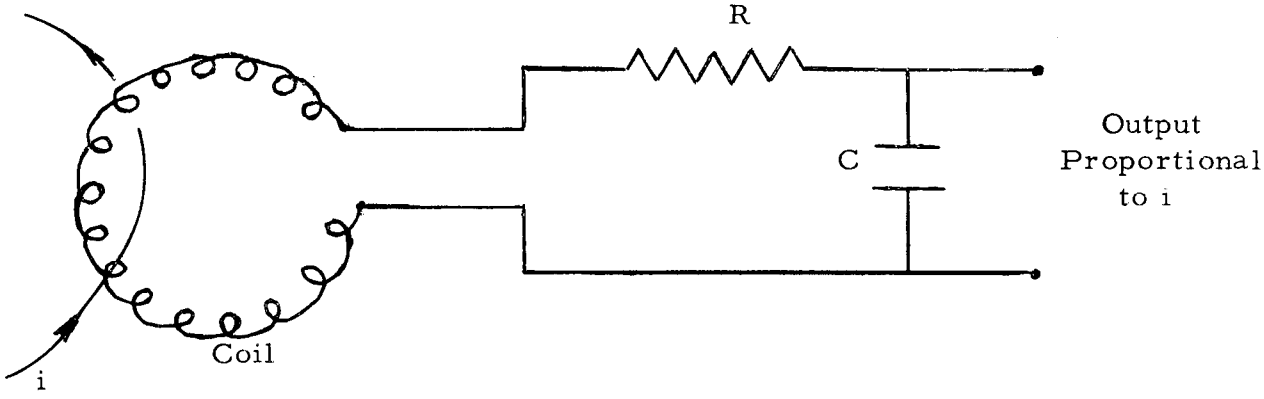

Fig. 1

The azimuthal flux produced by the plasma current (i) links the individual turns of the pick-up coil producing an (open-circuit) voltage at the coil terminals equal to M(di/dt), where M is the mutual inductance between the plasma loop and the pick-up coil. For sufficiently large R, the current flowing through the capacitor is then (M/R)(di/dt). The output voltage is then

$$\frac{1}{C}\int \frac{M}{R}\frac{di}{dt}\,dt = \frac{M}{RC}i$$

with suitable assumptions about initial conditions.

Current Pick-up Coils

Such a toroidal coil (sometimes referred to in the literature as a Rogovsky or Rogowski belt or coil) has the property that, for a sufficiently large number of uniformly spaced turns on the coil, the mutual inductance between the primary loop (plasma in this case) and the coil is independent of the spatial location of the primary loop so long as it passes through the "window" of the coil. This independence can, perhaps, best be seen by imagining the process to be reversed as indicated in Fig. 2.

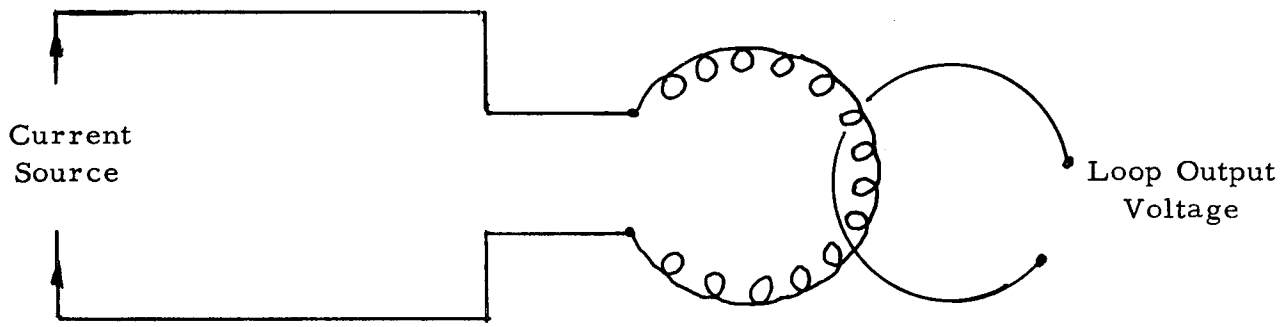

Fig. 2

If the toroidally-wound coil in Fig. 2 has a sufficient number of uniformly spaced turns, it will behave essentially like a uniform (current-sheet) solenoid closed on itself, and confine its own magnetic flux to the interior of the toroidal region. Under these conditions the same flux will link the single-turn secondary regard-

less of the position of the loop in the window of the toroid. Hence, the mutual inductance between the two circuits is a constant independent of positioning. It is clear from this discussion that it is not even necessary for the axis of the "toroidal" windings to be a circle so long as the coil confines its own flux to a closed tube. The output of the actual plasma-current measuring system in Fig. 1 is independent of the spatial distribution of current density in the plasma so long as the pick-up coil surrounds the plasma discharge tube. This analysis, of course, neglects the fact, to be considered later, that the toroidal coil also constitutes a one-turn loop around its window.

The mutual inductance of a toroidal pick-up coil (with respect to a single turn linking it) can be calculated from its geometry to a high degree of precision. The special case of a coil form having a rectangular cross-section will be considered because this is the simplest type to build. Assume a linear filamentary current centered in the toroid, and consider a plane containing this current, as shown in Fig. 3.

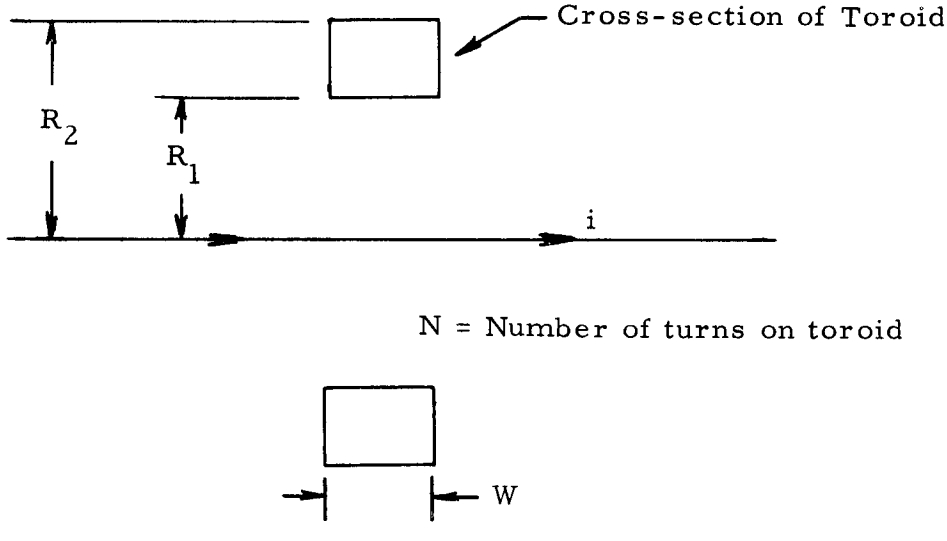

Fig. 3

Using MKS units, since $\oint \underline{H} \cdot \underline{d\ell} = \int\int \underline{j} \cdot \underline{dA} = i$, the total flux in the toroidal region is:

$$\phi = \mu W \int_{R_1}^{R_2} \frac{i}{2\pi r}\, dr = \frac{\mu W i}{2\pi} \ell n \frac{R_2}{R_1} \quad .$$

The coil output voltage, e_o, is just $N(d\phi/dt)$ and therefore $e_o/(di/dt) = M = (N\mu W/2\pi)\, \ell n(R_2/R_1) = 2 \times 10^{-7} NW\, \ell n(R_2/R_1)$, assuming that the coil form is made of non-magnetic material. For convenience if W is expressed in inches:

M (henries) $= 5.08 \times 10^{-9}\, NW\, \ell n(R_2/R_1)$.

In the event the primary quantity of interest is not a current, but is a magnetic field or its gradient at a single point, a useful reference for coil design is M. W. Garrett, J. Appl. Phys. 22, 1091 (1951).

L/R Integration (Current Transformer)

Another means of integration besides the RC integration already considered is L/R integration, as indicated in Fig. 4.

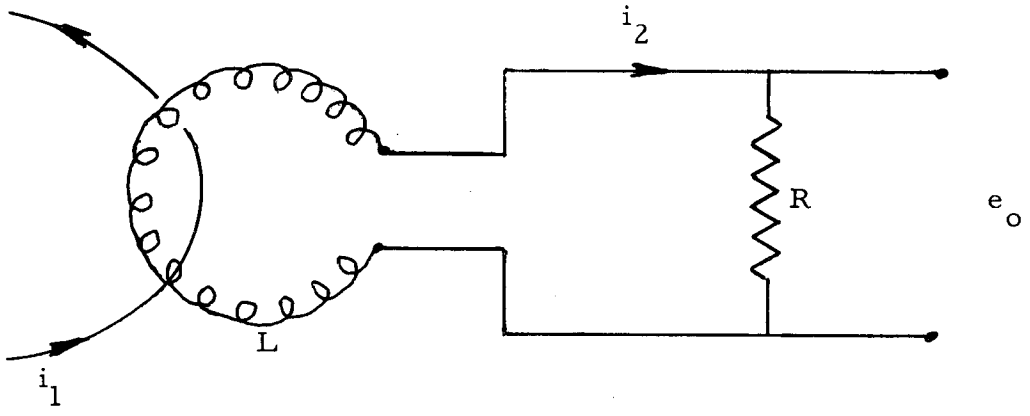

Fig. 4

In Fig. 4 the voltage induced in the pick-up coil is M(di/dt). For sufficiently small R, the current flowing in R is then $(1/L) \int M(di/dt)dt = Mi/L$, where L is the self-inductance of the coil, and hence $e_o = RMi/L = (\frac{M}{L/R})i$. For either system of integration the "sensitivity" of the system, i.e., e_o/i, is given by an expression of the form (mutual inductance/time constant).

It is interesting to note that the L/R integration system is usually analyzed as a "current transformer" without reference to differentiation and integration. In other words, for sufficiently small R, and sufficiently many turns, Lenz's law assures that the flux in the toroidal region will remain zero and hence $i = Ni_2$. But for N sufficiently large, $N = L/M$, and hence $i_2 = i/N = Mi/L$, which is essentially the same result obtained above.

Integrator Low-Frequency Limitation

All continuous integration schemes eventually fail at sufficiently low frequencies (or for sufficiently long times). This is most easily seen in the response of an actual system to a square current pulse:

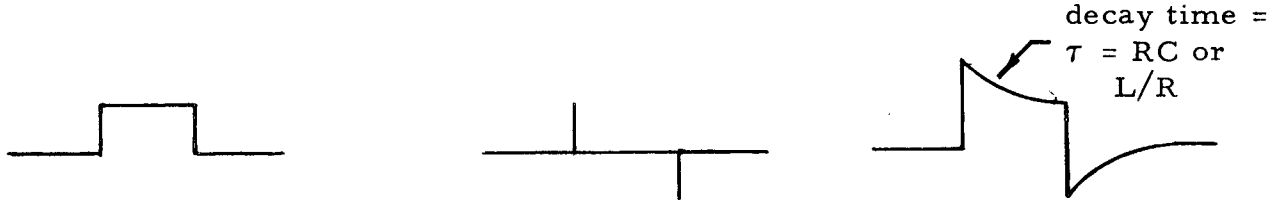

(a) Current to be measured

(b) Derivative of original signal

(c) Signal electrically re-integrated

Fig. 5

The integrated output signal will be a reasonably accurate replica of the current to be measured only if the integrator time constant, τ, is long compared to the duration of the pulse of current to be measured. Quantitatively, for a square pulse of duration T, short compared to τ, the maximum fractional error will be T/τ. Thus for 1% accuracy, τ should exceed the pulse length by a factor of 100.

Conflicting requirements on τ may arise, since a large τ necessary to minimize decay errors may make the sensitivity of the system too small to be useful. Additional gain may be incorporated in the system in such cases, and it is convenient to do so by use of the "Miller" integrator, the circuit of which is shown in Fig. 6.

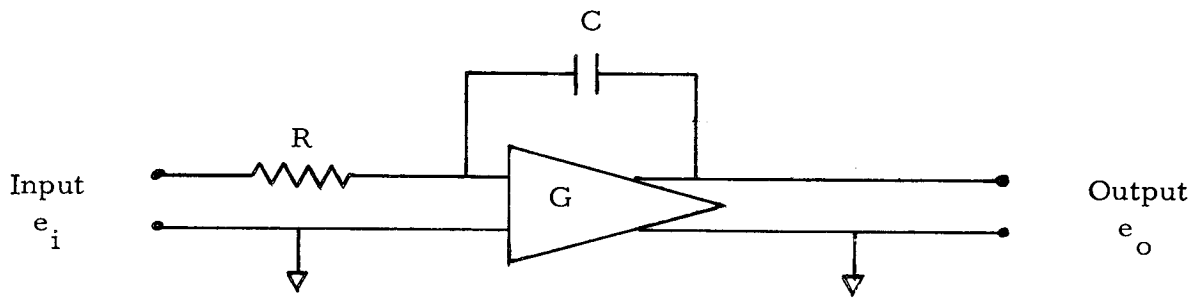

Fig. 6

The additional element introduced in Fig. 6 is a high-gain (inverting) amplifier whose (absolute) gain is G. Perhaps the simplest grasp of the operation of the Miller integrator may be had by assuming the amplifier gain is infinite in magnitude and negative in sign, the amplifier input impedance is infinite, and the amplifier output impedance is zero. Because of the infinite negative gain, the amplifier will act to keep its own input voltage virtually zero. The current in the

resistor is thus e_i/R. Since the amplifier input impedance is infinite, the same current must flow in C that flows in R. The charge on the capacitor (initially zero) is therefore $\int (e_i/R)dt$, and the output (and capacitor) voltage is $(1/RC)\int e_i dt$. This is just the result obtained for the simple RC integrator in the frequency range for which it is useful. The idealized Miller integrator does not "decay", however; when e_i is zero the voltage across R is also zero and there is thus no leakage from the capacitor. If the gain, G, is finite then a fraction 1/G of the capacitor voltage appears across R, and the capacitor discharge current is 1/G as large as it would be in the simple RC case. Hence, the effective decay time constant for the Miller integrator is GRC.

It is also instructive to consider an integrator from the point of view of its response to sinusoidal signals as a function of frequency. An ideal integrator may be characterized solely by its response to an ac voltage of arbitrary angular frequency, ω. Let $e_o = K\int e_i dt$, where K is a real proportionality constant. To find the performance as a function of frequency, let $e_i = \mathrm{Re}\ A\, e^{j\omega t}$. Then

$$e_o = K\,\mathrm{Re}\int A\, e^{j\omega t}dt = K\,\mathrm{Re}\,\frac{A\, e^{j\omega t}}{j\omega} ,$$

or, in terms of the usual complex magnitudes of ac circuit theory,

$$E_o = \frac{K E_i}{j\omega} \qquad \text{or} \qquad \frac{E_o}{E_i} = \frac{K}{j\omega} .$$

It can be shown that this latter equation is a sufficient as well as a necessary condition for a linear device to be an integrator. The frequency response

of an ideal and of some practical integrators are shown in Fig. 7.

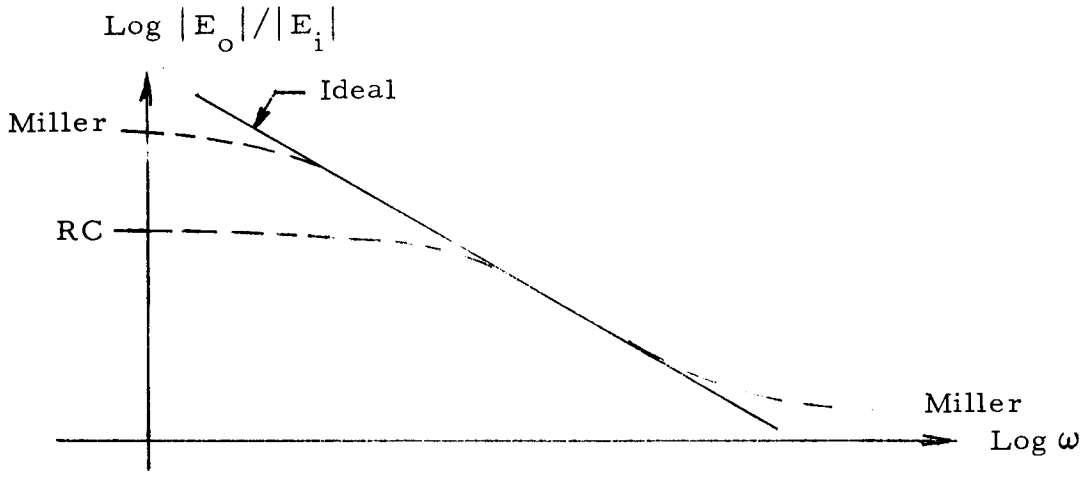

Fig. 7

The circuit diagram of a practical Miller integrator is shown in Fig. 8.

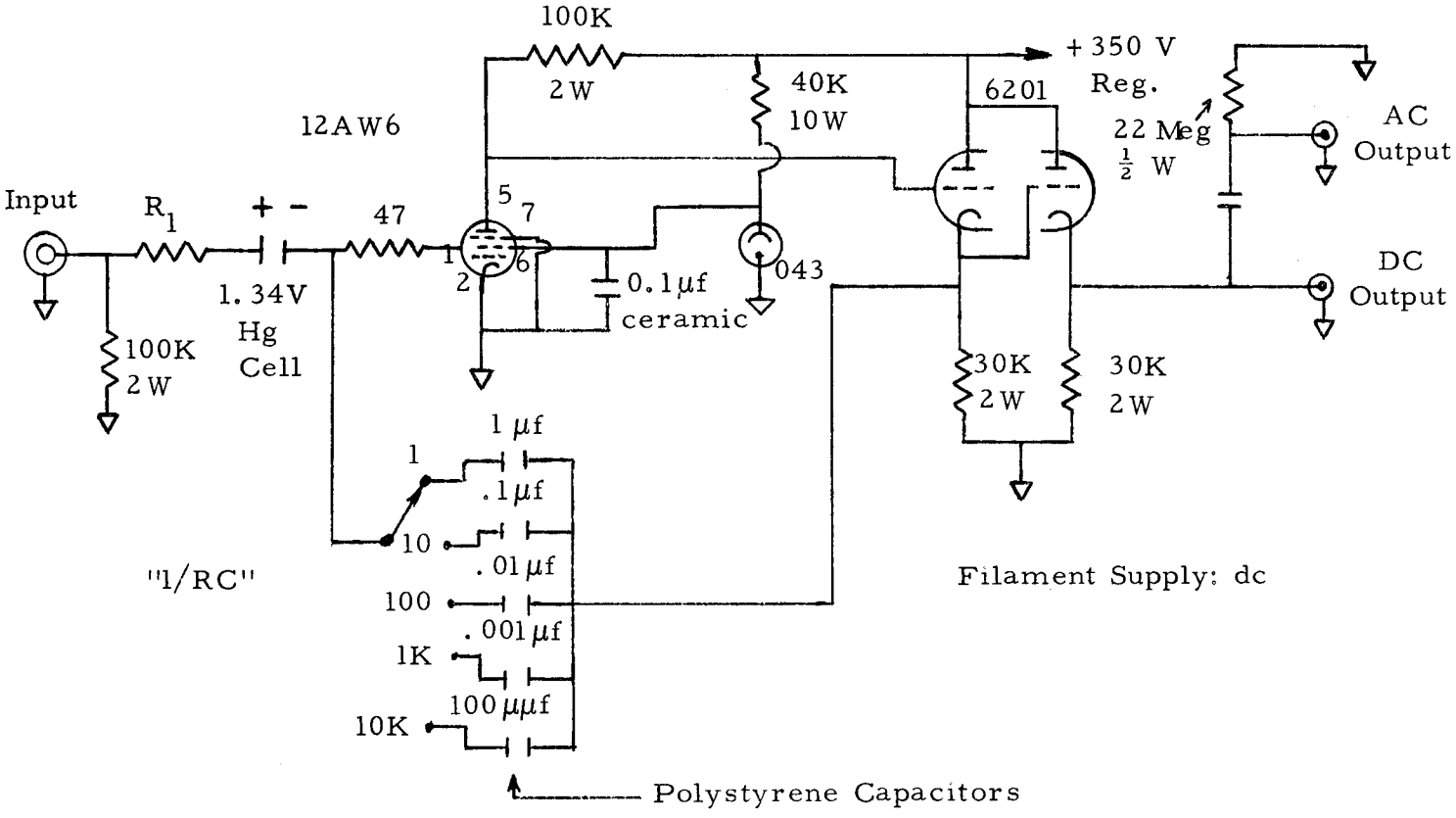

Fig. 8

With no input, the dc voltage at the dc output terminal should be between 100 and 200 volts dc, and should be checked periodically to detect tube aging. Adequate shielding and placement of parts are rather critical. Note that the grid of the output cathode-follower is connected to the cathode of that cathode-follower which is in the feedback loop. This connection rather than a parallel connection of the grids of the two cathode-followers is necessary to preserve high-frequency performance. R_1 may be 1 meg carbon, but if a 1% resistor is desired a Weston vamistor may be used. Some other resistor types exhibit excessive voltage coefficient or high effective shunt capacitance. Polystyrene capacitors exhibit a lower dielectric soak effect than any others tested in this laboratory.

Integrator High-Frequency Limitation

In some applications, the high-frequency response of even a well-designed Miller integrator is inadequate (as indicated in Fig. 7). This departure from the response of an ideal integrator typically will begin at a frequency of 1 megacycle or lower. This difficulty arises because of the non-zero output impedance of the amplifier. At some sufficiently high frequency the reactance of the feedback capacitor becomes low compared to the output impedance of the amplifier. Then even in a well-designed integrator, the transmission $|E_o/E_i|$ begins to level off to the value R_{out}/RG, where R_{out} is the amplifier output resistance. In a poorly designed integrator, the transmission may even rise with increasing frequency because of direct input-to-output capacitive coupling.

The high-frequency performance of the Miller integrator may be improved by keeping the amplifier output impedance low, as by use of a stacked cathode-follower output stage.

This improvement is usually small, however; an alternative scheme would be to use two integrators, one an RC type for good high-frequency response, and one a Miller type for proper low-frequency response. Fortunately, a system somewhat similar to this can be devised in which the two outputs add to give the correct final result, as shown in Fig. 9.

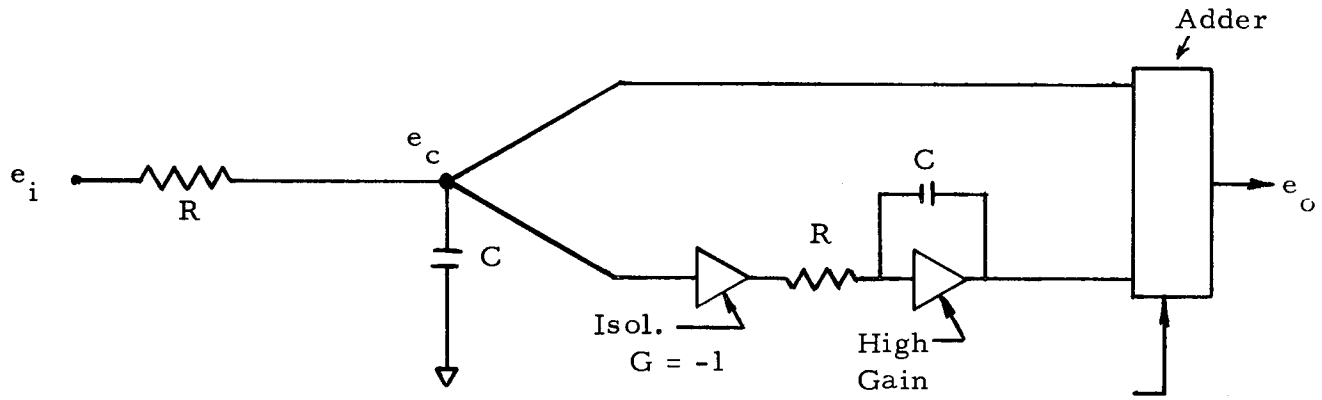

Fig. 9

If no loading is presented to the input RC circuit by either the adder or the isolating amplifier, then:

$$\frac{1}{RC}\int e_i = e_c + \frac{1}{RC}\int e_c dt \quad .$$

The second term in this equation is negligibly small at sufficiently high frequencies, but is the term that accounts for the failure of the simple RC integrator at low frequencies. The output of the adder, e_o, is just the sum of its two input signals:

$$e_o = e_c + \frac{1}{RC}\int e_c dt \quad .$$

The second term in this equation is just the usual expression for the output of a Miller integrator over the frequency range for which it is a useful integrator. Comparison of the above two equations shows that for this case:

$$e_o = \frac{1}{RC} \int e_i dt \quad ,$$

which is the desired result. Furthermore, this result is good even at the high frequencies at which the Miller integrator transmission has leveled out, since at such frequencies its contribution to the adder output is negligible compared to e_c. Thus Fig. 9 gives an integrator which is as good as the Miller integrator at low frequencies but also as good as the simple RC integrator at high frequencies. Incidentally, if the magnitude of the gain of the isolating amplifier is not exactly 1, then the ratio of the RC product in the input circuit to the RC product in the Miller circuit must be proportionately adjusted.

If it is desired merely to present the output (integral) to an oscilloscope, then the circuit of Fig. 9 can be simplified by the use of a differential type preamplifier in the oscilloscope. When two input signals (say, E_A and E_B) are presented to the two input terminals of such a preamplifier, the quantity displayed is $E_A - E_B$. The integrator used in this case is shown in Fig. 10.

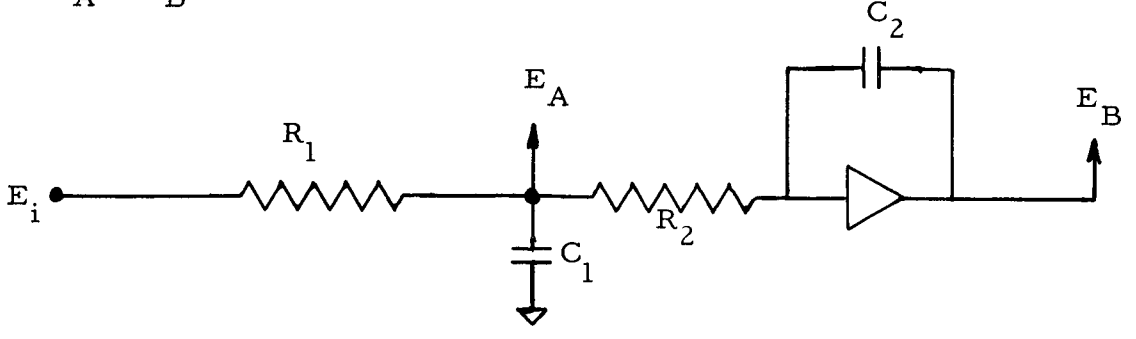

Fig. 10

Assuming a virtual ground at the amplifier input (because of the high negative feedback):

$$E_A = E_i \frac{\frac{R_2}{j\omega C_1} / \left(R_2 + \frac{1}{j\omega C_1}\right)}{R_1 + \frac{R_2}{j\omega C_1} / \left(R_2 + \frac{1}{j\omega C_1}\right)} .$$

From the previously derived result for the general property of an integrator in the frequency domain it follows that:

$$E_B = - E_A \frac{1/j\omega C_2}{R_2} .$$

Combining the above two equations and simplifying gives:

$$\frac{E_A - E_B}{E_i} = \frac{1}{j\omega} \times \frac{1 + j\omega R_2 C_2}{(R_1 + R_2)C_2 + j\omega C_1 C_2 R_1 R_2} .$$

C_2 should be chosen so that:

$$C_2 = \frac{C_1 R_1}{R_1 + R_2} .$$

With this choice, then:

$$\frac{E_A - E_B}{E_i} = \frac{1/R_1 C_1}{j\omega} ,$$

which is the desired result. Note again that when the transmission of the Miller

integrator portion of Fig. 10 levels out at high frequencies, E_B is already negligibly small compared to E_A. The final presentation, $E_A - E_B$, is as good at high frequencies as the simple RC circuit, and as good at low frequencies as the Miller integrator.

Another circuit useful in removing the high-frequency limitation imposed by the Miller integrator is shown in Fig. 11.

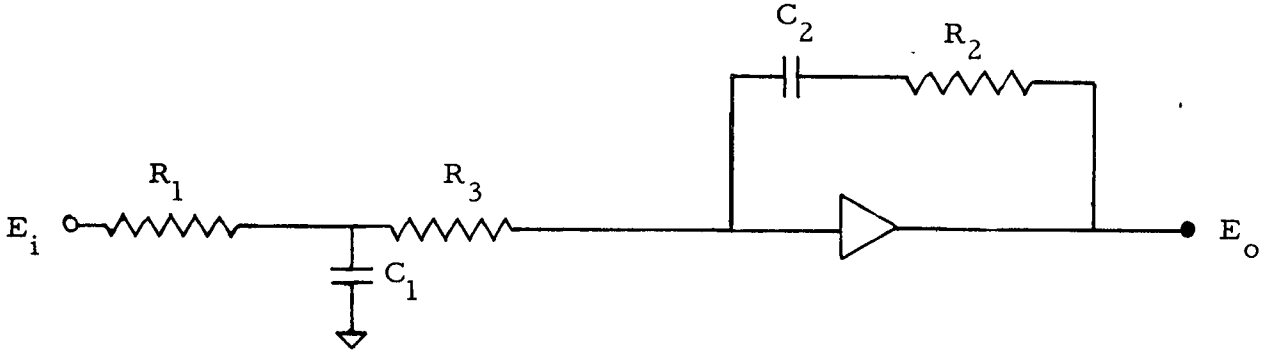

Fig. 11

With the usual assumptions about the amplifier in Fig. 11 (infinite gain, infinite input impedance, zero output impedance), if the R_2C_2 product is chosen so that:

$$R_2C_2 = \frac{R_1R_3}{R_1 + R_3} C_1 \quad ,$$

then it can be shown that:

$$\frac{E_o}{E_i} = \frac{1}{(R_1 + R_3)C_3} \times \frac{1}{j\omega} \quad .$$

In the case of Fig. 11, the high-frequency limitation of the normal Miller

integrator is not present since the required feedback loop contains resistance as well as capacitance. The feedback loop impedance never becomes small compared to the amplifier output impedance.

A further variation of this idea is shown in Fig. 12.

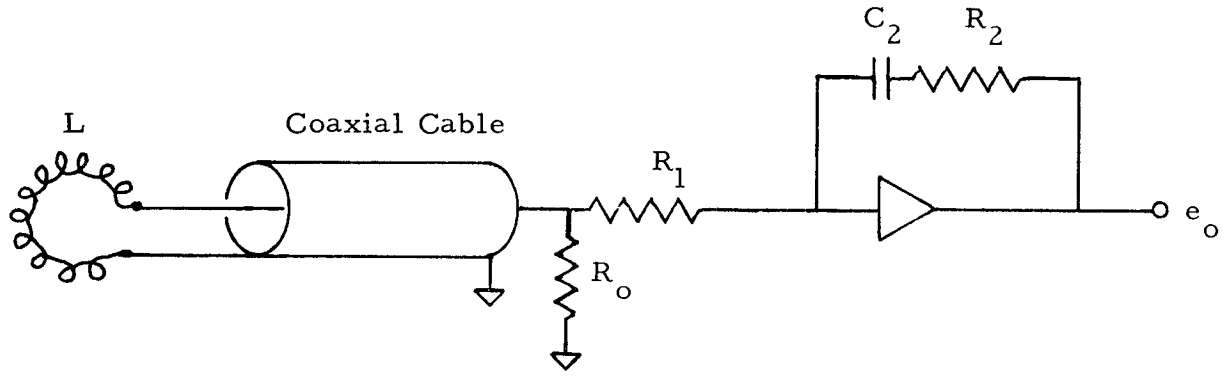

Fig. 12

In Fig. 12, L is the inductance of the pick-up coil, and E_i is the voltage induced in the coil. R_o (in parallel with R_1) is the proper resistance to terminate the coaxial cable used. The L and R_o by themselves constitute a simple L/R type integrator. It can be shown that if:

$$R_2C_2 = \frac{L}{R_o} \times \frac{R_1 + R_o}{R_1} \quad ,$$

then:

$$\frac{E_o}{E_i} = \frac{-R_o R_2}{L(R_1 + R_o)} \times \frac{1}{j\omega} \quad .$$

As with the previous example, the high-frequency performance is preserved by the required presence of R_2 in the feedback loop.

Frequency Limitation of Current Pick-up Coils

In a current measuring system, the toroidal pick-up coil may impose the high-frequency limitation on the system. The equivalent circuit of Fig. 13 is assumed in analyzing this problem.

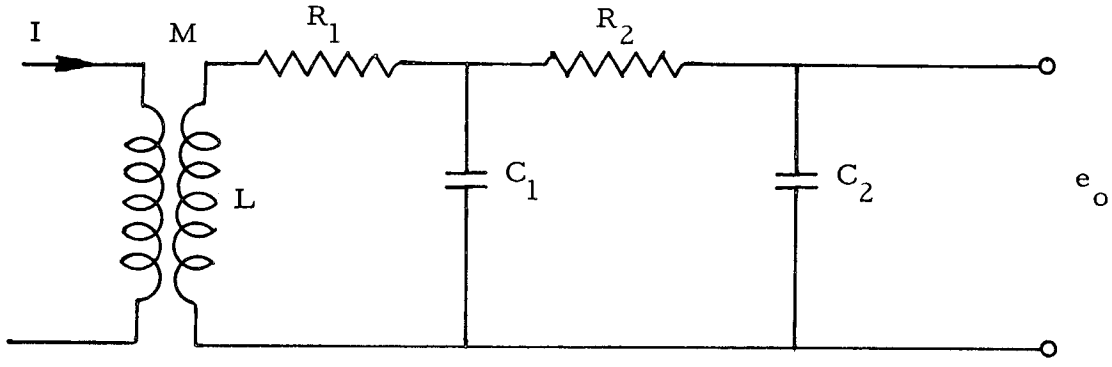

Fig. 13

This circuit is appropriate to the case of RC integration in which R_2C_2 form the integrator. C_1 is a lumped approximation to the distributed capacitance of the pick-up coil plus capacitance of any cable used to connect the pick-up coil to the integrating resistor, R_2. R_1 and L represent the resistance and self-inductance, respectively, of the pick-up coil. The following quantities are defined:

$$\omega_o \equiv \frac{1}{\sqrt{LC_1}} \qquad \tau \equiv R_2C_2$$

$$Q \equiv \frac{1}{R_1\sqrt{\frac{C_1}{L_1}} + \frac{1}{R_2}\sqrt{\frac{L}{C_1}}} \qquad Z \equiv \frac{1}{1 - \frac{\omega^2}{\omega_o^2} + \frac{j\omega}{Q\omega_o}}$$

Q is approximately the ordinary "figure of merit" or sharpness of resonance of a tuned circuit, while Z is the normalized sensitivity (or trans-impedance)of the system.

The following reasonable assumptions are made:

$\omega >> 1/\tau$ (the usual low-frequency limitation on integration, i.e., we fix our attention on the high-frequency behavior)

$R_2 >> R_1$, $C_2 >> C_1$.

It can then be shown that:

$$\frac{E_o}{I} = \frac{M}{\tau} Z \quad .$$

In short, departures of the complex quantity Z from (real) unity give departures of the system performance from the ideal performance expected at low frequencies. It is clear from a cursory inspection of the expression for Z that the system performance will be very bad at $\omega = \omega_o$ regardless of the value of Q. Figure 14 shows $|Z|$ and arg Z versus ω/ω_o for three different values of Q(Q = 10, 1, 0.1). Arg Z is shown dotted.

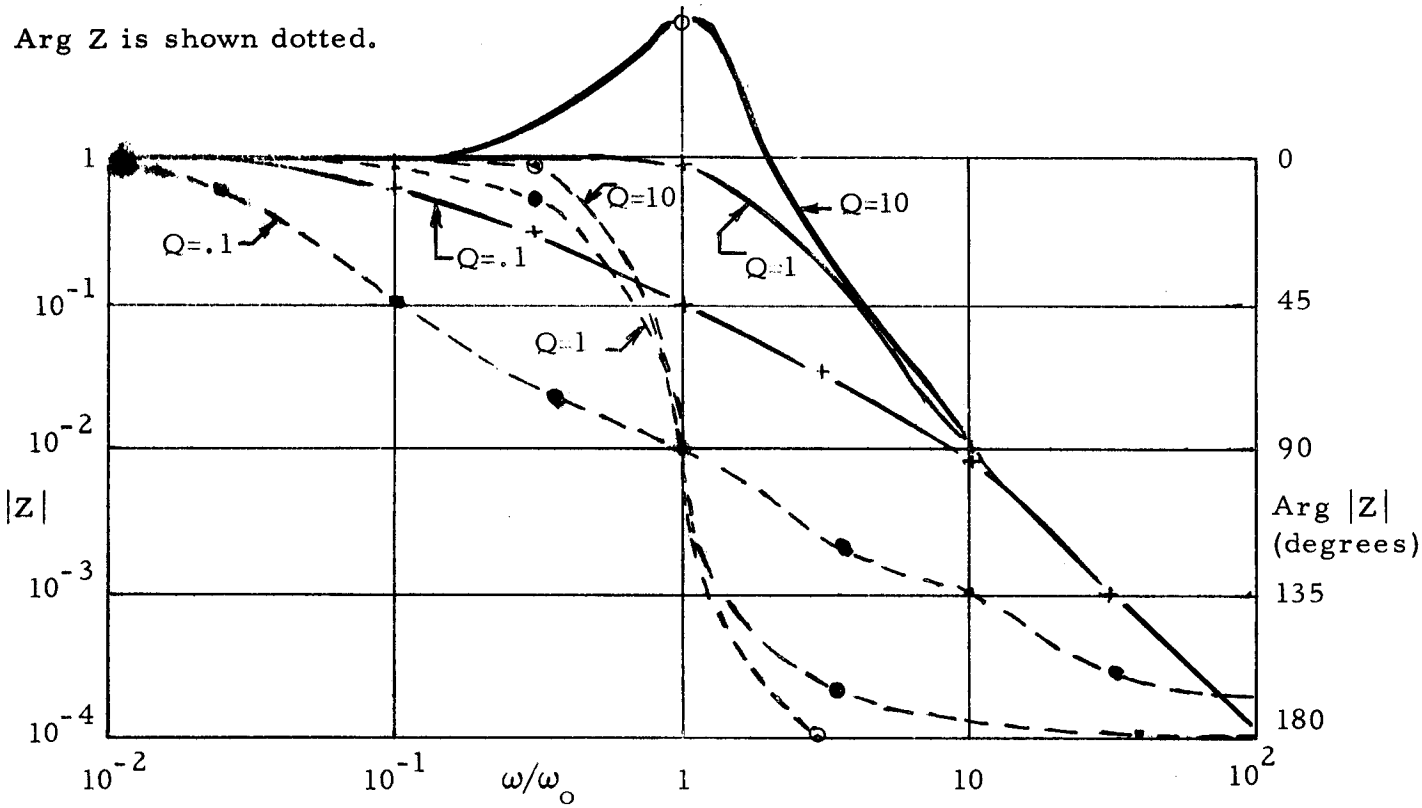

Fig. 14. High-frequency response of pick-up coil and RC integrator

If the Q is too high, the system response will be so peaked in the vicinity of $\omega = \omega_o$ that the system will exhibit undesirable "ringing" effects from shock excitation even though ω_o may be well beyond the highest frequency of interest. On the other hand too low a value of Q may cause inaccuracies in the system response (particularly in phase angle) many decades in frequency below ω_o. A Q of approximately unity is a reasonable compromise. In order to achieve this low Q, toroidal pick-up coils (for use with RC integration) are frequently wound with small diameter resistance wire (say, 0.01" diameter nichrome).

The behavior (both for low and high frequencies) of a pick-up coil and L/R integrator can be deduced from the circuit of Fig. 15.

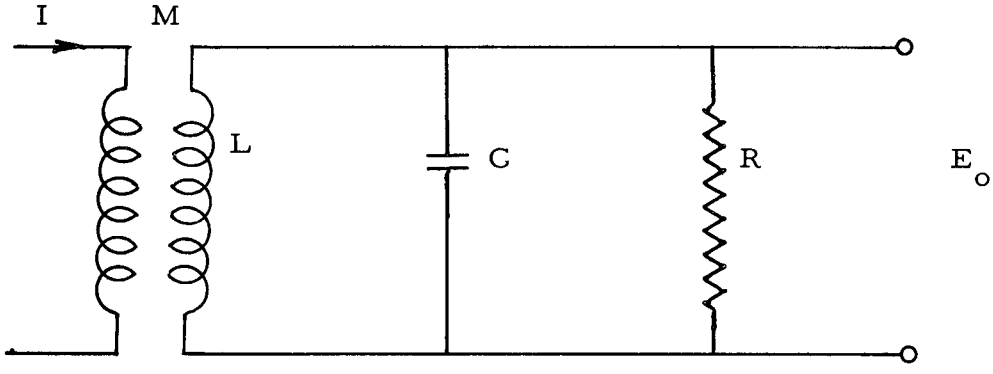

Fig. 15

Define $\omega_o \equiv 1/\sqrt{LC}$, $\tau \equiv L/R$. Then, omitting algebra:

$$\frac{E_o}{I} = \frac{M}{\tau} \cdot \frac{1}{1 + \frac{1}{j\omega\tau} - \frac{\omega}{j\tau\omega_o^2}} .$$

By inspection of the above expression, it is clear that E_o is a good replica of I if $\omega\tau >> 1$ and if $\omega << \omega_o\tau$. Together these requirements are that $\frac{1}{\tau} << \omega << \omega_o^2\tau$. It is, of course, implied that $\omega_o >> \frac{1}{\tau}$. The low-frequency limit for ω

(i.e., $1/\tau$) is the usual one for any integrator. It is also seen that ω_o is the geometric mean between the low-frequency limit ($1/\tau$) and the high-frequency limit ($\omega_o^2 \tau$). Therefore, for a given resonant frequency of the coil, this system (L/R) gives very much better high frequency performance than does the RC system. At $\omega = \omega_o$, the response of the L/R system is theoretically perfect, whereas at $\omega = \omega_o$ the response of the RC system is hopelessly bad.

For very small values of R in the L/R system, the resistance of the coil must also be taken into account, but this consideration does not materially affect the above conclusion concerning frequency response.

Calibration of Current Measuring Systems

It is difficult to measure the small mutual inductance of a toroidal pick-up coil, since a large current is required to give a useful coil voltage. A large ac current, as ordinarily produced in the laboratory, is very likely to contain appreciable but unknown percentages of harmonics. Since the coil differentiates, the harmonics contribute proportionately more to the output signal than does the fundamental. Also, for both the coil and the integrator separately the input and output waveshapes are different, which contributes to the difficulty of making accurate comparisons.

It is thus preferable to calibrate the whole system (coil plus integrator), rather than to calibrate coil and integrator separately. The quantity desired is ratio of output voltage to current being measured, and this ratio has the dimensions of resistance. In fact the coil plus integrator could be replaced by a resistor (meter shunt) if it were not for the impossibility of putting a meter shunt in series with a plasma loop, or, in some cases, if it were not for the voltage

isolation problem. This suggests comparing the coil plus integrator with a resistor, preferably by a null bridge method. A simplified schematic method for this calibration is shown in Fig. 16.

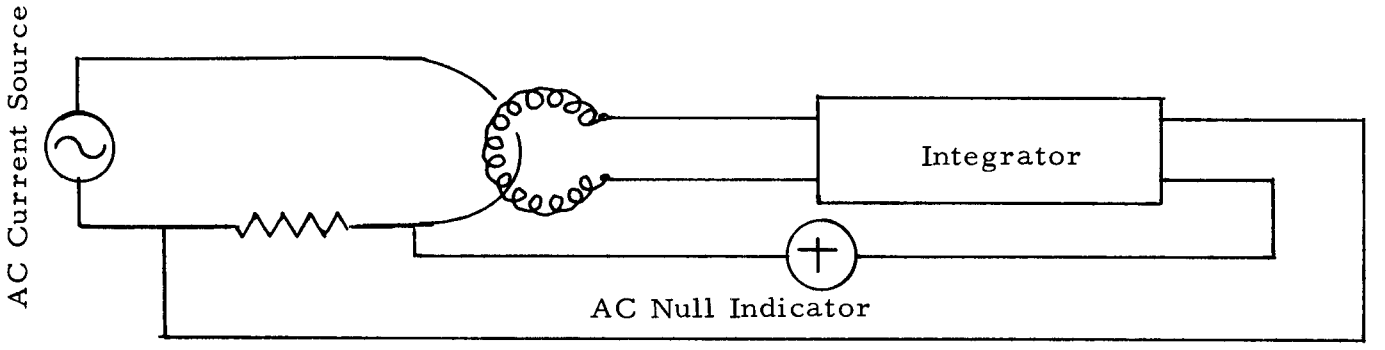

Fig. 16

A somewhat more practical circuit for this calibration is shown in Fig. 17.

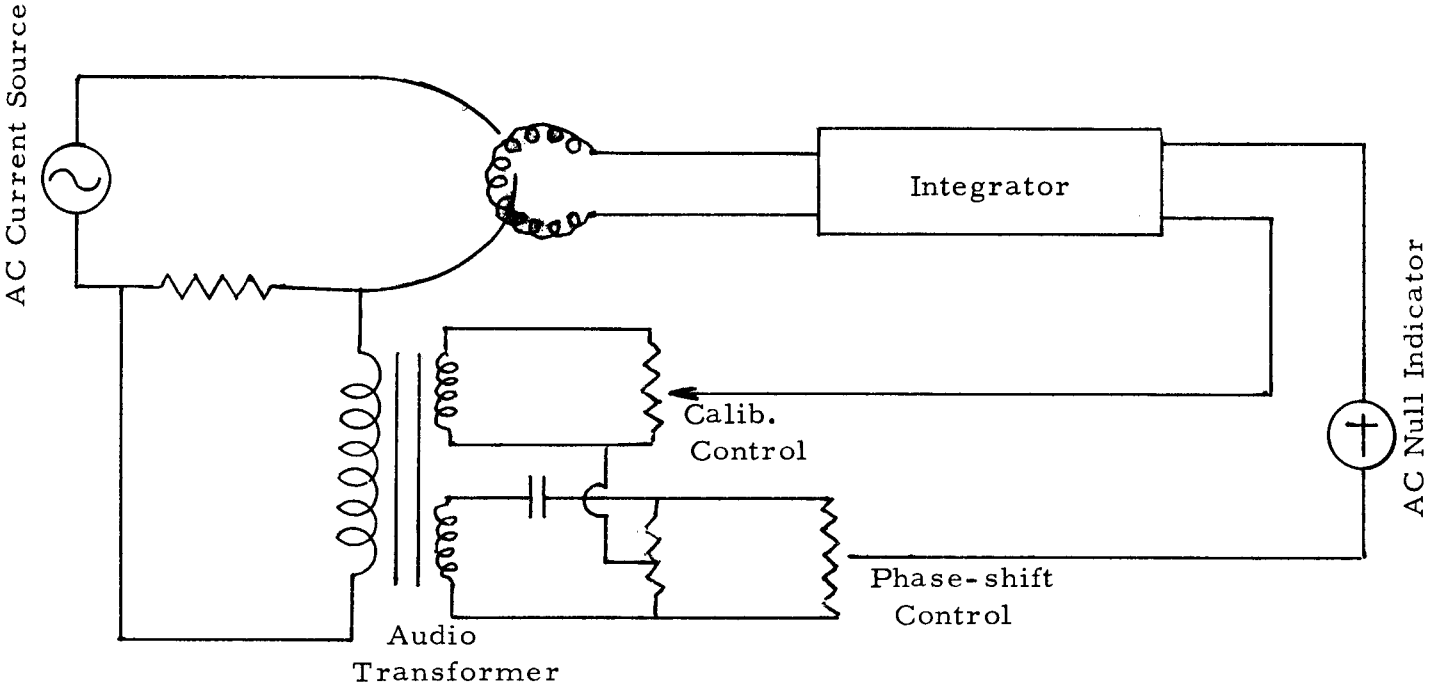

Fig. 17

The principal point of the circuit modification shown in Fig. 17 is to allow a lower source frequency (say 60 cps) to be used successfully. With a sinusoidal input, as the lowest useful frequency of the integrator is approached, the first noticeable deviation from perfect performance is the appearance of an out-of-phase, or quadrature, component in the integrator output. This quadrature voltage may interfere with obtaining a sharp null in the calibration method even though the in-phase component of the integrator output is still reliable. The addition of a "phase-shift control" in Fig. 17 enables the quadrature component to be canceled, and a sharp null to be obtained. It is not necessary to observe the exact setting of the "phase-shift control", but circuit values should be so chosen as to prevent the development of a quadrature component greater than a few per cent of the in-phase component. An inability to obtain a sharp null even at an extreme setting of the "phase-shift control" (for appropriate time constants) usually indicates a drastic loss of gain in the amplifier section of the integrator. A drawing of an actual calibrator of this type (Dwg. No. G-1046-S) will be separately provided. The drawing shows the calibrator built in two parts, along with various accessories required in actual operation.

Corrections for Large Extraneous Field

When a toroidal pick-up coil is used to measure the plasma current in a stellarator, the magnetic confinement field of the stellarator passes through the window of the pick-up coil. The coil acts as a one-turn loop around the confining field flux and thereby generates an undesired signal proportional to the rate of

change of the confining field. A first order correction for this effect can be made by proper lead placement ("backwinding" of the coil) as shown:

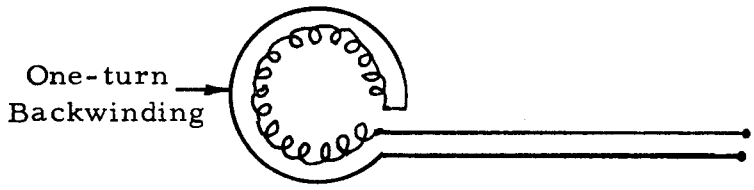

Fig. 18

This simple solution is usually not sufficient, however, since it is nearly impossible to place the backwinding at the exact radius necessary to effect complete cancellation of the confining field signal. Better cancellation can be achieved by the circuit of Fig. 19.

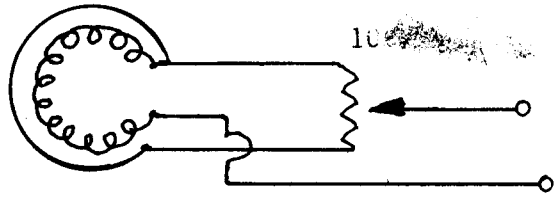

Fig. 19

The correct potentiometer setting can be found by trial and error, the correct setting resulting in a zero or minimum signal when the confining field is pulsed but no plasma current flows (either no gas in the machine or no plasma

heating voltage applied). In some cases, even this correction may not be sufficient. A residual pick-up-coil voltage may remain which appears to be proportional to the second derivative of the confining field. This occurs most frequently when the coil holders for the confining field windings are metallic, and hence have eddy currents induced in them by the confining field. If the eddy current field contribution does not vary radially in the same way the confining field varies radially, and if the major diameter of the pick-up coil is not large enough to keep the actual coil windings out of the strongest part of the confining field, then the second derivative signal may be particularly troublesome. A correction signal may be provided for the second derivative signal by use of an auxiliary loop to pick up a signal proportional to the derivative of the confining field and then an RC differentiator to differentiate this signal. A sketch (SK-1238) of such a system used on the B-3 stellarator will be separately provided.

Peak-Value Measurement

All the preceding methods of measurement present a time-varying signal to an oscilloscope. Accuracy is thus limited to the accuracy with which the oscilloscope trace can be read, say 2% or so. In some cases higher accuracy by means of a digital display may be desired. A digital display with any appreciable degree of time resolution would be a very complicated and expensive device. A compromise may be suitable in which the peak value of the pulse is read digitally to an accuracy of, say, $\pm$ 0.1%. A diode rectifier may be used in an RC integrator to cause the capacitor to charge up to a value corresponding to the peak field, and then stay at that value while it is being read with a digital

voltmeter. The basic circuit for accomplishing this is shown in Fig. 20.

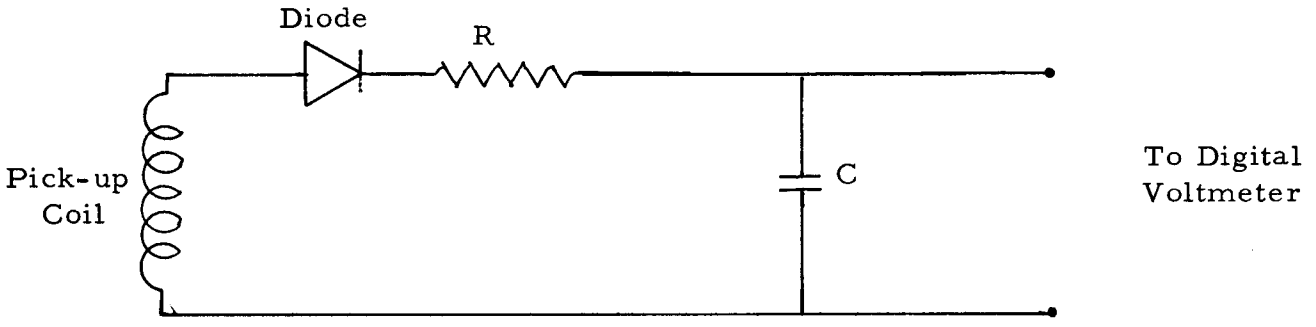

Fig. 20

Several precautions are necessary. The peak voltage developed by the pick-up coil should be of the order of 100 volts in order to avoid error introduced by the non-linear behavior of the diode at low voltages. The polystyrene capacitor should be kept short-circuited except for a few seconds during which the pulse occurs and the measurement is made (this assumes a pulse rate of no greater than three or so per minute). The digital voltmeter must have a very high input impedance in order that it not run the capacitor down during the time it takes to digitalize. This latter feature has been found obtainable on a relatively inexpensive commercial digital voltmeter by modifying it so that the input voltage is fed directly to a tube grid (differential amplifier) rather than through the resistive attenuator normally provided. A complete system is shown in a drawing (1367 D 001 WD) separately provided. The system shown has a reproducibility of $\pm$ 0.1% for pulses of the order of 20 ms duration provided the waveshape is reasonably reproducible. The RC time constant used (1 second) is not long enough to give complete independence of waveshape for the pulse durations used and for the precision desired.